# Spin functional renormalization group analysis of quantum Heisenberg ferromagnets

Dissertation
zur Erlangung des Doktorgrades
der Naturwissenschaften

vorgelegt beim Fachbereich Physik
der Johann Wolfgang Goethe-Universität
in Frankfurt am Main

von
Raphael Goll
aus
Heidelberg

Frankfurt 2021
(D30)

vom Fachbereich Physik der
Johann Wolfgang Goethe-Universität
als Dissertation angenommen.

Dekan: Prof. Dr. Harald Appelshäuser

Gutachter: Prof. Dr. Peter Kopietz
Prof. Dr. Roser Valentí

Datum der Disputation:

# Abstract

In this thesis we investigate the thermodynamic and dynamic properties of the $D$-dimensional quantum Heisenberg ferromagnet within the spin functional renormalization group (FRG); a formalism describing the evolution of the system's observables as the magnetic exchange interaction is artificially deformed. Following an introduction providing a self contained summary of the conceptual and mathematical background, we present the spin FRG as developed by Krieg and Kopietz in references [1] and [2] in chapter two. Thereto, the generating functional of the imaginary time-spin correlation functions and its exact flow equation describing the deformation process of the exchange interaction are introduced. In addition, it is highlighted that - in contrast to conventional field-theoretic FRG approaches - the related Legendre transformed functional cannot be defined if the exchange interaction is initially switched off. Next, we show that this limitation can be circumvented within an alternativ hybrid approach, which treats transverse and longitudinal spin fluctuations differently. The relevant functionals are introduced and the relations of the corresponding functional Taylor coefficients with the spin correlation functions are discussed. Lastly, the associated flow equations are derived and the possibility of explicit or spontaneous symmetry breaking is taken into account.

In chapter three, we benchmark the hybrid formalism against a calculation of the thermodynamic properties of the one and two-dimensional Heisenberg model at low temperatures $T$ and finite magnetic field $H$. For this purpose, we devise an anisotropic deformation scheme of the exchange interaction which allows for a controlled truncation of the infinite hierarchy of FRG flow equations. Thereby, contact with mean-field and spin-wave theory is made and the violation of the Mermin-Wagner theorem is discussed. To fulfill the latter, the truncation scheme is then complemented by a Ward identity relating the transverse self-energy and the magnetization. The resulting magnetization $M(H,T)$ and isothermal susceptibility $\chi^I(H,T)$ are in quantitative agreement with the literature and the established behavior of the transverse correlation length and the zero-field susceptibility close to the critical point is qualitatively reproduced in the limit $H \to 0$.

Finally, we investigate the longitudinal dynamics at low temperatures. To this end, the hierarchy of flow equations is solved within the same anisotropic deformation scheme complemented by an expansion in the inverse interaction range, and the resulting longitudinal dynamic structure factor is calculated within a low-momentum expansion. In $D = 3$, the large phase space accessible for the decay into transverse magnons yields only a broad hump centered at zero frequency whose width scales linearly in momentum. In contrast, at low temperatures and in a certain range of magnetic fields, a well-defined quasiparticle peak with linear dispersion emerges in $D \leq 2$, which we identify as zero-magnon sound. Sound velocity and damping are discussed as a function of temperature and magnetic field, and the relevant momentum-frequency window is estimated and compared to the hydrodynamic second-magnon regime.

# Publications

This work is partially based on the following two publications (titles and abstracts reprinted with permission © [2018-2020] American Physical Society):

Raphael Goll, Dmytro Tarasevych, Jan Krieg, and Peter Kopietz
**Spin functional renormalization group for quantum Heisenberg ferromagnets: Magnetization and magnon damping in two dimensions**
Phys. Rev. B **100**, 174424 (2019) [3]

We use the spin functional renormalization group recently developed by two of us [Krieg and Kopietz, Phys. Rev. B **99**, 060403(R) (2019)] to calculate the magnetization $M(H,T)$ and the damping of magnons due to classical longitudinal fluctuations of quantum Heisenberg ferromagnets. In order to guarantee that for vanishing magnetic field $H \to 0$, the magnon spectrum is gapless when the spin rotational invariance is spontaneously broken, we use a Ward identity to express the magnon self-energy in terms of the magnetization. In two dimensions, our approach correctly predicts the absence of long-range magnetic order for $H = 0$ at finite temperature $T$. The magnon spectrum then exhibits a gap from which we obtain the transverse correlation length. We also calculate the wave-function renormalization factor of the magnons. As a mathematical byproduct, we derive a recursive form of the generalized Wick theorem for spin operators in frequency space which facilitates the calculation of arbitrary time-ordered connected correlation functions of an isolated spin in a magnetic field.

Raphal Goll, Andreas Rückriegel, and Peter Kopietz
**Zero-magnon sound in quantum Heisenberg ferromagnets**
Phys. Rev. B **102**, 224437 (2020) [4]

Using a functional renormalization-group approach, we show that at low temperatures and in a certain range of magnetic fields, the longitudinal dynamic structure factor of quantum Heisenberg ferromagnets in dimensions $D \leq 2$ exhibits a well-defined quasiparticle peak with linear dispersion that we identify as zero-magnon sound. In $D > 2$, the larger phase space available for the decay into transverse spin waves leads only to a broad hump centered at zero frequency whose width scales linearly in momentum.

Besides, the following article - albeit not covered in the present monograph - was published during the term of this PhD:

Raphael Goll and Peter Kopietz
**Renormalization group for the $\varphi^4$ theory with long-range interaction and the critical exponent $\eta$ of the Ising model**
Phys. Rev. E **98**, 022135 (2018) [5]

We calculate the critical exponent $\eta$ of the $D$-dimensional Ising model from a simple truncation of the functional renormalization group flow equations for a scalar field theory with long-range interaction. Our approach relies on the smallness of the inverse range of the interaction and on the assumption that the Ginzburg momentum defining the width of the scaling regime in momentum space is larger than the scale where the renormalized interaction crosses over from long range to short range; the numerical value of $\eta$ can then be estimated by stopping the renormalization group flow at this scale. In three dimensions our result $\eta = 0.03651$ is in good agreement with recent conformal bootstrap and Monte Carlo calculations. We extend our calculations to fractional dimensions D and obtain the resulting critical exponent $\eta(D)$ between two and four dimensions. For dimensions $2 \leq D \leq 3$ our result for $\eta$ is consistent with previous calculations.

# Contents

## III Formalia

# I

# Spin functional renormalization group analysis of quantum Heisenberg ferromagnets

# Chapter 1

# Introduction

## 1.1 Preface

The birth of our present-day understanding of magnetic phenomena in solids as a cooperative interplay of the material's microscopic electrons traces back to the wake of the last century. At that time, the discovery of the normal Zeeman effect and its subsequent interpretation by Lorentz and Langevin using Maxwell's classical formalism had established the electron as the essential source of magnetic phenomena in gaseous matter. Furthermore, P. Curie had extended upon earlier work of Faraday and others and successfully classified a plethora of solid materials into the three classes of dia, para, and ferromagnetic materials, depending on their response with respect to an external magnetic field. It must thus have come as a surprise, when in 1911 Bohr - and independently a few years later van Leeuwen - showed that any bulk magnetic phenomena could by no means be explained in terms of an ensemble of classical electrons, whose statistical mechanic treatment simply predicts no magnetic behavior at all [6, 7]. It took another 20 years, and the revolutionary ideas of the newly formulated quantum mechanics, to solve this puzzle. As is well described in the literature, many of the radical ideas which emerged within that time, arose from the necessity to interpret the spectral line-structures and the chemical behavior of different elements. By the early 1920s Bohr's shell model of the atom had successfully explained the spectral properties of the hydrogen like-atoms, and Langmuir had suggested that the structure of the periodic table could be explained in terms of some clustering properties of the atomic electrons within these shells. An essential step forward was then made by Pauli, who noticed that the presumed atomic electron configurations could be explained in terms of the simple rule of one electron per state [8]. The necessity to develop a particular quantum mechanical labeling of these states hereby led to the postulation of an additional two-valued quantum number, lacking any classical interpretation. Shortly afterwards, Uhlenbeck and Goudsmit interpreted this quantum number as a manifestation of a so far overlooked intrinsic angular momentum property of the electron, the spin [9]. Meanwhile, Heisenberg and Schrödinger had successfully put the new quantum theory on firm mathematical ground, and the concept of the wave function as a probability amplitude describing the state of a given system, entered the stage. This, in turn, allowed Pauli to develop a proper mathematical treatment of the (non-relativistic) electron, describing its spin properties in terms of the nowadays famous three Pauli matrices and a wave function which had been upgraded to two components [10]. Finally, based on

all these novel ideas, the problem of the microscopic origin of magnetic phenomena in solid material was about to be reconsidered, too. In particular, Heisenberg [11] and Dirac [12] independently suggested that in a many-atom system the requirement of the antisymmetry of the wave function upon electron exchange in combination with the Coulomb interaction of the electrons would favor a ferromagnetic alignment of the spins of electrons localized in the outer shells of neighboring atoms. Further elaboration of this idea was interwoven with the development of a quantum many-particle theory by the likes of Heitler, London, Slater [6] and by 1929 the modern formulation of the Heisenberg exchange term

$$\mathcal{V}_{ij} = -\frac{1}{2} J_{ij} \boldsymbol{S}_i \cdot \boldsymbol{S}_j, \tag{1.1}$$

describing the low energy magnetic properties of a many-atom system in terms of an ensemble of SU(2) spin operators $\boldsymbol{S}_i$ localized on the sites $i$ and $j$ of an underlying lattice, first appeared in the publication of Dirac [13].[1]

Ever since, Heisenberg exchange interaction terms have been included in model-Hamiltonians whenever localized microscopic magnetic moments are expected to play a role, and as such have served as a cornerstone in the modern many-body description of the electromagnetic phases of matter. An accurate list of applications is inexhaustible, but prominent historic examples - which all have developed into vast research fields of their own - include the analysis of antiferromagnets [16], the investigation of magnetic impurities in metals [17, 18], as well as for instance, the quest for exotic spin-liquid phases of matter [19], possibly resulting from an interplay of geometric frustration and quantum fluctuations. In addition, the $n$-vector model - where the spin operators in the exchange term are interpreted as classical vectors of $n$ components - has played a crucial role in the development of our modern understanding of phase transition and universality [20].

However, keeping the general relevance of Heisenberg exchange terms in mind, the present thesis will primarily focus on the simplest possible benchmark model, the isotropic quantum Heisenberg ferromagnet on a $D$-dimensional hypercubic lattice. Given the long history of this model, the phase behavior in arbitrary dimensions is well established, and one would expect that the same holds true for the elementary dynamical excitations in the ordered phase. Certainly, this is the case for the transverse spin-dynamics (the dynamics of the spin components orthogonal to the direction of the macroscopic magnetization), which are usually explained in terms of spin waves (magnons) forming a weakly interacting gas of quasiparticles [21]. Interestingly, such a simple picture is not available for the longitudinal spin dynamics, which is still subject of ongoing research [22–24]. In this case, the absence of a clear perception probably also stems from the fact, that the majority of the developed analytical approaches towards quantum spin systems do not directly consider the spin degrees of freedom, but are based on auxiliary bosonic or fermionic particle representations. While these methods present the benefit that the well-known machinery of many-body theory can be applied, they all suffer from an artificial increase of the corresponding Hilbert space, which may lead to technical complications as well as non-physical effects. This is exemplified in a debate about

[1] Noteworthy, the original mechanism proposed by Heisenberg and Dirac is, however, slightly to simple to account for the origin of the exchange term in real materials. In addition, models of localized magnetic moments only account for a subarea of the magnetic phenomena observed in nature, as, e.g. the magnetism of metals usually derives from the magnetic moments of itinerant electrons [14, 15].

the possible existence of a zero-magnon mode in three dimensional Heisenberg ferromagnets, which took place in the late 1960s early 1970s. In the preceding decade, the *random phase* calculations of Bohm and Pines had successfully established a microscopic theory of the density fluctuations in charged and neutral Fermi liquids, explaining the observed wave like excitations, plasmons and zero-sound respectively, as emergent collective modes resulting from a coherent superposition of particle-hole states around the Fermi surface [25]. This early success of the many-body formalism, led to a number of works investigating the possible existence of related wave-like fluctuations of the magnetization density in the ferromagnetic phase of a Heisenberg magnet [26–32], mostly by mapping the spin system onto an ensemble of interacting bosons in the presence of a condensate. Original claims of the existence of such a zero-magnon mode for momenta at the boundary of the Brillouin zone [27] were, however, soon rejected as an artifact of the auxiliary representation [29] and subsequent works could not find any evidence of a well-defined finite frequency collective mode anywhere in the Brillouin zone [30–32]. Having said this, the precise calculations in Refs. [26–32] are complicated and often obscured by the auxiliary nature of the spin representation, while even more importantly, the question about the possible existence of such collective modes in lower dimensional Heisenberg models (i.e. a chain, respectively a planar lattice of interacting SU(2) spins) has hardly received any interest. This thesis aims to account for these shortcomings.

To this end, we build on recent advances in the application of the functional renormalization group (FRG) to quantum spin systems, and develop an analytical framework which allows for a non-perturbative calculation of the static and dynamic observables of the Heisenberg ferromagnet in the ordered phase. This framework, denoted *hybrid spin functional renormalization group* [3] is a special version of the *spin functional renormalization group* (spin FRG) method, which was developed in our group by Krieg and Kopietz [1, 2]. Technically, the spin FRG method rests on the modern language of generating functionals and the renormalization group, while its conceptual roots trace back to an old diagrammatic technique, which has been introduced in two seminal papers by Vaks, Larkin and Pikin (VLP) in 1968 [33, 34]. In particular, this technique enables the calculation of the various correlation functions of a Heisenberg system in a perturbation series in the exchange interaction, without resorting to any intermediate auxiliary representation. Given that the associated diagrammatic language is rather involved, the method has, however, not gained widespread attention and only little further development ever since [35, 36]. That said, the present thesis is an attempt to exemplify that the renaissance of these ideas within the modern spin FRG formulation presents not only a conceptual progress but also delivers noteworthy physical results. In order to do so, we do not only consider the aforementioned problem of the possible existence of a zero-sound mode, but also test the spin FRG method against a calculation of the magnetization and susceptibility curves of the one and two-dimensional Heisenberg model.

Thereto, the thesis is structured as follows: the following introduction presents a short review of the relevant physical and methodological background. In particular, we briefly discuss possible microscopic origins of the exchange interaction term (1.1), and establish the phase behavior of the ferromagnetic Heisenberg model in different dimensions. In addition, a short introduction to Matsubara's imaginary time formalism, which presents the formal basis of the spin FRG, is given and the relation to the relevant experimental observables is established. Lastly, we introduce a classification of different types of collective sound excitations, which is mandatory in order to contextualize the discussion of the zero-magnon

problem given in the last chapter. The second chapter introduces the spin FRG formalism in its original form, and its hybrid version, which is tailored to investigate quantum spin systems in the ordered phase. As such we define a number of mutually related generating functionals and derive corresponding exact FRG flow equations, describing the evolution of these functionals as the exchange interaction between the spins is gradually switched on. The calculation of the various spin correlation functions hereby reduces to the solution of an infinite set of coupled integro-differential equations, whose lowest order forms are explicitly given. As a first application of the hybrid spin FRG, chapter 3 provides an analysis of the thermodynamic response functions of the D-dimensional isotropic Heisenberg ferromagnet at temperatures and magnetic fields small compared to the intrinsic exchange interaction. The explicit temperature and magnetic-field dependence of the magnetization and susceptibility is investigated and compared to the benchmark results of the literature. Finally, we come back to the historic zero-sound discussion in the last chapter and investigate the longitudinal spin dynamics at low temperatures and finite magnetic fields. In particular, it is shown that in $D \leq 2$ a well-defined zero-magnon mode can indeed exist in in a certain range of magnetic fields. We end with a brief summary and an outlook to future studies.

## 1.2 The Heisenberg model

The following section introduces the Heisenberg model as an effective low energy description of the qualitative magnetic behavior of certain materials. Furthermore, we review the phase behavior of the ferromagnetic model as a function of temperature and dimension of the underlying lattice.

### 1.2.1 Exchange mechanisms

The magnetic ordering in insulators arises from a combination of the electrons' elementary properties, their spin and kinetic energy, and the interaction effects provoked by the Coulomb repulsion and the Pauli exclusion principle [37]. In the literature, a plethora of mechanisms have been suggested as the origin of a low energy description in terms of the Heisenberg model, and the present introduction is by no means able to present an exhaustive review. Instead, we follow the spirit of the reviews given in Ref. [38, 39], and shortly discuss the concepts of Coulomb and kinetic exchange on the basis of two simple two-particle models. These two exchange-processes present the basis of more complicated mechanisms, which presumably account for the origin of magnetic exchange interactions in insulators.

#### Two coupled $S = 1/2$ spins

In order to facilitate the upcoming discussion, let us shortly review the eigensystem of two spin-$S$ particles coupled by the Heisenberg term

$$-\boldsymbol{S}_1 \cdot \boldsymbol{S}_2 = -\sum_{\alpha=\{x,y,z\}} S_1^\alpha S_2^\alpha. \tag{1.2}$$

Here the operators $S_i^\alpha$ should be interpreted as direct products, i.e. $S_1^\alpha = \tilde{S}_1^\alpha \otimes \mathbb{1}_2$ respectively $S_2^\alpha = \mathbb{1}_1 \otimes \tilde{S}_2^\alpha$, where $\tilde{S}_i^\alpha$ is the spin operator acting on the $2S+1$-dimensional Hilbert-space of a single particle. These spin operators fulfill the normalization condition $\tilde{\boldsymbol{S}}_i^2 = S(S+1)$, and satisfy the SU(2)-algebra

$$\left[\tilde{S}_i^\alpha, \tilde{S}_j^\beta\right] = i\delta_{ij}\varepsilon^{\alpha\beta\gamma}\tilde{S}_i^\gamma, \tag{1.3}$$

where $\varepsilon^{\alpha\beta\gamma}$ is the completely antisymmetric Levi-Civita tensor. To simplify the discussion, we choose here $S = 1/2$ and describe the Hilbert-space of a single spin in the common spinor formulation where the components of $\tilde{S}_i^\alpha$ are expressed in terms of the Pauli matrices[2]

$$\tilde{S}_i^\alpha = \frac{1}{2}\sigma^\alpha, \quad \sigma^x = \begin{pmatrix} 0 & 1 \\ 1 & 0 \end{pmatrix}, \quad \sigma^y = \begin{pmatrix} 0 & -i \\ i & 0 \end{pmatrix}, \quad \sigma^z = \begin{pmatrix} 1 & 0 \\ 0 & -1 \end{pmatrix}. \tag{1.4}$$

The Hilbert-space of the coupled system is then four dimensional and a possible basis is given by the product states

$$\{(|\uparrow\rangle_1, |\downarrow\rangle_1) \otimes (|\uparrow\rangle_2, |\downarrow\rangle_2)\rangle\} = \{|\uparrow,\uparrow\rangle, |\uparrow,\downarrow\rangle, |\downarrow,\uparrow\rangle, |\downarrow,\downarrow\rangle\}, \tag{1.5}$$

[2] To simplify the notation, we set the reduced Planck constant $\hbar \to 1$ throughout this work. Likewise, the Boltzmann constant is set to $k_B \to 1$, i.e. frequency and temperature are measured in units of energy.

where the single particle basisvectors, $\{|\uparrow\rangle_i, |\downarrow\rangle_i\} = \{\chi_i^{\uparrow}, \chi_i^{\downarrow}\}$, are chosen as eigenstates of the $\tilde{S}_i^z$ operator. Evaluating the Heisenberg term (1.2) in the given basis yields the Matrix representation

$$-\boldsymbol{S}_1 \cdot \boldsymbol{S}_2 = -\frac{1}{4}\begin{pmatrix} 1 & 0 & 0 & 0 \\ 0 & -1 & 2 & 0 \\ 0 & 2 & -1 & 0 \\ 0 & 0 & 0 & 1 \end{pmatrix}. \tag{1.6}$$

This can be readily diagonalized in terms of the states

$$\begin{aligned} \{|S_{\text{tot}}, S_{\text{tot}}^z\rangle\} &= \{|1,1\rangle, |1,0\rangle, |1,-1\rangle; |0,0\rangle\} \\ &= \left\{|\uparrow,\uparrow\rangle, (|\uparrow,\downarrow\rangle + |\downarrow,\uparrow\rangle)/\sqrt{2}, |\downarrow,\downarrow\rangle, ; (|\uparrow,\downarrow\rangle - |\downarrow,\uparrow\rangle)/\sqrt{2}\right\}, \end{aligned} \tag{1.7}$$

where the quantum numbers $S_{\text{tot}}$ and $S_{\text{tot}}^z$ label the eigenvalues of the total spin operators $\boldsymbol{S}_{\text{tot}} = \boldsymbol{S}_1 + \boldsymbol{S}_2$ and $S_{\text{tot}}^z = S_1^z + S_2^z$. Here, the triplet states ($S_{\text{tot}} = 1$) are three-fold degenerate with eigenvalue $\varepsilon_t = -1/4$, while $\varepsilon_s = 3/4$ is the eigenvalue of the singlet state ($S_{\text{tot}} = 0$).

Having established the relevant eigensystem, we shall now discus two introductory examples which illustrate that the low energy sector of some electronic systems can be described solely in terms of the electrons' spin degrees of freedom.

### Coulomb exchange

To begin with, let us come back to Heisenberg's original suggestion that two electrons bound to different atomic sites would favor the (ferromagnetic) alignment of their spin due to an interplay of their mutual Coulomb repulsion and the Pauli principle. Although this picture was certainly the first to provide a microscopic explanation of the observed magnetostatic energies more detailed considerations reveal, that it can only scarcely explain the origin of the exchange term in real materials [40]. Instead of focusing on a possible inter-atomical exchange interaction, we therefore remain on firm ground and formalize his idea for the intra-atomical interaction between two electrons in different orthogonal orbitals. The following consideration is then simply a formalization of the first of Hund's famous rules, which states that the ground state of an isolated atom with a given configuration of one-electron orbitals has the largest of the possible $S_{\text{tot}}$ values [15]. For this purpose, consider a simple two electron Hamiltonian

$$\mathcal{H}(\boldsymbol{r}_1, \boldsymbol{r}_2) = \mathcal{H}_0(\boldsymbol{r}_1) + \mathcal{H}_0(\boldsymbol{r}_2) + \mathcal{H}_{ee}(\boldsymbol{r}_1, \boldsymbol{r}_2) \tag{1.8}$$

where $\mathcal{H}_0(\boldsymbol{r}_i)$ is some effective spin-independent one-electron Hamiltonian and

$$\mathcal{H}_{ee}(\boldsymbol{r}_1, \boldsymbol{r}_2) = \frac{\tilde{e}^2}{|\boldsymbol{r}_1 - \boldsymbol{r}_2|}, \quad \tilde{e}^2 = e^2/(4\pi\epsilon_0), \tag{1.9}$$

is the Coulomb interaction of the two electrons with $e$ the electron's charge and $\epsilon_0$ the dielectric constant. The latter is considered as a perturbation, i.e. we assume that the uncoupled system is solved by a set of appropriate orthonormal one electron eigenfunctions $\varphi_a^{\alpha}(\boldsymbol{r})$ with eigenenergies $\varepsilon_a$, where $a$ labels the orbital and $\alpha$ the spin state. A corresponding orthonormal basis of the two-electron states is then formed by the *slater determinants*

$$\Psi_{ab}^{\alpha\beta}(\boldsymbol{r}_1, \boldsymbol{r}_2) = \frac{1}{\sqrt{2}}\left(\varphi_a^{\alpha}(\boldsymbol{r}_1)\varphi_b^{\beta}(\boldsymbol{r}_2) - \varphi_a^{\alpha}(\boldsymbol{r}_2)\varphi_b^{\beta}(\boldsymbol{r}_1)\right), \tag{1.10}$$

whose eigenenergies are degenerate in all possible spin configurations. However, this degeneracy is lifted if the Coulomb interaction is taken into account. In order to show this, let us introduce the shorthand $\Psi^{\alpha\beta} = \Psi^{\alpha\beta}_{ab}(\boldsymbol{r}_1, \boldsymbol{r}_2)$ and consider the matrix elements of $H_{ee}$ in the basis $\{\Psi^{\uparrow\uparrow}, \Psi^{\uparrow\downarrow}, \Psi^{\downarrow\uparrow}, \Psi^{\downarrow\downarrow}\}$. A straightforward evaluation of the corresponding matrix elements then yields

$$\mathcal{H}_{ee} = \begin{pmatrix} K_{ab} - J_{ab} & 0 & 0 & 0 \\ 0 & K_{ab} & -J_{ab} & 0 \\ 0 & -J_{ab} & K_{ab} & 0 \\ 0 & 0 & 0 & K_{ab} - J_{ab} \end{pmatrix}, \tag{1.11}$$

where we introduced the *Coulomb- and exchange-integrals*

$$K_{ab} = \tilde{e}^2 \int d\boldsymbol{r}_1 d\boldsymbol{r}_2 \frac{\phi^*_a(\boldsymbol{r}_1)\phi^*_b(\boldsymbol{r}_2)\phi_a(\boldsymbol{r}_1)\phi_b(\boldsymbol{r}_2)}{|\boldsymbol{r}_1 - \boldsymbol{r}_2|}, \tag{1.12}$$

$$J_{ab} = \tilde{e}^2 \int d\boldsymbol{r}_1 d\boldsymbol{r}_2 \frac{\phi^*_a(\boldsymbol{r}_1)\phi^*_b(\boldsymbol{r}_2)\phi_b(\boldsymbol{r}_1)\phi_a(\boldsymbol{r}_2)}{|\boldsymbol{r}_1 - \boldsymbol{r}_2|}, \tag{1.13}$$

and $\phi_a(\boldsymbol{r})$, which is the orbital part of the eigenfunctions, i.e. $\varphi^\alpha_a(\boldsymbol{r}) = \phi_a(\boldsymbol{r})\chi^\alpha_a$ . Similar to the two-particle Heisenberg interaction (1.2), the Hamiltonian (1.11) is diagonalized in terms of a set of triplet and singlet states, $\{\Psi_t; \Psi_s\}$, constructed analogous to the states in (1.7), and with the respective eigenenergies $\varepsilon_t = K_{ab} + J_{ab}$ and $\varepsilon_s = K_{ab} - J_{ab}$. By comparing the Hamiltonian (1.11) to the matrix representation of the Heisenberg term (1.6), we can thus simply construct the equivalent representation

$$\mathcal{H}_{ee} = \left(K_{ab} - \frac{J_{ab}}{2}\right) - 2J_{ab}\boldsymbol{S}_a \cdot \boldsymbol{S}_b, \tag{1.14}$$

in terms of the spin operators $\boldsymbol{S}_{a,b}$ acting on the spin state of the electron in the corresponding orbital. Note, that the sign of the exchange integral (1.13) determines the character of the interaction. In the present case, where the spatial part of the states is constructed in terms of othogonal one-electron eigenfunctions, it is ferromagnetic ($J_{ab} > 0$) [38]. Hence, the ground state manifold is given by the three triplet states $S_{\text{tot}} = 1$, thus reproducing Hund's first rule for the simple two-electron model considered.

### Kinetic exchange

If spatially extended lattice systems are considered, the hybridization of atomic orbitals belonging to neighboring sites will in general allow for a tunneling of the electrons. In contrast to the previous discussion the double occupancy of a single orbital is thus possible, although penalized by the Coulomb interaction of the involved electrons. In order to show how the occurrence of these additional states affects the low energy properties of a given lattice system, let us neglect the multi-orbital structure of a single lattice site, and consider two electrons in the simple two-site Hubbard model

$$\mathcal{H}_{\text{Hub.}} = -t \sum_\sigma \left(c^\dagger_{1\sigma} c_{2\sigma} + c^\dagger_{1\sigma} c_{2\sigma}\right) + U \sum_{i=1,2} c^\dagger_{i\uparrow} c_{i\uparrow} c^\dagger_{i\downarrow} c_{i\downarrow}. \tag{1.15}$$

Here, we introduced the fermionic creation (annihilation) operators $c^\dagger_{i\sigma}$ ($c_{i\sigma}$) which create an electron of spin $\sigma$ at site $i$ from the vacuum $|\cdot,\cdot\,\rangle$, respectively remove it from a filled state, i.e.[3]

$$c^\dagger_{1\uparrow}|\cdot,\cdot\,\rangle = |\uparrow,\cdot\,\rangle, \quad c_{1\uparrow}|\uparrow,\cdot\,\rangle, = |\cdot,\cdot\,\rangle. \tag{1.16}$$

The first term in the Hamiltonian (1.15) thus accounts for the inter-site hopping of the electrons with a matrix element $t$, and the second captures the on-site Coulomb interaction in terms of the effective parameter $U$. Following the lines of the previous discussion, the Hamiltonian can readily be expressed in the six dimensional state space $\{|\uparrow,\uparrow\rangle, |\downarrow,\downarrow\rangle, |\uparrow,\downarrow\rangle, |\downarrow,\uparrow\rangle, |\uparrow\downarrow,\cdot\,\rangle, |\cdot\,,\uparrow\downarrow\rangle\}$. The ferromagnetic states $|\uparrow,\uparrow\rangle$ and $|\downarrow,\downarrow\rangle$ have a vanishing eigenenergy and do not couple to the rest. For the remaining states we find the matrix representation

$$\mathcal{H}_{\text{Hub.}} = U \begin{pmatrix} 0 & 0 & -t & -t \\ 0 & 0 & t & t \\ -t & t & U & 0 \\ -t & t & 0 & U \end{pmatrix}, \tag{1.17}$$

which can be straightforwardly diagonalized. In the limit $U/|t| \gg 1$, one finds a high energy sector consisting of two states with an eigenenergy $\varepsilon \sim \mathcal{O}(U)$, and the low energy sector

$$\left\{ \frac{|\uparrow,\downarrow\rangle + |\downarrow,\uparrow\rangle}{\sqrt{2}}, \frac{|\uparrow,\downarrow\rangle - |\downarrow,\uparrow\rangle - \epsilon\,[|\uparrow\downarrow,\cdot\,\rangle - |\cdot\,,\uparrow\downarrow\rangle]}{\sqrt{2+\eta^2}} \right\}, \tag{1.18}$$

with $\eta = 2t/U$, and eigenenergy $\varepsilon = \{0, -4t^2/U\}$. In the present limit ($U/|t| \gg 1$), the contribution of the doubly-occupied states in the second of these low energy eigenstates can be safely neglected, and including the ferromagnetic states we recover the familiar singlet-triplet structure of the $\boldsymbol{S}_1 \cdot \boldsymbol{S}_2$ state space, cf. (1.7). Similar to the previous discussion, the low energy sector of the Hubbard model can thus be described by constructing the effective Heisenberg Hamiltonian

$$\mathcal{H}_{U/|t|\gg 1} = \frac{4t^2}{U}\left(\boldsymbol{S}_1 \cdot \boldsymbol{S}_2 - \frac{1}{4}\right). \tag{1.19}$$

This is now of antiferromagnetic character and the corresponding ground state is thus given by the singlet state $S_{\text{tot}} = 0$. Note, that such a description is not restricted to the simple two-site model, but can also be derived for the extended Hubbard model at half filling, which results in an effective description with the Heisenberg term (1.19) summed over all nearest neighbor pairs [38].

### Realistic exchange mechanisms

While the presented kinetic exchange mechanism is conceptually simple, it is usually not able to account for the magnetism observed in common insulators as e.g. the transition metal oxides. In these multicomponent crystals, metallic ions are spatially separated by intermediate oxygen anions, such that there are no direct electron hopping processes between the metallic ions. This has led to the proposition of a *superexchange* mechanism [41,42]. Here, the antiferromagnetic coupling between electrons in the d-orbitals of metallic ions, arises from multiple

[3] The operators $c^\dagger_{i\sigma}, c_{i\sigma}$ fulfill the familiar anticommutation relations $\{c^\dagger_{i\sigma}, c_{j\sigma'}\} = \delta_{ij}\delta_{\sigma\sigma'}$ and $\{c_{i\sigma}, c_{j\sigma}\} = 0$.

hopping processes involving the intermediate p-orbitals of the oxygen anions [15]. In general, these interactions must not be antiferromagnetic and certain geometric configurations of the involved oxygen and ionic orbitals can also lead to a ferromagnetic exchange [43]. However, in this case the electrons in the d-orbitals of two neighboring ions are not connected via intermediate hopping processes, but the hopping between the involved p- and d-orbitals mediates an intrinsic ferromagnetic Coulomb exchange of the electrons in the oxygen orbitals onto its neighbors [38]. It is thus considered as a combined effect of Coulomb and kinetic exchange. Historically, these observations had been collected in the empirical Goodenough–Kanamori rules, which, based on the symmetry properties, and the electron occupancy of the involved orbitals allow to predict the sign of effective Heisenberg descriptions [44, 45].

Having said that, it is worth mentioning that the Heisenberg interaction term is of course only the dominant of several further contributions to the total exchange interaction, such as dipolar or Dzyaloshinskii–Moriya interactions, with the latter being present in materials where inversion symmetry is broken [46, 47]. Likewise, an application of the Heisenberg Hamiltonian is by far not restricted to insulating materials, but is also used e.g. in the description of metallic 4-f systems, where the magnetic and electronic properties arise from different electron groups. In this case, itinerant valence electrons mediate an effective Heisenberg interaction between magnetic ions giving rise to an exchange coupling which oscillates as a function of the interionic distance [40]. Finally, let us highlight that the strength of the Heisenberg exchange interaction in certain materials can also be highly anisotropic in the spatial direction [48, 49]. Within the appropriate energy scales, these materials are then effectively described by low-dimensional models, i.e. chains or planar lattices of interacting localized moments, thereby providing experimental access to a plethora of highly non-trivial quantum phenomena [50].

### 1.2.2 The isotropic ferromagnet

In order to set the stage for the upcoming chapters, let us introduce the general mathematical description of the Heisenberg model. In the following, we consider a hypercubic lattice system with a single $SU(2)$ spin occupying each lattice site. The spins on different sites interact via a ferromagnetic exchange interaction term, and we furthermore extend the model by a Zeeman-coupling to an external magnetic field $\boldsymbol{H} = H\boldsymbol{e}_z$, where $H$ is given in units of energy. The corresponding Hamiltonian reads

$$\mathcal{H} = -H\sum_{i=1}^{N} S_i^z - \frac{1}{2}\sum_{ij}^{N} J_{ij}\boldsymbol{S}_i \cdot \boldsymbol{S}_j, \tag{1.20}$$

where the indices $i$ and $j$ denote the $N$ sites of a $D$-dimensional lattice, while

$$J_{ij} = J(r_{ij}) > 0 \tag{1.21}$$

with $r_{ij} = |\boldsymbol{r}_i - \boldsymbol{r}_j|$ is the spatially isotropic exchange interaction.

#### Ground state & order parameter

Following the general theory of phase transitions and critical phenomena, the phase behavior of the model (1.20) is characterized in terms of a spontaneous magnetization $M(T)$, which

is a function of the temperature $T$ of the system. For the present translationally invariant system, this order-parameter is defined in terms of the singular limit

$$M(T) = \lim_{H\to 0}\lim_{N\to\infty}\frac{1}{N}\Big\langle\sum_i S_i^z\Big\rangle = \lim_{H\to 0}\lim_{N\to\infty}\langle S_i^z\rangle, \tag{1.22}$$

where the expectation value of the single spin operator $S_i^z$ is given by

$$\langle S_i^z\rangle = \begin{cases}\langle 0|S_i^z|0\rangle & T=0,\\ \frac{1}{Z}\mathrm{Tr}\left(e^{-\beta\mathcal{H}}S_i^z\right) & T>0.\end{cases} \tag{1.23}$$

Here, $|0\rangle$ represents the ground state of the Hamiltonian (1.20), $\beta = 1/T$ is the inverse temperature (measured in units of energy), and

$$Z = \mathrm{Tr}\, e^{-\beta\mathcal{H}} = \sum_n \langle n|e^{-\beta\mathcal{H}}|n\rangle, \tag{1.24}$$

the associated canonical partition function, where $\{|n\rangle\}$ denotes a complete set of states of the corresponding Hilbert space. Let us discuss the order parameter in the zero temperature case first. For this purpose it is worth to recall that for a vanishing magnetic field, the spin rotational invariance of the Hamiltonian (1.20) leads to a highly degenerate ground state manifold (cf. the previous section where the case $N = 2$ was explicitly considered). In a finite system, this manifold is represented in terms of the $(2S_{\mathrm{tot}}+1)$-fold degenerate multiplet

$$|0\rangle = \{|S_{\mathrm{tot}}, S_{\mathrm{tot}}^z\rangle\}, \tag{1.25}$$

where the quantum numbers $S_{\mathrm{tot}} = NS$ and $S_{\mathrm{tot}}^z = \{NS, NS-1,\ldots,-NS\}$ label the eigenvalues of the total spin operators $\boldsymbol{S}_{\mathrm{tot}}^2 = (\sum_i \boldsymbol{S}_i)^2$ and $S_{\mathrm{tot}}^z = \sum_i S_i^z$. The combined procedure of adding the Zeeman term to the Hamiltonian (1.20) and subsequently taking the limit of vanishing magnetic field singles out the state with all spins aligned parallel to the magnetic field as the true groundstate, i.e.

$$|0\rangle = |S_{\mathrm{tot}}, S_{\mathrm{tot}}^z = NS\rangle = \bigotimes_{i=1}^{N}|S\rangle_i. \tag{1.26}$$

The corresponding groundstate energy is thereby given by

$$E_0 = -N\left(HS + \frac{S^2 J_0}{2}\right). \tag{1.27}$$

where

$$J_{\boldsymbol{k}} = \sum_{\boldsymbol{r}} J(\boldsymbol{r})e^{-i\boldsymbol{k}\cdot\boldsymbol{r}}, \tag{1.28}$$

is the Fourier transformation of the exchange interaction. By construction, the groundstate breaks the continuous spin rotational symmetry of the Hamiltonian, which is reflected in the finite order-parameter $M(T=0) = S$. However, this breaking of a continuous symmetry comes at the price of the occurrence of gapless bosonic Nambu-Goldstone modes which dominate the low temperature behavior of the static and dynamic properties of the system [51,52].

As a side remark, let us note that the Heisenberg ferromagnet has the peculiarity that only a single type of Nambu-Goldstone mode is excited, although two of the three SU(2) symmetry generators are broken. Loosely speaking, this is a consequence of the fact that the order parameter operator $S^z_{\rm tot}$ is itself a symmetry generator and thus a constant of motion, i.e. $[\mathcal{H}, S^z_{\rm tot}] = 0$ [53–56].

### Elementary excitations

The Nambu-Goldstone modes of the isotropic Heisenberg ferromagnet can be identified with the well-known spin wave excitation introduced by Bloch in his seminal treatment of the Heisenberg model [57]. To sketch the characteristics of these modes let us briefly analyze the excitation spectrum.[4] For this purpose, the Hamiltonian is expressed in the form

$$\mathcal{H} = \mathcal{H}_0 - \frac{1}{2}\sum_{ij} J_{ij}\left(S_i^+ S_j^- + S_i^- S_j^+ + S_i^z S_j^z\right), \tag{1.29}$$

where

$$\mathcal{H}_0 = -H\sum_{i=1}^{N} S_i^z, \tag{1.30}$$

abbreviates the Zeeman term, while the exchange interaction is expressed in terms of the spin ladder operators

$$S_i^{\pm} = \frac{1}{\sqrt{2}}\left(S_i^x \pm i S_i^y\right). \tag{1.31}$$

Please note, that such a representation is convenient whenever the expectation value $\langle S_i^z\rangle$ is finite, and will be used throughout the following chapters. The corresponding commutation relations

$$\left[S_i^z, S_i^+\right] = S_i^+, \quad \left[S_i^z, S_i^-\right] = -S_i^-, \quad \left[S_i^+, S_i^-\right] = S_i^z, \tag{1.32}$$

hereby follow from the original SU(2)-algebra defined in Eq. (1.3). Likewise, their action on the eigenstate $|m\rangle_i$ of a singe spin is given by

$$S_i^{\pm}|m\rangle_i = \frac{1}{\sqrt{2}}\sqrt{(S\mp m)(S+1\pm m)}|m\pm 1\rangle_i. \tag{1.33}$$

(Please recall that $S^z|m\rangle = m|m\rangle$ with $m = S, S-1, \ldots, -S$). Noteworthy, the lowest energy eigenstate above the groundstate can now be constructed from a superposition of the *spin flip* state

$$|i\rangle = \frac{1}{\sqrt{S}} S_i^-|0\rangle = |S-1\rangle_i \bigotimes_{j\neq i} |S\rangle_j. \tag{1.34}$$

In order to show this, note that the Hamiltonian operator mixes spin flip states on different sites, i.e.

$$\mathcal{H}|i\rangle = E_0|i\rangle + H|i\rangle + S\sum_{ij} J_{ij}\left(|i\rangle - |j\rangle\right). \tag{1.35}$$

[4] The following derivation of the low energy excitation follows Ref. [58]

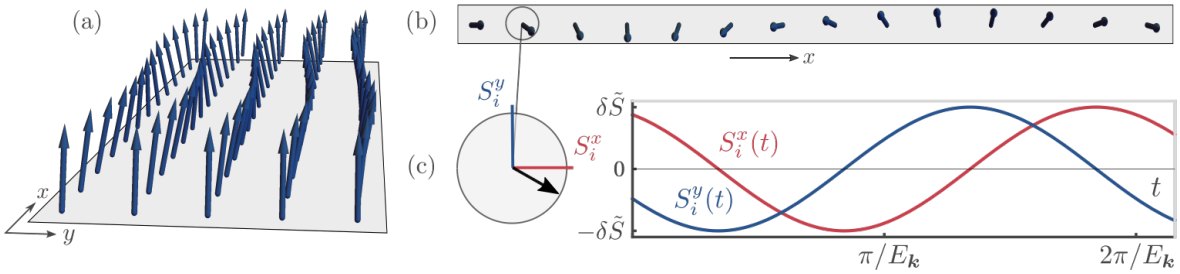


Figure 1.1: Classical spin wave picture of the elementary excitation in a Heisenberg ferromagnet: (a) Initial configuration of a spin wave with wave vector $\boldsymbol{k} \propto \boldsymbol{e}_x$. (b) Top view of the initial configuration. (c) Time evolution of the transverse spin components $S_i^x$ and $S_i^y$, showing an oscillation of frequency $E_{\boldsymbol{k}}$ and amplitude $\delta\tilde{S} \propto 1/N$. The underlying approximate solution to the equations of motion of the spin operators can be retraced in appendix A.1.

Hence, the state $|i\rangle$ is obviously not an eigenstate, which, however, can be constructed in terms of the one magnon state

$$|\boldsymbol{k}\rangle = \sum_i e^{-i\boldsymbol{k}\cdot\boldsymbol{r}_i}|i\rangle, \tag{1.36}$$

defined in terms of the Fourier transformation of the spin flip state. The corresponding energy is hereby given by

$$\mathcal{H}|\boldsymbol{k}\rangle = (E_0 + E_{\boldsymbol{k}})\,|\boldsymbol{k}\rangle, \tag{1.37}$$

where we introduced the excitation energy

$$E_{\boldsymbol{k}} = H + S\,(J_0 - J_{\boldsymbol{k}})\,, \tag{1.38}$$

which vanishes in the limits $|\boldsymbol{k}| \to 0$ and $H \to 0$, thus reflecting the gapless nature of the excitation. An intuitive picture of the one magnon state is obtained from an analysis of the associated equations of motion of the spin operators within the simplification $S_i^z \approx S$. As shown in detail in appendix A.1, the spins can in this limit be interpreted as classical vectors and the resulting solution yields a synchronized precession of the spin vectors around the z-axes. This spin wave, which is graphically depicted in Fig. 1.1, represents the classical counterpart of the magnon mode $|\boldsymbol{k}\rangle$. Finally, let us note that the higher order eigenstates can unfortunately not be constructed as a superposition of states with multiple spin flips. A proper quantum statistical calculation of the finite temperature observables - e.g. the order parameter - thus generally requires approximation methods.

### Hohenberg-Mermin-Wagner theorem

Let us now discuss the behavior of the order parameter in the finite temperature case. A priori, it is not clear that the order parameter remains finite once thermal fluctuations set in at $T > 0$. If this is indeed the case the spin rotational symmetry is said to be *spontaneously broken*. A hand-waving test can be carried out by simply assuming a finite order parameter and considering the corrections which would arise from the thermal excitation of the necessarily present magnon modes. The details of this self consistent argument will be formulated in chapter 3. For the moment it is sufficient to state, that these corrections diverge in spatial

dimensions $D \leq 2$, thus indicating the absence of a spontaneously symmetry broken phase at finite temperature in low-dimensional Heisenberg ferromagnets. A formal proof of this conjecture is given by the famous Hohenberg-Mermin-Wagner theorem [59, 60], which, quoting the original paper of Mermin and Wagner, states, that

> *"[...] at any nonzero temperature, a one-or two-dimensional isotropic spin-S Heisenberg model with finite-range exchange interaction can be neither ferromagnetic nor antiferromagnetic."* [59]

In the present formulation this translates to the assertion, that the ferromagnetic order parameter

$$M_{D\leq 2}(T) = 0 \quad \text{for} \quad T > 0, \tag{1.39}$$

provided that the exchange interaction fulfills

$$\frac{1}{N}\sum_{ij} J_{ij}|\boldsymbol{r}_i - \boldsymbol{r}_j| < \infty. \tag{1.40}$$

Note, that the theorem neither rules out the existence of any order at zero temperature, which leaves the previous discussion unaffected. Nor does it generally exclude the possibility of different kinds of phase transitions in Hamiltonian systems invariant under a continuous symmetry, as exemplified in the well-known work of Berezinskii, Kosterlitz, Thouless, and Nelson on the two-dimensional xy-model and superfluids [61–64]. As for the three-dimensional model, the existence of a symmetry broken phase below a critical *Curie-temperature* $T_c$ of the order of the exchange interaction is well established, although there apparently exist no rigorous proof of true long range order at $T > 0$, see e.g. Ref. [65]. Given the absence of a finite temperature magnetization in $D \leq 2$ (at vanishing magnetic field $H$), there is in principle no simple picture for the corresponding elementary excitations. However, at sufficiently small temperatures the system appears ordered at length scales smaller than the correlation length $\xi(T)$, which is defined in terms of functional dependence of the spin-spin correlation function

$$\langle S_i^z S_j^z \rangle \sim \exp[-|\boldsymbol{r}_i - \boldsymbol{r}_j|/\xi(T)]. \tag{1.41}$$

Since $\xi(T)$ diverges as the critical temperature $T_c = 0$ is approached from above, spin waves with a wave vector $|q| > 1/\xi$ can - in this regime - still be considered as well-defined excitations [66]. Evidently, the same holds true, if an external magnetic field is applied such that the expectation value $\langle S_i^z \rangle_{D\leq 2} \neq 0$ by construction. However, in this case the gap in the corresponding spectrum is significantly altered, as will be discussed in detail in chapter 3.

## 1.3 Response and correlation functions

The present thesis is entirely built upon a functional formalism which provides a non-pertubative framework to calculate imaginary-time ordered correlation functions of quantum spin models. Such imaginary-time correlation functions are generally the central objects in the widely used Matsubara approach to quantum many body systems. By contrast, all prominent experimental techniques applied in the study of magnetism, such as neutron-, x-ray- or Brillouin-light scattering, effectively probe the momentum-frequency representation of real-time correlation functions. The following pages introduce the form in which both

of these types of correlations functions are commonly expressed, and establish their mutual connection.

### 1.3.1 Linear response theory

The general theory describing the response of a given system to a weak external perturbation was formulated by Kubo in 1957 [67, 68]. Let us shortly recapitulate his formalism using the Heisenberg ferromagnet as an example [69]. For this purpose consider the effect of an additional external time dependent magnetic field $h_p(t)$ which minimally couples to the spins in terms of the time-dependent Hamiltonian

$$\mathcal{H}_{\text{tot}}(t) = \mathcal{H} - \sum_j S_j^\beta h_p(t). \tag{1.42}$$

Due to the presence of the external perturbation, any observable acquires a time-dependence. E.g. the expectation value of a single spin component reads

$$\langle S_i^\alpha \rangle(t) = \text{Tr}\left(\rho(t) S_i^\alpha\right), \tag{1.43}$$

where the distribution function $\rho(t)$ is determined by the von Neumann equation

$$\partial_t \rho(t) = \frac{1}{i}\left[\mathcal{H}_{\text{tot}}(t), \rho(t)\right], \tag{1.44}$$

subject to the boundary condition $\rho(t = -\infty) = \rho_e = e^{-\beta\mathcal{H}}/Z$. To linear order in the external field, the von Neumann Eq. (1.44) is solved by the distribution function

$$\rho(t) = \rho_e + \Delta\rho(t) + \mathcal{O}(h_p^2(t)), \tag{1.45}$$

with

$$\Delta\rho(t) = i\sum_j \int_{-\infty}^{t} dt'\, e^{-i(t-t')\mathcal{H}}[S_j^\beta, \rho_e] e^{i(t-t')\mathcal{H}} h_p(t'). \tag{1.46}$$

Substituting the solution (1.45) into the general expression (1.43) of the expectation value $\langle S_i^\alpha \rangle(t)$, the time evolution is thus given by

$$\langle S_i^\alpha \rangle(t) = \langle S_i^\alpha \rangle + \sum_j \int_{-\infty}^{\infty} dt'\, \chi_{R,ij}^{\alpha\beta}(t-t') h_p(t') + \mathcal{O}(h_p^2(t)). \tag{1.47}$$

Here, we introduced the retarded response function $\chi_{R,ij}^{\alpha\beta}(t-t')$, which using the cyclic properties of the trace, can be recast in the form

$$\chi_{R,ij}^{\alpha\beta}(t) = i\text{Tr}\left(\rho_e[S_i^\alpha(t), S_j^\beta(0)]\right)\Theta(t) = i\langle[S_i^\alpha(t), S_j^\beta(0)]\rangle\Theta(t), \tag{1.48}$$

and the time-dependence of the single spin operators is given in the Heisenberg picture of the equilibrium system, i.e. $S_i^\alpha(t) = \exp[it\mathcal{H}] S_i^\alpha \exp[-it\mathcal{H}]$. These considerations exemplify that the response of the system can be formulated in terms of equilibrium correlation functions, provided the external perturbation is sufficiently weak. Noteworthy, a similar link can also established in the theoretical description of scattering experiments.

### Scattering experiments and the dynamical structure factor

The unique success of thermal neutron scattering in the investigation of the magnetic properties of matter is owed to two of the neutron's elementary properties: While it is electrically neutral it possesses a magnetic moment. In a scattering experiment these particles hence do not only interact with the atomic nuclei of the sample but also couple to possibly present net magnetic moments of the corresponding orbital electrons. Since both of these interactions are in general relatively weak, the neutron has a large penetration length such that the bulk properties of the sample can be probed. For the same reason, the measurement process can be described within a linear response ansatz. In addition, the wavelength and energy of thermal neutrons may be tuned to the order of the interatomic spacing, respectively of the expected excitation energy, which allows to probe the magnetic order of a given sample, but also to investigate the associated dynamic properties within inelastic scattering experiments [70]. In case the scattering from the atomic nuclei of the sample can be neglected, the measured differential cross section effectively probes the pair-correlation function of the magnetization density. Under the assumption that this magnetization effectively originates from a system of localized spins, a straightforward calculation starting from Fermi's golden rule then shows that the differential scattering cross section of unpolarized inelastic neutron scattering can be expressed in the form [70–72]

$$\frac{d^2\sigma}{d\Omega d\omega}(\boldsymbol{q},\omega) \propto \frac{k'}{k}\sum_{\alpha\beta}\left(\delta_{\alpha\beta}-\frac{q_\alpha q_\beta}{q^2}\right)\mathcal{S}^{\alpha\beta}(\boldsymbol{q},\omega). \tag{1.49}$$

Here, $k$ and $k'$ are the absolute values of the momenta of the incoming and scattered neutrons, and the polarization factor $\left(\delta_{\alpha\beta}-q_\alpha q_\beta/q^2\right)$ accounts for the fact that the neutrons only couple to spin fluctuations perpendicular to the momentum transfer $\boldsymbol{q}$. The central element which contains the microscopic information in the expression (1.49) is the dynamical structure factor

$$\mathcal{S}^{\alpha\beta}(\boldsymbol{q},\omega) = \sum_{ij} e^{-i\boldsymbol{q}(\boldsymbol{r}_i-\boldsymbol{r}_j)}\mathcal{S}_{ij}^{\alpha\beta}(\omega) = \sum_{ij}\int_{-\infty}^{\infty} dt\, e^{-i(\boldsymbol{q}(\boldsymbol{r}_i-\boldsymbol{r}_j)-\omega t)}\mathcal{S}_{ij}^{\alpha\beta}(t), \tag{1.50}$$

determined by the space and time Fourier transformation of the equilibrium spin-spin correlation function

$$\mathcal{S}_{ij}^{\alpha\beta}(t) = \frac{1}{2\pi}\langle S_i^\alpha(t)S_j^\beta(0)\rangle = \frac{1}{2\pi}\mathrm{Tr}\left(\rho_e S_i^\alpha(t)S_j^\beta(0)\right). \tag{1.51}$$

Inelastic neutron scattering cross sections thus give access to the sum of correlation functions of different spin components $\alpha,\beta$. If the sample is in a magnetically ordered phase, it is natural to divide the structure factor into a longitudinal part $\mathcal{S}^{zz}(\boldsymbol{q},\omega)$, describing the correlation of the components parallel to the order parameter $\boldsymbol{M} = M\boldsymbol{e}_z$, and a transverse part $\mathcal{S}^{\perp}(\boldsymbol{q},\omega)$ which contains the information about the dispersion relations and lifetimes of the corresponding Goldstone modes. Experimentally, these contributions can in principle be separated using more sophisticated set ups relying on neutron polarization filters [73]. Finally, let us remind ourselves that the structure factor and the retarded response defined in Eq. (1.48) are both determined by equilibrium spin-spin correlation functions, and are thus mutually related. Before discussing the precise relation, known as *fluctuation-dissipation theorem*, it is useful to briefly recapitulate Matsubara's imaginary time formalism.

### 1.3.2 Matsubara formalism

While the previous real time correlation function can be readily linked to experimental observations, their direct calculation based on a perturbative separation of the Hamiltonian into a reference part and a small perturbation is cumbersome, as indicated by the simultaneous presence of the Boltzmann factor and the time evolution operators. Although there exists a framework for the general non-equilibrium scenario, known as Keldysh formalism [74], this method is rather cumbersome. Fortunately, most equilibrium many body problems can be formulated in the significantly easier Matsubara formalism, developed in the early 1950s by Matsubara [75], followed by important contribution from Kubo [67], and Martin and Schwinger [76]. The key idea of this formalism is to treat time and temperature in a uniform manner by analytically continuing real time into the complex plane, performing a Wick rotation $t \to -i\tau$. The time dependence of a general operator $O$ in the Heisenberg picture can then be formulated in imaginary time as

$$O(t) \to O(it) = O(\tau) = e^{\tau\mathcal{H}} O e^{-\tau\mathcal{H}}. \tag{1.52}$$

In analogy to the different real time correlation functions, let us therefore introduce the imaginary time-ordered spin-spin correlation functions (also denoted Matsubara Green function)

$$G_{ij}^{\alpha\beta}(\tau) = \langle \mathcal{T} S_i^\alpha(\tau) S_j^\beta(0) \rangle = \frac{\mathrm{Tr}\left(e^{-\beta H} \mathcal{T} S_i^\alpha(\tau) S_j^\beta(0)\right)}{\mathrm{Tr}\left(e^{-\beta H}\right)}, \tag{1.53}$$

where the time ordering operator $\mathcal{T}$ orders earlier times to the right, i.e.

$$\mathcal{T} S_i^\alpha(\tau) S_j^\beta(0) = S_i^\alpha(\tau) S_j^\beta(0)\Theta(\tau) + S_j^\beta(0) S_i^\alpha(\tau)\Theta(-\tau). \tag{1.54}$$

Before elaborating on the precise relation to the different real time correlation functions discussed previously, it is worth to shortly recapitulate a few benefits of the Matsubara formalism, which primarily arise from the functional similarity of the Boltzmann factor $\exp[-\beta\mathcal{H}]$ and the imaginary time evolution operator $\exp[-\tau\mathcal{H}]$. First of all, using the cyclic properties of the trace, it is straightforward to show that the imaginary-time ordered correlation functions fulfill the Kubo-Martin-Schwinger boundary condition

$$G_{ij}^{\alpha\beta}(\tau) = G_{ij}^{\alpha\beta}(\tau + \beta), \tag{1.55}$$

such that the imaginary time is effectively restricted to the interval $\tau \in [0, \beta]$. Given this periodicity, the functions can be expanded in the Fourier series,

$$G_{ij}^{\alpha\beta}(\tau) = \frac{1}{\beta} \sum_{\omega_n} e^{-i\omega_n \tau} G_{ij}^{\alpha\beta}(i\omega_n) \tag{1.56}$$

with a set of discrete Matsubara frequencies, $\omega_n = 2n\pi/\beta$ with $n \in \mathbb{Z}$, and the corresponding Fourier coefficients

$$G_{ij}^{\alpha\beta}(i\omega_n) = \int_0^\beta d\tau\, G_{ij}^{\alpha\beta}(\tau) e^{i\omega_n \tau}. \tag{1.57}$$

In addition, a perturbative calculation of the correlation functions is now at hand. To sketch this, let us express the Heisenberg Hamiltonian (1.20) in the form

$$\mathcal{H} = \mathcal{H}_0 + \mathcal{V}, \tag{1.58}$$

where

$$\mathcal{V} = -\frac{1}{2}\sum_{ij} J_{ij}\boldsymbol{S}_i \cdot \boldsymbol{S}_j, \tag{1.59}$$

abbreviates the exchange interaction contribution. Likewise, it is useful to express the imaginary-time dependence of the spin operators in the interaction picture,

$$S_i^\alpha(\tau) = \mathcal{U}(0,\tau)\tilde{S}_i^\alpha(\tau)\mathcal{U}(\tau,0), \tag{1.60}$$

where we introduced the interaction representation of the operators given by

$$\tilde{S}_i^\alpha(\tau) = \exp[\tau\mathcal{H}_0]S_i^\alpha \exp[-\tau\mathcal{H}_0], \tag{1.61}$$

and the corresponding evolution operator, $\mathcal{U}(\tau,\tau') = \exp[\tau\mathcal{H}_0]\exp[-(\tau-\tau')\mathcal{H}]\exp[-\tau'\mathcal{H}_0]$ (usually denoted S-matrix), which is best expressed in terms of the time ordered expression

$$\mathcal{U}(\tau,\tau') = \mathcal{T}e^{-\int_{\tau'}^{\tau} d\tau\, \tilde{\mathcal{V}}(\tau)}. \tag{1.62}$$

Substituting the interaction representation of the spin operators (1.60), the imaginary-time correlation functions introduced in Eq. (1.53) can be readily expressed in a form which allows for a perturbative expansion. To do so, note that the Boltzmann factor can be rewritten in terms of the S-matrix as $\exp[-\beta\mathcal{H}] = \exp[-\beta\mathcal{H}_0]\mathcal{S}(\beta,0)$. Upon using the cyclic property $\mathcal{U}(\tau_1,\tau_2)\mathcal{U}(\tau_2,\tau_3) = \mathcal{U}(\tau_1,\tau_3)$, and the properties of the time ordering operator, the correlation function then assumes the form

$$G_{ij}^{\alpha\beta}(\tau) = \frac{\mathrm{Tr}\left(e^{-\beta H_0}\mathcal{T}\tilde{S}_i^\alpha(\tau)\tilde{S}_j^\beta(0)\mathcal{U}(\beta,0)\right)}{\mathrm{Tr}\left(e^{-\beta H_0}\mathcal{U}(\beta,0)\right)} = \frac{\langle\mathcal{T}\tilde{S}_i^\alpha(\tau)\tilde{S}_j^\beta(0)\mathcal{U}(\beta,0)\rangle_0}{\langle\mathcal{U}(\beta,0)\rangle_0}, \tag{1.63}$$

where

$$\langle O\rangle_0 = \frac{\mathrm{Tr}\left(e^{-\beta\mathcal{H}_0}O\right)}{\mathrm{Tr}\, e^{-\beta\mathcal{H}_0}} \tag{1.64}$$

denotes the expectation value of the non-interacting system. Expanding the S-matrix $\mathcal{U}(\beta,0)$ in the nominator and denominator of Eq. (1.53) thus allows to generate a perturbative expansion of $G_{ij}^{\alpha\beta}(\tau)$ in the exchange interaction $J_{ij}$. Of course, the calculation of the resulting n-point non-interacting expectation values is still a non-trivial task, and we will come back to this point. For the moment let us solely remark, that a representation of the spin correlation functions in the form of Eq. (1.53) also presents the basis of the spin FRG formalism, to be introduced in the following chapter.

### Analytic continuation and fluctuation-dissipation theorem

Having discussed the different real and imaginary time correlation functions, their mutual relation remains to be established. This is straightforwardly done considering the spectral representations of the respective frequency representations. The frequency representations of the dynamical structure factor $\mathcal{S}_{ij}^{\alpha\beta}(\omega)$ and the Matsubara Green function $G_{ij}^{\alpha\beta}(i\omega)$ were defined in Eqs. (1.50) and (1.57), while the frequency representation of the retarded response function is analogously defined as

$$\chi_{R,ij}^{\alpha\beta}(\omega) = \int_{-\infty}^{\infty} dt\, \chi_{R,ij}^{\alpha\beta}(t)e^{i\omega t}. \tag{1.65}$$

The explicit construction of the corresponding spectral representations is retraced in appendix A.2 (see also Ref. [14]), and we solely state the final forms which read

$$\chi^{\alpha\beta}_{R,ij}(\omega) = -\frac{1}{Z}\sum_{nm}\langle n|S^\alpha_i|m\rangle\langle m|S^\beta_j|n\rangle\frac{e^{-\beta E_n}-e^{-\beta E_m}}{E_n - E_m + \omega + i\delta}, \tag{1.66}$$

$$\mathcal{S}^{\alpha\beta}_{ij}(\omega) = \frac{1}{Z}\sum_{nm}\langle n|S^\alpha_i|m\rangle\langle m|S^\beta_j|n\rangle e^{-\beta E_n}\delta(E_n - E_m + \omega), \tag{1.67}$$

$$G^{\alpha\beta}_{ij}(i\omega_n) = -\frac{1}{Z}\sum_{nm}\langle n|S^\alpha_i|m\rangle\langle m|S^\beta_j|n\rangle\frac{e^{-\beta E_n}-e^{-\beta E_m}}{E_n - E_m + i\omega_n}. \tag{1.68}$$

Here, the states $\{|n\rangle\}$ and $\{|m\rangle\}$ denote the eigenstates of the Hamiltonian (1.20) with respective energy eigenvalues $E_{n,m}$, and the infinitesimal real shift $\delta > 0$ was introduced in order to guarantee convergence of the Fourier transformation of the response function. A comparison of the spectral representations of the response function and the Matsubara Green function in Eqs. (1.66) and (1.68) thus shows that the former can be obtained by analytically continuing the Matsubara frequency to the real axes, i.e.

$$\chi^{\alpha\beta}_{R,ij}(\omega) = G^{\alpha\beta}_{ij}(i\omega_n \to \omega + i\delta). \tag{1.69}$$

Similarly, the relation between the structure factor and the retarded response follows by extending the latter into the complex plane. For this purpose, let us introduce the dynamical susceptibility

$$\chi^{\alpha\beta}_{ij}(z) = \int_{-\infty}^{\infty}\frac{d\omega'}{\pi}\frac{\chi''^{\alpha\beta}_{ij}(\omega')}{\omega' - z}, \quad z \in \mathbb{C}, \tag{1.70}$$

and the spectral function $\chi''^{\alpha\beta}_{ij}(\omega)$, which is defined as

$$\chi''^{\alpha\beta}_{ij}(\omega) = \frac{\pi\left(1 - e^{-\beta\omega}\right)}{Z}\sum_{nm}\langle n|S^\alpha_i|m\rangle\langle m|S^\beta_j|n\rangle e^{-\beta E_n}\delta(E_n - E_m + \omega). \tag{1.71}$$

According to these definitions, the retarded response function can be obtained by evaluating the $\chi^{\alpha\beta}_{ij}(z)$ just above the real axis, i.e.

$$\chi^{\alpha\beta}_{R,ij}(\omega) = \chi^{\alpha\beta}_{ij}(\omega + i\delta). \tag{1.72}$$

Likewise, we can use the Cauchy-Dirac relation, $(\omega + i\delta)^{-1} = \mathcal{P}(1/\omega) - i\pi\delta(\omega)$, where $\mathcal{P}$ denotes the Cauchy principle value, to separate the dynamical susceptibility on the right side of Eq. (1.72) into the real and imaginary parts

$$\chi^{\alpha\beta}_{ij}(\omega + i\delta) = \chi'^{\alpha\beta}_{ij}(\omega) + i\chi''^{\alpha\beta}_{ij}(\omega), \tag{1.73}$$

which allows to identify the spectral function with the imaginary part of the response function, i.e. $\mathrm{Im}\,\chi^{\alpha\beta}_{R,ij}(\omega) = \chi''^{\alpha\beta}_{ij}(\omega)$. Finally, let us compare the definition of the spectral function and the spectral representation of the structure factor, given in Eqs. (1.71) respectively (1.67). This yields the fluctuation dissipation relation

$$\mathcal{S}^{\alpha\beta}_{ij}(\omega) = \frac{1}{\pi}\frac{e^{\beta\omega}}{e^{\beta\omega}-1}\chi''^{\alpha\beta}_{ij}(\omega), = \frac{1}{\pi}\frac{e^{\beta\omega}}{e^{\beta\omega}-1}\mathrm{Im}\,\chi^{\alpha\beta}_{R,ij}(\omega). \tag{1.74}$$

which completes the formal relations of the different correlation functions.

## 1.4 Collective sound excitations

Chapter 4 of this thesis investigates the possible existence of a wave-like excitation of the magnetization density in isotropic Heisenberg ferromagnets. In general, such coherent density fluctuations close to equilibrium are known as sound waves. Depending on the time and energy scales involved, different types of sound have been established in the literature. In order to contextualize the present work in this respect, this section briefly introduces the most prominent phenomena: zero, first, and second sound. To this end, let us use the framework of linear response theory and sketch the qualitative response of a system to an external scalar field $\varphi(\boldsymbol{r}, t)$, coupling to a generalized density operator[5] $\rho(\boldsymbol{r})$ within the perturbing Hamiltonian

$$\delta\mathcal{H}(t) = -\int_{\boldsymbol{r}} \rho(\boldsymbol{r})\varphi(\boldsymbol{r}, t). \tag{1.75}$$

Depending on the scenario of interest $\rho(\boldsymbol{r})$ may be interpreted as the charge density of an electron system, the mass density of a classical fluid, or, e.g. the magnetization density in a system of localized magnetic moments. In any case, the density fluctuation in the system follows within linear response theory as

$$\delta\rho(\boldsymbol{r}, t) = \langle\rho(\boldsymbol{r}, t)\rangle - \langle\rho(\boldsymbol{r})\rangle = -\int_{\boldsymbol{r}'}\int_{-\infty}^{\infty} dt'\, \chi_R(\boldsymbol{r} - \boldsymbol{r}', t - t')\varphi(\boldsymbol{r}', t'), \tag{1.76}$$

where $\chi_R(\boldsymbol{r}, t)$ is the retarded density-density response function. Possible well-defined sound excitations then manifest as distinct poles in the imaginary part of the corresponding momentum frequency representation, $\chi_R(\boldsymbol{q}, \omega)$ which can be detected, e.g. by appropriate scattering techniques. In particular, the density-density response function is traditionally classified into two different frequency regimes, a *collision-dominated* regime at sufficiently small frequencies and a *collisionless* regime at high frequencies [25]. This terminology is usually applied whenever the system can be modeled in terms of an ensemble of interacting quasiparticles and an associated Boltzmann equation, accounting for the spatio-temporal evolution of the corresponding distribution function. In this picture, the collision rate of two quasiparticles $\omega_{\text{col}}$ naturally separates the response function $\chi_R(\boldsymbol{q}, \omega)$ into the two regimes

$$\omega \gg \omega_{\text{col}} \quad \text{(collisionless regime)}, \tag{1.77}$$

respectively

$$\omega \ll \omega_{\text{col}} \quad \text{(collision-dominated regime)}. \tag{1.78}$$

In the former case collisions between the individual particles are sufficiently infrequent and a collective response of all particles to the external perturbation can develop. In a charged respectively neutral Fermi liquid this phenomenon is known as plasmon sound or zero sound, and the characteristics can be inferred from a solution of the Boltzmann equation neglecting the terms describing the collisions. In the opposite limit, collisions between individual particles are sufficiently frequent such that the Boltzmann equation is governed by the collision terms. This regime can equally host a wave-like density excitation - conventional first sound - albeit of different origin. On the following pages, we briefly review the derivation of these two sound types and discuss the range of validity of the associated regimes, mostly referring

[5] Not to be confused with the non-equilibrium distribution function $\rho(t)$, introduced in Sec. 1.3.

to the neutral Fermi liquid as an example. In addition, we briefly comment on a third class of sound modes, second sound.

### 1.4.1 Zero sound in Fermi liquids

The characteristics of zero sound were first derived within Landau's Fermi liquid theory in the scope of a Boltzmann-Eq. [25], while the subsequent explanation of the same phenomena from a microscopic perspective was provided by Pines, Bohm and others [77–79]. Although various formulations of these calculations - nowadays summarized as *random phase approximation* (RPA) - can be found in standard textbooks on many-body physics [14,80,81], a short recap seems appropriate given the similarity of the approach employed in chapter 4. To this end, consider a system of interacting fermions described in second-quantized notation by the grand canonical operator

$$\mathcal{K} = \mathcal{H} - \mu\mathcal{N} = \mathcal{K}_0 + \mathcal{V}, \tag{1.79}$$

where

$$\mathcal{K}_0 = \sum_{\boldsymbol{k}\sigma} \epsilon_{\boldsymbol{k}} c^\dagger_{\boldsymbol{p}\sigma} c_{\boldsymbol{k}\sigma}, \quad \mathcal{V} = \frac{1}{2}\sum_{\sigma\sigma'}\sum_{\boldsymbol{k}\boldsymbol{k}'\boldsymbol{q}} J_{\boldsymbol{q}} c^\dagger_{\boldsymbol{k}+\boldsymbol{q}\sigma} c^\dagger_{\boldsymbol{k}'-\boldsymbol{q}\sigma'} c_{\boldsymbol{k}'\sigma'} c_{\boldsymbol{k}\sigma}, \tag{1.80}$$

denote the kinetic and the interacting parts. Here, $c^\dagger_{\boldsymbol{k}\sigma}$ and $c_{\boldsymbol{k}\sigma}$ present the familiar fermionic creation-annihilation operators creating respectively annihilating an electron in momentum state $\boldsymbol{k}$ and spin state $\sigma$ (cf. the commutation relations defined in the footnote on page 10). Furthermore,

$$\epsilon_{\boldsymbol{k}} = \frac{\boldsymbol{k}^2}{2m} - \mu, \tag{1.81}$$

is the shifted single particle energy, where $m$ is the mass of the fermions and $\mu$ the chemical potential. The interaction potential $J_{\boldsymbol{q}}$ is not specified for the moment. For the case of a Coulomb interaction

$$J_{\boldsymbol{q}} = 4\pi\tilde{e}^2 \frac{1-\delta_{q,0}}{q^2}, \tag{1.82}$$

one recovers the *jellium model* describing a gas of interacting electrons immersed in a positive background [80]. Akin to the discussion of the previous section, the system's dynamics close to equilibrium can be calculated within the Matsubara framework, and the experimentally relevant response functions are obtained by analytical continuation. Hence, let us consider the frequency representation of the imaginary time density-density correlation function [81]

$$G_{\rho\rho}(Q) = -\int_0^\beta d\tau\, e^{i\nu_n\tau} \langle \mathcal{T}\rho(\boldsymbol{q},\tau)\rho(-\boldsymbol{q},0)\rangle. \tag{1.83}$$

Here, we introduced the collective label $Q = (\boldsymbol{q}, i\nu_n)$, where $\nu_n$ is a bosonic Matsubara frequency. In addition, the density operator in second quantized notation reads

$$\rho(\boldsymbol{q}) = \sum_{\boldsymbol{p}\sigma} c^\dagger_{\boldsymbol{p}+\boldsymbol{q},\sigma} c_{\boldsymbol{p},\sigma}, \tag{1.84}$$

while the time dependence is in the Heisenberg picture, i.e. $\rho(\tau) = \exp[\tau\mathcal{K}]\hat{\rho}\exp[-\tau\mathcal{K}]$. Switching to the interaction picture the correlation function can be recast in the form

$$G_{\hat{\rho}\hat{\rho}}(Q) = -\int_0^\beta d\tau\, e^{i\nu_n\tau} \frac{\langle \mathcal{T}\tilde{\rho}(\boldsymbol{q},\tau)\tilde{\rho}(-\boldsymbol{q},0)\mathcal{U}(\beta,0)\rangle_0}{\langle \mathcal{U}(\beta,0)\rangle_0}, \tag{1.85}$$

which allows for a perturbative evaluation by expanding the S-matrix $\mathcal{U}(\beta,0)$, which is defined analogously to Eq. (1.62). Likewise, please note that the interaction representation $\tilde{\rho}(\tau)$ and the non-interacting averages $\langle\ldots\rangle_0$ are defined according to Eqs. (1.61) and (1.64), substituting $\mathcal{H}_0$ by $\mathcal{K}_0$. The resulting non-interacting averages can be evaluated using the fermionic Wick-theorem [80]. To zeroth order one obtains the non-interacting polarization

$$\pi_0(Q) = -\int_0^\beta d\tau\, e^{i\nu_n\tau}\langle\mathcal{T}\tilde{\rho}(\boldsymbol{q},\tau)\tilde{\rho}(-\boldsymbol{q},0)\rangle_0 = 2\int_K g_0(K)g_0(K-Q), \tag{1.86}$$

which is graphically depicted in Fig. 1.2. Here, we introduced the abbreviation $\int_K = (\beta V)^{-1}\sum_{\boldsymbol{k},\omega_m}$, where $\omega_m$ is a fermionic Matsubara frequency and $V$ the volume of the system. Furthermore, the non-interacting fermionic single-particle Green function $g_0(K)$ describing particle, respectively hole excitations above and below the Fermi sea at $|\boldsymbol{k}| = k_F$ is given by

$$g_0(K) = \frac{1}{i\omega_m - \epsilon_{\boldsymbol{k}} + i\delta\,\mathrm{sgn}(|\boldsymbol{k}| - k_F)}, \tag{1.87}$$

with $\delta$ an infinitesimal positive constant. The higher order contributions are best considered diagrammatically as shown in Fig. 1.2. Naturally each of these diagrams is either reducible with respect to cutting a single interaction line or not, and it is thus useful to regroup all irreducible contributions in the general polarization function $\pi(Q)$ [81]. The full series expansion in $J_{\boldsymbol{q}}$ can then be recast in the form of a geometric series in $\pi(Q)$, which yields the Dyson equation of the density-density correlation function

$$\begin{aligned} G_{\rho\rho}(Q) &= \pi(Q) + \pi(Q)J_{\boldsymbol{q}}\pi(Q) + \pi(Q)J_{\boldsymbol{q}}\pi(Q)J_{\boldsymbol{q}}\pi(Q) + \ldots \\ &= \frac{\pi(Q)}{1 - J_{\boldsymbol{q}}\pi(Q)}. \end{aligned} \tag{1.88}$$

### Random phase approximation

In evaluating the interaction irreducible polarization function one needs to resort to suitable approximations. One obvious choice is (again) an expansion in the interaction. Formally, this can be justified by generalizing the two-spin component system ($\sigma = \{\uparrow,\downarrow\}$) to a system with $N = 2S+1$ spin components ($S \gg 1$) [14]. In order for the interaction energy to be extensive in $N$ the interaction is likewise rescaled as $J_{\boldsymbol{q}} = \mathcal{J}_{\boldsymbol{q}}/N$, which hence allows for a direct classification of the contribution to the polarization in terms of powers of $1/N$, cf. Fig. 1.2. For the original model with $N = 2$ this is certainly questionable, but fortunately, the zeroth order approximation

$$\pi(Q) \approx \pi_0(Q), \tag{1.89}$$

known as random phase approximation, leads to a number of reasonable predictions for the physical properties of metals [81]. In particular, this approximation presents the simplest possibility to consistently take into account the effect of particle-hole fluctuations around the Fermi surface, which - in turn - give rise to a well-defined collective mode. In order to analyze this, let us consider the associated spectral function, which can be obtained from the imaginary time density-density correlation function by analytically continuing the Matsubara

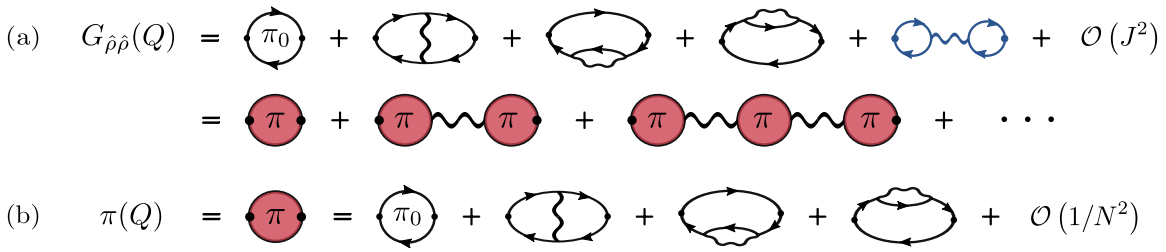


Figure 1.2: (a) Graphical representation of the perturbative expansion of $G_{\hat{\rho}\hat{\rho}}(Q)$ in powers of $J$. Irreducible (reducible) contributions are shown in black (blue). In the second line all irreducible contributions are regrouped in the polarization $\pi(Q)$ and the expansion is expressed as a geometric series. (b) Graphical representation of the expansion of $\pi(Q)$ in inverse powers of the number of spin components $N$. Arrowed lines represent the fermionic single particle Green functions $g_0(K)$ and wavy lines represent the interaction $J_{\boldsymbol{k}}$. Momentum and frequency conservation is implicit at each vertex.

frequency to the real axes. Upon substituting the non-interacting polarization $\pi_0(Q)$ in the Dyson Eq. (1.88) the spectral function reads

$$\begin{aligned}\chi''(\boldsymbol{q},\omega) &= \operatorname{Im} G_{\rho\rho}(\boldsymbol{q}, i\nu_n \to \omega + i\delta) \\ &= \frac{\operatorname{Im}\pi_0(\boldsymbol{q},\omega+i\delta)}{\left(1 - J_{\boldsymbol{q}}\operatorname{Re}\pi_0(\boldsymbol{q},\omega+i\delta)\right)^2 + \left(J_{\boldsymbol{q}}\operatorname{Im}\pi_0(\boldsymbol{q},\omega+i\delta)\right)^2}.\end{aligned} \tag{1.90}$$

This expression can be further analyzed by simplifying $\pi_0(Q)$. Performing the sum over the internal Matsubara frequencies in the corresponding definition (1.86), the non-interacting polarization reads

$$\pi_0(\boldsymbol{q},\omega+i\delta) = \frac{2}{V}\sum_{\boldsymbol{k}} \frac{n_F(\epsilon_{\boldsymbol{k}}) - n_F(\epsilon_{\boldsymbol{k}+\boldsymbol{q}})}{\epsilon_{\boldsymbol{k}} - \epsilon_{\boldsymbol{k}+\boldsymbol{q}} + \omega + i\delta}. \tag{1.91}$$

At sufficiently low temperatures, the fermionic distribution function $n_F(\epsilon_{\boldsymbol{k}})$ can be approximated by its zero temperature limit $n_F(\epsilon_{\boldsymbol{k}}) = \Theta(|\boldsymbol{k}| - k_F)$, such that the real and imaginary parts of the polarization reduce to [14]

$$\operatorname{Re}\pi_0(\boldsymbol{q},\omega+i\delta) = -D(\epsilon_F)\mathcal{L}_R(\tilde{q},\tilde{\omega}), \tag{1.92a}$$
$$\operatorname{Im}\pi_0(\boldsymbol{q},\omega+i\delta) = -D(\epsilon_F)\mathcal{L}_I(\tilde{q},\tilde{\omega}), \tag{1.92b}$$

where we introduced the density of states at the Fermi energy $D(\epsilon_F) = mk_F/(\pi^2)$, the rescaled momentum $\tilde{q} = q/(2k_F)$ and frequency $\tilde{\omega} = \omega/(4\epsilon_F)$ ($\epsilon_F = k_F^2/(2m)$), and the real and imaginary parts of the dimensionless *Lindhard function*

$$\mathcal{L}_R(\tilde{q},\tilde{\omega}) = \frac{1}{2} + \frac{1}{8\tilde{q}}\left[\frac{\tilde{q}^2 - (\tilde{q}^2+\tilde{\omega})^2}{\tilde{q}^2}\ln\left|\frac{\tilde{q}^2+\tilde{q}+\tilde{\omega}}{\tilde{q}^2-\tilde{q}+\tilde{\omega}}\right| + (\tilde{\omega}\to-\tilde{\omega})\right], \tag{1.93}$$

$$\mathcal{L}_I(\tilde{q},\tilde{\omega}) = -\frac{\pi}{8\tilde{q}}\left[\frac{\tilde{q}^2 - (\tilde{q}^2+\tilde{\omega})^2}{\tilde{q}^2}\Theta\left(\tilde{q}^2 - (\tilde{q}^2+\tilde{\omega})^2\right) - (\tilde{\omega}\to-\tilde{\omega})\right]. \tag{1.94}$$

From the form of the spectral function in Eq. (1.90) it is evident, that the system possesses a well-defined excitation with dispersion $\tilde{\omega}_s(\tilde{q})$, if

$$1 + J_{\boldsymbol{q}} D(\epsilon_F)\mathcal{L}_R\left(\tilde{q},\tilde{\omega}_s(\tilde{q})\right) = 0, \tag{1.95}$$

provided that the damping term $J_{\boldsymbol{q}} D(\epsilon_F)\mathcal{L}_I\left(\tilde{q},\tilde{\omega}_s(\tilde{q})\right)$ is sufficiently small. Before discussing the numerical solution of Eq. (1.95) it is worth mentioning, that the low momentum limit of the corresponding dispersion can be obtained analytically with the help of the expansion

$$\mathcal{L}_R(\tilde{q},\tilde{\omega}) \overset{q\ll 1}{\approx} \mathcal{L}_R(z=\tilde{\omega}/\tilde{q}) = 1 - \frac{z}{2}\ln\left|\frac{z+1}{z-1}\right|. \tag{1.96}$$

In case of a Coulomb interaction as specified in Eq. (1.82), the dispersion relation defined implicitly in terms of Eq. (1.95) is obtained by expanding the logarithm in Eq. (1.96) in $1/z$, which recovers the plasmon solution

$$\tilde{\omega}_s(\tilde{q}) = \tilde{\omega}_p + \mathcal{O}\left(\tilde{q}^2\right), \tag{1.97}$$

where $\tilde{\omega}_p = e^2 n/(4\epsilon_F\epsilon_0 m)$ is the dimensionless plasma frequency with $n = k_F^3/(3\pi^2)$ the density of a non-interacting electron gas. This gapped dispersion is a consequence of the singular nature of the Coulomb interaction and implies that the mode sits well above the particle-hole continuum, where $\operatorname{Im}\pi_0(\boldsymbol{q},\omega+i\delta)\neq 0$. In this region, which is bound by

$$\tilde{q}(\tilde{q}+1) < \tilde{\omega} < \tilde{q}(\tilde{q}-1), \tag{1.98}$$

any density excitation dissipates into particle-hole pairs and a coherent response to an external perturbation cannot build up. This damping mechanism is known as *Landau damping*. In the neutral case, i.e. for a small contact interaction $J_{\boldsymbol{q}} = J_0$ with $D(\epsilon_F)J_0 \ll 1$, Eqs. (1.95) and (1.96) yield the linear dispersion

$$\tilde{\omega}_s(\tilde{q}) = \tilde{q}\,(1+c_n), \quad c_n = e^{-2+2/(D(\epsilon_F)J_0)}. \tag{1.99}$$

For sufficiently small $\tilde{q} < c_n$ this mode sits just above the particle-hole continuum and the corresponding spectral function thus displays a well-defined sound-peak. Noteworthy, the dimensionless sound velocity $(1+c_n)$ is non-analytic in the interaction $J_0$ which indicates the non-perturbative nature of the result [80] (restoring the proper units one finds $\omega_s(q) = v_0 q$ with $v_0 = v_F(1+c_n)$). The contact and the Coulomb scenarios are compared in Fig. (1.3) a), where the numerical solution of Eq. (1.95) is shown for the dimensionless coupling strengths $\alpha_N = D(\epsilon_F)J_0 = 5$ respectively $\alpha_C = D(\epsilon_F)J_{\tilde{q}}\tilde{q}^2 = 1$.[6] In both cases two solutions are found, one above and a second well within the particle-hole continuum. While the former leads to a sharp excitation peak whose damping is determined by processes not captured within the RPA, the second is completely overdamped by the finite continuum contribution. Increasing the momentum, the upper solution enters the particle-hole continuum and is strongly damped until both solution merge at a certain critical momentum above which no distinct excitation-features can be observed. This behavior is reflected in the corresponding spectral function of the neutral case shown in Fig. 1.3 b). Note, that although the weak coupling solution Eq. (1.99) is not applicable for the chosen $\alpha_N$, the dispersion relation remains linear at small momenta with a corresponding speed of sound of the order of the Fermi velocity (this characteristic is also confirmed by an analysis of Landau's Fermi liquid theory in the strong

[6] $\alpha_N \gg 1$ was chosen in order to allow for a graphical distinction of the dispersion relation and the upper limit of the particle hole continuum. Note, that the large-$N$ expansion, which formally justifies the RPA procedure, is independent of the coupling strenght [14].

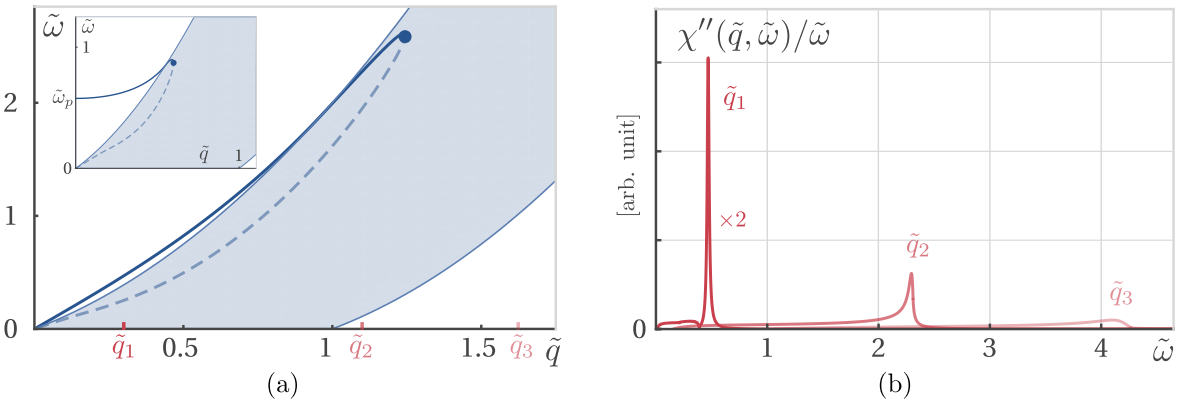


Figure 1.3: (a) Zero-sound dispersion relation $\tilde{\omega}_s(\tilde{q})$ obtained from the numerical solution of Eq. (1.95) for a dimensionless coupling strength $\alpha_N = 5$ (full line). The dashed line depicts a second solution lying inside the particle-hole continuum (shaded area, bounded by Eq. (1.98)). The inset shows the corresponding solutions in case of a Coulomb interaction of coupling strength $\alpha_C = 1$. (b) Spectral function $\chi''(\tilde{q},\tilde{\omega})/\tilde{\omega}$ (Eq. (1.90)) for the three different momenta $\tilde{q} = 0.30, 1.24, 1.63$ . Note, that a phenomenological damping constant $\delta \sim 10^{-2}$ was included in Eq. (1.90) in order to render the width of the zero sound peak at $\tilde{\omega}_s(\tilde{q}_1)$ finite.

coupling limit [82]).

Finally, please note that these results are only applicable if the temperature is significantly smaller than the frequency and the chemical potential, i.e. $T \ll \omega$ and $T \ll \mu$. It is only in this regime, that an approximation of the elementary particle-hole excitations in terms of the non-interacting Green function $g_0$ is justified, and temperature effects can - at least qualitatively - be neglected. Within this parameter range, the system's response to an external perturbing field of the form $\varphi(\boldsymbol{r}, t) \sim \exp[i\omega t]$, can thus be interpreted as the coherent superposition of particle-hole states, excited in a range $\omega$ around the Fermi surface.

### 1.4.2 Hydrodynamic sound

Let us now once more assume an external perturbing field of the form $\varphi(\boldsymbol{r}, t) \sim \exp[i\omega t]$, but discuss the response of an ensemble of (thermally excited) quasiparticles in the limit of low frequencies, i.e. $\omega \ll T$. In this case, a proper discussion of the dynamics requires a solution of the aforementioned full Boltzmann equation, which is notoriously complicated if not impossible. However, at frequency scales $\omega \ll \omega_{\text{col}}$ and momentum scales $q \ll 1/l$, where $l$ is the mean free path of the particles (essentially dominated by the various collisions), a simplified hydrodynamic picture emerges. In this regime, the system can be described in terms of a set of coarse-grained, and locally conserved variables, the mass, momentum, and energy densities, which follow from taking appropriate moments of the distribution function [83]. This hydrodynamic regime also hosts a characteristic sound mode which is briefly characterized in the following.

### First Sound

The dynamical excitations in the hydrodynamic regime close to equilibrium are well described by a linearized form of the universal Navier-Stokes equations of fluid dynamics. Notably, within such a description any microscopic details enter solely in terms of a set of empirical parameters which allows for a general discussion. A concise solution of this set of equations and the resulting density-density correlation functions were first derived by Kadanoff and Martin in Ref. [84], whose approach is also summarized in the monograph of Forster [85]. Instead of delving into details, let us solely highlight the structure of this work, and the characteristics of the associated sound mode. As emphasized before, the dynamics of a system become accessible to a hydrodynamic description if the mass, momentum, and energy densities of the system, $\rho(\boldsymbol{r},t)$, $\boldsymbol{g}(\boldsymbol{r},t)$ and $\varepsilon(\boldsymbol{r},t)$, vary sufficiently slowly in space and time. If this is the case, the system can be partitioned into sub-parts with each part almost in thermodynamic equilibrium, and the dynamics are constrained by the conservation laws

$$\partial_t \rho(\boldsymbol{r},t) + \nabla \cdot \boldsymbol{g}(\boldsymbol{r},t) = 0, \tag{1.100a}$$
$$\partial_t g_i(\boldsymbol{r},t) + \nabla_j \tau_{ij}(\boldsymbol{r},t) = 0, \tag{1.100b}$$
$$\partial_t \varepsilon(\boldsymbol{r},t) + \nabla \cdot \boldsymbol{j}(\boldsymbol{r},t) = 0. \tag{1.100c}$$

This set of continuity equations needs to be complemented by two *constitutive relations* for the stress tensor $\tau_{ij}(\boldsymbol{r},t)$ and the energy current $\boldsymbol{j}(\boldsymbol{r},t)$,

$$\tau_{ij}(\boldsymbol{r},t) = f_{1;\{\xi\}}\left[P(\boldsymbol{r},t), T(\boldsymbol{r},t), \boldsymbol{g}(\boldsymbol{r},t)\right], \tag{1.101a}$$
$$\boldsymbol{j}(\boldsymbol{r},t) = f_{2;\{\xi\}}\left[P(\boldsymbol{r},t), T(\boldsymbol{r},t), \boldsymbol{g}(\boldsymbol{r},t)\right], \tag{1.101b}$$

which are linear functions of the momentum density and of the local pressure $P(\boldsymbol{r},t)$ and temperature $T(\boldsymbol{r},t)$ of the system. The precise form of $f_{1,2}$ (cf. Eq. 4.17 in Ref. [85]) can be inferred from a mix of phenomenological and symmetry considerations, while $\{\xi\}$ denotes a set of three transport coefficients - shear and bulk-viscosity $\eta$ and $\zeta$ and heat conductivity $\kappa$ - which enter as empirical parameters. Furthermore, close to equilibrium any changes in the local pressure and temperature are related to the mass and energy densities by

$$\nabla P(\boldsymbol{r},t) = \left.\frac{\partial P}{\partial \rho}\right|_{\varepsilon} \nabla\rho(\boldsymbol{r},t) + \left.\frac{\partial P}{\partial \varepsilon}\right|_{\rho} \nabla\varepsilon(\boldsymbol{r},t), \tag{1.102a}$$
$$\nabla T(\boldsymbol{r},t) = \left.\frac{\partial T}{\partial \rho}\right|_{\varepsilon} \nabla\rho(\boldsymbol{r},t) + \left.\frac{\partial T}{\partial \varepsilon}\right|_{\rho} \nabla\varepsilon(\boldsymbol{r},t), \tag{1.102b}$$

where $P$, $\rho$ and $\varepsilon$ denote the corresponding uniform thermodynamic equilibrium values. Together, the set of Eqs. (1.100)-(1.102) thus presents a closed system of partial differential equations, which can be solved working with Fourier respectively Laplace transformed variables. In particular, the explicit solution shows that an initial non-uniform density configuration $\rho(\boldsymbol{r}, t=0)$ relaxes to its uniform equilibrium value in a mix of damped wave-like propagation and diffusion. Similar to the collisionless regime, this behavior is best analyzed in terms of the associated spectral function,

$$\frac{1}{\tilde{\omega}}\chi''(\tilde{q},\tilde{\omega}) \propto \left(\alpha \frac{\tilde{q}^4\Gamma}{(\tilde{\omega}^2-\tilde{q}^2)^2 + (\tilde{\omega}\tilde{q}^2\Gamma)^2} + (1-\alpha)\,\frac{\tilde{q}^2 D}{\tilde{\omega}^2 + (\tilde{q}^2 D)^2}\right), \tag{1.103}$$

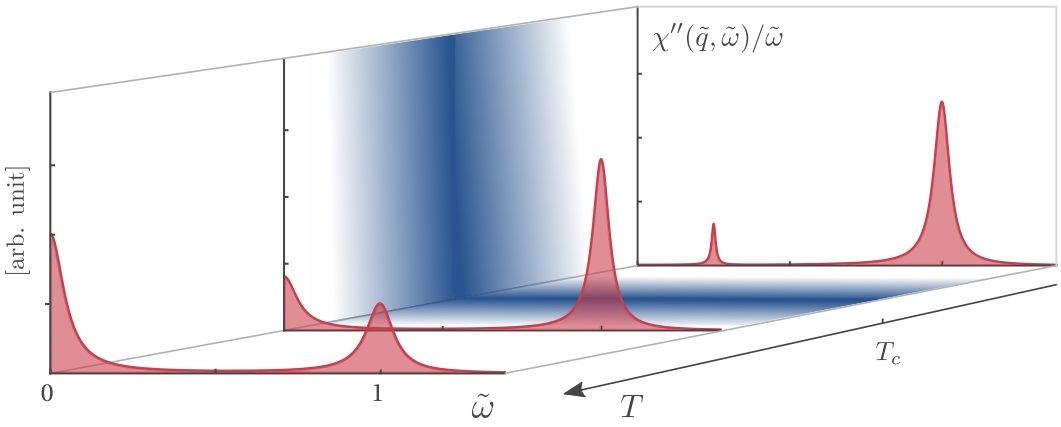


Figure 1.4: Qualitative temperature dependence of the generalized hydrodynamic (density-density) spectral function $\chi''(\tilde{q},\tilde{\omega})/\tilde{\omega}$. First and second layer: $\chi''(\tilde{q}=1,\tilde{\omega})/\tilde{\omega}$ (Eq. (1.103)) evaluated for the Landau-Platceck ratios $R_{\rm LP}=1$ and $R_{\rm LP}=0.25$ and dimensionless diffusion constants $D=D_T=0.05$. Third layer: Qualitative form of a hydrodynamic spectral function in the symmetry broken phase showing an additional second sound peak. The shading indicates a continuous phase transition at $T=T_c$.

which can be obtained from the explicit solution of Eqs. (1.100)-(1.102) within a linear response construction [84, 85]. Here, we introduced the dimensionless variables $\tilde{\boldsymbol{q}}=\boldsymbol{q}/(mv_1)$ and $\tilde{\omega}=\omega/(mv_1^2)$[7], and the sound velocity

$$v_1^2=\frac{1}{\alpha}\frac{\partial P}{\partial\rho}\bigg|_T,\quad \alpha=C_v/C_p, \tag{1.104}$$

where $C_v$ and $C_p$ denote the specific heat at constant volume respectively pressure. Note, that the ratio of the two specific heats is usually expressed in terms of the *Landau-Platceck* ratio $R_{\rm LP}=1/\alpha-1$. In addition, the diffusion and damping coefficients are given in terms of the transport coefficients as

$$D=\frac{1}{\rho}\left(\frac{4}{3}\eta+\zeta\right),\quad D_T=\frac{\kappa}{\rho C_p},\quad \Gamma=D+D_T\frac{1-\alpha}{\alpha}. \tag{1.105}$$

Hydrodynamic sound hence manifests as a well defined peak in the density-density spectral functions with linear dispersion and quadratic momentum dependence of the corresponding width. Furthermore, the sound peak is accompanied by a diffusive central peak which accounts for the coupling of density and temperature (entropy) fluctuations. Although the precise form of the spectral function depends on the scenario of interest, some general behavior is, moreover, hidden in the temperature dependence of the Landau-Platceck ratio [85]. In common classical fluids, $R_{\rm LP}$ grows as the temperature is increased and the response is thus dominated by a narrow diffusive central peak ($R_{\rm LP}\gg 1\Leftrightarrow C_p\gg C_v$), while at low temperatures a sharp sound peak dominates since $C_p\approx C_v$ ($R_{\rm LP}\ll 1$, cf. first and second layer in Fig. 1.4). However please keep in mind, that this discussion is only sensible as long as the system remains in a temperature range where the hydrodynamic approach is justified.

[7] The mass $m$ is determined by the equilibrium mass density $\rho=mn$ where $n$ is a dimensionless density.

That said, for the majority of the systems modeled in terms of an ensemble of fermionic quasi-particles, i.e. normal metals or electron gases in semiconductors, this is only seldom the case [86,87]. In these systems, electron-phonon and impurity scattering processes, which do not conserve the momentum and energy of the electron ensemble, present the dominant contribution to the collision integrals and hence prevent any collective hydrodynamic behavior [88]. Notable Fermi systems, which indeed show hydrodynamic behavior are Graphene (see e.g. the recent experiments presented in Refs. [89,90]), respectively liquid He-3, whose low temperature behavior is described in terms of a neutral Fermi liquid. For this system, the order of magnitude of the corresponding hydrodynamic speed of sound $v_1$, can be estimated from the thermodynamic response of a non-interacting Fermi gas [80]

$$v_1 \sim \sqrt{\frac{1}{\alpha}\frac{\partial P}{\partial \rho}\bigg|_T} = \frac{v_F}{\sqrt{3}}, \tag{1.106}$$

which is of the same order as the zero-sound velocity $v_0 \approx v_F$ obtained for the case of small contact interaction. This suggests that the transition from zero to first sound can be traced experimentally while crossing from the collisionless regime at low temperatures into the collision-dominated regime upon increasing the temperature. Noteworthy, such a transition has indeed been observed some 50 years ago in low temperature transport measurements on liquid He-3 [91,92], where two sound regimes were observed separated by a maximum in the sound damping.

### Second sound

To complete the discussion of different sound types let us briefly mention another hydrodynamic phenomenon, second sound, which generally denotes a wave-like propagation of temperature fluctuations in the symmetry broken phase of a system. Historically, this phenomenon was first debated in the scope of liquid He-4, which shows a phase transition into a superfluid phase upon cooling the system below the critical temperature $T_\Lambda \approx 2\text{K}$, but similar phenomena have been observed, e.g. in very pure crystalline solids [93] or sand [94]. A hydrodynamic description of this phase is given by the phenomenological *two-fluid model*, originally developed by Tisza [95] and later refined by Landau [96]. In this description the three variables $\rho(\boldsymbol{r},t)$, $\boldsymbol{g}(\boldsymbol{r},t)$, and $\varepsilon(\boldsymbol{r},t)$ are complemented by an additional conserved quantity, the superfluidity velocity field $\boldsymbol{v}_s(\boldsymbol{r},t)$ whose dynamics is described by another constitutive relation of the form of Eq. (1.101) [85,97].[8] While the detailed discussion of these equations is beyond the scope of this introduction, the corresponding solution predicts a wave-like propagation of temperature inhomogeneities instead of the usual diffusive process, which - loosely speaking - is a consequence of the fact that a superfluid flow carries no entropy [25]. Due to the coupling of temperature and (mass)-density fluctuations, this phenomenon is also reflected in the (density-density) spectral function of the liquid: upon cooling liquid He-4 below $T_\Lambda$ the diffusive central peak vanishes and a second low-frequency sound peak emerges, albeit of very small spectral weight, while the original first sound peak remains largely unaffected by the phase transition (cf. Fig. 1.4).

[8] Microscopically, superfluidy is commonly related to the formation of a Bose-Einstein condensate in an ensemble of interacting bosons, and the field $\boldsymbol{v}_s$ can be defined as gradient of the phase of the associated complex order parameter $\langle\psi(\boldsymbol{r})\rangle$, where $\psi(\boldsymbol{r})$ denotes a bosonic field operator in second quantization notation.

---

The classification of sound modes presented here concludes our review of the conceptual background of this thesis. For now, let us continue by introducing the methodical foundation of this work, the spin functional renormalization group.

# Chapter 2

# Spin functional renormalization group

## 2.1 Outline

In the previous introduction we recapitulated Matsubara's imaginary time formalism in the context of the ferromagnetic Heisenberg model. Therein, we indicated that the relevant observables, such as the magnetization and the dynamical structure factor, can in principle be calculated in a series expansion in the exchange interaction once an external magnetic field is taken into account. The explicit evaluation of such a perturbative ansatz then requires the calculation of non-interacting n-point time-ordered spin correlation functions, cf. Eq. (1.64). This structure is reminiscent of the standard perturbative treatment of bosonic and fermionic many-body systems, albeit with the essential difference, that the pairwise commutation relations of the involved spin operators is not a complex number, as in the case of bosonic or fermionic operators, but an operator itself. By consequence, the Wick-contraction of a given non-interacting n-point spin correlation function, i.e. the reduction to a sum of pair correlation functions - which themselves are straightforwardly calculable - is considerably more complicated. As recapitulated in the introduction, the explicit rules for such a reduction scheme and the associated diagrammatic language, were developed in the late 1960s by Vaks *et al.* [33, 34]. Notably, their approach did not only recover the low-temperature reference results of that time, in particular Dyson's general spin wave theory findings [98, 99], but could also establish the existence of spin-wave excitations for all temperatures below the Curie temperature $T_c$, a statement still contested up to that point. Nevertheless, the technique was never established as a standard approach, while Heisenberg spin systems were instead investigated by a plethora of other methods. Thereto, the majority of the analytical approaches do not consider the spin degrees of freedom, but are based on auxiliary representations. Important examples include the bosonic Holstein-Primakoff [100] and Dyson-Maleev formalism [98, 101], which allow to analyze the magnetically ordered phase in a perturbative treatment in the inverse spin magnitude $1/S$. Similar techniques applicable to the disordered phase are given by the Schwinger-Boson [102, 103] and Abrikosov pseudo-fermion formulations [104]. However, all of these methods have in common that the corresponding Hilbert space is artificially increased, which has to be accounted for by implementing additional constraints and projection-techniques. Of course, there also exist various other methods which

do not rely on a mapping of the spin Hamiltonian onto bosonic or fermionic counterpart. The most prominent example being the Bethe ansatz [105], which provides an exact solution framework for certain one-dimensional systems. Other methods that can in principle be applied to spin systems in arbitrary dimensions, include the Bogoliubov-Tyablikov Green's function method [106], which is based on different decoupling strategies of the spins' equation of motions, and the analysis in terms of a coherent state path integral as introduced by Haldane [107, 108]. In addition, the Heisenberg model can of course also be studied within a wealth of powerful numerical methods, such as exact diagonalization [109], density matrix renormalization group [110] and various quantum Monte Carlo methods [111, 112] (for an overview see e.g. Ref. [109]).

The following chapter recapitulates a further contribution to the vast methodology sketched above, the *spin functional renormalization group* (spin FRG). In what follows, the original formalism as developed in Ref. [1, 2] is shortly reviewed, and certain limitations of its applicability are discussed. In a second step we then introduce the alternative hybrid formalism, published in our work Ref. [3], which allows for an investigation of the Heisenberg ferromagnet in the ordered phase. We finish the chapter by deriving a universal solution framework of the corresponding FRG flow equation, which presents the basis of the forthcoming chapters. To prevent any misconceptions, it should be stated that the essential concepts presented in this chapter were developed by Krieg and Kopietz and not by the author. Nonetheless, the following pages contain some useful novel additions to the original formulations.

## 2.2 Original formalism

The following pages summarize the essential technical details of the formalism introduced in Ref. [1], though the notation is hereby slightly adjusted for consistency-reasons. To begin with, please remember that we parameterized the Heisenberg Hamiltonian (1.20) in the form $\mathcal{H} = H_0 + \mathcal{V}$, where $\mathcal{H}_0$ represents the Zeeman Hamiltonian and $\mathcal{V}$ the exchange interaction contribution [cf. Eq. (1.59)]. Given that the following formalism is partially based on an asymmetrical treatment of the longitudinal and transverse fluctuations, the exchange interaction part will from now on be given in the form

$$\mathcal{V} = -\frac{1}{2}\sum_{ij}\left[J^{\perp}_{ij}\left(S^{+}_{i}S^{-}_{j} + S^{-}_{i}S^{+}_{j}\right) + J^{z}_{ij}S^{z}_{i}S^{z}_{j}\right], \tag{2.1}$$

which accounts for a possible anisotropy of the transverse and longitudinal parts of the exchange interaction, $J^{\perp}_{ij}$ and $J^{z}_{ij}$. In addition, the transverse part of the spin interaction is hereby expressed in terms of the spin ladder operators $S^{\pm}_{i}$ introduced in Eq. (1.31) on page 13. Following the central idea of the spin FRG, we now replace the exchange interactions $J^{\perp}_{ij}$ and $J^{z}_{ij}$ in Eq. (2.1) by the modified versions

$$J^{\perp}_{ij} \to J^{\perp}_{\Lambda,ij} = J^{\perp}_{ij} - R^{\perp}_{\Lambda,ij}, \quad \text{and} \quad J^{z}_{ij} \to J^{z}_{\Lambda,ij} = J^{z}_{ij} - R^{z}_{\Lambda,ij}. \tag{2.2}$$

Here, the regulators $R^{\perp}_{\Lambda,ij}$ and $R^{z}_{\Lambda,ij}$ account for a general deformation process which is parameterized by the deformation variable $\Lambda \in (\Lambda_0, \Lambda_{\text{final}})$. This can be a simple switching-on procedure, i.e. $J_{\Lambda,ij} = \Lambda J_{ij}$ with $\Lambda \in (0, 1)$, or a more complicated deformation scheme, as

e.g. cutting off a long range interaction $J_{ij}$ for distances $|\boldsymbol{r}_i - \boldsymbol{r}_j| > d_\Lambda \in (a, \infty)$, where $a$ is the underlying lattice spacing. In any case, the regulators need to be chosen such as to enable a controlled solution of the deformed model at $\Lambda = \Lambda_0$, while in the limit $\Lambda \to \Lambda_{\text{final}}$ the full model should be recovered. Building upon the discussion of the Matsubara formalism in section 1.3.2, let us now introduce the central entity of the work of Krieg and Kopietz [1]: The $\Lambda$-dependent *generating functional of the connected imaginary time-ordered spin correlation functions*

$$\mathcal{G}_\Lambda[\boldsymbol{h}] = \ln \mathrm{Tr}\left[e^{-\beta\mathcal{H}_0}\mathcal{T}e^{\int_0^\beta d\tau\left[\sum_i \boldsymbol{h}_i(\tau)\cdot\boldsymbol{S}_i(\tau) - \mathcal{V}_\Lambda(\tau)\right]}\right]. \tag{2.3}$$

Here, $\boldsymbol{h} = \{\boldsymbol{h}_i(\tau)\}$ denotes a set of three-component source-fields, $\mathcal{T}$ is the imaginary time-ordering operator introduced in section 1.3.2 and the time-dependence of all operators is in the interaction picture with respect to $\mathcal{H}_0$, cf. Eq. (1.61) on page 19. In addition, we introduced the abbreviation $\mathcal{V}_\Lambda(\tau)$, which represents the exchange interaction term (2.1), with substituted interactions $J^\perp_{\Lambda,ij}$ and $J^z_{\Lambda,ij}$, and time-dependent spin operators. Note, that the functional $\mathcal{G}_\Lambda[\boldsymbol{h}]$ encapsulates the imaginary time version of the physically relevant correlation functions in an elegant way. To illustrate this let us express the scalar product which couples source-fields and spin operators in the form

$$\boldsymbol{h}_i(\tau)\cdot\boldsymbol{S}_i(\tau) = h^+_I S^-_I + h^-_I S^+_I + h^z_I S^z_I = \sum_{\alpha=\{+,-,z\}} h^{\bar\alpha}_I S^\alpha_I, \tag{2.4}$$

where we introduced the collective site- and imaginary time index $S^\alpha_I = S^\alpha_i(\tau_i)$ and the notation

$$(\alpha, \bar\alpha) \in \{(+-), (-+), (zz)\}, \tag{2.5}$$

for the spin and source-field components. Explicit differentiating of the functional $\mathcal{G}_\Lambda[\boldsymbol{h}]$ with respect to the sources $h^\alpha_I$ then defines the set of time-ordered connected spin correlation functions,

$$G^{\alpha_1\ldots\alpha_n}_{\Lambda,I_1\ldots I_n} = \langle\mathcal{T}\left[S^{\alpha_1}_{I_1}\ldots S^{\alpha_n}_{I_n}\right]\rangle_{\Lambda,c} = \left.\frac{\delta^n\mathcal{G}_\Lambda[\boldsymbol{h}]}{\delta h^{\bar\alpha_1}_{I_1}\ldots\delta h^{\bar\alpha_n}_{I_n}}\right|_{\boldsymbol{h}=0}. \tag{2.6}$$

Evidently, these correlation functions cannot be calculated exactly for any non-vanishing interaction part $\mathcal{V}_\Lambda(\tau)$. Nevertheless, the spin FRG formalism rests on the idea that it is still possible to formulate exact flow equations describing their evolution as $\mathcal{V}_\Lambda(\tau)$ is modified along $\Lambda$. The respective system of coupled integro-differential equations can be obtained from the flow of the generating functional $\mathcal{G}_\Lambda[\boldsymbol{h}]$, which follows from the definition (2.3) as

$$\partial_\Lambda\mathcal{G}_\Lambda[\boldsymbol{h}] = -\frac{1}{2}\sum_{IJ}\sum_\alpha\left[\left(\partial_\Lambda\mathcal{R}^{\bar\alpha\alpha}_{\Lambda,IJ}\right)\left[\frac{\delta^2\mathcal{G}_\Lambda[\boldsymbol{h}]}{\delta h^{\bar\alpha}_I\delta h^\alpha_J} + \frac{\delta\mathcal{G}_\Lambda[\boldsymbol{h}]}{\delta h^{\bar\alpha}_I}\frac{\delta\mathcal{G}_\Lambda[\boldsymbol{h}]}{\delta h^\alpha_J}\right]\right]. \tag{2.7}$$

Here, we introduced the abbreviation $\sum_I = \int_0^\beta d\tau\sum_i$, and formulated the $\Lambda$-derivation of the interactions $\partial_\Lambda J^\perp_\Lambda = \partial_\Lambda R^\perp_\Lambda$ and $\partial_\Lambda J^z_\Lambda = \partial_\Lambda R^z_\Lambda$ in terms of the regulator matrix

$$\mathcal{R}_{\Lambda,IJ} = \delta(\tau_i - \tau_j)\mathcal{M}_{\pm\mp z}\left(R^\perp_{\Lambda,ij}, R^\perp_{\Lambda,ij}, R^z_{\Lambda,ij}\right), \tag{2.8}$$

where $\mathcal{M}_{\pm\mp z}$ is a matrix in component space $\alpha$, with matrix elements

$$\mathcal{M}_{\pm\mp z}(R^\perp_{\Lambda,ij}, R^\perp_{\Lambda,ij}, R^z_{\Lambda,ij}) = \begin{pmatrix} 0 & R^\perp_{\Lambda,ij} & 0 \\ R^\perp_{\Lambda,ij} & 0 & 0 \\ 0 & 0 & R^z_{\Lambda,ij}\end{pmatrix}. \tag{2.9}$$

Expanding both sides of the flow equation (2.7) in a functional Taylor expansion around $\boldsymbol{h} = 0$ then yields the infinite hierarchy of coupled flow equations for the different connected correlation functions $G^{\alpha_1 \dots \alpha_n}_{\Lambda, I_1 \dots I_n}$. As noted in the work of Krieg and Kopietz [1], this hierarchy can for example be used to generate the systematic expansion of the n-point correlation functions in powers of the interaction. Noteworthy, this allows one to reproduce the notoriously complicated spin diagrammatic results of VLP [33, 34] in a considerably simpler way. However, similar to the bosonic and fermionic FRG formulations, it is significantly more efficient to calculate the connected correlation functions not directly, but to consider their irreducible building blocks, the one-particle irreducible vertices as the essential elements of interest. In practice, this is implemented by introducing their corresponding generating functional $\mathcal{L}_\Lambda[\boldsymbol{M}]$ via a subtracted Legendre transformation of $\mathcal{G}_\Lambda[\boldsymbol{h}]$ as

$$\mathcal{L}_\Lambda[\boldsymbol{M}] = \sum_{I,\alpha} M^{\bar{\alpha}}_I h^\alpha_I - \mathcal{G}_\Lambda[\boldsymbol{h}] - \frac{1}{2} \sum_{IJ} \sum_{\alpha} M^{\bar{\alpha}}_I \mathcal{R}^{\bar{\alpha}\alpha}_{\Lambda, IJ} M^\alpha_J. \tag{2.10}$$

Here, the fields $h^\alpha_I$ on the right side of the definition (2.10) are implicitly determined by inverting the relations

$$M^\alpha_I = \frac{\delta \mathcal{G}_\Lambda[\boldsymbol{h}]}{\delta h^{\bar{\alpha}}_I}, \tag{2.11}$$

such that the new sources $M^\alpha_I$ can be interpreted as field dependent magnetizations. Note however, that $\mathcal{L}_\Lambda[\boldsymbol{M}]$ is only well defined if the actual inverse functions can be constructed for all values of $\Lambda$. Let us for the moment assume that this is the case. Differentiating the functional $\mathcal{L}_\Lambda[\boldsymbol{M}]$ with respect to the sources then gives rise to the set of irreducible vertices

$$L^{\alpha_1 \dots \alpha_n}_{\Lambda, I_1 \dots I_n} = \left. \frac{\delta^n \mathcal{L}_\Lambda[\boldsymbol{M}]}{\delta M^{\bar{\alpha}_1}_{I_1} \dots \delta M^{\bar{\alpha}_n}_{I_n}} \right|_{\boldsymbol{M}=0}, \tag{2.12}$$

which can be related to the connected correlation functions $G^{\alpha_1 \dots \alpha_n}_{\Lambda, I_1 \dots I_n}$ via the functional Taylor expansion of the identity

$$[\boldsymbol{G}[\boldsymbol{h}]]^{\alpha\alpha'}_{IJ} = \left[ \left( \boldsymbol{\mathcal{L}}''[\boldsymbol{M}] + \boldsymbol{\mathcal{R}}_\Lambda \right)^{-1} \right]^{\bar{\alpha}\bar{\alpha}'}_{IJ}, \tag{2.13}$$

a procedure usually called *tree expansion* [113]. In particular, Eq. (2.13) follows by construction from the definition (2.10) with the matrix elements of the *Hessian* matrices $\boldsymbol{G}[\boldsymbol{h}]$ and $\boldsymbol{\Gamma}''_\Lambda[\boldsymbol{M}]$ given by

$$[\boldsymbol{G}_\Lambda[\boldsymbol{h}]]^{\alpha\alpha'}_{IJ} = \frac{\delta^2 \mathcal{G}_\Lambda[\boldsymbol{h}]}{\delta h^{\bar{\alpha}}_I \delta h^{\bar{\alpha}'}_J}, \tag{2.14a}$$

$$\left[\boldsymbol{\mathcal{L}}''_\Lambda[\boldsymbol{M}]\right]^{\alpha\alpha'}_{IJ} = \frac{\delta^2 \mathcal{L}_\Lambda[\boldsymbol{M}]}{\delta M^{\bar{\alpha}}_I \delta M^{\bar{\alpha}'}_J}, \tag{2.14b}$$

and $(\boldsymbol{\mathcal{R}}_\Lambda)^{\alpha\alpha'}_{IJ} = \mathcal{R}^{\alpha\alpha'}_{\Lambda, IJ}$.[1] We may now continue along the lines of the usual FRG formalism and derive the corresponding exact flow equation of the functional $\mathcal{L}_\Lambda[\boldsymbol{M}]$. Differentiating

[1] Eq. (2.14) follows from the identity

$$\delta^{\alpha\beta}_{AB} = \frac{\delta M^\alpha_A}{\delta M^\beta_B} = \sum_{C,\gamma} \frac{\delta h^{\bar{\gamma}}_C}{\delta M^\beta_B} \frac{\delta M^\alpha_A}{\delta h^{\bar{\gamma}}_C} = \sum_{C,\gamma} \left( \frac{\delta^2 \mathcal{L}}{\delta M^\beta_B \delta M^\gamma_C} + R^{\beta\gamma}_{BC} \right) \frac{\delta^2 G}{\delta h^{\bar{\gamma}}_C \delta h^{\bar{\alpha}}_A},$$

where we used Eq. (2.11) and the complementary relation $h^{\bar{\alpha}}_A = \delta \mathcal{L} / \delta M^\alpha_A + \sum_B M^{\bar{\alpha}}_B R^{\bar{\alpha}\alpha}_{BA}$.

the definition (2.10) of $\mathcal{L}_\Lambda[\boldsymbol{M}]$ with respect to $\Lambda$ yields

$$\partial_\Lambda \mathcal{L}_\Lambda[\boldsymbol{M}] = \frac{1}{2}\sum_{IJ}\sum_{\alpha}\left(\partial_\Lambda \mathcal{R}^{\bar{\alpha}\alpha}_{\Lambda,IJ}\right)\frac{\delta^2 \mathcal{G}_\Lambda[\boldsymbol{h}]}{\delta h^{\bar{\alpha}}_I \delta h^{\alpha}_J}. \tag{2.15}$$

Note, that the flow of the regulator term, which was added in the definition (2.10), cancels the second term inside the brackets of the flow equation (2.7) of the functional $\mathcal{G}_\Lambda[\boldsymbol{h}]$. In order to express the right side of the flow equation as a functional of the magnetizations $M^\alpha_I$, we make use of the identity (2.13) which relates the corresponding Hessian matrices. This allows to rewrite the flow equation in compact form as

$$\partial_\Lambda \mathcal{L}_\Lambda[\boldsymbol{M}] = \frac{1}{2}\mathrm{Tr}\left[\left(\boldsymbol{\mathcal{L}}''[\boldsymbol{M}] + \boldsymbol{\mathcal{R}}_\Lambda\right)^{-1}\partial_\Lambda \boldsymbol{\mathcal{R}}_\Lambda\right], \tag{2.16}$$

where we introduced the shorthand $\mathrm{Tr} = \sum_{IJ,\alpha}$. Eq. (2.16) formally resembles the Wetterich equation of a bosonic field theory [114]. This algebraic similarity is noteworthy, given that in the present case the underlying generating functionals are not formulated as path integrals. However, let us emphasize that the regulator terms in Eq. (2.16) have a different origin than in standard FRG approaches to bosonic field theories. In the latter case the regulators are commonly introduced in the quadratic part of the corresponding action in order to suppress low energy modes of momentum $|\boldsymbol{k}| < \kappa$ from the functional integral. Along the FRG flow, the cutoff parameter $\kappa$ is then continuously lowered from the intrinsic ultraviolet cutoff to $\kappa = 0$, thereby successively including fluctuations at longer and longer wavelengths [113,114]. In the present case the regulator terms modify the interaction operator of the Hamiltonian directly. While it is in principle possible to chose the regulator terms in order to mimic a similar mode-elimination scheme, the approach is not restricted to that. In particular, in the present work we choose a simple switching-on procedure of the interaction term. The FRG flow then does not describe any transition from a microscopic to a macroscopic effective theory but rather an adiabatic interpolation from the non-interacting to the interacting system. Furthermore, let us point out, that the SU(2) nature of the underlying spin operators entered the derivation of (2.16) at no point. It is nevertheless fully taken into account by the initial condition of the connected correlation functions, respectively their corresponding initial vertices. Actual calculations thus require a suitable deformation scheme which allows for a controlled calculation and classification of the initial conditions. In addition, please bear in mind, that the flow equation (2.16) is only applicable if the generating functional $\mathcal{L}_\Lambda[\boldsymbol{M}]$ can actually be constructed for all values of $\Lambda$. However, as indicated in Ref. [1] this is not always possible.

### Non-applicability for initially decoupled sites

Let us shortly discuss why the above-presented approach fails, if we choose a vanishing initial exchange interaction $\mathcal{V}_{\Lambda_0} = 0$. While such a choice presents the benefit that the initial time-ordered spin correlation functions $G^{\alpha_1\ldots\alpha_n}_{\Lambda_0,I_1\ldots I_n}$ can be calculated exactly, the functional $\mathcal{L}_{\Lambda_0}[\boldsymbol{m}]$ introduced in Eq. (2.10) cannot be defined. Recall, that the definition (2.10) implies, that in the vicinity of $\boldsymbol{h} = 0$ we may invert the relation (2.11) and express the source fields $h^\alpha_I$ in terms of the local magnetizations $M^\alpha_I$. This is in general possible if the corresponding Jacobian matrix $\boldsymbol{G}_\Lambda = \boldsymbol{G}_\Lambda[\boldsymbol{h} = 0]$ is invertible, which is not the case for a system of decoupled sites.

In order to exemplify this, let us discretize continuous imaginary time as $\tau \in (0,\beta) \to \tau_i = i\,d\tau, i \in (0,1,2,..,n)$ where $n = \beta/\,d\tau$. The discrete version of the initial Jacobian matrix is then given by

$$\boldsymbol{G}_{\Lambda_0} = \begin{pmatrix} g_{00} & \cdots & g_{0n} \\ \vdots & \ddots & \vdots \\ g_{n0} & \cdots & g_{nn} \end{pmatrix}, \tag{2.17}$$

where the indices denote the position on the imaginary time axes, and

$$g_{ij} = \mathcal{M}_{\pm\mp z}\left(G^{+-}_{\Lambda_0}(i\,d\tau, j\,d\tau), G^{-+}_{\Lambda_0}(i\,d\tau, j\,d\tau), G^{zz}_{\Lambda_0}(i\,d\tau, j\,d\tau)\right) \tag{2.18}$$

is a matrix in component space. Here $G^{+-}_{\Lambda_0}(i\,d\tau, j\,d\tau) = G^{-+}_{\Lambda_0}(j\,d\tau, i\,d\tau)$, and $G^{zz}_{\Lambda_0}(i\,d\tau, j\,d\tau)$ are the initial transverse and longitudinal two point connected correlation functions. Their explicit form is not important at this point, but it is sufficient to state that, while the transverse part is explicitly time-dependent, the longitudinal sector has no quantum dynamics,

$$G^{zz}_{\Lambda_0}(i\,d\tau, j\,d\tau) = \text{constant} \quad \forall(i,j). \tag{2.19}$$

However, this implies that $\boldsymbol{G}_{\Lambda_0}$ is not invertible since its determinant vanishes such that the Legendre transformation (2.10) is not defined.[2] In fact, this non-existence is not a peculiarity of the Heisenberg model, but generally arises whenever one of the operators simultaneously couples to a source field and commutes with the initial Hamiltonian $\mathcal{H}_{\Lambda_0}$. In order to render the above approach well-defined, the deformation scheme needs thus to be chosen such as to ensure a particular quantum dynamics of all operators. This can be achieved, e.g. by coupling the spin operators to an additional bath of fermionic or bosonic particles. An example for this procedure can be found in Ref. [115], where the *poor man's scaling* equations of the Kondo model are re-derived within a similar operator-based FRG formalism. Another possibility is to directly work with the flow equations of the connected correlation functions $G^{\alpha_1\ldots\alpha_n}_{\Lambda,I_1\ldots I_n}$, though one then looses the benefits of the irreducible structure of $\mathcal{L}_\Lambda[\boldsymbol{M}]$. In the following we choose a different approach and define an alternative hybrid functional which allows for initial conditions of decoupled sites, albeit maintaining an irreducible structure with respect to the essential fluctuations.

## 2.3 Hybrid formalism

The formalism here presented constitutes the formal basis of the calculations carried out in the forthcoming chapters. It was first presented in a brief form in the PhD thesis of Krieg [2], and in a slightly different way in our publication Ref. [3]. To this end, the following section introduces an alternative hybrid functional and its subtracted Legendre transform, which possesses two main benefits compared to the original functionals of the previous section. First of all, their construction is based on an asymmetric treatment of the longitudinal and transverse fluctuations, which yields a formalism predestined to investigate Heisenberg-systems in the magnetically ordered phase. Furthermore, the corresponding subtracted Legendre transformed functional remains well-defined in the limit of vanishing interaction $\mathcal{V}_\Lambda(\tau) \to 0$, thus

[2] Note, that since $G^{zz}_{\Lambda_0}(i\,d\tau, j\,d\tau) = \text{constant}$, each $h^z_i$-row of $\boldsymbol{G}_{\Lambda_0}$ is equivalent. Interchanging two rows leaves $\boldsymbol{G}_{\Lambda_0}$ unchanged, but its determinant changes sign. Consequently, $\det \boldsymbol{G}_{\Lambda_0} = -\det \boldsymbol{G}_{\Lambda_0} = 0$.

eventually enabling a controlled calculation and classification of the initial conditions of the respective FRG flow equations.

### 2.3.1 Construction of the hybrid functionals

The following definitions are based on a Hubbard-Stratonovich (HS) decoupling of the longitudinal part of the interaction $\mathcal{V}_\Lambda(\tau)$. To this end, consider in particular the generating functional of the connected correlation functions $\mathcal{G}_\Lambda[\boldsymbol{h}]$ at vanishing longitudinal source $h_i^z(\tau) = 0$. If we decouple the longitudinal part of the interaction within a HS-transformation, the latter can be rewritten as

$$e^{\mathcal{G}_\Lambda[\boldsymbol{h}^\perp, h^z=0]} = \frac{\int \mathcal{D}[\eta] e^{-\frac{1}{2}\sum_{IJ}[\mathbb{J}^z_\Lambda]^{-1}_{IJ}\eta_I\eta_J} \mathrm{Tr}\left[e^{-\beta\mathcal{H}_0}\mathcal{T}e^{\sum_I \eta_I S^z_I} e^{\sum_{I,\alpha=\pm} h^{\bar{\alpha}}_I \cdot S^\alpha_I - \int_\tau \mathcal{V}^\perp_\Lambda(\tau)}\right]}{\int \mathcal{D}[\eta] e^{-\frac{1}{2}\sum_{IJ}[\mathbb{J}^z_\Lambda]^{-1}_{IJ}\eta_I\eta_J}}. \tag{2.20}$$

Here, we collected the transverse part of the interaction (2.1) in $\mathcal{V}^\perp_\Lambda(\tau)$, introduced the shorthand $\int_\tau = \int_0^\beta d\tau$, and regrouped the exchange couplings in the Matrix

$$[\mathbb{J}_\Lambda]_{IJ} = \mathcal{M}_{\pm\mp z}(\mathbb{J}^\perp_{\Lambda,IJ}, \mathbb{J}^\perp_{\Lambda,IJ}, \mathbb{J}^z_{\Lambda,IJ}) = \delta(\tau_i - \tau_j)\mathcal{M}_{\pm\mp z}(J^\perp_{\Lambda,ij}, J^\perp_{\Lambda,ij}, J^z_{\Lambda,ij}). \tag{2.21}$$

Let us now couple a longitudinal source field $s_I$ to the HS-field, and introduce the hybrid functional

$$e^{\mathcal{F}_\Lambda[\boldsymbol{h}^\perp, s]} = \frac{\int \mathcal{D}[\eta] e^{-\frac{1}{2}\sum_{IJ}[\mathbb{J}^z_\Lambda]^{-1}_{IJ}\eta_I\eta_J} \mathrm{Tr}\left[e^{-\beta\mathcal{H}_0}\mathcal{T}e^{\sum_I \eta_I \left(S^z_I + s_I\right)} e^{\sum_{I,\alpha=\pm} h^{\bar{\alpha}}_I \cdot S^\alpha_I - \int_\tau \mathcal{V}^\perp_\Lambda(\tau)}\right]}{\int \mathcal{D}[\eta] e^{-\frac{1}{2}\sum_{IJ}[\mathbb{J}^z_\Lambda]^{-1}_{IJ}\eta_I\eta_J}}. \tag{2.22}$$

While this definition highlights the connection to the underlying HS-decoupling, it is rather cumbersome. An alternative definition which is certainly easier to use can be obtained by integrating out the HS-field, which yields

$$\mathcal{F}_\Lambda[\boldsymbol{h}^\perp, s] = \mathcal{G}_\Lambda\left[\boldsymbol{h}^\perp_i, h^z_i = \sum_j J^z_{\Lambda,ij} s_j\right] + \frac{1}{2}\sum_{IJ} \mathbb{J}^z_{\Lambda,IJ} s_I s_J. \tag{2.23}$$

Note, that in case this HS-decoupling strategy is applied to the whole interaction, the resulting functional is usually identified as the generating functional of the effective interaction [116] and the corresponding functional Taylor coefficients are known as *amputated connected Green functions* [113]. Following this nomenclature we denote the corresponding functional Taylor coefficients.

$$F^{\alpha_1\ldots\alpha_n}_{\Lambda,I_1\ldots I_n} = \left.\frac{\delta^n \mathcal{F}_\Lambda[\boldsymbol{h}^\perp, s]}{\delta j^{\bar{\alpha}_1}_{I_1} \ldots \delta j^{\bar{\alpha}_n}_{I_n}}\right|_{(\boldsymbol{h}^\perp, s)=(0,0)}, \quad j^\alpha_I \in \{h^+_I, h^-_I, s_I\}, \tag{2.24}$$

*partially-amputated connected correlation functions*, i.e. correlation functions, which in a diagrammatic sense are connected with respect to transverse and amputated connected with respect to longitudinal fluctuations. Given the alternative definition (2.23) of $\mathcal{F}_\Lambda[\boldsymbol{h}^\perp, s]$, these correlation functions may be straightforwardly expressed in terms of the corresponding

connected correlation functions $G^{\alpha_1,..,\alpha_n}_{\Lambda,I_1...I_n}$. The longitudinal lowest-order functions are for example given by

$$F^z_{\Lambda,I} = \sum_J \mathbb{J}^z_{\Lambda,IJ} G^z_{\Lambda,J}, \tag{2.25a}$$

$$F^{zz}_{\Lambda,IJ} = \sum_{KL} \mathbb{J}^z_{\Lambda,IK} \mathbb{J}^z_{\Lambda,JL} G^{zz}_{\Lambda,KL} + \mathbb{J}^z_{\Lambda,IJ}. \tag{2.25b}$$

It should be noted at this point, that any correlation function with at least one longitudinal leg involves powers of the longitudinal exchange interaction $J^z_{\Lambda,ij}$, and thus vanishes in the limit $J^z_{\Lambda,ij} \to 0$. At first sight, the functional $\mathcal{F}_\Lambda[\boldsymbol{h}^\perp, s]$ therefore does not seem to give rise to convenient initial conditions if $\mathcal{V}_{\Lambda_0} = 0$. Let us ignore this possible complication for the moment and restrict to the case of a finite interaction. We will explicitly discuss the limit $\mathcal{V}_{\Lambda_0} \to 0$ at the end of section 2.3.2. For now we continue along the lines of the previous section and introduce the generating functional of the corresponding irreducible vertices via a subtracted Legendre transformation.

### Symmetry-breaking

When defining an appropriate subtracted Legendre functional we have to ensure that the possibility of an explicit or spontaneous breaking of the spin rotational symmetry is properly incorporated. As discussed in the introduction, the symmetry-broken phase is characterized by the finite expectation value

$$\langle S^\alpha_I \rangle_\Lambda = \left. \frac{\delta \mathcal{G}_\Lambda[\boldsymbol{h}]}{\delta h^{\bar{\alpha}}_I} \right|_{\boldsymbol{h}=0} = M_\Lambda \delta^{\alpha z}, \tag{2.26}$$

where $M_\Lambda$ presents the $\Lambda$-dependent generalization of the order parameter introduced in section 1.2.2. In the present hybrid formalism this finite expectation value appears in the corresponding zero field limit of the first order amputated connected correlation function

$$\left. \frac{\delta \mathcal{F}_\Lambda[\boldsymbol{j}]}{\delta j^z_I} \right|_{\boldsymbol{j}=0} = \bar{\Phi}^\alpha_{I,\Lambda} = \phi_\Lambda \delta^{\alpha z}, \quad \phi_\Lambda = J^z_{\Lambda,0} M_\Lambda. \tag{2.27}$$

Here we regrouped the source fields $\{\boldsymbol{h}^\perp_I, s_I\}$ into the three component fields $\boldsymbol{j}_I$ introduced in Eq. (2.24) and defined the longitudinal exchange field $\phi_\Lambda$, with $J^z_{\Lambda,0}$ being the $\boldsymbol{k} = 0$ Fourier-coefficient of the exchange coupling $J^z_{ij}$ [cf. Eq. (2.27)]. Due to the finite order parameter the pure Legendre transformation

$$L_\Lambda[\boldsymbol{\Phi}] = \sum_{I,\alpha} \Phi^{\bar{\alpha}}_I j^\alpha_I - \mathcal{F}_\Lambda[\boldsymbol{j}], \tag{2.28}$$

where the $j^\alpha_I$-fields are understood as functionals of the fields $\Phi^\alpha_I \in \{\Phi^+_I, \Phi^-_I, \Phi^z_I\}$ by inverting

$$\Phi^\alpha_I = \frac{\delta \mathcal{F}_\Lambda[\boldsymbol{j}]}{\delta j^{\bar{\alpha}}_I}, \tag{2.29}$$

has an extremum at $\Phi^\alpha_I = \bar{\Phi}^\alpha_I$, since by construction $\delta L_\Lambda[\boldsymbol{\Phi}]/\delta \Phi^{\bar{\alpha}}_I|_{\bar{\boldsymbol{\Phi}}} = j^\alpha_I[\bar{\boldsymbol{\Phi}}] = 0$. In defining the generating functional of the irreducible vertices, it is then convenient to introduce the

regulator terms such that they do not alter the position of this extremum [117]. We therefore consider the fluctuations around the extremal source-configuration,

$$\varphi_I^\alpha \in \{\Phi_I^+, \Phi_I^-, \Phi_I^z - \phi_\Lambda\} \tag{2.30}$$

as the relevant source fields and define the generating functional of the one-line irreducible vertices as

$$\Gamma_\Lambda[\boldsymbol{\varphi}] = \sum_{I,\alpha} \left(\bar{\Phi}_\Lambda^\alpha + \varphi_I^\alpha\right) j_I^{\bar{\alpha}} - \mathcal{F}_\Lambda[\boldsymbol{j}] - \frac{1}{2}\sum_{IJ}\sum_{\alpha\alpha'} \varphi_I^\alpha R_{\Lambda,IJ}^{\alpha\alpha'} \varphi_J^{\alpha'}. \tag{2.31}$$

At this point, we introduced the regulator matrix

$$[\boldsymbol{R}_\Lambda]_{IJ} = \mathcal{M}_{\pm\mp z}(R_{\Lambda,IJ}^\perp, R_{\Lambda,IJ}^\perp, R_{\Lambda,IJ}^\phi), \tag{2.32}$$

where the transverse regulator $R_{\Lambda,IJ}^\perp = R_{\Lambda,ij}^\perp \delta(\tau_i - \tau_j)$ was introduced in Eq. (2.2), and the longitudinal regulator is defined by

$$R_{\Lambda,IJ}^\phi = [\mathbb{J}_\Lambda^z]_{IJ}^{-1} - [\mathbb{J}^z]_{IJ}^{-1}. \tag{2.33}$$

Concerning the definition of the functional $\Gamma_\Lambda[\boldsymbol{\varphi}]$, a few comments are in order: first, please note that $\Gamma_\Lambda[\boldsymbol{\varphi}]$ implicitly also depends on the $\Lambda$-dependent extremal source-configuration $\bar{\Phi}_\Lambda^\alpha$, although this is not highlighted in the argument. In order to prevent any misconceptions, let us furthermore state that the definition (2.31) is not consistent with the one used in Ref. [3]. In this work, the subtracted Legendre transformation is defined with a regulator term coupling to the full longitudinal source field $\Phi_I^z$, and the possibility of a finite vacuum expectation value is subsequently incorporated by expanding the resulting functional around its extremal source-configuration. However, within this formalism the corresponding Taylor coefficients can effectively be identified with the connected correlation functions at finite external source field $h_I^z = (1 - J_{\Lambda,0}^z/J_0^z)\phi_\Lambda$.[3] In the present scheme, this technical inconvenience does not arise, as can be seen by relating the corresponding set of irreducible vertices

$$\Gamma_{\Lambda,I_1\ldots I_n}^{\alpha_1\ldots\alpha_n} = \left.\frac{\delta^n \Gamma_\Lambda[\boldsymbol{\varphi}]}{\delta\varphi_{I_1}^{\bar{\alpha}_1}\ldots\delta\varphi_{I_n}^{\bar{\alpha}_n}}\right|_{\boldsymbol{\varphi}=0}, \tag{2.34}$$

to the partially-amputated connected correlation functions $F_{\Lambda,I_1\ldots I_n}^{\alpha_1\ldots\alpha_n}$ within the tree-expansion which will be formulated in the following section. Thereto, the identity

$$[\boldsymbol{F}[\boldsymbol{j}]]_{IJ}^{\alpha\alpha'} = \left[\left(\boldsymbol{\Gamma}''[\boldsymbol{\varphi}] + \boldsymbol{R}_\Lambda\right)^{-1}\right]_{IJ}^{\bar{\alpha}\bar{\alpha}'}, \tag{2.35}$$

which is derived analogously to the corresponding relation in the original formalism given in Eq. (2.13), is expanded around $\boldsymbol{j} = 0$, respectively $\boldsymbol{\varphi} = 0$. Likewise, the associated Hessian matrices are given by

$$[\boldsymbol{F}_\Lambda[\boldsymbol{j}]]_{IJ}^{\alpha\alpha'} = \frac{\delta^2 \mathcal{F}_\Lambda[\boldsymbol{j}]}{\delta j_I^{\bar{\alpha}} \delta j_J^{\bar{\alpha}'}}, \tag{2.36a}$$

$$\left[\boldsymbol{\Gamma}_\Lambda''[\boldsymbol{\Phi}]\right]_{IJ}^{\alpha\alpha'} = \frac{\delta^2 \Gamma_\Lambda[\boldsymbol{\Phi}]}{\delta\Phi_I^{\bar{\alpha}}\delta\Phi_J^{\bar{\alpha}'}}. \tag{2.36b}$$

[3] In Ref. [3] this does pose practical problems since the longitudinal interaction is not deformed, i.e. $J_\Lambda^z = J^z$.

**Exact FRG flow equations**

Similar to the previously introduced functionals $\mathcal{G}_\Lambda[\boldsymbol{h}]$ and $\mathcal{L}_\Lambda[\boldsymbol{M}]$, the hybrid functional $\mathcal{F}_\Lambda[\boldsymbol{j}]$ and its Legendre-transformed companion $\Gamma_\Lambda[\boldsymbol{\varphi}]$ each satisfy a formally exact flow equation. The flow equation of the hybrid functional $\mathcal{F}_\Lambda[\boldsymbol{j}]$ can be best derived using its definition given in Eq. (2.22), and reads

$$\begin{aligned}\partial_\Lambda \mathcal{F}_\Lambda[\boldsymbol{j}] = \frac{1}{2}\sum_{IJ}\left(\partial_\Lambda \mathbb{J}^\perp_{\Lambda,IJ}\right)\sum_{\alpha=\pm}\left(\frac{\delta^2\mathcal{F}_\Lambda[\boldsymbol{j}]}{\delta j_I^{\bar\alpha}\delta j_J^{\alpha}} + \frac{\delta\mathcal{F}_\Lambda[\boldsymbol{j}]}{\delta j_I^{\bar\alpha}}\frac{\delta\mathcal{F}_\Lambda[\boldsymbol{j}]}{\delta j_J^{\alpha}}\right)\\ - \frac{1}{2}\sum_{IJ}\left(\partial_\Lambda\left[\mathbb{J}^z_\Lambda\right]^{-1}_{IJ}\right)\left(\frac{\delta^2\mathcal{F}_\Lambda[\boldsymbol{j}]}{\delta j_I^{z}\delta j_J^{z}} + \frac{\delta\mathcal{F}_\Lambda[\boldsymbol{j}]}{\delta j_I^{z}}\frac{\delta\mathcal{F}_\Lambda[\boldsymbol{j}]}{\delta j_J^{z}}\right) + \frac{1}{2}\sum_{IJ}\mathbb{J}^z_{\Lambda,IJ}\partial_\Lambda\left[\mathbb{J}^z_\Lambda\right]^{-1}_{IJ}. \quad (2.37)\end{aligned}$$

Along the same lines, the flow of the generating functional of the irreducible vertices $\Gamma_\Lambda[\boldsymbol{\varphi}]$ is straightforwardly obtained from the relation with the functional $\mathcal{F}_\Lambda[\boldsymbol{j}]$ given in Eq. (2.31). Using the identity $j_I^z = \delta\Gamma_\Lambda[\boldsymbol{\varphi}]/\delta\varphi_I^z + \sum_J R^\phi_{\Lambda,IJ}\varphi_J^z$, we obtain,

$$\begin{aligned}\partial_\Lambda\Gamma_\Lambda[\boldsymbol{\varphi}] = \ &(\partial_\Lambda\phi_\Lambda)\left(\sum_I\frac{\delta\Gamma_\Lambda[\boldsymbol{\varphi}]}{\delta\varphi_I^z} + \sum_{IJ}R^\phi_{\Lambda,IJ}\varphi_J^z\right)\\ &- \partial_\Lambda\mathcal{F}_\Lambda[\boldsymbol{j}] - \frac{1}{2}\sum_{IJ}\sum_{\alpha\alpha'}\varphi_i^\alpha\left(\partial_\Lambda R^{\alpha\alpha'}_{\Lambda,IJ}\right)\varphi_J^{\alpha'}. \quad (2.38)\end{aligned}$$

Substituting the expression for $\partial_\Lambda\mathcal{F}_\Lambda[\boldsymbol{j}]$, derived in Eq. (2.37), and using $\partial_\Lambda\left[\mathbb{J}^z_\Lambda\right]^{-1}_{IJ} = \partial_\Lambda R^\phi_{\Lambda,IJ}$ respectively $\partial_\Lambda\left[\mathbb{J}^\perp_\Lambda\right]^{-1}_{IJ} = -\partial_\Lambda R^\perp_{\Lambda,IJ}$, this reduces to

$$\begin{aligned}\partial_\Lambda\Gamma_\Lambda[\boldsymbol{\varphi}] = \frac{1}{2}\sum_{IJ}\left(\left(\partial_\Lambda R^\perp_{\Lambda,IJ}\right)\sum_{\alpha=\pm}\frac{\delta^2\mathcal{F}_\Lambda[\boldsymbol{j}]}{\delta j_I^{\bar\alpha}\delta j_J^{\alpha}} + \left(\partial_\Lambda R^\phi_{\Lambda,IJ}\right)\frac{\delta^2\mathcal{F}_\Lambda[\boldsymbol{j}]}{\delta j_I^{z}\delta j_J^{z}}\right) - \frac{1}{2}\sum_{IJ}\mathbb{J}^z_{\Lambda,IJ}\partial_\Lambda R^\phi_{\Lambda,IJ}\\ + (\partial_\Lambda\phi_\Lambda)\sum_I\frac{\delta\Gamma_\Lambda[\boldsymbol{\varphi}]}{\delta\varphi_I^z} + \sum_{IJ}\varphi_I^z\partial_\Lambda\left(R^\phi_{\Lambda,IJ}\phi_\Lambda\right) - \frac{1}{2}\sum_{IJ}\phi_\Lambda\left(\partial_\Lambda R^\phi_{\Lambda,IJ}\right)\phi_\Lambda. \quad (2.39)\end{aligned}$$

Similar to the previous section, the relation of the corresponding Hessian matrices of $\mathcal{F}_\Lambda[\boldsymbol{j}]$ and $\Gamma_\Lambda[\boldsymbol{\varphi}]$ given in Eq. (2.35), then allows to rewrite this exact flow equation for the generating functional of the irreducible vertices in compact form as

$$\begin{aligned}\partial_\Lambda\Gamma_\Lambda[\boldsymbol{\varphi}] = \frac{1}{2}\mathrm{Tr}\left[\left(\left(\boldsymbol{\Gamma}''_\Lambda[\boldsymbol{\varphi}] + \mathbf{R}_\Lambda\right)^{-1} - \mathbf{J}^z_\Lambda\right)\partial_\Lambda\mathbf{R}_\Lambda\right]\\ + (\partial_\Lambda\phi_\Lambda)\sum_I\frac{\delta\Gamma_\Lambda[\boldsymbol{\varphi}]}{\delta\varphi_I^z} + \sum_{IJ}\varphi_I^z\partial_\Lambda\left(R^\phi_{\Lambda,IJ}\phi_\Lambda\right) - \frac{1}{2}\sum_{IJ}\phi_\Lambda\left(\partial_\Lambda R^\phi_{\Lambda,IJ}\right)\phi_\Lambda, \quad (2.40)\end{aligned}$$

where $\mathbf{J}^z_\Lambda$ is a matrix in all labels with matrix elements $[\mathbf{J}^z_\Lambda]^{\alpha\alpha'}_{IJ} = \delta^{z\alpha}\delta^{z\alpha'}\mathbb{J}^z_{\Lambda,IJ}$. Formally, Eq. (2.40) presents the basis of the forthcoming calculations. In practice it is albeit convenient to express this flow equation as an infinite hierarchy of coupled integro-differential equations, describing the flow of the corresponding irreducible vertices $\Gamma^{\alpha_1\ldots\alpha_n}_{\Lambda,I_1\ldots I_n}$. In order to interpret the corresponding equations, let us first establish the relation of the irreducible vertices $\Gamma^{\alpha_1\ldots\alpha_n}_{\Lambda,I_1\ldots I_n}$ to the physically relevant connected correlation functions $G^{\alpha_1\ldots\alpha_n}_{\Lambda,I_1\ldots I_n}$. In the course of this, we will furthermore show, that the Legendre transformation scheme defined in Eqs. (2.31) and (2.29) remains well-defined in the limit $\mathcal{V}_{\Lambda_0}\to 0$.

### 2.3.2 Tree expansion

The following section establishes the relations of the functional Taylor coefficients of the three functionals $\mathcal{G}_\Lambda[\boldsymbol{h}]$, $\mathcal{F}_\Lambda[\boldsymbol{j}]$ and $\Gamma_\Lambda[\boldsymbol{\varphi}]$. For this purpose, let us switch to momentum-frequency representation and introduce the Fourier expansion of the source fields

$$\{h_I^\alpha, j_I^\alpha, \varphi_I^\alpha\} = \int_K e^{i(\boldsymbol{k}\cdot\boldsymbol{r}_i - \omega_n \tau)} \{h_K^\alpha, j_K^\alpha, \varphi_K^\alpha\}. \tag{2.41}$$

Here, we introduced the abbreviation $\int_K = (\beta N)^{-1} \sum_{\boldsymbol{k},\omega_n}$, where the momentum-sum runs over all momenta $\boldsymbol{k}$ inside the first Brillouin-zone of the underlying lattice. Furthermore, $K = (\boldsymbol{k}, i\omega_n)$ is a collective label which contains momenta and the bosonic Matsubara frequencies $\omega_n = 2\pi n/\beta$ with $n \in \mathbb{Z}$. We can now formally expand the three functionals in a Taylor series around the origin in field space as

$$\begin{aligned}
\mathcal{G}_\Lambda[\boldsymbol{\varphi}] = \mathcal{G}_\Lambda[0] &+ \int_K G^z_K h^z_{-K} + \int_{K_1K_2} \left( G^{+-}_{\Lambda,K_1K_2} h^-_{-K_1} h^+_{-K_2} + \frac{1}{2!} G^{zz}_{\Lambda,K_1K_2} h^z_{-K_1} h^z_{-K_2} \right) \\
&+ \int_{K_1\ldots K_3} \left( G^{+-z}_{\Lambda,K_1K_2K_3} h^-_{-K_1} h^+_{-K_2} h^z_{-K_3} + \frac{1}{3!} G^{zzz}_{\Lambda,K_1K_2K_3} h^z_{-K_1} h^z_{-K_2} h^z_{-K_3} \right) \\
&+ \int_{K_1\ldots K_4} \left( \frac{1}{(2!)^2} G^{++--}_{\Lambda,K_1K_2K_3K_4} h^-_{-K_1} h^-_{-K_2} h^+_{-K_3} h^+_{-K_4} + \frac{1}{2!} G^{+-zz}_{\Lambda,K_1K_2K_3K_4} h^-_{-K_1} h^+_{-K_2} h^z_{-K_3} h^z_{-K_4} \right. \\
&\qquad \left. + \frac{1}{4!} G^{zzzz}_{\Lambda,K_1K_2K_3K_4} h^z_{-K_1} h^z_{-K_2} h^z_{-K_3} h^z_{-K_4} \right) + \ldots \,,
\end{aligned} \tag{2.42a}$$

respectively,

$$\mathcal{F}_\Lambda[\boldsymbol{j}] = \mathcal{F}_\Lambda[0] + \int_K F^z_K j^z_{-K} + \int_{K_1K_2} \left( F^{+-}_{\Lambda,K_1K_2} j^-_{-K_1} j^+_{-K_2} + \frac{1}{2!} F^{zz}_{\Lambda,K_1K_2} j^z_{-K_1} j^z_{-K_2} \right) + \ldots, \tag{2.42b}$$

$$\Gamma_\Lambda[\boldsymbol{\varphi}] = \Gamma_\Lambda[0] + \int_{K_1K_2} \left( \Gamma^{+-}_{\Lambda,K_1K_2} \varphi^-_{-K_1} \varphi^+_{-K_2} + \frac{1}{2!} \Gamma^{zz}_{\Lambda,K_1K_2} \varphi^z_{-K_1} \varphi^z_{-K_2} \right) + \ldots \,. \tag{2.42c}$$

The corresponding Taylor coefficients

$$A^{\alpha_1\ldots\alpha_n}_{\Lambda,K_1\ldots K_n} = \left. \frac{\delta^n \mathcal{A}_\Lambda[\boldsymbol{x}]}{\delta x^{\bar{\alpha}_1}_{-K_1} \ldots\, \delta x^{\bar{\alpha}_n}_{-K_n}} \right|_{\boldsymbol{x}=0} = \delta\left(K_1 + \ldots + K_n\right) A^{\alpha_1,\ldots\alpha_n}_\Lambda(K_1, \ldots, K_n), \tag{2.43}$$

with $\mathcal{A}_\Lambda[\boldsymbol{x}] \in \{\mathcal{G}_\Lambda[\boldsymbol{h}], \mathcal{F}_\Lambda[\boldsymbol{j}], \Gamma_\Lambda[\boldsymbol{\varphi}]\}$ and $\delta(K) = \beta N \delta_{\omega,0} \delta(\boldsymbol{k})$ , should be interpreted as the Fourier space versions of the correlation functions and irreducible vertices introduced in Eqs. (2.6), (2.24) and (2.34). The relation of these three sets of coefficients $G^{\alpha_1,\ldots\alpha_n}_{\Lambda,K_1\ldots K_n}$, $F^{\alpha_1,\ldots\alpha_n}_{\Lambda,K_1\ldots K_n}$ and $\Gamma^{\alpha_1,\ldots\alpha_n}_{\Lambda,K_1\ldots K_n}$ can be constructed by combining Eq. (2.22), where the hybrid functional $\mathcal{F}_\Lambda[\boldsymbol{j}]$ is expressed in terms of the original functional $\mathcal{G}_\Lambda[\boldsymbol{h}]$, with the momentum frequency analogue of the relation of the Hessian matrices given in Eq. (2.35),

$$[\boldsymbol{F}_\Lambda[\boldsymbol{j}]]_{aa'} = \left[ \left( \boldsymbol{\Gamma}''_\Lambda[\boldsymbol{\varphi}] + \boldsymbol{R}_\Lambda \right)^{-1} \right]_{\bar{a}\bar{a}'}. \tag{2.44}$$

At this point, we regrouped the momentum-frequency label $K = (\boldsymbol{k}, i\omega)$ and the component index $\alpha = \{+, -, z\}$ in the collective label

$$(a, \bar{a}) = ((K, \alpha), (-K, \bar{\alpha})), \tag{2.45}$$

and the elements of the Hessian matrices $\boldsymbol{F}_\Lambda[\boldsymbol{h}, s]$ and $\boldsymbol{\Gamma}''_\Lambda[\boldsymbol{m}, \phi]$ are given by

$$[\boldsymbol{F}_\Lambda[\boldsymbol{j}]]_{aa'} = F^{\alpha\alpha'}_{\Lambda,KK'}[\boldsymbol{j}], \tag{2.46a}$$

$$\left[\boldsymbol{\Gamma}''_\Lambda[\boldsymbol{\Phi}]\right]_{aa'} = \Gamma^{\alpha\alpha'}_{\Lambda,KK'}[\boldsymbol{\Phi}]. \tag{2.46b}$$

Furthermore, we introduced the momentum-frequency representation of the regulator matrix (2.8),

$$[\boldsymbol{R}_\Lambda]_{KK'} = \mathcal{M}_{\pm\mp z}\left(R^\perp_{\Lambda,KK'}, R^\perp_{\Lambda,KK'}, R^\phi_{\Lambda,KK'}\right) = \delta(K-K')\mathcal{M}_{\pm\mp z}\left(R^\perp_{\Lambda,\boldsymbol{k}}, R^\perp_{\Lambda,\boldsymbol{k}}, R^\phi_{\Lambda,\boldsymbol{k}}\right), \tag{2.47}$$

with the longitudinal and transverse regulators given by

$$R^\perp_{\Lambda,\boldsymbol{k}} = J^\perp_{\boldsymbol{k}} - J^\perp_{\Lambda,\boldsymbol{k}}, \tag{2.48a}$$

$$R^\phi_{\Lambda,\boldsymbol{k}} = \frac{1}{J^z_{\Lambda,\boldsymbol{k}}} - \frac{1}{J^z_{\boldsymbol{k}}}. \tag{2.48b}$$

The relation of the Hessian matrices given in Eq. (2.44) can now be used to systematically construct the higher order vertices $\Gamma^{\alpha_1\ldots\alpha_n}_{\Lambda,K_1..K_n}$ in terms of the amputated connected correlation functions $F^{\alpha_1\ldots\alpha_n}_{\Lambda,K_1..K_n}$. At this point, we restrict to the relations of the second order coefficients, while the third and fourth order relations can be found in appendix B.1. Setting $\boldsymbol{\varphi} = 0$ and $\boldsymbol{j} = 0$ in Eq. (2.44) and introducing the notation

$$A^{\alpha\alpha'}_{\Lambda,KK'} = \delta(K + K')A^{\alpha\alpha'}_\Lambda(K), \tag{2.49}$$

we obtain

$$F^{+-}_\Lambda(K) = F^{-+}_\Lambda(-K) = \left[\Gamma^{+-}_\Lambda(K) + R^\perp_{\Lambda,\boldsymbol{k}}\right]^{-1}, \tag{2.50a}$$

$$F^{zz}_\Lambda(K) = F^{zz}_\Lambda(-K) = \left[\Gamma^{zz}_\Lambda(K) + R^\phi_{\Lambda,\boldsymbol{k}}\right]^{-1}, \tag{2.50b}$$

where the symmetries $F^{+-}_\Lambda(K) = F^{-+}_\Lambda(-K)$ and $F^{zz}_\Lambda(K) = F^{zz}_\Lambda(-K)$ follow from the properties of the time ordering operator. Furthermore, the relation between the hybrid functional $\mathcal{F}_\Lambda[\boldsymbol{j}]$ and the original functional $\mathcal{G}_\Lambda[\boldsymbol{h}]$ given in Eq. (2.23) allows to express the amputated-connected correlation functions in terms of the connected correlation functions. The transverse two-point correlation functions are equivalent

$$G_\Lambda(K) = G^{+-}_\Lambda(K) = F^{+-}_\Lambda(K), \tag{2.51}$$

whereas the relation of the longitudinal two-point functions is given by the Fourier transformed version of Eq. (2.25b)

$$F_\Lambda(K) = F^{zz}_\Lambda(K) = \left(J^z_{\Lambda,\boldsymbol{k}}\right)^2 G^{zz}_\Lambda(K) + J^z_{\Lambda,\boldsymbol{k}}. \tag{2.52}$$

Here, we introduced the abbreviations $G_\Lambda(K)$ and $F_\Lambda(K)$, in the following referred to as transverse and longitudinal propagator. In chapter 3 it is shown that the former is simply a $\Lambda$-dependent version of the common spin wave propagator, while the latter should be interpreted as effective longitudinal exchange interaction. Substituting these identities into the expressions of the two point vertices in Eq. (2.50b) and using the expression (2.48) for the regulator terms finally yields the tree expansion of the two point vertices

$$\Gamma^{+-}_\Lambda(K) = G^{-1}_\Lambda(K) + J^\perp_{\Lambda,\boldsymbol{k}} - J^\perp_{\boldsymbol{k}}, \tag{2.53a}$$

$$\begin{aligned}\Gamma^{zz}_\Lambda(K) &= \frac{1}{F_\Lambda(K)} - R^\phi_{\Lambda,\boldsymbol{k}} = \frac{1}{J^z_{\Lambda,\boldsymbol{k}}\left[1 + J^z_{\Lambda,\boldsymbol{k}} G^{zz}_\Lambda(K)\right]} - \left(\frac{1}{J^z_{\Lambda,\boldsymbol{k}}} - \frac{1}{J^z_{\boldsymbol{k}}}\right) \\ &= -\frac{G^{zz}_\Lambda(K)}{1 + J^z_{\Lambda,\boldsymbol{k}} G^{zz}_\Lambda(K)} + \frac{1}{J^z_{\boldsymbol{k}}}.\end{aligned} \tag{2.53b}$$

The relations of the higher order coefficients can be obtained analogously. We refer at this point to appendix B.1, where the explicit connections of the third and fourth order coefficients are derived.

### The hybrid functionals in the limit of decoupled sites

Please recall, that the original formalism presented in section 2.2 had the disadvantage that the inverse of the relations $M^\alpha_I(\boldsymbol{h})$, defined in Eq. (2.11), possibly does not exist. In particular, this became manifest in the case of decoupled sites, where the lack of longitudinal quantum dynamics renders the corresponding Jacobian matrix non-invertible. In the present formalism, the situation appears to be even more complicated, given that the longitudinal Taylor coefficients of the respective Jacobian matrix $\boldsymbol{F}_\Lambda[\boldsymbol{j} = 0]$ involve powers of $J^z_{\Lambda,ij}$ and thus vanish completely if the sites are decoupled. Expressing the source fields $j^\alpha_I$ in terms of the Legendre source fields $\varphi^\alpha_I$ seems thus again not possible when choosing an initially vanishing interaction $\mathcal{V}_{\Lambda_0} = 0$. However, in contrast to the previous section, the corresponding vertices can still be unambiguously defined by considering the limiting case

$$\Gamma_{\Lambda_0}[\boldsymbol{\varphi}] = \lim_{\Lambda\to\Lambda_0} \Gamma_\Lambda[\boldsymbol{\varphi}], \tag{2.54}$$

which remains well-defined thanks to the regulator terms which were added in the definition of $\Gamma_\Lambda[\boldsymbol{\varphi}]$, cf. Eq. (2.31). Here, the relation of the second order coefficients given in Eq. (2.53b) can serve as an illustrative example. The initial longitudinal two point vertex

$$\Gamma^{zz}_{\Lambda_0}(K) = \lim_{\Lambda\to\Lambda_0}\left(\frac{1}{F_\Lambda(K)} - R^\phi_{\Lambda,\boldsymbol{k}}\right) = -G^{zz}_{\Lambda_0}(K) + \frac{1}{J^z_{\boldsymbol{k}}}, \tag{2.55}$$

remains finite, although the terms $F^{-1}_\Lambda(K)$ and $R^\phi_{\Lambda,\boldsymbol{k}}$ each separately diverge if $J^z_{\Lambda_0,\boldsymbol{k}} = 0$. As can be seen from the according relations derived in appendix B.1, this cancellation mechanism is not a peculiarity of the second order relation but enters the tree expansion of all higher order vertices in a similar way. It should thus be kept in mind that the present approach rests on an inversion of the relations $\varphi^\alpha_I(\boldsymbol{j})$ at finite interaction $\mathcal{V}_\Lambda$ and a subsequent definition of the corresponding initial irreducible vertices by taking the $\Lambda \to \Lambda_0$ limit of the respective tree-expanded expressions.

### 2.3.3 Vertex expansion of the flow equation

Having established the different vertex expansions, we are now in the position to express the exact flow equation of the functional $\Gamma_\Lambda[\boldsymbol{\varphi}]$ in a computationally more accessible form. Substituting the corresponding tree expansion given in Eq. (2.42c) into the appropriate flow equation (2.40), and comparing the coefficients on both sides allows us to derive an infinite hierarchy of coupled integro-differential equations, which describe the flow of the vertices $\Gamma^{\alpha_1\ldots\alpha_n}_{\Lambda,K_1\ldots K_n}$. The flow of the constant term $\Gamma_\Lambda[0] = \beta N f_\Lambda$, where $f_\Lambda$ can be identified with the free energy per lattice site, is accordingly obtained as

$$\partial_\Lambda f_\Lambda = \int_K G_\Lambda(K)\partial_\Lambda R^\perp_{\Lambda,\boldsymbol{k}} + \int_K \frac{1}{2}\left[F_\Lambda(K) - J^z_{\Lambda,\boldsymbol{k}}\right]\partial_\Lambda R^\phi_{\Lambda,\boldsymbol{k}} - \frac{1}{2}\phi^2_\Lambda \partial_\Lambda R^\phi_{\Lambda,0}. \tag{2.56}$$

Next, consider the flow equation of the exchange field $\phi_\Lambda$. Following the construction-scheme discussed in the previous section, this can be obtained from the condition that the expansion of the generating functional $\Gamma_\Lambda[\boldsymbol{\varphi}]$ does not have a term linear in the fluctuations $\varphi^\alpha_K$ (see also Refs. [113, 117]). This is guaranteed if the flow of the exchange field $\phi_\Lambda$ satisfies

$$\begin{aligned}\Gamma^{zz}_\Lambda(0)\partial_\Lambda\phi_\Lambda = &-\partial_\Lambda\left(R^\phi_{\Lambda,0}\phi_\Lambda\right)\\ &-\int_K \dot{G}_\Lambda(K)\Gamma^{+-z}_\Lambda(K,-K,0) - \frac{1}{2}\int_K \dot{F}_\Lambda(K)\Gamma^{zzz}_\Lambda(K,-K,0),\end{aligned} \tag{2.57}$$

where we introduced the transverse and longitudinal single-scale propagators

$$\dot{G}_\Lambda(K) = -\left[G_\Lambda(K)\right]^2\partial_\Lambda R^\perp_{\Lambda,\boldsymbol{k}}, \tag{2.58a}$$

$$\dot{F}_\Lambda(K) = -\left[F_\Lambda(K)\right]^2\partial_\Lambda R^\phi_{\Lambda,\boldsymbol{k}}. \tag{2.58b}$$

Note, that the exchange field is given by $\phi_\Lambda = J^z_{\Lambda,0}M_\Lambda$, hence Eq. (2.57) can be recast in a form which gives access to the flow of the magnetization $M_\Lambda$, as will be shown in the following chapter. Finally, let us specify the flow equations for the transverse and longitudinal two-point vertices,

$$\begin{aligned}\partial_\Lambda\Gamma^{+-}_\Lambda(K) = &\,\Gamma^{+-z}_\Lambda(K,-K,0)\partial_\Lambda\phi_\Lambda\\ &-\int_Q \left[G_\Lambda(Q)F_\Lambda(Q-K)\right]^\bullet\Gamma^{+-z}_\Lambda(K,-Q,Q-K)\Gamma^{+-z}_\Lambda(Q,-K,K-Q)\\ &+\int_Q \dot{G}_\Lambda(Q)\Gamma^{+-zz}_\Lambda(K,Q,-Q,-K) + \frac{1}{2}\int_Q \dot{F}_\Lambda(Q)\Gamma^{+-zz}_\Lambda(K,-K,Q,-Q),\end{aligned} \tag{2.59}$$

$$\begin{aligned}\partial_\Lambda\Gamma^{zz}_\Lambda(K) = &\,\Gamma^{zzz}_\Lambda(K,-K,0)\partial_\Lambda\phi_\Lambda\\ &-\int_Q \left[G_\Lambda(Q)G_\Lambda(Q-K)\right]^\bullet\Gamma^{+-z}_\Lambda(Q,K-Q,-K)\Gamma^{+-z}_\Lambda(Q-K,-Q,K)\\ &-\frac{1}{2}\int_Q \left[\dot{F}_\Lambda(Q)F_\Lambda(Q-K)\right]^\bullet\Gamma^{zzz}_\Lambda(Q,K-Q,-K)\Gamma^{zzz}_\Lambda(Q-K,-Q,K)\\ &+\int_Q \dot{G}_\Lambda(Q)\Gamma^{+-zz}_\Lambda(Q,-Q,K,-K) + \frac{1}{2}\int_Q \dot{F}_\Lambda(Q)\Gamma^{zzzz}_\Lambda(Q,-Q,K,-K),\end{aligned} \tag{2.60}$$

where we introduced the shorthand

$$[G_\Lambda(K_1)G_\Lambda(K_2)]^\bullet = \dot{G}_\Lambda(K_1)G_\Lambda(K_2) + \dot{G}_\Lambda(K_2)G_\Lambda(K_1). \tag{2.61}$$

A graphical representation of the flow equations (2.57), (2.59) and (2.60) is shown in Fig. 2.1. For reason of compactness, we will not discuss any of the higher order flow equations at this point. In principle these can be constructed analogously, and we postpone their introduction to chapter 4, where the flow of the three and four point vertices will be discussed in a certain truncation scheme.

---

The above set of coupled integro-differential equations completes the present chapter. Up to this point, no approximations were applied. Hence, all static and dynamic properties of the Heisenberg model are included in the presented tower of FRG equations, and should thus be extractable if meaningful approximation strategies can be found. This is the scope of the following two chapters.

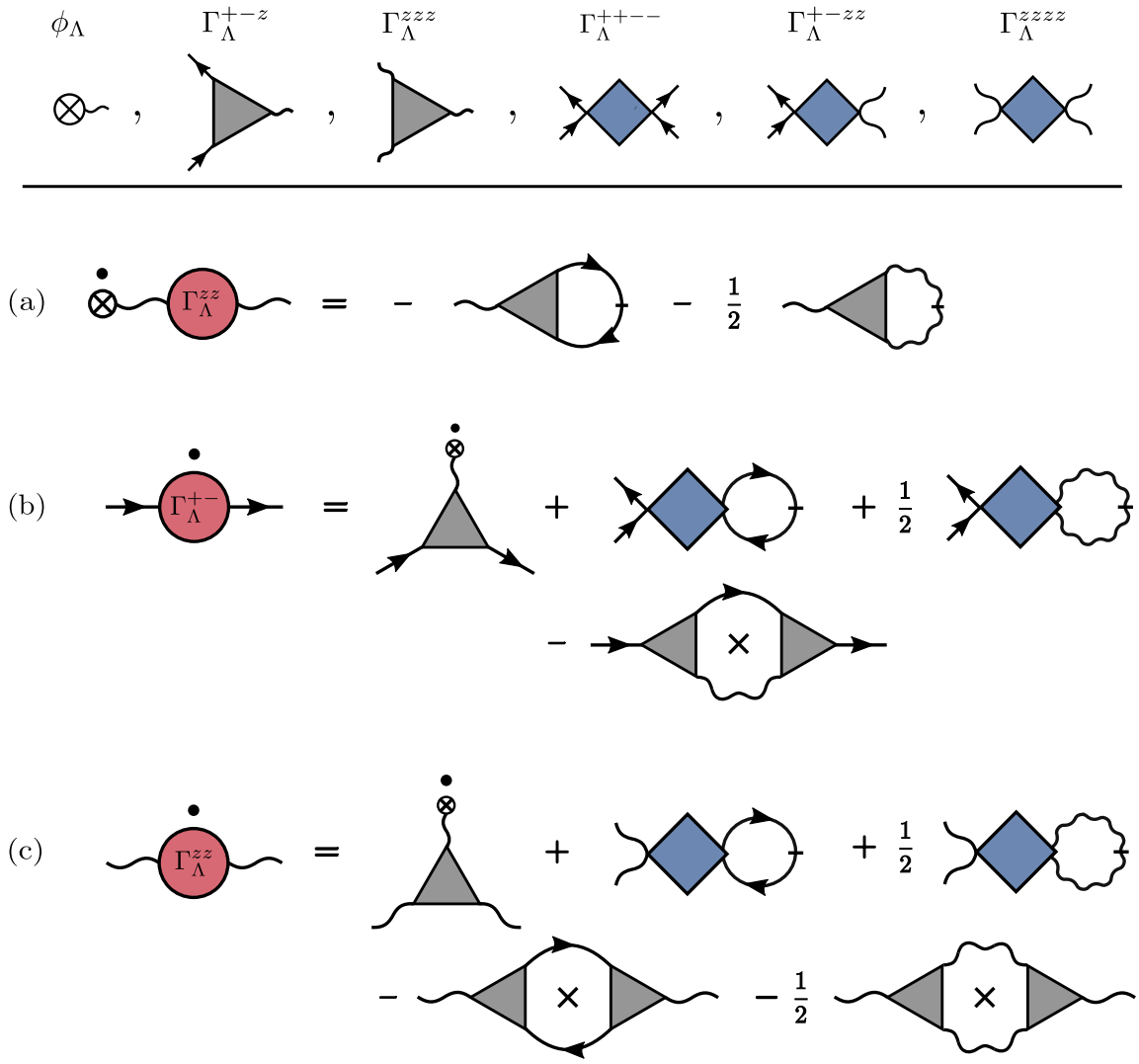


Figure 2.1: Graphical representation of the exact FRG flow equations (2.57), (2.59) and (2.60) for (a) the exchange field $\phi_\Lambda$, (b) the transverse two-point vertex $\Gamma^{+-}_\Lambda(K)$, and (c) for the longitudinal two-point vertex $\Gamma^{zz}_\Lambda(K)$. The nomenclature of the different symbols is depicted at the top. Outgoing (incoming) arrowed legs represent the spherical component of the transverse magnetization field $\varphi^+_K$ ($\varphi^-_K$), and the wavy legs are associated with the fluctuating part $\varphi^z_K$ of the longitudinal exchange field. A dot above a symbol represents the derivative of the same with respect to the deformation parameter $\Lambda$. Closed loops of arrowed and wavy lines represent transverse and longitudinal propagators, while lines with an extra slash represent the corresponding single-scale propagators. A diagram with a cross inside the loop is equivalent to the sum of two similar diagrams with each of the propagators successively replaced by the corresponding single-scale propagator [cf. Eq. (2.61)].

# Chapter 3

# Thermodynamics in low dimensions

## 3.1 Outline

As a first application of the spin FRG formalism, this chapter provides an analysis of the thermodynamic response functions of the $D$-dimensional isotropic Heisenberg ferromagnet at temperatures and external magnetic fields both small compared to the intrinsic exchange interaction. In particular, we will derive expressions for the magnetization and the isothermal susceptibility and briefly discuss the corresponding specific heat in the following. Given the long history of the analysis of the Heisenberg model, the field- and temperature-dependence of these response functions is well established and their calculation therefore presents an excellent benchmark problem. To this end, recall, that the low-temperature phase behavior of the system is distinctly different in dimensions $D = 3$ and $D \leq 2$. While the three-dimensional model is magnetically ordered and therefore well described by conventional spin-wave theory [21, 98, 99], the spin rotational symmetry cannot be spontaneously broken at finite temperatures in the lower-dimensional case. A naive application of this spin-wave theory breaks down in the limit $H \to 0$ and other approaches are thus required in order to describe the low-dimensional model in the vicinity of the critical point $(H_c, T_c) = (0, 0)$. In one dimension a series of variations of the Bethe ansatz technique - mostly developed by M. Takahashi and co-workers - was especially successful in calculating the thermodynamic properties of the $S = 1/2$ Heisenberg ferromagnet [118–120]. This includes in particular the explicit form of the zero temperature divergence of the isothermal zero-field susceptibility derived in Ref. [119]. Likewise, the low-temperature thermodynamics of the two-dimensional ferromagnet have been investigated by various methods, many of whom were developed in the late 80's, when a renewed interest in two-dimensional quantum spin systems was triggered by the discovery of high-temperature superconductivity. Explicit calculations of the temperature dependence of the zero-field susceptibilities and the spin-spin correlation length were for example carried out using Schwinger-Boson techniques [103], renormalization-group approaches [121] and variations of conventional spin-wave theory [122]. In addition, various authors have calculated the thermodynamic response functions at finite field, e.g. using Green-function techniques [106, 123, 124], exact diagonalization [109] and Monte Carlo methods [125, 126].

The following now presents an independent calculation of the static magnetic properties with a focus on the one and two-dimensional model. According to the general idea of the

spin FRG we thereby start from a system of uncoupled sites and incorporate the interaction effects by explicitly solving the hierarchy of flow equations, which were derived at the end of the previous chapter. This is done in several truncation steps, each building on one another. Note, that the presence of an external magnetic field is hereby crucial, since it assures well-defined initial vertices and allows for the possibility to truncate the hierarchy of FRG flow equations in a controlled way. Fortunately, the qualitative behavior of the magnetization and the susceptibility in the zero-field limit can - to a large extent - still be extracted by extrapolation.

## 3.2 Spin FRG formulation

The following analysis is based on the exact flow equation for the hybrid generating functional derived in Eq. (2.40) of chapter 2. In particular, we determine in the following the magnetization curves $M(H,T)$ and the corresponding isothermal susceptibility $\chi^I(H,T) = \partial_H M(H,T)$ in $D \leq 2$, as functions of temperature and magnetic field, by solving the flow equation (2.57) of the exchange field $\phi_\Lambda$. In addition, the specific heat, which can be obtained from the flow of the free energy per lattice site $f_\Lambda$, derived in Eq. (2.56), will also briefly be discussed.

### 3.2.1 Deformation scheme

Let us shortly outline the general deformation scheme of the transverse and longitudinal exchange interactions, $J^\perp_{\Lambda,\boldsymbol{k}}$ and $J^z_{\Lambda,\boldsymbol{k}}$, which will be chosen in the following. In order to establish the relation of our approach to the conventional formulations of spin-wave theory, we choose here a scheme, where the transverse and longitudinal interactions are switched on one after another. In the first part of the flow, we turn on the longitudinal interaction and solve the flow equations within a *tadpole* truncation. This recovers the familiar mean-field solution. In a second step, the transverse interaction is then turned on, which amounts to analyzing the effect of the transverse dynamics on the thermodynamic properties of the system. Formally, the whole deformation process can be encapsulated in terms of the deformation parameter $\Lambda$ as

$$J^\alpha_{\Lambda,\boldsymbol{k}} = \Big(\delta^{\alpha z}\left[\Theta(-\Lambda)(\Lambda+1)+\Theta(\Lambda)\right] + \delta^{\alpha\perp}\Theta(\Lambda)\Lambda\Big)\, J_{\boldsymbol{k}} \quad , \quad \Lambda \in (-1,1), \tag{3.1}$$

which is graphically summarized in Fig. 3.1. Note, that the same scheme will also be employed in chapter 4, where the longitudinal spin-spin dynamics are analyzed. Note, that this is in principle not the optimal scheme to analyze the model close to the critical point $(H_c, T_c) = (0,0)$. Akin to the conventional FRG descriptions of critical phenomena, a regularization of the long-wavelength modes of the exchange interaction combined with a wise rescaling of the flowing quantities should be more appropriate in this region [113, 114]. While such a scheme was partially applied in our original publication [3], the essential critical properties can also be inferred from the present deformation process and we therefore adhere to the latter for reasons of clarity and consistency.

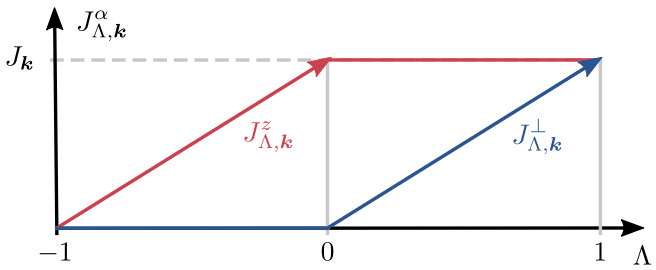


Figure 3.1: Anisotropic deformation scheme of the longitudinal and transverse exchange interaction $J^{\alpha}_{\Lambda,\boldsymbol{k}}$, with $\alpha \in (\perp, z)$, employed in the present chapter. Starting from a system of decoupled spins at $\Lambda_0 = -1$, the longitudinal interaction is gradually switched on and fully restored at $\Lambda = 0$. In the second part of the flow, from $\Lambda = 0$ to $\Lambda = 1$, the same procedure is applied to the transverse interaction.

### 3.2.2 Initial conditions

The initial conditions of the ensemble of FRG flow equations are obtained by calculating the connected correlation functions of a single spin subject to an uniform magnetic field $\boldsymbol{H} = H\boldsymbol{e}^z$. The detailed expressions of the respective frequency representations $G^{\alpha_1\ldots\alpha_n}_{\Lambda_0}(i\omega_1,\ldots,i\omega_n)$ are derived in App. B.2 and the corresponding initial vertices $\Gamma^{\alpha_1\ldots\alpha_n}_{\Lambda_0}(i\omega_1,\ldots,i\omega_n)$ can be obtained by the limiting procedure outlined at the end of section 2.3.2: Substituting the initial connected correlation functions, derived in Eqs. (B.21)-(B.23) of App. B.2, in the tree expansion relations Eqs. (B.9)-(B.13), formulated in App. B.1, the lowest order transverse and mixed transverse-longitudinal vertices read,

$$\Gamma^{+-}_{\Lambda_0}(K) = G^{-1}_{\Lambda_0}(i\omega) - J_{\boldsymbol{k}}, \tag{3.2a}$$

$$\Gamma^{+-z}_{\Lambda_0}(i\omega_1, i\omega_2, i\omega_3) = \frac{1}{b_{\Lambda_0}}\left[1 - \delta(\omega_3) b'_{\Lambda_0} G^{-1}_{\Lambda_0}(-i\omega_2)\right] \tag{3.2b}$$

$$\begin{aligned}\Gamma^{++--}_{\Lambda_0}(i\omega_1, i\omega_2, i\omega_3, i\omega_4) = \frac{1}{b^2_{\Lambda_0}}\Big[&G^{-1}_{\Lambda_0}(-i\omega_3) + G^{-1}_{\Lambda_0}(-i\omega_4) \\ &- \left[\delta(\omega_1+\omega_3) + \delta(\omega_1+\omega_4)\right] b'_{\Lambda_0} G^{-1}_{\Lambda_0}(-i\omega_3) G^{-1}_{\Lambda_0}(-i\omega_4)\Big]\end{aligned} \tag{3.2c}$$

$$\begin{aligned}\Gamma^{+-zz}_{\Lambda_0}(i\omega_1, i\omega_2, i\omega_3, i\omega_4) = \frac{1}{b^2_{\Lambda_0}}\Big[&\delta(\omega_3)\delta(\omega_4)[2(b')^2 - b_{\Lambda_0} b''_{\Lambda_0}] G^{-1}_{\Lambda_0}(-i\omega_2) \\ &- \left[\delta(\omega_3) + \delta(\omega_4)\right] b'_{\Lambda_0}\Big].\end{aligned} \tag{3.2d}$$

Here, we introduced the initial transverse propagator

$$G_{\Lambda_0}(i\omega) = \frac{b_{\Lambda_0}}{H - i\omega}, \tag{3.3}$$

and the abbreviations $\delta(\omega) = \beta\delta_{\omega,0}$, $b_{\Lambda_0} = b(\beta H)$, and $b^{(n)}_{\Lambda_0} = b^{(n)}(\beta H)$, where,

$$b(y) = \left(S + \frac{1}{2}\right)\coth\left[\left(S + \frac{1}{2}\right)y\right] - \frac{1}{2}\coth\left[\frac{y}{2}\right], \tag{3.4}$$

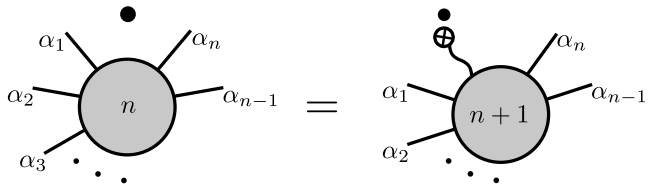


Figure 3.2: Graphical representation of the mean-field (tadpole) truncation of the FRG flow equation (3.8) for the irreducible vertices with $n \geq 2$. The nomenclature is the same as in Fig. 2.1

is the spin-$S$ Brillouin function, and $b^{(n)}(y)$ its nth-derivative. Analogously, the purely longitudinal vertices are given by

$$\Gamma^{zz}_{\Lambda_0}(K) = -\delta(\omega) b'_{\Lambda_0} + \frac{1}{J_{\boldsymbol{k}}}, \tag{3.5a}$$

$$\Gamma^{zzz}_{\Lambda_0}(i\omega_1, i\omega_2, i\omega_3) = -\delta(\omega_1)\delta(\omega_1)\delta(\omega_1) b''_{\Lambda_0}, \tag{3.5b}$$

$$\vdots$$

$$\Gamma^{z\ldots z}_{\Lambda_0}(i\omega_1, \ldots, i\omega_n) = -\delta(\omega_1)\ldots\delta(\omega_n) b^{(n)}_{\Lambda_0}. \tag{3.5c}$$

## 3.3 Solving the vertex-expanded flow equation

Having established proper initial conditions we are now in the position to tackle the vertex expansion of the flow equation of the hybrid functional, derived in section 2.3.3 on page 44. As a warm-up problem, let us begin by constructing the familiar mean-field solutions from these equations. An analysis of the resulting vertices then reveals that a controlled truncation of the infinite hierarchy of flow equations becomes accessible at low temperatures.

### 3.3.1 Mean-field truncation

In the literature, mean-field theory of localized spin systems is commonly introduced by expressing the spin operators in terms of fluctuations $\delta \boldsymbol{S}_i$ around the spatially constant order parameter, i.e. $\boldsymbol{S}_i = M\boldsymbol{e}^z + \delta \boldsymbol{S}_i$ [127]. Neglecting terms of the order $\mathcal{O}(\delta \boldsymbol{S}^2)$ in the corresponding Hamiltonian then yields an effective single-site description. For the Heisenberg model, the mean-field Hamiltonian reads

$$\mathcal{H}_{\mathrm{MF}} = -(H + J_0 M_0) \sum_i S^z_i, \tag{3.6}$$

where the mean-field magnetization $M_0$ is determined by the self consistency equation

$$\langle S^z_i \rangle_{\mathrm{MF}} = \frac{\mathrm{Tr}\ S^z_i e^{-\beta \mathcal{H}_{\mathrm{MF}}}}{\mathrm{Tr}\ e^{-\beta \mathcal{H}_{\mathrm{MF}}}} = b\left(\beta(H + J_0 M_0)\right) = M_0. \tag{3.7}$$

In general, this approximation describes the system well in $D > 4$, respectively in the limit of a long range exchange interaction [127]. To recover the Mean field description, we should hence assume, that the Fourier transform of the interaction is dominated by momenta $|\boldsymbol{k}| < \kappa_0$,

where $1/(\kappa_0 a) \gg 1$ is a measure of the interaction radius in units of the underlying lattice spacing $a$. In this case, each loop integration in the FRG flow equations yields a factor $\kappa_0^D$ and to lowest order in $\kappa_0$ we can simply neglect all loop contributions. The flow equations for the irreducible vertices with more than one external leg then simplify to

$$\partial_\Lambda \Gamma_\Lambda^{\alpha_1\dots\alpha_n}(K_1,\dots,K_n) = \Gamma_\Lambda^{\alpha_1\dots\alpha_n z}(K_1,\dots,K_n,0)\partial_\Lambda\phi_\Lambda, \quad n \geq 2, \tag{3.8}$$

which is graphically represented in Fig. 3.2. Note, that such a truncation is equivalent to the spin-diagrammatic procedure of summing up all tadpole diagrams, as described in Ref. [35]. The formal solution of this hierarchy of equations for the different vertices $\Gamma_\Lambda^{\alpha_1\dots\alpha_n}(\{K\}) = \Gamma_\Lambda^{\alpha_1\dots\alpha_n}(K_1,\dots,K_n)$ is given by

$$\Gamma_\Lambda^{\alpha_1\dots\alpha_n}(\{K\}) = \Gamma_{\Lambda_0}^{\alpha_1\dots\alpha_n}(\{K\})\big|_H + \int_{\Lambda_0}^{\Lambda} d\Lambda'\, \Gamma_{\Lambda'}^{\alpha_1\dots\alpha_n z}(\{K\},0)\partial_{\Lambda'}\phi_{\Lambda'}, \tag{3.9}$$

where $|_H$ highlights the magnetic field dependence of the initial vertices $\Gamma_{\Lambda_0}^{\alpha_1\dots\alpha_n}(\{K\}) = \Gamma_{\Lambda_0}^{\alpha_1\dots\alpha_n}(\{K\})\big|_H$. Iterating the above solution, the $\Lambda$-dependent vertices read

$$\begin{aligned}\Gamma_\Lambda^{\alpha_1\dots\alpha_n}(\{K\}) &= \sum_{m=0}^{\infty} \frac{\phi_\Lambda^m}{m!} \Gamma_{\Lambda_0}^{\alpha_1\dots\alpha_n \overbrace{z\dots z}^{m}}(\{K\},\underbrace{0,\dots,0}_{m})\big|_H \\ &= \sum_{m=0}^{\infty} \frac{\phi_\Lambda^m}{m!} \partial_H^m \Gamma_{\Lambda_0}^{\alpha_1\dots\alpha_n}(\{K\})\big|_H = \Gamma_{\Lambda_0}^{\alpha_1\dots\alpha_n}(\{K\})\big|_{H+\phi_\Lambda},\end{aligned} \tag{3.10}$$

where we used the identity $\Gamma_{\Lambda_0}^{\alpha_1\dots\alpha_n z}(\{K\},0)|_H = \partial_H \Gamma_{\Lambda_0}^{\alpha_1\dots\alpha_n}(\{K\})|_H$ in the second step. Starting from the non-interacting system and summing up all tadpole diagrams in the FRG flow equations thus corresponds to a shift $H \to H + \phi_\Lambda$ in the magnetic field. Here, the exchange field $\phi_\Lambda$ is determined by the flow equation,

$$\Gamma_\Lambda^{zz}(0)\partial_\Lambda\phi_\Lambda = -\partial_\Lambda\left(R_{\Lambda,0}^\phi \phi_\Lambda\right), \tag{3.11}$$

which follows from the corresponding flow equation (2.57) upon neglecting the loop contributions. Substituting the expression $\Gamma_{\Lambda_0}^{zz}(0)|_{H+\phi_\Lambda}$ for the longitudinal two-point vertex, the flow of the exchange field then reduces to

$$\partial_\Lambda\left(\phi_\Lambda / J_{\Lambda,0}\right) = \partial_\Lambda b\left(\beta(H+\phi_\Lambda)\right). \tag{3.12}$$

Integrating Eq. (3.12) from $\Lambda_0$ to $\Lambda$ and expressing the exchange field as $\phi_\Lambda = J_{\Lambda,0}M_\Lambda$, the flowing magnetization $M_\Lambda$ is hence given by a $\Lambda$-dependent version of the self consistency Eq. (3.7),

$$M_\Lambda = b\left(\beta(H + J_{\Lambda,0}M_\Lambda)\right). \tag{3.13}$$

Likewise, the flow of the free energy per lattice site simplifies in this truncation to

$$\partial_\Lambda f_\Lambda = -\frac{1}{2}\phi_\Lambda^2 \partial_\Lambda R_{\Lambda,0}^\phi = \frac{1}{2} M_\Lambda^2 J_0, \tag{3.14}$$

which is solved by

$$f_\Lambda = \frac{1}{2}\frac{\phi_\Lambda^2}{J_{\Lambda,0}^z} - \frac{B\left(\beta(H+\phi_\Lambda)\right)}{\beta}, \quad B(y) = \ln\frac{\sinh\left[(s+1/2)y\right]}{\sinh[y/2]}, \tag{3.15}$$

where $B(y)$ is the (primitive) integral of the Brillouin function $b(y)$. Once the longitudinal interaction is completely restored, i.e. at $\Lambda = 0$, we hence recover the mean-field solution magnetization $M_0$ introduced in Eq. (3.7), and the corresponding energy density

$$u_0 = \partial_\beta (\beta f_0) = -(H + M_0 J_0) M_0. \tag{3.16}$$

Likewise, the higher order vertices at $\Lambda = 0$ are given by

$$\Gamma_0^{\alpha_1 \dots \alpha_n}(i\omega_1, \dots, i\omega_n) = \Gamma_{\Lambda_0}^{\alpha_1 \dots \alpha_n}(i\omega_1, \dots, i\omega_n)\big|_{H \to H + J_0 M_0}, \tag{3.17}$$

such that their explicit values hence simply follow from the expressions derived in the previous section. Note however, that in the limit of small temperatures $T \ll S J_0$, the Brillouin function $b_0 = b\left(\beta(H + J_0^z M_0)\right)$ and its derivatives $b_0^{(n)} = b^{(n)}\left(\beta(H + J_0^z M_0)\right)$ satisfy the hierarchy

$$b_0 \ll b_0' \ll b_0'' \dots \ . \tag{3.18}$$

At low temperatures, it should therefore be reasonable to neglect all vertices whose mean-field values are of the order $\mathcal{O}(b_0')$ and higher. This truncation scheme will be employed in the following sections, where the flow from $\Lambda = 0$ to $\Lambda = 1$ is evaluated.

### 3.3.2 One-loop truncation

In a second step, let us now consider the flow in the region from $\Lambda = 0$ to $\Lambda = 1$, where the effect of the magnons on the thermodynamic properties of the system is taken into account. Since the longitudinal regulator $R_\Lambda^\phi$ vanishes for $\Lambda > 0$, the flow of the free energy, derived in Eq. (2.56), simplifies to

$$\partial_\Lambda f_\Lambda = \int_K G_\Lambda(K) \partial_\Lambda R_{\Lambda, \boldsymbol{k}}^\perp, \tag{3.19}$$

while the flow of the exchange field, Eq. (2.57), becomes

$$\partial_\Lambda \phi_\Lambda = J_0 \partial_\Lambda M_\Lambda = -\frac{1}{\Gamma_\Lambda^{zz}(0)} \int_K \dot{G}_\Lambda(K) \Gamma_\Lambda^{+-z}(K, -K, 0). \tag{3.20}$$

Here, the transverse propagator introduced in Eq. (2.51) can be expressed in the form

$$G_\Lambda(K) = \frac{M_0}{E_{\Lambda, \boldsymbol{k}} - i\omega + M_0 \Sigma_\Lambda(K)}, \tag{3.21}$$

where we introduced the $\Lambda$-dependent magnon dispersion,

$$E_{\Lambda, \boldsymbol{k}} = \Delta_\Lambda + \Lambda \varepsilon_{\boldsymbol{k}}, \tag{3.22}$$

with the abbreviations $\Delta_\Lambda = H + M_0 J_0 (1 - \Lambda)$ and $\varepsilon_{\boldsymbol{k}} = M_0 (J_0 - J_{\boldsymbol{k}})$. In addition, the transverse self energy

$$\Sigma_\Lambda(K) = \Gamma_\Lambda^{+-}(K) - \Gamma_0^{+-}(K), \tag{3.23}$$

is introduced, which encodes all interaction effects beyond mean-field level. A simple approximation, which recovers the well-known linear spin-wave theory results for the magnetization and the internal energy, is to neglect the renormalization of the higher order vertices on

the right side of the flow equations (3.19) and (3.20). The vertices are then given by their mean-field values,

$$\Sigma_0(K) = 0, \quad \Gamma_0^{zz}(0) = \frac{1}{J_0} + \mathcal{O}(b'), \quad \Gamma_0^{+-z}(K, -K, 0) = \frac{1}{M_0} + \mathcal{O}(b'), \tag{3.24}$$

where the terms $\propto b_0' = b'(\beta(H + J_0 M_0))$ can be neglected at low temperatures. In this one-loop approximation, the flow of the magnetization simplifies to

$$\partial_\Lambda M_\Lambda = -\frac{1}{M_0} \int_K \dot{G}_\Lambda(K), \tag{3.25}$$

while the single scale propagator introduced in Eq. (2.58a) is simply a total derivative, i.e. $\dot{G}_\Lambda(K) = \partial_\Lambda G_\Lambda(K)$. Thus Eq. (3.25) can be straightforwardly integrated. After summation over the internal Matsubara frequencies we hence find for the flowing magnetization

$$M_\Lambda = M_0 - \frac{1}{N} \sum_{\boldsymbol{k}} \left[ n\left(\beta E_{\Lambda,\boldsymbol{k}}\right) - n\left(\beta E_{\Lambda=0}\right) \right], \tag{3.26}$$

where

$$n(x) = \frac{1}{\exp(x) - 1}, \tag{3.27}$$

is the Bose distribution function. The flow of the free energy $f_\Lambda$ can be equally integrated, and the corresponding energy density reads

$$u_\Lambda = u_0 + \frac{1}{N} \sum_{\boldsymbol{k}} \left[ E_{\Lambda,\boldsymbol{k}} n\left(\beta E_{\Lambda,\boldsymbol{k}}\right) - E_{\Lambda=0} n\left(\beta E_{\Lambda=0}\right) \right]. \tag{3.28}$$

The resulting magnetization and the energy density at $\Lambda = 1$ hereby recover the first order expression of perturbative spin-wave theory in $1/S$ [40], respectively the low-temperature expressions of the diagrammatic approach followed by VLP [33].

### Infrared catastrophe

As discussed in the literature, the one-loop solution to the magnetization given in Eq. (3.26) describes the low-temperature behavior of the Heisenberg ferromagnet in three dimensions reasonably well, but fails to do so in $D \leq 2$ [39, 40]. In order to recapitulate this, let us shortly rewrite the magnetization in Eq. (3.26) into a form, which allows for a straightforward analysis. Note, that in the given temperature range, the contributions proportional to the mean-field distribution function $n\left(\beta E_{\Lambda=0}\right)$ are exponentially small and can thus be neglected. Similarly, the momentum sum in Eq. (3.26) is dominated by small momenta and it is hence possible to replace the momentum dependent part of the magnon dispersion $\varepsilon_{\boldsymbol{k}}$ by its long wavelength approximation, $\varepsilon_{\boldsymbol{k}} \approx \boldsymbol{k}^2/(2m)$, where the magnon mass $m$ depends on the precise nature of the exchange interaction. The thermal wave vector $k_{\mathrm{th}} = \sqrt{2mT}$ then acts as an effective ultraviolet cutoff of the corresponding momentum sums and by replacing the momentum sum by an integration in the usual way the magnetization derived in Eq. (3.26) reads

$$M_{\Lambda=1} = M_0 - \frac{(k_{\mathrm{th}} a)^D}{c_D} \mathrm{Li}_{D/2}\left(e^{-\beta H}\right), \quad c_D = 2^D \pi^{D/2}, \tag{3.29}$$

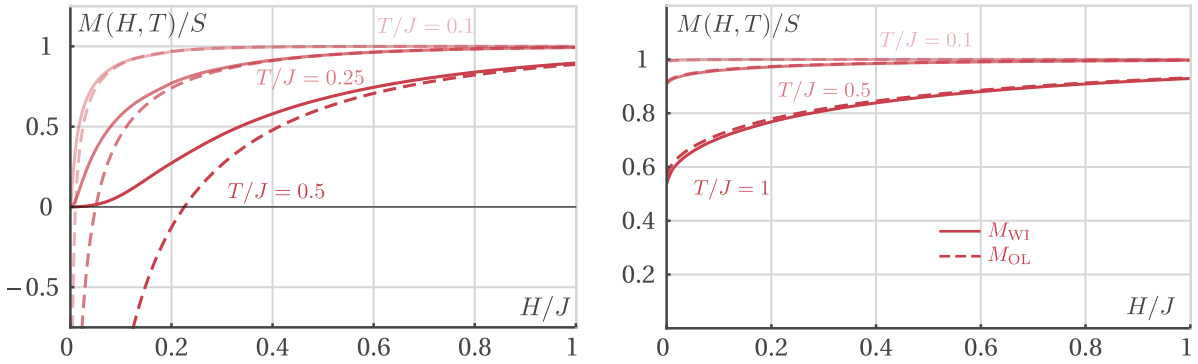


(a) $D = 1$ (b) $D = 3$

Figure 3.3: Infrared catastrophe of the one-loop solution to the Magnetization in lower dimensions: Magnetization $M$ in $D = 1$ (a) and $D = 3$ (b) as a function of magnetic field $H$ for three different temperatures (the energy scale is chosen assuming a nearest neighbor exchange interaction of strength $J$). The dashed line represents the one-loop solution (3.29), whereas the full line shows the integrated solution of Eq. (3.39), which takes into account the Ward-identity Eq. (3.35). In contrast to the one-loop solution, the latter does not predict nonphysical negative values at low magnetic fields in $D = 1$. This erroneous behavior of the one-loop solution is also present in $D = 2$, albeit at significantly smaller magnetic fields and thus not displayed.

where $a$ is the underlying lattice spacing, and

$$\mathrm{Li}_s(z) = \frac{1}{\Gamma(s)} \int_0^\infty d\epsilon \, \frac{\epsilon^{s-1}}{e^\epsilon/z - 1}, \tag{3.30}$$

the Polylogarithm function with $\Gamma(s)$ the Gamma function. (For the technical details of this low momentum expansion see appendix C.1.1). Given the asymptotic behavior of the polylogarithm function

$$\lim_{|z|\to 1} \mathrm{Li}_s(z) = \begin{cases} \zeta(s) & s > 1, \\ \infty & s \leq 1, \end{cases} \tag{3.31}$$

where $\zeta(s)$ is the Riemann-zeta function, we note straightaway that the magnon contribution diverges for small magnetic fields $H \ll T$ in $D \leq 2$. This non-physical behavior, known as *infrared catastrophe*, is graphically depicted in Fig. 3.3, where the resulting one and three-dimensional magnetization curves are compared for several temperatures as a function of magnetic field. Technically, this breakdown originates from the neglect of the self energy contribution which leads to a gapless magnon dispersion in the limit $H \to 0$. As discussed in the introduction, the occurrence of such gapless modes is intimately linked to the presence of a spontaneously symmetry-broken phase, and thus in clear conflict with the Mermin-Wagner theorem. In contrast, the one-loop result (3.26) is well-behaved in three dimensions, where Eq. (3.26) predicts a small correction of the saturated magnetization proportional to $T^{3/2}$, a behavior known as *Bloch law* [40], while the corresponding isothermal zero-field susceptibility $\chi^I_{H=0}$ diverges as $T/\sqrt{H}$ (cf. Fig. 3.3 (b); see also Ref. [34]).

Note, that in contrast to the result for the magnetization, the magnon contribution to the internal energy do not lead to a potentially diverging specific heat. Applying the same

approximations as above, the internal energy at low temperatures reads

$$u = u_0 + \frac{(k_{\mathrm{th}}a)^D}{c_D}\left[H\mathrm{Li}_{D/2}\left(e^{-\beta H}\right) + \frac{1}{\beta}\mathrm{Li}_{D/2+1}\left(e^{-\beta H}\right)\right]. \tag{3.32}$$

At small magnetic fields, the first contribution inside the brackets can be neglected since it vanishes irrespective of the dimensions and the specific heat is solely governed by the second term. Given that the polylogarithm $\mathrm{Li}_{D/2+1}\left(\exp(-\beta H)\right)$ reduces to a constant in the limit of vanishing magnetic field, one thus finds the usual $T^{D/2}$ dependence of the specific heat at low temperatures, characteristic for Nambu-Goldstone modes with a quadratic dispersion. Unfortunately, the present deformation scheme does not allow to discuss the explicit magnetic field and temperature dependence of the specific heat beyond this simple result. Technically, this is a result of the non-simultaneous deformation of longitudinal and transverse interaction, which prevents proper incorporation of the longitudinal exchange interaction contribution to the internal energy. In the present scheme, these contributions are only taken into account on the mean-field level and the magnon contribution to the longitudinal two-point vertex $\Gamma^{zz}_\Lambda(K)$ is neglected in the free energy flow in Eq. (3.19) since the longitudinal regulator $R^\phi_\Lambda$ vanishes for $\Lambda > 0$. As shown e.g. in Ref. [123], magnetic field and temperature dependence of the specific heat are, however, determined by the interplay of the longitudinal and transverse exchange interaction contributions to the internal energy. An extended analysis of the specific heat thus requires an isotropic deformation scheme.

### 3.3.3 Ward-identity truncation

Following the discussion of the previous section, it should be clear, that in order to prevent the infrared catastrophe the transverse propagator $G_\Lambda(K)$ must satisfy the appropriate $K \to 0$ behavior. Fortunately, the exact value in an isotropic system, $G(0) = G_{\Lambda=1}(0)$, can be obtained within a simple geometric construction which goes back to the work of Patashinskii and Prokrovskii [128]. To recapitulate their reasoning, let us suppose that the system is perturbed by a small uniform and time-independent transverse magnetic field $\delta h^x$. The perturbed magnetization $\boldsymbol{M}_p = \langle \boldsymbol{S}_i \rangle_p$ then slightly grows in magnitude and aligns along the field $\boldsymbol{H}_p = H\boldsymbol{e}^z + \delta h^x \boldsymbol{e}^x$, as sketched in Fig. 3.4. The resulting change of the magnetization components can be readily calculated within the generating functional approach discussed in the previous chapter. In the limiting case $\delta h^x \to 0$ we find in particular

$$\begin{aligned}\lim_{\delta h^x \to 0} \frac{\delta M^x_p}{\delta h^x} &= \lim_{\delta h^x \to 0} \frac{\delta \mathcal{G}\left[\{h^\alpha_i(\tau) = \delta h^x \delta^{\alpha x}\}\right]}{\delta h^x \delta h^x} \\ &= G^{xx}(K=0),\end{aligned} \tag{3.33}$$

where we introduced the notation $\mathcal{G}[\boldsymbol{h}] = \mathcal{G}_{\Lambda=1}[\boldsymbol{h}]$. Following Fig. 3.4, the ratio of transverse magnetization and

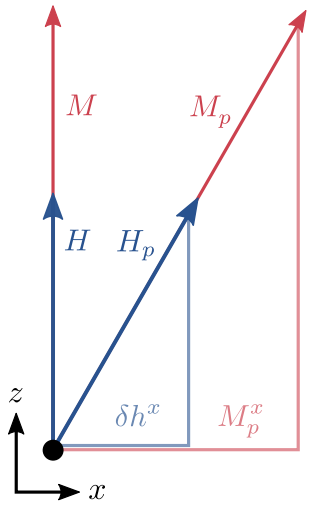


Figure 3.4: Geometrical construction of the Ward-identity Eq. (3.35). Magnetic field and magnetization vectors are depicted in blue respectively red.

perturbing field can, however, be expressed as $\delta M_p^x/\delta h^x = M_p/H_p$, where $M_p$ and $H_p$ denote the absolute values of the perturbed magnetization and the total magnetic field. By expressing $G^{xx}(0)$ in terms of the transverse propagator as

$$G^{xx}(0) = \frac{G^{+-}(0) + G^{-+}(0)}{2} = G(0), \tag{3.34}$$

we hence recover the Ward-identity

$$G(0) = \lim_{\delta h^x \to 0} \frac{\delta M_p^x}{\delta h^x} = \lim_{\delta h^x \to 0} \frac{M_p}{H_p} = \frac{M}{H}, \tag{3.35}$$

which relates the value of the isotropic transverse propagator at vanishing momentum and frequency to the magnetization of the system[1]. In order to fulfill this requirement, we choose an appropriate self energy in the following. In particular, we demand that the self energy at vanishing momentum and frequency is related to the flowing magnetization as

$$\Sigma_\Lambda(0) = \frac{H}{M_\Lambda} - \frac{H}{M_0}. \tag{3.36}$$

If we neglect the momentum and frequency dependent part of the self energy, the propagator in Eq. (3.21) is then given by

$$G_\Lambda(K) = \frac{M_0}{\tilde{E}_{\Lambda,\boldsymbol{k}} - i\omega}, \tag{3.37}$$

where

$$\tilde{E}_{\Lambda,\boldsymbol{k}} = \tilde{\Delta}_\Lambda + \Lambda\varepsilon_{\boldsymbol{k}}, \quad \tilde{\Delta}_\Lambda = H\frac{M_0}{M_\Lambda} + M_0 J_0(1-\Lambda), \tag{3.38}$$

is the magnon-dispersion with the modified energy gap $\tilde{\Delta}_\Lambda$. Upon performing the Matsubara summation over the internal frequencies, the flow equation for the magnetization (3.25) then modifies to

$$\partial_\Lambda M_\Lambda = -\frac{M_0\beta}{N}\sum_{\boldsymbol{k}} J_{\boldsymbol{k}} n\big(\beta\tilde{E}_{\Lambda,\boldsymbol{k}}\big)\Big[n\big(\beta\tilde{E}_{\Lambda,\boldsymbol{k}}\big)+1\Big]. \tag{3.39}$$

In order to compare the resulting magnetization curves to last section's linear one-loop results, let us apply the previous low-temperature approximation and replace the momentum dependent part of dispersion by its low momentum expansion $\varepsilon_{\boldsymbol{k}} \approx \boldsymbol{k}^2/2m$. Within this approximation the momentum dependency of the exchange interaction $J_{\boldsymbol{k}}$ can equally be neglected and the flow equation of the magnetization (3.39) can be recast in the more convenient form

$$\partial_\Lambda M_\Lambda \approx -M_0 J_0 \beta \frac{(k_{\mathrm{th}}a)^D}{\Lambda^{D/2} c_D \Gamma(D/2)} \int_0^\Lambda d\epsilon \, \frac{\epsilon^{\frac{D-2}{2}} e^{\beta\tilde{\Delta}_\Lambda+\epsilon}}{\left(e^{\beta\tilde{\Delta}_\Lambda+\epsilon}-1\right)^2}, \tag{3.40}$$

which allows for a straightforward numerical integration. (For the technical details of the above low momentum expansion see again appendix C.1.1). The resulting magnetization curves in one and three dimensions are displayed together with last section's results in Fig. 3.3.

[1] A more formal derivation of the Ward-identity Eq. (3.35) follows from an analysis of the corresponding equations of motion, see App. C in our publication Ref. [3].

While the implementation of the Ward-identity does not have a significant influence on the magnetization curves in $D = 3$, it clearly cures the infrared catastrophe in $D \leq 2$: In contrast to the simple one-loop results the magnetization now vanishes in the limit $H \to 0$, as demanded by the Mermin-Wagner theorem. Likewise, the energy gap of the magnon dispersion $\tilde{\Delta}_{\Lambda=1} \propto H/M_{\Lambda=1}$ remains finite in this limit.

**Zero-field susceptibility and transverse correlation length within the Katanin substitution**

Having guaranteed the Mermin-Wagner condition $M_{D\leq 2}(H = 0, T > 0) = 0$, we are now in the position to briefly analyze the critical region close to $(H_c, T_c) = (0, 0)$. To this end, note, that the single scale propagator can be expressed in the form

$$\dot{G}_\Lambda(K) = \partial_\Lambda G_\Lambda(K) - \frac{H}{M_\Lambda^2} G_\Lambda^2(K) \partial_\Lambda M_\Lambda. \tag{3.41}$$

If we neglect the second term on the right hand side, the flow equation of the magnetization (3.25) can be straightforwardly integrated, and the resulting magnetization is given by the self consistent solution of

$$M_{\mathrm{Kat},\Lambda} = M_0 - \frac{1}{N} \sum_{\boldsymbol{k}} \left[ n(\beta \tilde{E}_{\Lambda,\boldsymbol{k}}) - n(\beta \tilde{E}_{\Lambda=0}) \right], \tag{3.42}$$

where the new magnon dispersion $\tilde{E}_{\Lambda,\boldsymbol{k}}$ is given Eq. (3.38) with $M_\Lambda$ replaced by $M_{\mathrm{Kat},\Lambda}$. This approximation, which amounts to the replacement of the single scale propagator $\dot{G}_\Lambda(K) \to \partial_\Lambda G_\Lambda(K)$, is commonly called Katanin substitution [129] - hence the above subscript - and is frequently employed in various FRG formulations such as in the pseudofermionic approach towards quantum spin systems [130]. In the limit $H \to 0$, the self consistent solution of Eq. (3.42) reproduces the flowing magnetization obtained by the integration of the flow Eq. (3.39). Naturally, this simply follows from the fact that the second term in the expression of the single scale propagator (3.41) vanishes in this case. Note however, that the same term still contributes to the resulting zero-field isothermal susceptibility, $\chi^I_\Lambda(0, T) = \partial_H M_\Lambda(0, T)$, which is therefore not reproduced by the corresponding Katanin-substituted version

$$\chi^I_{\mathrm{Kat},\Lambda}(0, T) = \partial_H M_{\mathrm{Kat},\Lambda}(H, T)\big|_{H=0} = \lim_{H\to 0} \frac{M_{\mathrm{Kat},\Lambda}(H, T)}{H}. \tag{3.43}$$

Having said that, let us nevertheless shortly review the low-temperature behavior of $\chi^I_{\mathrm{Kat}}(0, T)$, for which we can find explicit analytical expressions. Since the self consistency equation (3.42) at $\Lambda = 1$ and $H = 0$ is solved by a vanishing magnetization, this susceptibility is implicitly determined by the condition

$$S = \frac{1}{N} \sum_{\boldsymbol{k}} n(\beta M_0/\chi^I_{\mathrm{Kat}}(0, T) + \beta \varepsilon_{\boldsymbol{k}}) \approx \frac{(k_{\mathrm{th}} a)^D}{c_D} \mathrm{Li}_{D/2}\left( e^{-\beta S/\chi^I_{\mathrm{Kat}}(0,T)} \right), \tag{3.44}$$

where we once more neglected the initial contribution, approximated $M_0 \approx S$ and applied the usual low momentum expansion of the energy dispersion. Assuming that the argument

of the polylogarithm satisfies $\lim_{T\to 0} \beta S/\chi^I = 0$, Eq. (3.44) can be straightforwardly solved with the help of the asymptotic behavior

$$\mathrm{Li}_s(e^{-\mu}) \overset{\mu\to 0^+}{\sim} \begin{cases} -\ln(\mu) & s = 1, \\ \Gamma(1-s)\mu^{s-1} & s < 1. \end{cases} \tag{3.45}$$

In order to compare the associated results to the literature, we furthermore fix the magnon-mass $m$ at this point assuming an underlying cubic lattice with a nearest neighbor exchange interaction of strength $J$, for which $(k_{\mathrm{th}}a)^D = [T/(JS)]^{D/2}$. The resulting zero temperature limit of the zero-field susceptibility of the one-dimensional model is then given by

$$\lim_{T\to 0} \chi^I_{\mathrm{Kat}}(0,T) = \frac{4JS^4}{T^2}, \quad (D=1). \tag{3.46}$$

For $S = 1/2$, this result recovers the solution obtained within the random phase approximation of Green-function theory [106], while the exact result $\chi^I(0,T) = J^2/(24T^2)$, found within Bethe ansatz calculations [119] and confirmed by Green-function theory [131], possesses the same temperature dependence but is slightly smaller. For the two-dimensional model we find analogously

$$\lim_{T\to 0} \chi^I_{\mathrm{Kat}}(0,T) = \frac{S}{T} e^{4\pi JS^2/T}, \quad (D=2). \tag{3.47}$$

This agrees up to a prefactor $T/(JS)$ with the susceptibility found in modified spin-wave theory [122], Schwinger Boson mean-field theory [103] and a one loop momentum shell renormalization group calculation [121].[2] Furthermore, the expression of the susceptibilities allow us to estimate the low-temperature limit of the corresponding zero-field transverse correlation length $\xi(T)$. The latter can be obtained, by writing the low momentum expansion of the magnon-dispersion $\tilde{E}(\boldsymbol{k})$ in the form

$$\tilde{E}(\boldsymbol{k}) \approx \frac{1}{2m}\left(\xi^{-2} + k^2\right). \tag{3.48}$$

We thus find $\xi^2(T) = \chi^I_{\mathrm{Kat}}(0,T)/(2mS)$, which yields for the nearest-neighbor exchange-interaction case

$$\frac{\xi(T)}{a} = \begin{cases} \frac{2JS^2}{T}, & (D=1), \\ \sqrt{\frac{JS}{T}} e^{2\pi JS^2/T}, & (D=2). \end{cases} \tag{3.49}$$

In the one-dimensional case, this result agrees with the exact Bethe ansatz [119], respectively the Green-function theory results [131], again up to a numerical prefactor. This is now also the case for the two dimensional expression, compared to the one-loop results found in Refs. [103, 121, 122]. Given the simplicity of the applied truncation the agreement of these results is surprising, although the underlying Katanin-substitution is per se not justified within the present low-temperature scheme. It remains thus to be discussed, to which extent these results can be reproduced from truncating the vertex expansion of the flow equation in a more controlled way. We will address this questions in the upcoming section.

[2] In this context, it is also worth to point out that the deformation scheme employed in our original publication Ref. [3], allows to make contact with the precise momentum-shell RG-equations of Ref. [121].

### 3.3.4 Higher-order vertex corrections

A consistent implementation of the low-temperature truncation scheme requires the inclusion of the vertex renormalization processes entering the flow equation of the magnetization, given in Eq. (2.57). This includes in particular the renormalization of the longitudinal two-point vertex at vanishing momentum and frequency $\Gamma^{zz}_\Lambda = \Gamma^{zz}_\Lambda(0)$, of the momentum and frequency dependent part of the self energy $\Sigma(K)-\Sigma(0)$, and of the mixed three-point vertex $\Gamma^{+-z}_\Lambda(Q,-Q,0)$, all of which were neglected so far. The flow equation of the longitudinal and transverse two-point vertices were derived at the end of the previous chapter, cf. Eqs. (2.59) and (2.60). Within the present truncation scheme, it is consistent to neglect all vertex contributions on the right side of these flow equations, whose initial conditions are of the order $\mathcal{O}(b_0')$ and higher. The flow equation of the longitudinal two-point vertex then simplifies to

$$\partial_\Lambda \Gamma^{zz}_\Lambda = -\int_Q [G_\Lambda(Q)G_\Lambda(Q)]^\bullet \, \Gamma^{+-z}_\Lambda(Q,-Q,0)\Gamma^{+-z}_\Lambda(Q,-Q,0), \tag{3.50}$$

while the flow equation of the self energy, $\Sigma_\Lambda(K) = \Gamma^{+-}_\Lambda(K) - \Gamma^{+-}_0(K)$, is given by

$$\begin{aligned}\partial_\Lambda \Sigma_\Lambda(K) = \int_Q \dot{G}_\Lambda(Q)\Big[&\Gamma^{++--}_\Lambda(K,Q,-Q,-K) - F_\Lambda(0)\Gamma^{+-z}_\Lambda(K,-K,0)\Gamma^{+-z}_\Lambda(Q,-Q,0) \\ &- F_\Lambda(Q-K)\Gamma^{+-z}_\Lambda(K,-Q,Q-K)\Gamma^{+-z}_\Lambda(Q,-K,K-Q)\Big].\end{aligned} \tag{3.51}$$

In principle, the flow of the three-point vertex could be obtained by truncating the corresponding flow equation within a similar procedure. At this point, we choose a different scheme, which once more exploits the Ward-identity introduced in the previous section. In order to develop this, let us parameterize the self energy in the form

$$\Sigma_\Lambda(K) = \Sigma_\Lambda(0) + M_0^{-1}\left[\left(1 - Z_\Lambda^{-1}\right) i\omega + \sigma_\Lambda(K)\right], \tag{3.52}$$

such that the propagator in Eq. (3.21) is given by

$$G_\Lambda(K) = \frac{Z_\Lambda M_0}{Z_\Lambda \tilde{E}_{\Lambda,\boldsymbol{k}} - i\omega + Z_\Lambda \sigma_\Lambda(K)}. \tag{3.53}$$

Here, $Z_\Lambda$ is the *wave-function renormalization*, which determines the spectral contribution of the magnons in the structure factor and $\sigma_\Lambda(K)$ contains the momentum and frequency dependent renormalization of the momentum dependent part of the magnon energy $\varepsilon_{\boldsymbol{k}}$ and a corresponding damping term. The renormalization of $\sigma_\Lambda(K)$ is neglected in the following. This is justified, given that to one-loop order, the self energy flow equation yields a magnon-damping of the order of $b_0'$, which can hence be neglected at low temperatures. (For the detailed calculations see appendix C.2). Likewise, the momentum sums in the resulting flow equations (e.g. of the magnetization) are (at low temperatures) dominated by the low momentum behavior of the dispersion relation which is not qualitatively modified by the higher order vertex corrections. Furthermore, please recall, that the fulfillment of the Ward-identity (3.35) was guaranteed by coupling the self energy at vanishing momentum and frequency $\Sigma_\Lambda(0)$ in Eq. (3.36) to the flowing magnetization $M_\Lambda$. To be consistent with this choice, the corresponding flow equations should hence satisfy

$$\partial_\Lambda \Sigma_\Lambda(0) = -\frac{H}{M_\Lambda^2}\partial_\Lambda M_\Lambda. \tag{3.54}$$

Substituting the explicit flow equations for $\partial_\Lambda \Sigma_\Lambda(0)$ and $\partial_\Lambda M_\Lambda$, (3.51) and (3.20), this condition can be reformulated as

$$\begin{aligned} 0 = \frac{H}{M_\Lambda^2 \Gamma_\Lambda^{zz} J_0} \Gamma_\Lambda^{+-z}(Q,-Q,0) - \Gamma_\Lambda^{++--}(0,Q,-Q,0) + F_\Lambda(0)\Gamma_\Lambda^{+-z}(0,0,0)\Gamma_\Lambda^{+-z}(Q,-Q,0) \\ + F_\Lambda(Q)\Gamma_\Lambda^{+-z}(0,-Q,Q)\Gamma_\Lambda^{+-z}(Q,0,-Q), \end{aligned} \tag{3.55}$$

which should be considered as an additional constraint on the involved two-, three-, and four-point vertices. However, note, that similar to the Ward-identity, Eq. (3.55) is a property of the isotropic system. Hence, it is violated in the present anisotropic deformation scheme, as can be verified by substituting the mean-field values of the corresponding vertices. In order to cure this, we thus need to resort to yet another approximation. Here, we choose in particular to ignore the terms which violate the constraint (3.55) at the mean-field level ($\Lambda = 0$). This amounts to neglecting the last term on the left side of Eq. (3.55) and to a replacement of the mean-field four-point vertex by

$$\Gamma_0^{++--}(K,Q,-Q,-K) \to G_0^{-1}(i\omega_k)/M_0^2. \tag{3.56}$$

In order to obtain a closed set of flow equations we now ignore the renormalization of this vertex and the momentum and frequency dependence of the three-point vertex, i.e. we set

$$\Gamma_\Lambda^{++--}(K,Q,-Q,-K) \to G_0^{-1}(i\omega_k)/M_0^2, \quad \Gamma_\Lambda^{+-z}(Q,-Q,0) \to \Gamma_\Lambda^{+-z}(0,0,0) = \Gamma_\Lambda^{+-z}. \tag{3.57}$$

Within these approximations, the constraint condition (3.55) then reduces to

$$\frac{H\Gamma_\Lambda^{+-z}}{M_\Lambda^2 J_0} - \frac{(H + M_0 J_0)\Gamma_\Lambda^{zz}}{M_0^3} + \left(\Gamma_\Lambda^{+-z}\right)^2 = 0, \tag{3.58}$$

which allows to determine the flowing three-point vertex in terms of the flowing magnetization and the longitudinal two-point vertex as

$$\Gamma_\Lambda^{+-z} = -\frac{H}{2M_\Lambda^2 J_0} + \sqrt{\left(\frac{H}{2M_\Lambda^2 J_0}\right)^2 + \frac{(H + M_0 J_0)\Gamma_\Lambda^{zz}}{M_0^3}}. \tag{3.59}$$

Moreover, the approximated four-point vertex in the flow equation of the self energy (3.51) yields a contribution to the flowing wave function renormalization $Z_\Lambda$ of the form

$$\partial_\Lambda Z_\Lambda = -\frac{Z_\Lambda^2}{M_0^2} \int_Q \dot{G}_\Lambda(Q). \tag{3.60}$$

Within the presented approximations we are thus left with a closed set of three flow equations for the magnetization, the longitudinal two-point vertex and the wave function renormalization. After performing the Matsubara summation over the internal frequencies, the respective

flow equations, (3.20), (3.50), and (3.60), are given as

$$\partial_\Lambda M_\Lambda = -\frac{\beta (M_0 Z_\Lambda)^2 \Gamma_\Lambda^{+-z}}{J_0 \Gamma_\Lambda^{zz} N} \sum_{\boldsymbol{k}} J_{\boldsymbol{k}} n\left(x_{\Lambda,\boldsymbol{k}}\right) \left[n\left(x_{\Lambda,\boldsymbol{k}}\right)+1\right], \tag{3.61a}$$

$$\partial_\Lambda \Gamma_\Lambda^{zz} = -\frac{\beta^2 (M_0 Z_\Lambda)^3 \left(\Gamma_\Lambda^{+-z}\right)^2}{2N} \sum_{\boldsymbol{k}} J_{\boldsymbol{k}} n\left(x_{\Lambda,\boldsymbol{k}}\right) \left[n\left(x_{\Lambda,\boldsymbol{k}}\right)+1\right] \left[2n\left(x_{\Lambda,\boldsymbol{k}}\right)+1\right], \tag{3.61b}$$

$$\partial_\Lambda Z_\Lambda = -\frac{\beta Z_\Lambda^4}{N} \sum_{\boldsymbol{k}} J_{\boldsymbol{k}} n\left(x_{\Lambda,\boldsymbol{k}}\right) \left[n\left(x_{\Lambda,\boldsymbol{k}}\right)+1\right], \tag{3.61c}$$

where we introduced the shorthand $x_{\Lambda,\boldsymbol{k}} = \beta Z_\Lambda \tilde{E}_{\Lambda,\boldsymbol{k}}$.(at low temperatures) The solution of this set of integro-differential equations is discussed in the following section.

## 3.4 Magnetization and isothermal susceptibility curves

The solution of the set of integro-differential equations (3.61) requires a specification of the underlying exchange interaction. In order to quantitatively compare our result to the literature, we here once more choose a nearest neighbor interaction of strength $J$, with the momentum space representation

$$J_{\boldsymbol{k}} = 2J \sum_{i=1}^{D} \cos(k_i a), \tag{3.62}$$

and evaluate the momentum sums without resorting to the low-momentum expansion of the magnon dispersion $\tilde{E}_{\Lambda,\boldsymbol{k}}$.[3]

### 3.4.1 Finite magnetic field

We first discuss the solution at finite magnetic field. Fig. 3.5 (a) and (b) show the resulting magnetization curves, $M(H,T) = M_{\Lambda=1}(H,T)$, in one and two dimensions as a function of temperature for different magnetic fields in the range $H/J = 0.1 - 1.0$. For magnetic fields $H \sim \mathcal{O}(J)$ and up to temperatures $T \sim \mathcal{O}(J)$, our one-dimensional calculations are in very good quantitative agreement with the Bethe ansatz results of Ref. [123]. The same holds true for the two-dimensional case, compared to the Monte Carlo simulations of Ref. [125]. Decreasing the magnetic field further to $H/J = 0.1$, the deviation of our results from the reference results becomes significant at lower and lower temperatures, though quantitative agreement is still observed up to temperatures $T \sim J/2$. This is also reflected in the associated wave function renormalization $Z(H,T) = Z_{\Lambda=1}(H,T)$ shown in part (c) and (d) of Fig. 3.5, whose behavior allows for a self consistency check of the present truncation scheme. For magnetic fields $H/J = 0.4 - 1$, $Z(H,T)$ remains of the order of unity for the whole range of displayed temperatures, thus indicating that the assumption of well-defined magnonic quasiparticles is justified. By contrast, for the smallest displayed magnetic field $H/J = 0.1$, this is only the case up to the limiting temperatures $T \sim J$ ($T \sim J/2$) in $D = 1$ ($D = 2$). For higher temperatures the wave function renormalization saturates to $Z \sim 1/4$ while the

[3]The numerical integration of Eqs. (3.61) is performed using the NDSolve routine in Wolfram Mathematica [132].

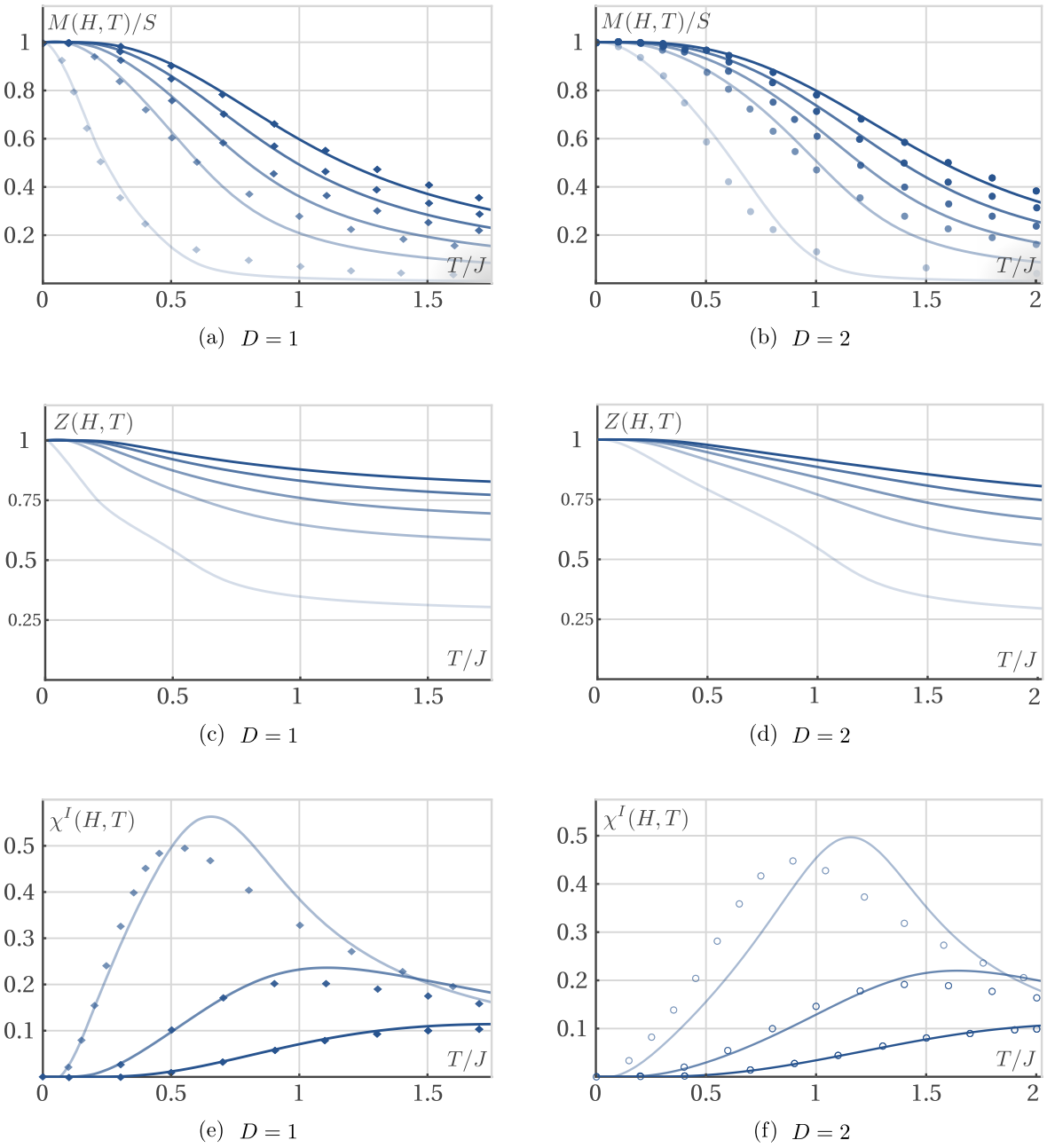


Figure 3.5: Magnetization, susceptibility, and wave-function renormalization of the one and two dimensional $S = 1/2$ Heisenberg ferromagnet as a function of temperature, obtained by numerically solving the set of flow equations (3.61). The energy scale is fixed assuming a nearest neighbor exchange interaction of strength $J$. (a) and (b): $M(H,T)/S$ in $D = 1$ and $D = 2$ for magnetic fields $H/J = 1.0, 0.8, 0.6, 0.4, 0.1$ (top to bottom) compared to the Bethe ansatz results of Ref. [123] (◆), respectively the Monte Carlo simulation results of Ref. [125] (●). (c) and (d): $Z(H,T)$ in $D = 1$ and $D = 2$ for the same magnetic fields. (e) and (f): $\chi^I(H,T)/S$ in $D = 1$ and $D = 2$ for magnetic fields $H/J = 0.4, 1, 2$ (top to bottom), compared to the Bethe ansatz results (◆), respectively the exact diagonalisation results of Ref. [123] (○).

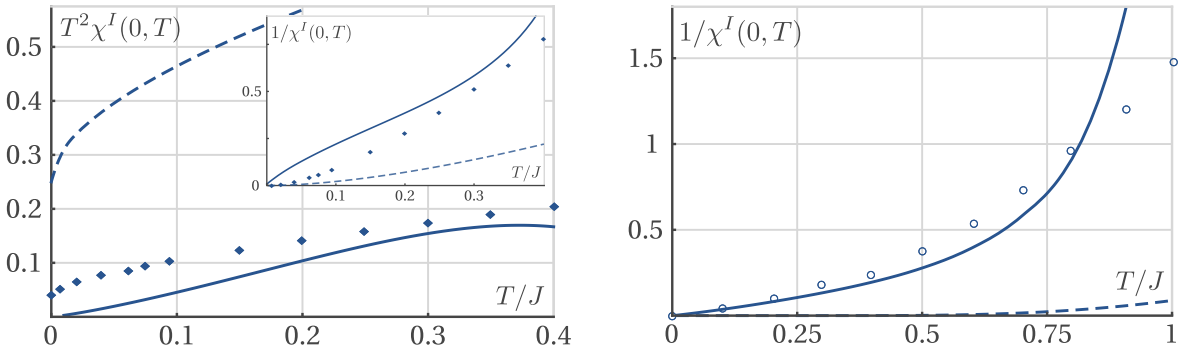


(a) $D = 1$ (b) $D = 2$

Figure 3.6: Zero-field isothermal susceptibilities of the one (a) and two-dimensional (b) model as function of temperature obtained from the numerical solution of Eqs. (3.61). The data points depict the Bethe ansatz (◆), respectively exact diagonalization results (○) of Ref. [123], and the dashed solution is obtained via the self consistency equation (3.42) derived within the Katanin-substitution.

relative deviation from the benchmark results in Ref. [123,125] increases. This is best observed in the susceptibility curves, $\chi^I(H,T) = \partial_H M(H,T)$ shown in part (e) and (f) of Fig. 3.5, which are in good quantitative agreement with Ref. [123, 125] at sufficiently low temperatures. (Note, that the low-temperature discrepancy of the two-dimensional susceptibility at $H/J = 0.4$ can probably be attributed to finite size effects in the exact diagonalisation data, as explained in Ref. [123].) Generally speaking, the deviations of our results from the benchmark results given in Ref. [123,125] at higher temperature were to be expected, given that all vertices, whose mean field values are of the order $\mathcal{O}(b_0')$ and higher, were neglected in solving the flow equations. Likewise, it is clear that the truncation scheme presented here is not well-controlled in the limit of arbitrary small magnetic fields since the underlying anisotropic (mean-field) deformation scheme is only justified for magnetic fields strong enough to induce long range order in the $S^z$-direction. Having said that, it is nevertheless interesting to extrapolate the given results to vanishing magnetic field and low-temperatures, i.e. into the vicinity of the phase transition occurring at $T_c = 0$.

### 3.4.2 The limit of vanishing magnetic field

In order to establish the connection with the Katanin solution of the zero-field susceptibility, discussed in section 3.3.3, let us briefly analyze the solution of the set of Eqs. (3.61) in the limit $H \to 0$. Unfortunately, the associated numerical evaluation becomes cumbersome at such low temperatures and low magnetic fields. Therefore, the zero field susceptibility $\chi^I(0,T)$ was determined by interpolation of $M(H^*,T)$ and $M(0,T) = 0$, where $H^*/J \sim 10^{-7}$ was chosen such that convergence of $\chi^I(0,T)$ was observed, while the temperature was not decreased below $T/J \sim 10^{-2}$. Fig. 3.6 shows the resulting one and two dimensional zero-field susceptibilities as a function of temperature compared to the results of Ref. [123], respectively to the numerical solution of the Katanin self-consistency equation (3.42).

In case of the one dimensional model, our calculations agree reasonably well with the the exact Bethe-ansatz results at small but non-zero temperatures $T/J \sim 0.1 - 0.4$. However, in the limit $T \to 0$ they equally fail to reproduce the $1/T^2$ divergence of the zero-field

susceptibility, which in turn is qualitatively reproduced by the Katanin-substituted solution, although with a wrong prefactor.

By contrast, the two-dimensional results seem to reproduce the exact diagonalisation data in the limit $T \to 0$. This should however be interpreted with caution, given that the latter is prone to finite size effects. By analogy with the one dimensional result we therefore expect that the observed behavior is also only valid within an intermediate temperature range and does not extend down to $T = 0$. This is also reflected in the fact that both, exact-diagonalization data and the integrated solution diverge more slowly than the Katanin-substituted version. The latter is governed by an exponential temperature dependence that is well-established in the literature results, and we thus conclude that neither the exact diagonalisation data, nor our zero-field solution can account for the quantitative behavior of $\chi(0, T)$ (cf. the discussion at the end of section 3.3.3). This is not surprising, given that we are in the close vicinity of the critical point.

---

The previous results complete the proof of principle calculations of the present chapter; in brief, it was demonstrated that the spin FRG formalism allows for an elegant calculation of the static magnetic properties of the low-dimensional Heisenberg ferromagnet at finite field and low temperatures. In what follows, we will now leave the safe harbor of established findings and tackle some longstanding questions about the existence of collective sound modes in quantum ferromagnets.

# Chapter 4

# Longitudinal spin dynamics at low temperatures

## 4.1 Outline

The dynamical properties of the isotropic Heisenberg ferromagnet are best discussed in terms of the dynamical structure factor $\mathcal{S}^{\alpha\beta}(\boldsymbol{q},\omega)$, introduced in chapter 1. In the paramagnetic phase, i.e. for temperatures $T \gg T_C$ in $D = 3$ respectively at zero magnetic field in $D \leq 2$, no distinct excitations exist leading to an isotropic structure factor dominated by a diffusive central peak, whose origin is usually explained in terms of a hydrodynamic picture [85] (for a recent microscopic spin FRG calculation, see Ref. [133]). In the presence of a finite magnetization transverse and longitudinal parts evidently require a separate analysis. As discussed previously, the transverse dynamics in this case are determined by magnons, which manifest as well-defined excitation peaks in $\mathcal{S}^{\perp}(\boldsymbol{q},\omega)$, cf. Appendix C.2. Notably, this picture results not only from microscopic calculations - valid at small timescales - but also within a phenomenological hydrodynamic approach presumably valid at very long timescales [134]. By contrast, no such simple picture exists for the characteristic fluctuations of the magnetization density, encoded in the longitudinal part $\mathcal{S}^{zz}(\boldsymbol{q},\omega)$. In particular, the longitudinal dynamics in the high- and low frequency limit - the collisionless respectively collision-dominated regimes - are not smoothly connected but separated into two different pictures. Both regimes have received a considerable amount of interest during the 60s and 70s of the previous century, which has lead to the following picture in $D = 3$:

In the collision-dominated regime the general form of $S^{zz}(\boldsymbol{q},\omega)$ for small momenta $|\boldsymbol{q}|$ and frequencies $\omega$ can be obtained from the continuity equations of the conserved quantities; the local magnetization, the local temperature and the momentum density. However, due to the spatial lattice structure, the latter is only conserved for sufficiently low temperatures, such that Umklapp scattering processes can be neglected. The resulting system of differential equations was first analyzed in the late 1960s, by Reiter [135] and independently by Schwabl and Michel [136, 137]. Both works stated that at low temperatures and in the presence of a finite external magnetic field $H$, $S^{zz}(\boldsymbol{q},\omega)$ exhibits a diffusive peak at $\omega = 0$ and a damped propagating mode with linear dispersion. In analogy with the second sound mode in phonon systems, this mode is denoted *second magnon* although it should be stressed that the excitation manifests primarily as a magnetization density wave and not - as in the case of

liquid He-4 - as a temperature wave. A few years later the problem was picked up again by Dewel [32] who concluded that the hydrodynamic description of the longitudinal dynamics is only valid at momentum scales $q < q_H$, where the momentum threshold $q_H^2 = 2ma^2H$ is effectively set by the relative strength of the magnetic field $H$ measured in terms of the magnon mass $m$. Technically, this breakdown of the hydrodynamic theory manifests as a singularity in the collision operator in the limit $H \to 0$, whose origin can be traced back to the gapless nature of the transverse magnons.

The picture in the collisionless regime is slightly less consistent. Early studies, conducted during the 60's and early 70's, focused on the possible occurrence of a collective density fluctuation mode in the three dimensional system. Analogous to Fermi systems, where particle hole fluctuations around the Fermi surface give rise to a collective zero-sound mode [25] (cf. chapter 1), such a *zero-magnon* mode could possibly arise from coherent creation and annihilation processes of magnons. However, an initial claim predicting the existence of such a zero magnon at the boundary of the Brillouin zone was soon interpreted as an artifact of the mapping onto the bosonic Holstein-Primakoff Hamiltonian [29]. This absence was confirmed by a number of subsequent works which analyzed the longitudinal spin dynamics in terms of auxiliary fermionic or bosonic representations. [30–32] Some 25 years later, the problem was reconsidered by Izyumov *et al.* [36], who reformulated the spin diagrammatic approach of Vaks *et al.* [33,34] allowing for non-perturbative calculations of the transverse and longitudinal correlation functions. In particular, the authors claimed to have successfully re-summed all loop diagrams contributing to the longitudinal correlation function. Although this tour de force of the spin diagrammatic technique remains impressive, their corresponding analysis of the longitudinal structure factor is somewhat inconclusive: While their spectral line shape shows broad maxima at finite frequency $\omega_{\boldsymbol{q}} \propto |\boldsymbol{q}|$, it is equally troubled by strange dip features, arising once more from the gapless nature of the magnons at vanishing magnetic field (cf. Ref. [32]). From our perspective, the finite frequency maxima in Ref. [36] should therefore not be interpreted as a signature of any collective excitation.

Interestingly, the fate of collective sound modes in the lower dimensional Heisenberg systems has - to our knowledge - only scarcely been investigated [28]. Having said this, the hybrid spin FRG formalism provides, fortunately, an ideal framework to deal with the expected complicated interplay of longitudinal and transverse fluctuations. In particular, we present in the following an investigation of the longitudinal dynamics of the $D = 1, 2, 3$-dimensional system in the collisionless regime at sufficiently high frequencies and low momenta. For this purpose we use a specific RPA-like truncation which recovers the analytic structure of the longitudinal correlation function as found by Izyumov *et al.*. A detailed analysis of this solution, then indeed reveals a well-defined zero-magnon mode in dimensions $D \leq 2$ at very low temperatures and in a certain rage of magnetic fields. Finally, these results are compared to the longitudinal dynamics in the collision-dominated regime.

## 4.2 Spin FRG formulation

The following analysis is based on the flow equation of the hybrid generating functional derived in Eq. (2.40) of chapter 2. Similar to the previous chapter we solve the associated tower of coupled integro-differential equations describing the flow of the corresponding vertices in a controlled approximation (cf. section 2.3.3). To set the stage for the upcoming calculations,

please recall that in the spin FRG formalism the longitudinal dynamics are encoded in the longitudinal two-point vertex

$$\Gamma^{zz}_{\Lambda}(Q) = \Gamma^{zz}_{\Lambda}(\boldsymbol{q}, i\nu) = \frac{1}{J^z_{\boldsymbol{q}}} - \Pi_{\Lambda}(Q), \tag{4.1}$$

where the polarization $\Pi_{\Lambda}(Q)$ represents the part of $\Gamma^{zz}_{\Lambda}(Q)$ that is modified along the flow. Following the relations of the second order vertices and connected correlation functions established in Eqs. (2.50)-(2.53) of Sec. 2.3.2, the longitudinal spin-spin correlation function is hereby given by

$$G^{zz}_{\Lambda}(Q) = \frac{\Pi_{\Lambda}(Q)}{1 - J^z_{\Lambda,\boldsymbol{q}}\Pi_{\Lambda}(Q)}. \tag{4.2}$$

Likewise, the longitudinal propagator introduced in Eq. (2.52) reads

$$F_{\Lambda}(Q) = \frac{J^z_{\Lambda,\boldsymbol{q}}}{1 - J^z_{\Lambda,\boldsymbol{q}}\Pi_{\Lambda}(Q)}, \tag{4.3}$$

and can hence be identified with the effective screened longitudinal interaction essentially determined by the many-body fluctuations encoded in $\Pi_{\Lambda}(Q)$.

### 4.2.1 Deformation scheme & initial conditions

In the analysis of the longitudinal dynamics, the same deformation scheme as in the previous chapter is applied, and longitudinal and transverse interaction are deformed consecutively (cf. Sec. 3.2.1). In addition, we also employ a similar truncation in the first part of the flow [$\Lambda \in (-1, 0)$], where all but the tadpole diagrams are omitted while the longitudinal interaction is restored. The resulting vertices at $\Lambda = 0$ are then given by their mean-field values, as derived in Sec. 3.3.1. The following analysis is concerned with the second part of the flow from $\Lambda = 0$ to $\Lambda = 1$ where $J^z_{\Lambda,\boldsymbol{k}} = J_{\boldsymbol{k}}$ and hence $\dot{F}_{\Lambda}(K) = 0$.

### 4.2.2 Zero-sound truncation

In order to investigate the structure of the low temperature fluctuations encoded in the longitudinal two point vertex, we need to resort to a suitable truncation of the infinite hierarchy of flow equations. This is done in two steps. First, we follow the lines of the previous chapter and classify the different vertices in terms of their mean field value at $\Lambda = 0$: Following the discussion of Sec. 3.2.2 and 3.3.1, these vertices are given as a sum of terms involving the Brillouin function $b_0 = b(\beta(H + J_0 M_0))$ and its higher derivatives $b_0^{(n)} = b^{(n)}(\beta(H + J_0 M_0))$. At low temperatures $T \ll SJ_0$, the Brillouin function satisfies $b_0 \gg b_0' \gg b_0'' \gg \ldots$, and all vertices whose initial condition are of the order $\mathcal{O}(b_0')$ and higher are neglected in the following. This involves the longitudinal three- and four-point vertices and the mixed four-point vertex, i.e.

$$\{\Gamma^{zzz}_{\Lambda}(K_1, K_2, K_3),\ \Gamma^{zzzz}_{\Lambda}(K_1, K_2, K_3, K_4),\ \Gamma^{+-zz}_{\Lambda}(K_1, K_2, K_3, K_4)\} \to 0. \tag{4.4}$$

In addition, we furthermore neglect the contributions of the five- and six-point vertices to the flow of the remaining transverse four-point vertex $\Gamma^{++--}_{\Lambda}(K_1, \ldots, K_4)$. This should be

reasonable, given that to one-loop order these vertices do not introduce any new form of dynamics in $\Gamma_\Lambda^{++--}(K_1,\ldots,K_4)$ as compared to the mean field value $\Gamma_0^{++--}(K_1,\ldots,K_4)$. Within these approximations, the hierarchy of flow equations decouples and one is left with a closed set of integro-differential equations involving the set of transverse self energy, the polarization, and the three- and four point vertices, i.e.

$$\{\Sigma_\Lambda(K),\ \Pi_\Lambda(K),\ \Gamma_\Lambda^{+-z}(K_1,K_2,K_3),\ \Gamma_\Lambda^{++--}(K_1,K_2,K_3,K_4)\}, \tag{4.5}$$

which is graphically represented in Fig. 4.1 (for the flow of the self energy see Fig. 2.1). In a second step, let us now analyze the resulting flow equations focusing on the possible existence of a well-defined collective mode.

To this end, recall that the essential features of the zero-sound phenomenon in Fermi systems can all be extracted from an approximation of the polarization function by its non-interacting counterpart. As recapitulated in Sec. 1.4.1, this approximation formally corresponds to the zeroth order term in an expansion in the effective interaction, and a similar strategy appears thus reasonable in the present case. In particular, note, that the different contributions on the right side of the flow equations presented in Fig. 4.1 can be classified according to the number of longitudinal propagators $F_\Lambda(K)$.

In the following, the higher-order contributions in the second and third column of Fig. 4.1 are neglected and only the terms of the order of $\mathcal{O}\left(F_\Lambda(K)^0\right)$ are retained. As originally emphasized by Vaks *et al.* [33, 34], such a classification effectively corresponds to a expansion in the inverse longitudinal interaction range. Formally, the present truncation may thus only be justified for a long range interaction, which implies, that $J_{\boldsymbol{k}}$ is enhanced for small $\boldsymbol{k}$. Nevertheless, we assume that this truncation remains at least qualitatively correct even for short-range interaction. Given this simplification, the flow of the transverse four-point vertex in Fig. 4.1 (c) is still driven by three different scattering processes, which can be labeled in analogy to an interacting Fermi system as zero sound (ZS), exchange (EX) and particle-particle (PP) channel. For interacting fermions, the ZS channel dominates the renormalization of the effective interaction if $J_{\boldsymbol{k}}$ is of long-range nature. Analogously, we assume that this holds true in the present case as well, and neglect the other two channels in the following.

### Flow equations in zero-sound truncation

The previous approximations render the set of flow equations analytically tractable. To write down the explicit forms, let us introduce the auxiliary function

$$\dot{L}_\Lambda(K,Q) = \left[G_\Lambda(K)G_\Lambda(K-Q)\right]^\bullet. \tag{4.6}$$

The analytical expression for the flow of the longitudinal polarization shown in Fig. 4.1 then reads

$$-\partial_\Lambda \Pi_\Lambda(Q) = -\int_K \dot{L}_\Lambda(K,Q)\Gamma_\Lambda^{+-z}(K,Q-K,-Q)\Gamma_\Lambda^{+-z}(K-Q,-K,Q), \tag{4.7a}$$

while the flow equations of the three- and four-point vertices are given by,

$$\begin{aligned}&\partial_\Lambda \Gamma_\Lambda^{+-z}(K+Q,-K,-Q) = \\ &-\int_{K'} \dot{L}_\Lambda(K,-Q)\Gamma_\Lambda^{+-z}(K'+Q,-K',-Q)\Gamma_\Lambda^{++--}(K+Q,K',-K'-Q,-K),\end{aligned} \tag{4.7b}$$

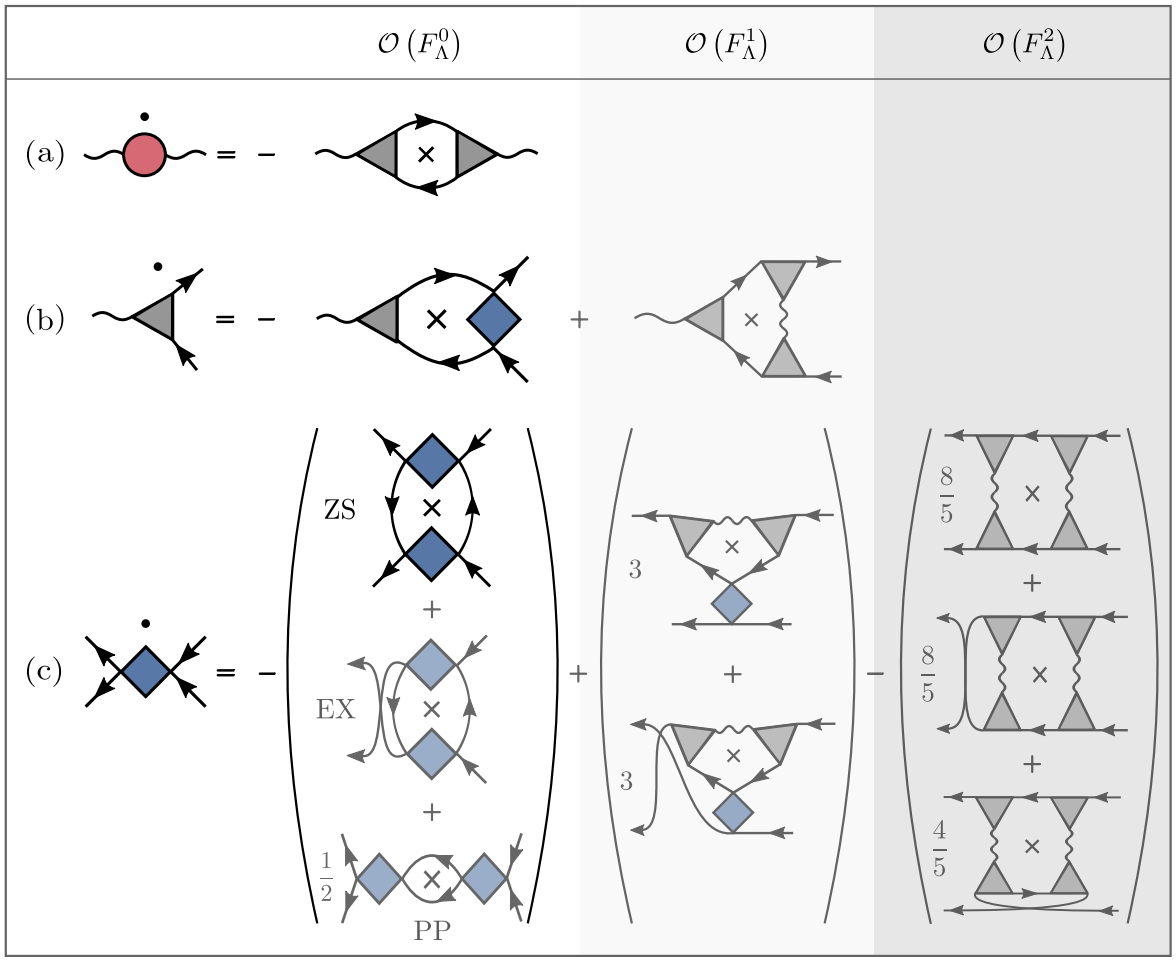


Figure 4.1: Graphical representation of the low temperature approximation of (a) the flow of the longitudinal two-point vertex $\Gamma_\Lambda^{zz}(K)$, and the corresponding flow of the higher-order vertices $\Gamma_\Lambda^{+-z}(K_1, K_2, K_3)$ (b) respectively $\Gamma_\Lambda^{++--}(K_1, \ldots, K_4)$ (c). The diagrammatic contributions on the right side of the flow equations are grouped in powers of the longitudinal effective interaction $F_\Lambda(K)$ defined in Eq. (4.3). In the present Zero-sound truncation, all higher order contributions, as well as the exchange and particle-particle contributions in the flow of $\Gamma_\Lambda^{++--}(K_1, \ldots, K_4)$ are neglected. The nomenclature of the different symbols follows Fig. 2.1.

respectively

$$\partial_\Lambda \Gamma_\Lambda^{++--}(K_1+Q, K_2-Q, -K_2, -K_1) = \\ -\int \dot{L}_\Lambda(K,Q)\Gamma_\Lambda^{++--}(K_1+Q, K-Q, -K, -K_1)\Gamma_\Lambda^{++--}(K_2-Q, K, Q-K, -K_2). \quad (4.7c)$$

In order to close this set of flow equations, the renormalization of the self energy $\Sigma_\Lambda(K)$ entering the transverse propagator

$$G_\Lambda(K) = \frac{M_0}{E_{\Lambda,\boldsymbol{k}} - i\omega + M_0\Sigma_\Lambda(K)}, \quad (4.8)$$

should be considered as well [for the definition of $E_{\Lambda,\boldsymbol{k}}$ see Eq. (3.22)]. In this respect it is useful to briefly reiterate an aspect of the previous chapter: the one-loop approximation $\Sigma_\Lambda(K) = 0$ led to qualitatively correct magnetization curves in dimensions $D = 3$ while this approximation predicted non-physical results $M_{D\leq 2}(H,T) < 0$ only for magnetic fields $H \ll T$. In the following, we therefore assume that the qualitative influence of the magnons on the longitudinal dynamics can be accounted for within the same approximation, provided that the magnetic field is restricted to the range

$$H_l(T) < H < T. \tag{4.9}$$

The lower bound $H_l(T)$ is hereby estimated via the condition $M_{\Lambda=1}(H_l(T),T) = 0$, where $M_\Lambda(H,T)$ is given by the one-loop solution (3.26) derived in Sec. 3.3.2. Upon applying the familiar low-temperature approximations - i.e. neglecting the initial contribution and setting $M_0 \approx S$ - this condition reduces to

$$\rho\big|_{H=H_l(T)} = 1, \tag{4.10}$$

where

$$\rho = \frac{1}{SN}\sum_{\boldsymbol{k}} n\left(\beta(H+\varepsilon_{\boldsymbol{k}})\right) \approx \frac{(k_{\mathrm{th}}a)^D}{Sc_D}\mathrm{Li}_{D/2}\left(e^{-\beta H}\right), \tag{4.11}$$

denotes the density of thermally excited magnons in units of $S$. Solving Eq. (4.10) using the asymptotic behavior of the polylogarithm in the limit $\beta H \ll 1$ (cf. appendix C.1.2), the lower bound is hence approximately given by

$$H_l(T) \approx \begin{cases} \frac{ma^2}{2S}T^2 & D = 1, \\ T\exp\left(-\frac{4\pi S}{ma^2 T}\right) & D = 2. \end{cases} \tag{4.12}$$

## 4.3 Generalized random phase solution

Having established the range of validity of the above truncation, we are left with an analysis of the three flow equations (4.7), which can be regarded as the spin FRG analog of the Bethe-Salpeter equations investigated by Izyumov *et al.* [36]. The following considerations are in most parts technical and have been outlined in concise form in appendix B of our publication Ref. [4], which I mostly quote here: [1]

*"[...] Given the structure of the set of flow equations (4.7), it is clear that in order to find an explicit solution for the polarization, we have to choose a suitable parameterization of the three- and four-point vertices."* This is done as follows in a form that is inspired by their corresponding mean-field conditions, derived in Sec. 3.3.1 as

$$\Pi_0(K) = 0, \tag{4.13a}$$

$$S\Gamma_0^{+-z}(K_1,K_2,K_3) = 1, \tag{4.13b}$$

$$S^2\Gamma_0^{++--}(K_1,K_2;K_3,K_4) = G_0^{-1}(-i\omega_3) + G_0^{-1}(-i\omega_4). \tag{4.13c}$$

[1] Reprinted with permission from Ref. [4] © [2020] American Physical Society. This appendix was written by the author in summer 2020. Any italic text is a literal copy of Ref. [4], while the normal text presents explanatory additions.

Here, all terms proportional to the derivatives of the Brillouin function were neglected and the mean field magnetization was approximated as $M_0 \approx S$. *"[...] Based on these initial conditions, we make the following ansatz for the three-point vertex*

$$S\Gamma_\Lambda^{+-z}(K_1, K_2, K_3) = \gamma_\Lambda^0(-K_3) + \gamma_\Lambda^1(-K_3)G_0^{-1}(-i\omega_2), \tag{4.14}$$

*and for the four-point vertex,*

$$\begin{aligned} S^2\Gamma_\Lambda^{++--}(K_1, K_2, K_3, K_4) = U_\Lambda^{00}(K_1 + K_4) \\ + U_\Lambda^{01}(K_1 + K_4)G_0^{-1}(-i\omega_4) \\ + U_\Lambda^{10}(K_1 + K_4)G_0^{-1}(-i\omega_3) \\ + U_\Lambda^{11}(K_1 + K_4)G_0^{-1}(-i\omega_3)G_0^{-1}(-i\omega_4). \end{aligned} \tag{4.15}$$

*This parametrization retains the initial frequency dependence of the vertices but promotes the corresponding coefficients to $\Lambda$-dependent functions. Furthermore, the additional terms $\gamma_\Lambda^1(K)$, $U_\Lambda^{00}(K)$ and $U_\Lambda^{11}(K)$ must necessarily be included since they are generated by the respective flow equation. With this ansatz, the flow equations (4.7) may be rewritten in compact matrix form as*

$$\partial_\Lambda \Pi_\Lambda(Q) = \boldsymbol{\gamma}_\Lambda^T(Q)\dot{\boldsymbol{P}}_\Lambda(Q)\boldsymbol{\gamma}_\Lambda(-Q), \tag{4.16a}$$

$$\partial_\Lambda \boldsymbol{\gamma}_\Lambda^T(Q) = -\boldsymbol{\gamma}_\Lambda^T(Q)\dot{\boldsymbol{P}}_\Lambda(Q)\boldsymbol{U}_\Lambda(Q), \tag{4.16b}$$

$$\partial_\Lambda \boldsymbol{U}_\Lambda(Q) = -\boldsymbol{U}_\Lambda(Q)\dot{\boldsymbol{P}}_\Lambda(Q)\boldsymbol{U}_\Lambda(Q), \tag{4.16c}$$

*where we introduced the two-component vector*

$$\boldsymbol{\gamma}_\Lambda(Q) = \begin{pmatrix} \gamma_\Lambda^0(Q) \\ \gamma_\Lambda^1(Q) \end{pmatrix}, \tag{4.17}$$

*and the $2 \times 2$ matrices*

$$\boldsymbol{U}_\Lambda(Q) = \begin{pmatrix} U_\Lambda^{00}(Q) & U_\Lambda^{01}(Q) \\ U_\Lambda^{10}(Q) & U_\Lambda^{11}(Q) \end{pmatrix}, \tag{4.18a}$$

$$\dot{\boldsymbol{P}}_\Lambda(Q) = \begin{pmatrix} \dot{P}_\Lambda^{00}(Q) & \dot{P}_\Lambda^{01}(Q) \\ \dot{P}_\Lambda^{10}(Q) & \dot{P}_\Lambda^{11}(Q) \end{pmatrix}. \tag{4.18b}$$

*Here, the four types of generalized differential polarization functions $\dot{P}^{\mu\nu}(Q)$ are defined by*

$$S^2\dot{P}_\Lambda^{00}(Q) = \int_K \dot{L}(K, Q) \tag{4.19a}$$

$$S^2\dot{P}_\Lambda^{01}(Q) = \int_K \dot{L}(K, Q)G_0^{-1}(i\omega), \tag{4.19b}$$

$$S^2\dot{P}_\Lambda^{10}(Q) = \int_K \dot{L}(K, Q)G_0^{-1}(i\omega - i\nu), \tag{4.19c}$$

$$S^2\dot{P}_\Lambda^{11}(Q) = \int_K \dot{L}(K, Q)G_0^{-1}(i\omega)G_0^{-1}(i\omega - i\nu). \tag{4.19d}$$

*The quadratic structure of Eqs. (4.16) allows us to construct a formal solution for the seven functions $\Pi_\Lambda(Q)$, $\gamma^\mu_\Lambda(Q)$ and $U^{\mu\nu}_\Lambda(Q)$. In particular, we note that the flow equation (4.16c) involving the four functions $U^{\mu\nu}_\Lambda(Q)$ is a matrix Ricatti equation, whose formal solution is*

$$\boldsymbol{U}_\Lambda(Q) = [1 + \boldsymbol{U}_0 \boldsymbol{P}_\Lambda(Q)]^{-1} \boldsymbol{U}_0, \quad \boldsymbol{U}_0 = \begin{pmatrix} 0 & 1 \\ 1 & 0 \end{pmatrix}, \tag{4.20}$$

*where, the form of $\boldsymbol{U}_0$ is determined by the initial conditions (4.13), while the coefficients of the matrix $\boldsymbol{P}_\Lambda(Q)$ read*

$$\big(\boldsymbol{P}_\Lambda(Q)\big)^{\mu\nu} = P^{\mu\nu}_\Lambda(Q) = \int_0^\Lambda d\Lambda'\, \dot{P}^{\mu\nu}_{\Lambda'}(Q). \tag{4.21}$$

*Moreover, the structure of the flow equations (4.16) allows to derive an explicit solution for $\boldsymbol{\gamma}_\Lambda(Q)$. Comparing Eqs. (4.16b) and (4.16c), we can identify the two independent solutions*

$$\boldsymbol{\gamma}_{\Lambda,1}(Q) = \begin{pmatrix} U^{00}_\Lambda(Q) \\ U^{01}_\Lambda(Q) \end{pmatrix}, \quad \textit{and} \quad \boldsymbol{\gamma}_{\Lambda,2}(Q) = \begin{pmatrix} U^{10}_\Lambda(Q) \\ U^{11}_\Lambda(Q) \end{pmatrix}. \tag{4.22}$$

*However, only the latter is compatible with the initial condition $\boldsymbol{\gamma}^T_{\Lambda=0}(Q) = (1, 0)$ and is thus chosen in the following. Substituting the solution $\boldsymbol{\gamma}_{\Lambda,2}(Q)$ into Eq. (4.16a) and using the symmetries $U^{00}_\Lambda(-Q) = U^{00}_\Lambda(Q)$ and $U^{01}_\Lambda(-Q) = U^{10}_\Lambda(Q)$, it is then straightforward to show that the flow of the polarization satisfies*

$$\partial_\Lambda \Pi_\Lambda(Q) = -\partial_\Lambda U^{11}_\Lambda(Q). \tag{4.23}$$

*Integrating both sides of Eq. (4.23) from $\Lambda = 0$ to $\Lambda = 1$ and explicitly evaluating the 11-matrix element of the solution (4.20) then yields the polarization*

$$\Pi_{\Lambda=1}(Q) = -U^{11}_{\Lambda=1}(Q) = \frac{P^{00}(Q)}{[1 + P^{10}(Q)]\,[1 + P^{01}(Q)] - P^{00}(Q)P^{11}(Q)}, \tag{4.24}$$

*with $P^{\mu\nu}(Q) = P^{\mu\nu}_{\Lambda=1}(Q)$. [...] The four different types of generalized polarizations $P^{\mu\nu}(Q)$ can be further simplified by explicitly carrying out the $\Lambda$-integration in Eq. (4.21). Since the transverse self energy was neglected, this is a trivial operation and we recover [...]"*

$$S^2 P^{00}(Q) = \int_K L(K, Q), \tag{4.25a}$$

$$S^2 P^{01}(Q) = S^2 P^{10}(-Q) = \int_K L(K, Q) G_0^{-1}(i\omega), \tag{4.25b}$$

$$S^2 P^{11}(Q) = \int_K L(K, Q) G_0^{-1}(i\omega) G_0^{-1}(i\omega - i\nu), \tag{4.25c}$$

where the function $L(K, Q)$ is defined by

$$L(K, Q) = G(K)G(K - Q) - G_0(i\omega)G_0(i\omega - i\nu), \tag{4.26}$$

with $G(K) = G_{\Lambda=1}(K)$ and $G_0(i\omega) = G_{\Lambda=0}(K)$ defined in Eq. (4.8). Substituting the polarization defined in (4.24) in the expression for the longitudinal correlation function Eq. (4.2), we finally obtain the longitudinal two-point correlation function

$$G^{zz}(Q) = \frac{P^{00}(Q)}{[1 + P^{01}(Q)][1 + P^{10}(Q)] - P^{00}(Q)[P^{11}(Q) + J^z_{\boldsymbol{q}}]}. \tag{4.27}$$

Please note, that this expression strongly resembles Eq. (5.13) of Ref. [36], although it is not equivalent because the generalized polarizations $P^{01}(Q), P^{10}(Q)$ and $P^{11}(Q)$ do not agree with the corresponding quantities of Ref. [36]. Following Ref. [36] we hence refer to Eq. (4.27) as *generalized random phase solution* (GRPA). This name follows from the structure of the corresponding one-loop solution

$$G^{zz}_{\mathrm{RPA}}(Q) = \frac{P^{00}(Q)}{1 - P^{00}(Q) J^z_{\boldsymbol{q}}}, \tag{4.28}$$

which presents the bosonic analogue of the RPA solution for the density-density correlation function of a Fermi gas (cf. Sec. 1.4.1). While this expression was first derived in the pioneering work of Vaks *et al.* [33, 34] we will show hereinafter that the additional terms in the generalized solution Eq. (4.27) lead to significantly different longitudinal dynamics as compared to the RPA result.

### 4.3.1 Low momentum approximation of the generalized polarizations

In order to analyze the dynamics encoded in the GRPA solution, the generalized polarizations defined in Eqs. (4.25) need to be evaluated. With the help of the transverse propagator $G_\Lambda(K)$ and its corresponding mean field value $G_0(i\omega)$ defined in Eq. (4.8), we can carry out the Matsubara sums to obtain

$$P^{00}(Q) = \frac{1}{N}\sum_{\boldsymbol{k}} \left[C(\boldsymbol{k}, \boldsymbol{q}, i\nu) + n_0' \delta_{\omega,0}\right], \tag{4.29a}$$

$$P^{01}(Q) = P^{10}(-Q) = \frac{1}{N}\sum_{\boldsymbol{k}} \left[C(\boldsymbol{k}, \boldsymbol{q}, i\nu) J_{\boldsymbol{k}+\frac{\boldsymbol{q}}{2}} + \frac{n_{\boldsymbol{k}} - n_0}{S}\right], \tag{4.29b}$$

$$P^{11}(Q) = \frac{1}{N}\sum_{\boldsymbol{k}} \left[C(\boldsymbol{k}, \boldsymbol{q}, i\nu) J_{\boldsymbol{k}+\frac{\boldsymbol{q}}{2}} J_{\boldsymbol{k}-\frac{\boldsymbol{q}}{2}} + \frac{2 n_{\boldsymbol{k}} J_{\boldsymbol{k}}}{S}\right], \tag{4.29c}$$

where we introduced the auxiliary function

$$C(\boldsymbol{k}, \boldsymbol{q}, i\nu) = \frac{n_{\boldsymbol{k}+\boldsymbol{q}/2} - n_{\boldsymbol{k}-\boldsymbol{q}/2}}{\varepsilon_{\boldsymbol{k}-\frac{\boldsymbol{q}}{2}} - \varepsilon_{\boldsymbol{k}+\frac{\boldsymbol{q}}{2}} + i\nu}, \tag{4.30}$$

and the abbreviations $n_{\boldsymbol{k}} = n(\beta E_{\Lambda=1,\boldsymbol{k}})$, respectively $n_0 = n(\beta E_{\Lambda=0})$. Following the analysis of the one-loop solution of the magnetization given in Sec. 3.3.2, the mean-field terms $n_0' = -n_0\left(n_0 + 1\right)/T$ and $n_0$ can be neglected in the examined temperature range $H < T \ll SJ_0$. In addition, please recall, that in this temperature regime the thermal momentum $k_{\mathrm{th}} = \sqrt{2mT}$ acts as an ultraviolet cutoff. For momenta $|\boldsymbol{q}| \ll k_{\mathrm{th}}$, the auxiliary function $C(\boldsymbol{k}, \boldsymbol{q}, i\nu)$ thus can be expanded as

$$C(\boldsymbol{k}, \boldsymbol{q}, i\nu) \approx c(\boldsymbol{k}, \boldsymbol{q}, i\nu) = -n_{\boldsymbol{k}}' \frac{\boldsymbol{v}_{\boldsymbol{k}} \cdot \boldsymbol{q}}{\boldsymbol{v}_{\boldsymbol{k}} \cdot \boldsymbol{q} - i\nu}, \tag{4.31}$$

where $n_{\boldsymbol{k}}' = -\beta n_{\boldsymbol{k}}(n_{\boldsymbol{k}} + 1)$ and $\boldsymbol{v}_{\boldsymbol{k}} = \nabla_{\boldsymbol{k}} \varepsilon_{\boldsymbol{k}}$ is the magnon velocity. Furthermore, to leading order in $\boldsymbol{q}$, the $\boldsymbol{q}$-dependence of the factors $J_{\boldsymbol{k}\pm\boldsymbol{q}/2}$ in the expressions of the generalized polarization functions can be neglected. This is justified, given that the longitudinal correlation

function (4.27) depends only on the sum $P^{01}(Q) + P^{10}(Q)$ and the product $P^{01}(Q)P^{10}(Q)$ which are even functions of $\boldsymbol{q}$. We hence approximate

$$P^{00}(Q) = \frac{1}{N}\sum_{\boldsymbol{k}} c(\boldsymbol{k}, \boldsymbol{q}, i\nu), \tag{4.32a}$$

$$P^{10}(Q) = P^{01}(Q) = \frac{1}{N}\sum_{\boldsymbol{k}} \left[\frac{n_{\boldsymbol{k}}}{S} + c(\boldsymbol{k}, \boldsymbol{q}, i\nu)J_{\boldsymbol{k}}\right], \tag{4.32b}$$

$$P^{10}(Q) = \frac{1}{N}\sum_{\boldsymbol{k}} \left[\frac{2n_{\boldsymbol{k}}J_{\boldsymbol{k}}}{S} + c(\boldsymbol{k}, \boldsymbol{q}, i\nu)J_{\boldsymbol{k}}^2\right]. \tag{4.32c}$$

Given that the momentum integrals in the present temperature regime are dominated by small momenta, we may finally also neglect the $\boldsymbol{k}$-dependence of $J_{\boldsymbol{k}}$ in the integrands and replace the momentum dependent part of the magnon dispersion $\varepsilon_{\boldsymbol{k}}$ by its long wavelength approximation $\varepsilon_{\boldsymbol{k}} \approx k^2/(2m)$. This allows to express the higher order generalized polarization function as,

$$P^{10}(Q) = P^{01}(Q) = J_0 P^{00}(Q) + \rho, \tag{4.33a}$$

$$P^{11}(Q) = J_0^2 P^{00}(Q) + 2J_0\rho, \tag{4.33b}$$

where $\rho$ is the density of thermally excited magnons, defined in Eq. (4.11). To simplify the upcoming numerical analysis let us rewrite the polarization $P^{00}(Q)$ in a more accessible form. For this purpose we evaluate the momentum summation in Eq. (4.32) within the usual low momentum expansion sketched in appendix C.1.1, such that the polarization reduces to

$$P^{00}(\boldsymbol{q}, i\nu) = P\left(\frac{i\nu}{v_{\mathrm{th}}q}\right), \tag{4.34}$$

where we introduced the thermal velocity $v_{\mathrm{th}} = k_{\mathrm{th}}/m$. Here the function $P(z)$ with $z \in \mathbb{C}$ is given by

$$P(z) = \beta\frac{(k_{\mathrm{th}}a)^D}{\tilde{c}_D}\int_0^\infty d\epsilon\, g_D\left(\frac{z}{\sqrt{\epsilon}}\right)\frac{\epsilon^{\frac{D-2}{2}}e^{\beta H+\epsilon}}{(e^{\beta H+\epsilon}-1)^2}, \quad \tilde{c}_D = \frac{2(2\pi)^D}{\Omega_D}, \tag{4.35}$$

with the angular average

$$g_D(z) = \frac{1}{\Omega_D}\int d\Omega_D \frac{\cos\vartheta}{\cos\vartheta - z}, \tag{4.36}$$

where the angle $\vartheta$ denotes the latitude on the surface of the $D$-dimensional unit sphere $\Omega_D$. Within these approximations we finally obtain the following simplified expression for the longitudinal two-point correlation function:

$$G^{zz}(\boldsymbol{q}, i\nu) = \frac{P\left(\frac{i\nu}{v_{\mathrm{th}}q}\right)}{(1+\rho)^2 + J_0 P\left(\frac{i\nu}{v_{\mathrm{th}}q}\right)}. \tag{4.37}$$

Note, that the higher order $\boldsymbol{q}$-dependence of $J_{\boldsymbol{q}}$ in the denominator of Eq. (4.27) was omitted, in order to be consistent with the previous low momentum expansion. Remarkably, the inclusion of the three and four-point vertices thus leads to a sign flip in the low momentum structure of the denominator as compared to the one-loop RPA result given in Eq. (4.28).

### 4.3.2 Zero-magnon sound

We are now in the position to investigate the existence of a collective zero-magnon excitation. To this end, let us evaluate the longitudinal dynamic structure factor, which following Sec. 1.3 is given as

$$S^{zz}(\boldsymbol{q},\omega) = \frac{1}{\pi}\frac{e^{\beta\omega}}{e^{\beta\omega}-1}\mathrm{Im}\, G^{zz}(\boldsymbol{q}, i\nu \to \omega + i\delta). \tag{4.38}$$

For this purpose, the integral defining the function $P(z)$ in Eq. (4.35) is calculated numerically. The details of this evaluation are summarized in appendix C.1.3, where the explicit expression for $g_D(z)$ as well as the resulting form of $P(z)$ are given. The resulting structure factor is shown in Fig. 4.2 in $D = 1, 2, 3$ and for magnetic fields in the regime $H < T$. Please note, that the relevant energy scale is set by the magnon stiffness $1/(ma^2)$. Remarkably, we indeed observe a finite frequency peak at position $\omega_s(\boldsymbol{q}) = v_0 q$ in dimensions $D = 1$ and $D = 2$, which we identify as a zero-magnon signature. In $D = 1$, this peak is sharp provided the magnetic field is only a little smaller than the temperature, while in $D = 2$, a similar well-defined mode is only present for significantly smaller magnetic fields. This observation should be contrasted with the three-dimensional case, where the structure factor is dominated by a zero frequency hump, whose width is $\propto q$. This suggests that there is no zero magnon in $D = 3$, which is consistent with the literature (see in particular Refs. [30–32, 138]).

#### Zero-magnon sound velocity and damping strength

To further analyze these observations, let us follow along the lines of Sec. 1.4.1 where the zero-sound mode in Fermi systems was discussed. In particular, recall that a zero-sound mode exists if the longitudinal two-point correlation function has a pole close to the real axes in the complex plane. The corresponding sound dispersion $\omega_{\boldsymbol{q}}$ is then given by

$$\omega_{\boldsymbol{q}}^{\parallel_0} = v_0 q, \quad v_0 = v_{\mathrm{th}} x_0, \tag{4.39}$$

where $x_0 \in \mathbb{R}$ is the positive solution of

$$(1+\rho)^2 + J_0 \mathrm{Re}\, P\,(x_0) = 0. \tag{4.40}$$

Likewise we can determine the corresponding damping strength. To this end, let us expand the longitudinal correlation function in Eq. (4.38) around $x_0$, such that the structure factor takes on the Lorentzian form

$$S^{zz}(\boldsymbol{q},\omega) = \left(\frac{e^{\beta\omega}}{e^{\beta\omega}-1}\right)\frac{\omega_{\boldsymbol{q}}}{2\pi J_0}\frac{\gamma_{\boldsymbol{q}}}{(\omega-\omega_{\boldsymbol{q}})^2+\gamma_{\boldsymbol{q}}^2}. \tag{4.41}$$

Here, we introduced the damping coefficient

$$\gamma_{\boldsymbol{q}} = y_0 v_{\mathrm{th}} q, \quad y_0 = \frac{\mathrm{Im}\, P(x_0+i\delta)}{\mathrm{Re}\, P'(x_0+i\delta)}, \tag{4.42}$$

where $P'(z) = dP(z)/\,dz$. The numerical results for the solution of the sound velocity $v_0/v_{\mathrm{th}}$ and the corresponding relative damping $\gamma_{\boldsymbol{q}}/\omega_{\boldsymbol{q}}$ are shown graphically in Fig. 4.3 for three different temperatures $T \ll 1/(ma^2)$. Note, that in $D = 3$ there is no solution to Eq. (4.40),

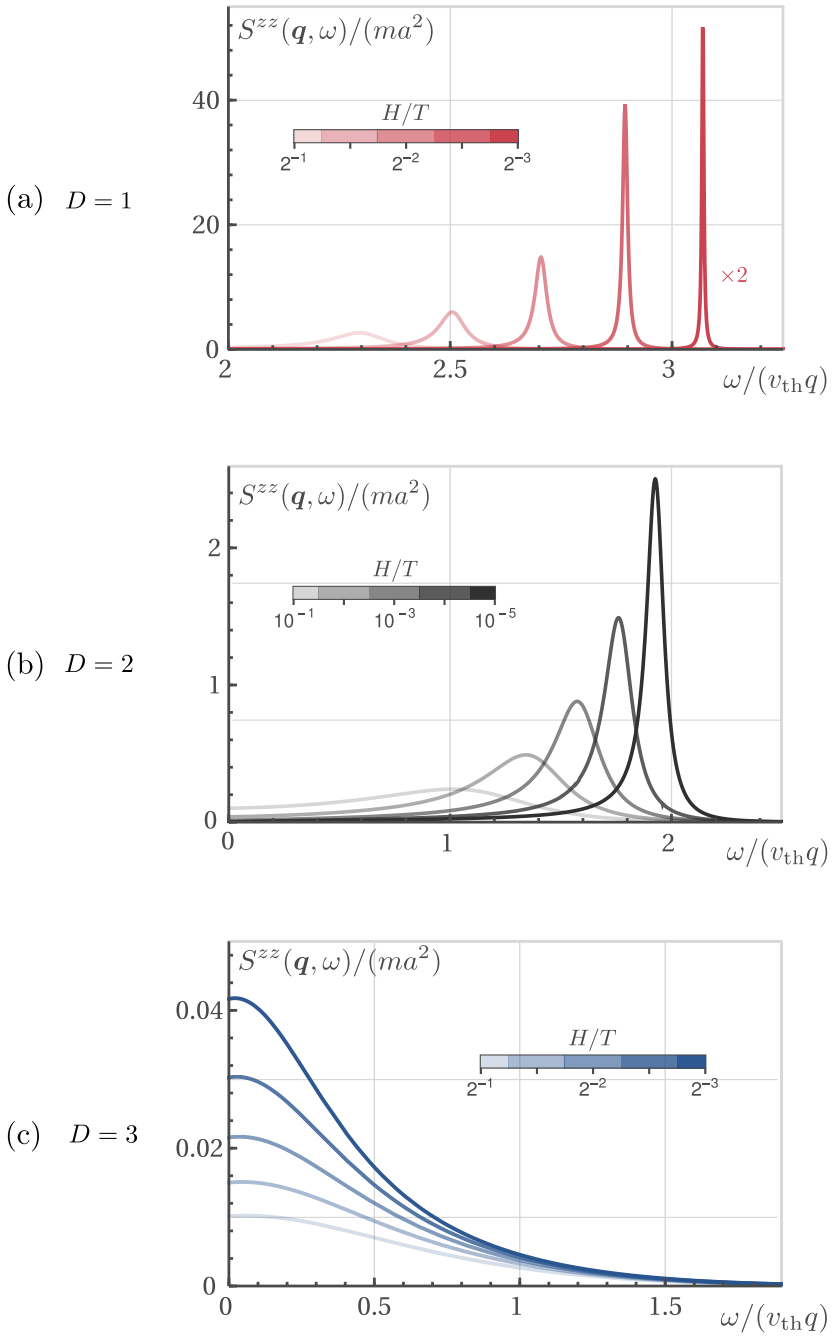


Figure 4.2: Longitudinal dynamic structure factor $S^{zz}(\boldsymbol{q},\omega)$ [Eq. (4.38)] of the $D$-dimensional, $S = 1/2$ Heisenberg ferromagnet for $q = k_{\rm th}/4$, temperature $Tma^2 = 10^{-2}$ and magnetic fields in the range $H < T \ll 1/(ma^2)$. Reprinted with permission from Ref. [4] © [2020] American Physical Society.

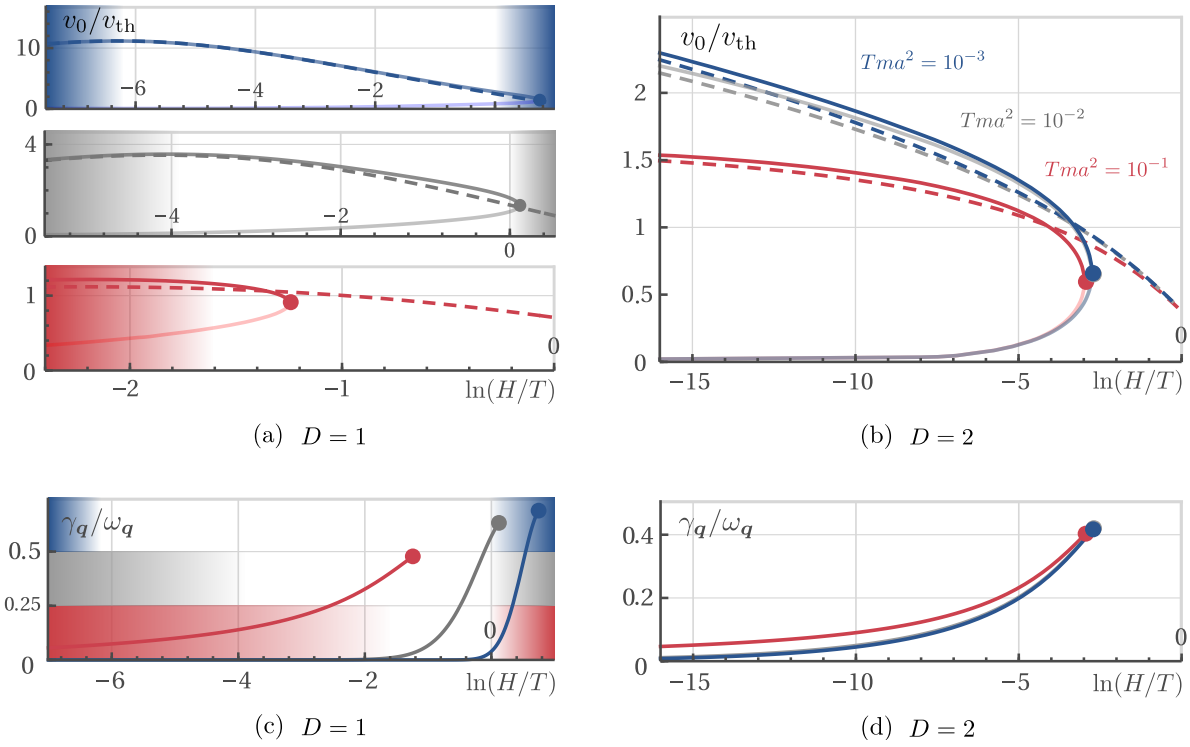


Figure 4.3: Zero-magnon velocity $x_0 = v_0/v_{\rm th}$ in (a) $D = 1$ and (b) $D = 2$ as a function of dimensionless magnetic field $H/T$ for temperatures $Tma^2 = 10^{-1}, 10^{-2}, 10^{-3}$ (red, gray, blue). The dashed line corresponds to the approximate solution (4.45), while the full line is obtained solving Eq. (4.40) numerically. For magnetic fields smaller than a certain upper limit (displayed as a full dot), Eq. (4.40) has two solutions [lower (opaque) and upper (full) branch], where the larger one may be identified as the corresponding zero-magnon velocity. The shading indicates the boundaries $H = H_l(T)$ and $H = T$ where our calculation breaks down. In $D = 2$, the calculation remains valid for the whole range of displayed magnetic fields. (c): Damping $y_0 = \gamma_{\boldsymbol{q}}/\omega_{\boldsymbol{q}}$ of the zero-magnon mode. Reprinted with permission from Ref. [4] © [2020] American Physical Society.

which confirms the absence of a zero-magnon mode, as indicated previously. In $D = 1$ and $D = 2$ we find a solution to Eq. (4.40) provided the magnetic field is smaller than a certain upper limit, which is indicated by the full dot in Fig. 4.3. However, for magnetic fields slightly smaller than this limit, the relative damping $\gamma_{\boldsymbol{q}}/\omega_{\boldsymbol{q}}$ is still quite large, and it is only for even smaller magnetic fields that a well-defined zero-magnon mode exists ($\gamma_{\boldsymbol{q}}/\omega_{\boldsymbol{q}} \ll 1$). Remarkably, the sound velocity in this regime is significantly larger than the thermal velocity $v_{\rm th}$, which allows us to derive an analytical expression for $v_0$. To this end recall, that in the relevant parameter regime the integral defining the function $P(z)$ is dominated by small $\epsilon \lesssim 1$. For $x_0 \gg 1$, it is thus possible to approximate the real part of the angular average in the integrand of $\mathrm{Re}\, P(x_0 + i\delta)$ by,

$$\mathrm{Re}\, g_D\left(\frac{x_0 + i\delta}{\sqrt{\varepsilon}}\right) \approx -\frac{\varepsilon}{D x_0^2}, \quad \frac{x_0}{\sqrt{\varepsilon}} \gg 1 \tag{4.43}$$

which allows us to express the function $P(x_0)$ in terms of the Polylogarithm as

$$\mathrm{Re}P\left(x_0+i\delta\right)=-\frac{\beta\left(k_{\mathrm{th}}a\right)^D}{2c_Dx_0^2}\mathrm{Li}_{D/2}(e^{-\beta H}). \tag{4.44}$$

Upon substituting this approximation into the condition (4.40), we hence find the analytical expression for the dimensionless zero-sound velocity

$$x_0=\frac{v_0}{v_{\mathrm{th}}}=\sqrt{\frac{\beta J_0\left(k_{\mathrm{th}}a\right)^D\mathrm{Li}_{D/2}(e^{-\beta H})}{2c_D(1+\rho)^2}}=\sqrt{\frac{\beta J_0S}{2}\frac{\rho}{(1+\rho)^2}}, \tag{4.45}$$

where we expressed the polylogarithm in the numerator in terms of the magnon density in the second identity. Moreover, given that the the normalized magnon density is bound by $\rho=1$, the maximal value of the sound velocity can be estimated as

$$\mathrm{Max}(x_0)=\frac{1}{2}\sqrt{\frac{\beta J_0S}{2}}. \tag{4.46}$$

### Analogy to fermionic zero sound

An intuitive picture of the previous results can be obtained from a graphical comparison of the involved energy scales. For this purpose, let us briefly sketch the evaluation of the polarization bubbles to second order in $q$. In particular, consider the imaginary parts $\mathrm{Im}\,P^{\mu\nu}(Q)$ which determine the damping of the zero-magnon mode. After analytical continuation to real frequencies, we obtain the general expression

$$\mathrm{Im}\,P^{\mu\nu}(\boldsymbol{q},\omega+i\delta)=-\frac{i\pi}{N}\sum_{\boldsymbol{k}}\left[A^{\mu\nu}_{\boldsymbol{k}}n_{\boldsymbol{k}}\delta\left(\varepsilon_{\boldsymbol{k}-\boldsymbol{q}}-\varepsilon_{\boldsymbol{k}}+\omega\right)+(\boldsymbol{q},\omega)\leftrightarrow(-\boldsymbol{q},-\omega)\right], \tag{4.47}$$

where, we introduced the shorthands $A^{00}_{\boldsymbol{k}}=1$, $A^{10}_{\boldsymbol{k}}=A^{01}_{\boldsymbol{k}}=J_{\boldsymbol{k}}$, and $A^{11}_{\boldsymbol{k}}=J_{\boldsymbol{k}}J_{\boldsymbol{k}-\boldsymbol{q}}$. In order to make contact with the fermionic zero-sound results discussed in the introduction, let us suppose the momentum integration in Eqs. (4.29) are evaluated within the approximation $\varepsilon_{\boldsymbol{k}}=k^2/(2m)$ restricting the momentum integration to the region $k\in(0,k_{\mathrm{th}})$. The simultaneous presence of the momentum cutoff $k_{\mathrm{th}}$ and the the delta function in the above integrand then leads to non-vanishing result $\mathrm{Im}\,P^{\mu\nu}(\boldsymbol{q},\omega+i\delta)\neq0$ only in the region

$$\tilde{q}(\tilde{q}+1)<\tilde{\omega}<\tilde{q}(\tilde{q}-1), \tag{4.48}$$

where

$$\tilde{\omega}=\frac{\omega}{4T},\quad \tilde{q}=\frac{q}{2k_{\mathrm{th}}}, \tag{4.49}$$

denote dimensionless frequency and momentum. In analogy to the Fermi liquid, this momentum-frequency range can be interpreted as the continuum region, in which any density fluctuation can dissipate into virtual magnon pairs and is thus strongly over-damped. For this reason, the second solution to $x_0$ (the lower branch in Fig. 4.3) does not lead to a well-defined excitation peak in the structure factor. Likewise, we can interpret the zero-magnon mode as the coherent superposition of virtual magnon states, excited in a range $\omega_q^{\|_0}$ around $\varepsilon_{\boldsymbol{k}}=T$.

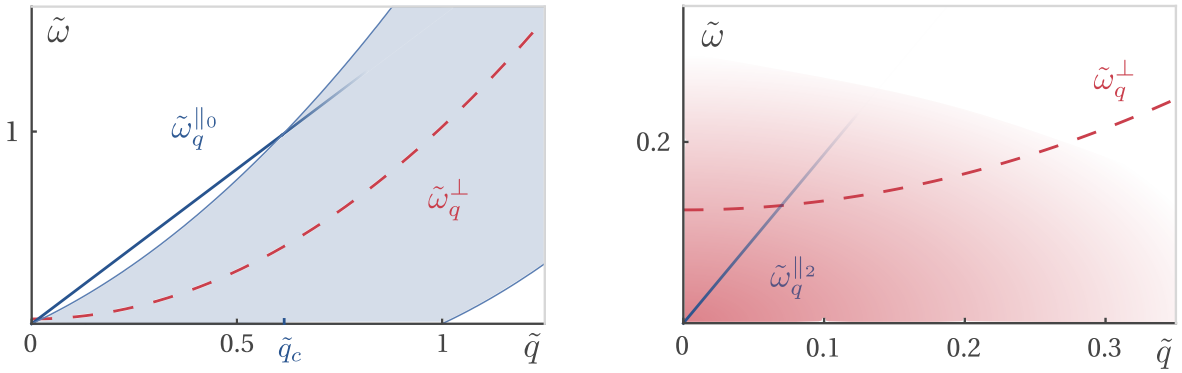


(a) $Tma^2 = 10^{-1}$, $Hma^2 = 10^{-2}$ (b) $Tma^2 = 1$, $Hma^2 = 0.5$

Figure 4.4: Comparison of the relevant momentum-frequency scales in the collisionless and collision-dominated regime of the two-dimensional Heisenberg ferromagnet. (a): dimensionless magnon (red) and zero-sound (blue) dispersions together with the two-magnon continuum (shaded area, bounded by Eq. (4.48). (b): dimensionless magnon (red) and second-sound (blue) dispersions together with the range of validity of the hydrodynamic description (shaded area, bounded by Eq. (4.54) with $\tilde{q} \lesssim \sqrt{\tilde{\omega}_{\text{col}}}$).

Having said that, we also expect that the zero-magnon mode is only well-defined up to a momentum $q_c$, above which it is absorbed in the magnon continuum. This scenario is depicted in Fig. 4.4 (a), where the magnon continuum is shown together with the dimensionless low momentum expansions of the magnon, and zero-sound dispersions

$$\tilde{\omega}_q^{\perp} = \frac{\beta H}{4} + \tilde{q}^2, \quad \tilde{\omega}_q^{\parallel} = 2x_0\tilde{q}. \tag{4.50}$$

Within theses approximations we can estimate the critical momentum as and corresponding critical frequency as

$$\tilde{q}_c \sim 2x_0 - 1, \quad \tilde{\omega}_c \sim 2x_0(x_0 - 1). \tag{4.51}$$

However, please keep in mind that a reliable determination of these values for $\tilde{q}_c \gg 1$ requires the evaluation of the zero-sound dispersion and damping for generic values of $q$, for which the momentum sums in $P^{\mu\nu}(Q)$ should be evaluated without any low momentum approximations. In addition, let us recall that the sharp onset of the magnon continuum is an artifact of the (artificially) introduced momentum cutoff $k_{\text{th}}$. While this procedure allows to highlight the relation to the fermionic zero-sound scenario, an exact momentum integration would also lead to a smooth transition.[2]

### Relation to second magnon sound

Finally, let us briefly make establish the connection with the second magnon phenomenon, which occurs in the collision-dominated regime of the Heisenberg ferromagnet and was investigated in detail in $D = 3$ by Reiter [135], and Schwabl and Michel [136, 137], respectively in $D = 2$ in the recent work of Rodriguez *et al.* [24]. Here, the system's dynamics are described

[2]Note, that in the numerical evaluation of the structure factor displayed in Fig. 4.2 this is mimicked by sending the upper integration boundary to infinity.

by a set coupled hydrodynamic equations for the the local temperature, magnetization, and momentum densities, which should be valid in the presence of a strong magnetic field, and in the temperature range where Umklapp and dipole scattering processes can be neglected. A detailed analysis of these equations gives rise to diffusive temperature fluctuations and two propagating modes accounting for the fluctuations of the spin components: the transverse spin-wave mode and a second magnon mode describing a wave-like propagation of the magnetization density.[3] Following Refs. [24, 135] the dimensionless dispersion relation of the latter is hereby given as

$$\tilde{\omega}_q^{\parallel 2} = 2x_2\tilde{q}, \tag{4.52}$$

with the dimensionless second magnon velocity

$$x_2 = \sqrt{r_D \frac{\mathrm{Li}_{D/2+1}(e^{-\beta H})}{\mathrm{Li}_{D/2}(e^{-\beta H})}}, \qquad r_D = \begin{cases} 5/6 & D = 3, \\ 1 & D = 2. \end{cases} \tag{4.53}$$

This second sound-scenario is depicted in Fig. 4.4 (b), where it should be kept in mind that a hydrodynamic description is only valid at frequency scales $\omega \ll \omega_{\mathrm{col}}$, with $\omega_{\mathrm{col}}$ the collision frequency of the magnons. In a clean system, the latter is dominated by momentum conserving two magnon-collisions which, following Ref. [24, 99], lead to a collision frequency of the form

$$\omega_{\mathrm{col}} \sim T\left(Tma^2\right)^D \rho^2, \quad (\tilde{\omega}_{\mathrm{col}} \sim \left(Tma^2\right)^D \rho^2). \tag{4.54}$$

Since this expression vanishes in the limit $T \to 0$, practical observations of the collision-dominated hydrodynamic regime are hence not feasible at low temperatures. Moreover, the occurrence of a second-magnon mode within the hydrodynamic regime is likewise bound to a momentum and frequency window, where the aforementioned dipole and Umklapp scattering processes can be neglected. As estimated in Ref. [136, 137] for the three-dimensional case, this window is probably negligibly small. It is therefore not surprising that an experimental confirmation of second magnon sound close to equilibrium has not been established yet. (For a recent experimental observation of second sound modes in parametrically pumped yttrium-iron garnet (YIG) films, see Ref. [139]).

---

This brief comparison with the hydrodynamic regime concludes the chapter. On the remaining pages, the essential results of this thesis are shortly categorized and an outlook to possible future studies is given.

[3] As stressed by Halperin and Hohenberg the transverse dynamics can thus be interpreted in analogy to liquid He-4: hydrodynamic spin waves bear the same relation to elementary magnon excitations as first sound bears to phonons in liquid helium He-4.

# Chapter 5

# Conclusion

## 5.1 Résumé

This thesis provides an investigation of the thermodynamic and dynamic properties of the $D$-dimensional quantum Heisenberg ferromagnet within the non-perturbative spin FRG method. Overall, this work can hereby be regarded as one of the first successful application of this novel technique, containing conceptual and technical progress on several levels.

On the methodological side, restrictions of the applicability of the original spin FRG formulation were sketched, and the significance of the hybrid formalism in the description of the symmetry broken phase was highlighted. Furthermore, it was shown that it is beneficial to introduce the Legendre transformation of the hybrid functional with the regulator terms coupling to the fluctuations around the extremal source configuration, since this saves the need to formulate the vertex expansion of the FRG flow equation around some self consistent source field.

As a proof of principle for the utility of the spin FRG method, chapter 2 presented an investigation of the thermodynamic properties of the model at low temperatures and finite magnetic fields. To this end we devised the anisotropic exchange interaction deformation scheme, which allowed for a controlled truncation of the infinite hierarchy of flow equations, making contact with conventional mean-field and linear spin-wave theory along the way. Moreover, we could show that the Mermin Wagner theorem - governing the low temperature behavior of the Heisenberg system in $D \leq 2$ - can be satisfied by complementing the FRG flow equations with a Ward-identity that was derived graphically. The resulting magnetization and isothermal susceptibility curves agree very well with the corresponding literature results. This demonstrates that thermodynamic properties of quantum spin systems can be quantitatively calculated within the spin FRG, provided that physically meaningful truncation strategies exist.

The benefits of the spin FRG method were further highlighted within the subsequent (re)investigation of the zero-magnon problem. In particular, the algebraic structure of the tower of FRG flow equation allowed us to clearly distinguish the different longitudinal and transverse processes contributing to the longitudinal two point correlation function. This simplicity is remarkable and in stark contrast to the complicated auxiliary bosonic and fermionic formulations of the problem respectively the idiosyncratic spin diagrammatic calculations of Izyumov *et al.* (cf. Refs. [29–32]) and Ref. [36]). In qualitative accordance with these works,

our generalized RPA results for the longitudinal structure factor predict that no collective zero-sound mode exists in $D = 3$. By contrast, in $D \leq 2$ we indeed find a collective sound mode with linear dispersion in the vicinity of the critical point, i.e. at low temperatures $T \ll SJ_0$ and in the magnetic field range $H_l(T) < H < T$ [cf. Eq. (4.12) for the explicit form of $H_l(T)$]. To our knowledge, this emergent property arising from the coherent superposition of spin wave states, has not been described before, while the fact that its existence is restricted to $D \leq 2$ is consistent with the expectation that long wavelength fluctuations do have drastically more influence in lower dimensional systems. Having said that, please note that the algebraic simplicity of the tower of FRG also allows us to clearly address the two critical assumptions underlying this central result: Firstly, that it is reasonable to classify the contributions in the tower of FRG flow equations according to the number of longitudinal propagators, which effectively corresponds to an expansion in the inverse interaction range and can hence formally only be justified for long range exchange interactions. Secondly, that the exchange and particle-particle processes depicted in Fig. 4.1 do not significantly alter the longitudinal dynamics at low temperatures, which can only be justified by an analogy to the related Fermi liquid system.[1] A detailed analysis of the influence of these terms would help to refine the precise conditions under which our results can be applied. In contrast to the here-presented calculation, such an analysis requires the numerical solution of the resulting set of coupled integro-differential equations. However, this would open a full new aspect of technical complexity and hence is postponed to future studies.

## 5.2 Outlook

With respect to the findings of this thesis, several future directions can be envisaged. On the level of the spin FRG it might be possible to analyze a possible zero-magnon signature in the specific heat $C(H,T)$ of the ferromagnetic Heisenberg chain. Noteworthy, for magnetic fields in the range $H \lesssim 0.01ma^2$, the exact Bethe calculations presented in Ref. [124] indeed show an additional low temperature maximum in $C(H,T)$ which could possibly be explained as such a thermodynamic signature. To investigate this hypothesis within the spin FRG, the flow equation of the free energy density

$$\partial_\Lambda f_\Lambda = -\int_K G_\Lambda(K) \dot{j}^\perp_{\Lambda,\boldsymbol{k}} - \frac{1}{2}\int_K G^{zz}_\Lambda(K) \dot{j}^z_{\Lambda,\boldsymbol{k}} + \frac{1}{2} M^2_\Lambda \dot{j}^z_{\Lambda,0}, \tag{5.1}$$

should be analyzed within a simultaneous deformation of longitudinal and transverse interaction. In contrast to the deformation scheme presented here, this would allow us to take into account a possible thermodynamic feedback of the zero-sound mode encoded in $G^{zz}_\Lambda(K)$. Let us, however, remember that the generalized RPA expression for $G^{zz}_\Lambda(K)$ is only valid in the regime of high frequency and low momentum, which renders the frequency summation in the flow equation (5.1) nontrivial.

Notwithstanding the above, the claim of the existence of a zero-magnon mode in $D \leq 2$ should be investigated within a complementary method. The most fruitful approach is probably an analysis of the longitudinal dynamics of the Heisenberg chain within the Bethe ansatz,

[1] Given the similarity of the algebraic structure of the longitudinal two point correlation function it is likely to assume that these simplifications are also implicitly applied in Ref. [36], although this is not explicitly extractable.

respectively DMRG calculations, focusing on the temperature and magnetic field range specified above. If such studies confirm the picture proclaimed here, it remains to be analyzed whether zero-magnon signatures can be detected in real materials. On the theoretical side, this calls for an investigation of the robustness of the phenomenon against additional perturbing effects, such as magnon-phonon coupling terms [140] or additional spin-spin interactions as e.g. dipole-dipole or spin-orbit coupling effects [141], all of which were neglected so far.

In addition, explicit experimental studies of suitable candidate materials would be required. Unfortunately, most quasi one-dimensional Heisenberg materials are of antiferromagnetic respectively ferrimagnetic character [50], but a plethora of quasi two-dimensional Heisenberg ferromagnet with small inter-layer exchange $J'$ exist [49, 142–144]. (See e.g. the recent publication of Ref. [49] where a candidate material with a negligible intra-inter exchange interaction ratio was proposed; apparently, the crystal sizes are sufficiently large to allow for experimental scattering studies). A verification of the zero-sound claim should hence be possible within polarized neutron scattering, provided the relevant momentum resolution $q \sim k_{\rm th}$ at temperatures $T \ll SJ_0$ can be achieved experimentally.

Finally, let us highlight that the dynamics of spins systems with more complicated exchange interaction configurations, such as antiferromagnetic, ferrimagnetic, or spin-dimer systems are considerably richer than the ferromagnet, especially in reduced dimensions [50, 145]. An example related to the longitudinal dynamics in ferromagnets discussed here, are the longitudinal modes detected in the neutron respectively Raman scattering data of low dimensional antiferromagnetic insulators such as $CsNiCl_3$ [146] and $Cu_2Te_2O_5Br_2$ [147]. Theoretically, these systems were modeled in terms of weakly coupled antiferromagnetic Heisenberg chains, respectively isolated spin clusters, and the longitudinal mode was described within mean-field [147, 148] and Ginzburg-Landau approaches [146, 149, 150], where the mode is interpreted as a two-magnon resonance process. Noteworthy, this is consistent with the recent spin diagrammatic approach of [23] where it is emphasized that the longitudinal dynamics of ordered three dimensional antiferromagnets are governed by multiple two-magnon processes, although no contact with the occurrence of longitudinal modes in low dimensional systems is made. A related spin FRG analysis could establish such a connection thereby providing a complementary microscopic description of the longitudinal mode. Eventually, it remains to be said that a similar operator based FRG approach can be applied to the Hubbard model formulated in terms of X-operators [151, 152], thus possibly allowing for non-pertubative insights into the complicated magneto-electronic properties of strongly coupled itinerant electron systems [15].

# II

# Appendices

# Additions to chapter 1

## A.1 Bloch spin wave theory

The following section complements the discussion of the elementary excitation of a Heisenberg ferromagnet given in section 1.2.2 providing a brief review of Bloch's semi-classical spin wave picture as discussed e.g. in Ref. [153]. To this end consider the equation of motions of the spin operators

$$\frac{d\boldsymbol{S}_i}{dt} = i\left[\mathcal{H}, \boldsymbol{S}_i\right], \tag{A.1}$$

where $\mathcal{H}$ is the Heisenberg Hamiltonian introduced in Eq. (1.20). Upon evaluating the commutator in Eq. (A.1) one obtains the three coupled equations of motions

$$\frac{1}{i}\frac{dS_i^{\pm}}{dt} = \mp \sum_j J_{ij}\left(S_j^z S_i^{\pm} - S_j^{\pm} S_i^z\right) \mp H S_i^{\pm}, \tag{A.2a}$$

$$\frac{1}{i}\frac{dS_i^{z}}{dt} = -\sum_j J_{ij}\left(S_j^+ S_i^- - S_i^+ S_j^-\right). \tag{A.2b}$$

At low energies, the operators $S_i^{\pm}$ can be regarded as classical quantities which deviate only slightly from the groundstate expectation value $\langle 0|S_i^{\pm}|0\rangle = 0$. Since the right side of the equation of motion of the $S_i^z$ component [Eq. (A.2b)] is of second order in $S_i^{\pm}$ it is therefore neglected in the following. Effectively, this corresponds to the approximation $S_i^z \to S$. Within this simplification the transverse equation of motion [Eq. (A.2a)] reduces to

$$\frac{1}{i}\frac{dS_i^{\pm}}{dt} = \mp S \sum_j J_{ij}\left(S_i^{\pm} - S_j^{\pm}\right) \mp H S_i^{\pm}, \tag{A.3}$$

which is readily solved in momentum space. Introducing the Fourier components

$$S_{\boldsymbol{k}}^{\alpha} = \sum_i S_i^{\alpha} e^{-i\boldsymbol{k}\cdot\boldsymbol{r}_i}, \tag{A.4}$$

we obtain

$$\frac{dS_{\boldsymbol{k}}^{\pm}}{dt} = \mp i E_{\boldsymbol{k}} S_{\boldsymbol{k}}^{\pm}, \tag{A.5}$$

where $E_{\boldsymbol{k}}$ is the excitation energy introduced in Eq. (1.38). The time dependence of the transverse spin components is thus given by

$$S_{\boldsymbol{k}}^{-}(t) = S_{\boldsymbol{k}}(0) e^{iE_{\boldsymbol{k}}t}, \quad S_{\boldsymbol{k}}^{+}(t) = S_{-\boldsymbol{k}}^{*}(0) e^{-iE_{\boldsymbol{k}}t}, \tag{A.6}$$

where $S_{\boldsymbol{k}}(0)$ is determined by the initial spin configuration. For the $x$ and $y$ components in real space we hence find

$$S_i^x(t) = \frac{1}{\sqrt{2}}\left(S_i^+ + S_i^-\right) = \frac{1}{\sqrt{2}}\frac{1}{N}\sum_{\boldsymbol{k}}\left(S^*_{-\boldsymbol{k}}(0)e^{-i(E_{\boldsymbol{k}}t-\boldsymbol{k}\cdot\boldsymbol{r}_i)} + S_{\boldsymbol{k}}(0)e^{i(E_{\boldsymbol{k}}t+\boldsymbol{k}\cdot\boldsymbol{r}_i)}\right), \tag{A.7a}$$

$$S_i^y(t) = \frac{1}{\sqrt{2}i}\left(S_i^+ - S_i^-\right) = \frac{1}{\sqrt{2}i}\frac{1}{N}\sum_{\boldsymbol{k}}\left(S^*_{-\boldsymbol{k}}(0)e^{-i(E_{\boldsymbol{k}}t-\boldsymbol{k}\cdot\boldsymbol{r}_i)} - S_{\boldsymbol{k}}(0)e^{i(E_{\boldsymbol{k}}t+\boldsymbol{k}\cdot\boldsymbol{r}_i)}\right). \tag{A.7b}$$

In case that a single mode of momentum $\boldsymbol{q}$ is excited, i.e. $S_{\boldsymbol{k}}(0) = \delta S\delta_{\boldsymbol{k},\boldsymbol{q}}$, this reduces to the spin wave solution

$$S_i^x(t) = \delta\tilde{S}\cos\left(E_{\boldsymbol{q}}t + \boldsymbol{q}\cdot\boldsymbol{r}_i\right), \tag{A.8a}$$

$$S_i^y(t) = -\delta\tilde{S}\sin\left(E_{\boldsymbol{q}}t + \boldsymbol{q}\cdot\boldsymbol{r}_i\right), \tag{A.8b}$$

with $\delta\tilde{S} = \sqrt{2}\delta S/N$, which is graphically depicted in Fig. 1.1 on page 14.

## A.2 Lehmann representations

To establish the relation of the different response and correlation functions, this section recapitulates the corresponding Lehmann representations (see also Ref. [14, 80]). For this purpose, consider the spectral representation of the retarded response function

$$\begin{aligned}\chi^{\alpha\beta}_{R,ij}(t-t') &= i\langle[S_i^\alpha(t), S_j^\beta(t')]\rangle\Theta(t-t')\\ &= \frac{i}{Z}\sum_{nm}\left(e^{-\beta E_n} - e^{-\beta E_m}\right)\langle n|S_i^\alpha|m\rangle\langle m|S_j|n\rangle e^{i(t-t')(E_n-E_m)}\Theta(t-t'),\end{aligned} \tag{A.9}$$

respectively the spectral representations of the structure factor and the Matsubara Green function

$$\mathcal{S}^{\alpha\beta}_{ij}(t-t') = \frac{1}{2\pi}\langle S_i^\alpha(t)S_j^\beta(t')\rangle = \frac{1}{2\pi Z}\sum_{nm}e^{-\beta E_n}\langle n|A|m\rangle\langle m|B|n\rangle e^{i(t-t')(E_n-E_m)}, \tag{A.10}$$

$$G^{\alpha\beta}_{ij}(\tau-\tau') = \langle\mathcal{T}A(\tau)B(\tau')\rangle = \frac{1}{Z}\sum_{nm}e^{-\beta E_n}\langle n|A|m\rangle\langle m|B|n\rangle e^{(\tau-\tau')(E_n-E_m)}. \tag{A.11}$$

The corresponding frequency representations are defined via the Fourier transformations

$$\chi^{\alpha\beta}_{R,ij}(\omega) = \int_{-\infty}^{\infty}dt\,\chi^{\alpha\beta}_{ij}(t)e^{i\omega t}, \tag{A.12}$$

$$\mathcal{S}^{\alpha\beta}_{ij}(\omega) = \int_{-\infty}^{\infty}dt\,\mathcal{S}^{\alpha\beta}_{ij}(t)e^{i\omega t}, \tag{A.13}$$

$$G^{\alpha\beta}_{ij}(\omega) = \int_0^\beta d\tau\,G^{\alpha\beta}_{ij}(t)e^{i\omega_n\tau}. \tag{A.14}$$

Note, that in order to guarantee convergence of the Fourier transformation of the retarded response function $\chi^{\alpha\beta}_{R,ij}(\omega)$, the frequency needs to be shifted to $\omega+i\delta$ where $\delta$ is an infinitesimal

positive constant. With the help of the identities

$$\int_0^\infty dt\, e^{it(\omega+i\delta+x)} = \frac{i}{x+\omega+i\delta}, \tag{A.15}$$

$$\int_{-\infty}^\infty dt\, e^{i\omega t} = 2\pi\delta(\omega), \tag{A.16}$$

$$\int_0^\beta d\tau\, e^{\tau(i\omega_n+x)} = \frac{e^{\beta x}-1}{x+i\omega_n}, \tag{A.17}$$

we hence recover the Lehmann representations

$$\chi^{\alpha\beta}_{R,ij}(\omega) = -\frac{1}{Z}\sum_{nm}\langle n|S^\alpha_i|m\rangle\langle m|S^\beta_j|n\rangle\frac{e^{-\beta E_n}-e^{-\beta E_m}}{E_n-E_m+\omega+i\delta}, \tag{A.18}$$

$$\mathcal{S}^{\alpha\beta}_{ij}(\omega) = \frac{1}{Z}\sum_{nm}\langle n|S^\alpha_i|m\rangle\langle m|S^\beta_j|n\rangle e^{-\beta E_n}\delta(E_n-E_m+\omega), \tag{A.19}$$

$$G^{\alpha\beta}_{ij}(i\omega_n) = -\frac{1}{Z}\sum_{nm}\langle n|S^\alpha_i|m\rangle\langle m|S^\beta_j|n\rangle\frac{e^{-\beta E_n}-e^{-\beta E_m}}{E_n-E_m+i\omega_n}, \tag{A.20}$$

which allow us to construct the mutual relations of the different response and correlation functions discussed in section 1.3.

# Additions to chapter 2

## B.1 Higher order tree expansion

This appendix constructs the tree expansion of the three- and four-point irreducible vertices $\Gamma^{\alpha_1,..\alpha_{3/4}}_{\Lambda,K_1...K_{3/4}}$ in terms of the connected correlation functions $G^{\alpha_1,..\alpha_{3/4}}_{\Lambda,K_1...K_{3/4}}$. It is in major parts a reformulation of the appendix A of Ref. [3], which was written by the author in 2019. Note, that a similar construction scheme can also be found in the PhD thesis of Jan Krieg [2]. We start with the relation

$$[\boldsymbol{F}_\Lambda[\boldsymbol{j}]]_{aa'} = \left[\left(\boldsymbol{\Gamma}''_\Lambda[\boldsymbol{\varphi}] + \boldsymbol{R}_\Lambda\right)^{-1}\right]_{\bar{a}\bar{a}'}, \tag{B.1}$$

which was introduced in Eq. (2.44) in section 2.3.2. Recall that $(a, \bar{a}) = ((\boldsymbol{k}, i\omega, \alpha), (-\boldsymbol{k}, -i\omega, \bar{\alpha}))$ is a collective label capturing momentum, frequency and component labels. Taking additional derivatives of Eq. (B.1) with respect to $\varphi^\alpha_K$, the third- and fourth-order derivative tensors read,

$$\left(\boldsymbol{\Gamma}^{(3)}_\Lambda[\boldsymbol{\varphi}]\right)_{a_1a_2a_3} = -\sum_{a'_1a'_2a'_3}\prod_{i=1}^{3}\left(\mathbf{F}''_\Lambda[\boldsymbol{j}]\right)^{-1}_{\bar{a}_i\bar{a}'_i}\left(\mathbf{F}^{(3)}_\Lambda[\boldsymbol{j}]\right)_{\bar{a}'_1\bar{a}'_2\bar{a}'_3}, \tag{B.2}$$

$$\begin{aligned}\left(\boldsymbol{\Gamma}^{(4)}_\Lambda[\boldsymbol{\varphi}]\right)_{a_1a_2a_3a_4} = &-\sum_{a'_1a'_2a'_3a'_4}\prod_{i=1}^{4}\left(\mathbf{F}''_\Lambda[\boldsymbol{j}]\right)^{-1}_{\bar{a}_i\bar{a}'_i}\left(\mathbf{F}^{(4)}_\Lambda[\boldsymbol{j}]\right)_{\bar{a}'_1\bar{a}'_2\bar{a}'_3\bar{a}'_4}\\ &+\mathcal{S}_{a_1,a_2;a_3,a_4}\frac{1}{2}\sum_{a'_1a'_2}\left(\boldsymbol{\Gamma}^{(3)}_\Lambda[\boldsymbol{\varphi}]\right)_{a_1a_2a'_1}\left(\mathbf{F}''_\Lambda[\boldsymbol{j}]\right)^{-1}_{\bar{a}'_1\bar{a}'_2}\left(\boldsymbol{\Gamma}^{(3)}_\Lambda[\boldsymbol{\varphi}]\right)_{a'_2a_3a_4}.\end{aligned} \tag{B.3}$$

Here, the operator $\mathcal{S}_{a_1,a_2;a_3,a_4}$ symmetrizes the expression to its right with respect to the exchange of all labels [113], and the summation over the internal labels implies $\sum_a = \int_K \sum_\alpha$. By setting $\boldsymbol{\varphi} = 0$ and $\boldsymbol{j} = 0$ in Eqs. (B.2) and (B.3) we obtain the desired expansion of the three- and four-point vertices generated by our hybrid functional $\Gamma_\Lambda[\boldsymbol{\varphi}]$ in powers of the correlation functions generated by $\mathcal{F}_\Lambda[\boldsymbol{j}]$. Using

$$\left(\mathbf{F}''_\Lambda[0]\right)^{+-}_{KK'} = \delta(K+K')G_\Lambda(K), \tag{B.4a}$$

$$\left(\mathbf{F}''_\Lambda[0]\right)^{-+}_{KK'} = \delta(K+K')G_\Lambda(-K), \tag{B.4b}$$

$$\left(\mathbf{F}''_\Lambda[0]\right)^{zz}_{KK'} = \delta(K+K')F_\Lambda(K), \tag{B.4c}$$

where the $\Lambda$-dependent transverse propagator $G_\Lambda(K)$ and the longitudinal effective interaction $F_\Lambda(K)$ were introduced in Eqs. (2.51) and (2.52) on page 42, we obtain from Eq. (B.2)

for the three-point vertices defined via the vertex expansion (2.42c),

$$\Gamma^{+-z}_{\Lambda}(K_1,K_2,K_3) = -\,G^{-1}_{\Lambda}(K_1)G^{-1}_{\Lambda}(-K_2)F^{-1}_{\Lambda}(K_3)F^{+-z}_{\Lambda}(K_1,K_2,K_3), \tag{B.5}$$

$$\Gamma^{zzz}_{\Lambda}(K_1,K_2,K_3) = -\,F^{zzz}_{\Lambda}(K_1,K_2,K_3)\prod_{i=1}^{3}F^{-1}_{\Lambda}(K_i). \tag{B.6}$$

Using the relation (2.23) between the hybrid functional $\mathcal{F}_\Lambda[\boldsymbol{j}]$ and the generating functional $\mathcal{G}_\Lambda[\boldsymbol{h}]$ of the connected spin correlation functions, we can express the three-point functions $F^{+-z}_{\Lambda}(K_1,K_2,K_3)$ and $F^{zzz}_{\Lambda}(K_1,K_2,K_3)$ on the right-hand side of Eqs. (B.5) and (B.6) in terms of the connected spin correlation functions as

$$\begin{aligned} F^{-1}_{\Lambda}(K_3)F^{+-z}_{\Lambda}(K_1,K_2,K_3) &= F^{-1}_{\Lambda}(K_3)J^{z}_{\Lambda,\boldsymbol{k_3}}G^{+-z}_{\Lambda}(K_1,K_2,K_3) \\ &= \left[1+J^{z}_{\Lambda,\boldsymbol{k_3}}G^{zz}_{\Lambda}(K_3)\right]^{-1}G^{+-z}_{\Lambda}(K_1,K_2,K_3), \end{aligned} \tag{B.7}$$

$$F^{zzz}_{\Lambda}(K_1,K_2,K_3)\prod_{i=1}^{3}F^{-1}_{\Lambda}(K_i) = G^{zzz}_{\Lambda}(K_1,K_2,K_3)\prod_{i=1}^{3}\left[1+J^{z}_{\Lambda,\boldsymbol{k_i}}G^{zz}_{\Lambda}(K_i)\right]^{-1}. \tag{B.8}$$

Substituting Eqs. (B.7) and (B.8) into Eqs. (B.5) and (B.6), we hence obtain the desired expansion of the three-point vertices in terms of the connected spin correlation functions,

$$\Gamma^{+-z}_{\Lambda}(K_1,K_2,K_3) = -\,G^{-1}_{\Lambda}(K_1)G^{-1}_{\Lambda}(-K_2)\left[1+J^{z}_{\Lambda,\boldsymbol{k_3}}G^{zz}_{\Lambda}(K_3)\right]^{-1}G^{+-z}_{\Lambda}(K_1,K_2,K_3), \tag{B.9}$$

$$\Gamma^{zzz}_{\Lambda}(K_1,K_2,K_3) = -\,G^{zzz}_{\Lambda}(K_1,K_2,K_3)\prod_{i=1}^{3}\left[1+J^{z}_{\Lambda,\boldsymbol{k_i}}G^{zz}_{\Lambda}(K_i)\right]^{-1}. \tag{B.10}$$

Analogously, using Eq. (B.3) we find for the four-point vertices,

$$\begin{aligned} &\Gamma^{++--}_{\Lambda}(K_1,K_2,K_3,K_4) = \\ &\quad -\,G^{-1}_{\Lambda}(K_1)G^{-1}_{\Lambda}(K_2)G^{-1}_{\Lambda}(-K_3)G^{-1}_{\Lambda}(-K_4)G^{++--}_{\Lambda}(K_1,K_2,K_3,K_4) \\ &\quad +\Big\{\Gamma^{+-z}_{\Lambda}(K_1,K_3,-K_1-K_3)F_{\Lambda}(-K_1-K_3)\Gamma^{+-z}_{\Lambda}(K_2,K_4,-K_2-K_4)+(K_3\leftrightarrow K_4)\Big\}, \end{aligned} \tag{B.11}$$

$$\begin{aligned} &\Gamma^{+-zz}_{\Lambda}(K_1,K_2,K_3,K_4) = \\ &\quad -\,G^{-1}_{\Lambda}(K_1)G^{-1}_{\Lambda}(-K_2)G^{+-zz}_{\Lambda}(K_1,K_2,K_3,K_4)\prod_{i=3,4}\left[1+J^{z}_{\Lambda,\boldsymbol{k_i}}G^{zz}_{\Lambda}(K_i)\right]^{-1} \\ &\quad +\Big\{\Gamma^{+-z}_{\Lambda}(K_1,-K_1-K_3,K_3)G_{\Lambda}(-K_1-K_3)\Gamma^{+-z}_{\Lambda}(-K_2-K_4,K_2,K_4)+(K_3\leftrightarrow K_4)\Big\} \\ &\quad +\Gamma^{zzz}_{\Lambda}(K_3,K_4,-K_3-K_4)F_{\Lambda}(-K_3-K_4)\Gamma^{+-z}_{\Lambda}(K_1,K_2,-K_1-K_2), \end{aligned} \tag{B.12}$$

$$\begin{aligned} &\Gamma^{zzzz}_{\Lambda}(K_1,K_2,K_3,K_4) = \\ &\quad -\,G^{zzzz}_{\Lambda}(K_1,K_2,K_3,K_4)\prod_{i=1}^{4}\left[1+J^{z}_{\Lambda,\boldsymbol{k_i}}G^{zz}_{\Lambda}(K_i)\right]^{-1} \\ &\quad +\Gamma^{zzz}_{\Lambda}(K_1,K_3,-K_1-K_3)\left[1+J^{z}_{\Lambda,-\boldsymbol{k}_1-\boldsymbol{k}_3}G^{zz}_{\Lambda}(-K_1-K_3)\right]^{-1}\Gamma^{zzz}_{\Lambda}(K_2,K_4,-K_2-K_4), \end{aligned} \tag{B.13}$$

where we have introduced the notation

$$\{f(..,K_3,..)+(K_3\leftrightarrow K_4)\} = \{f(..,K_3,..)+f(..,K_4,..)\}, \tag{B.14}$$

with $f(\ldots)$ any arbitrary function.

## B.2 On-site connected correlation functions

This section revises the derivation of the connected correlation functions of a single $SU(2)$ spin subject to a uniform magnetic field $\boldsymbol{H} = H\boldsymbol{e}^z$. Combined with the tree expansion derived in the previous appendix, these correlation functions determine the initial conditions of the hierarchy of flow equations solved in Chapters 3 and 4. In case the exchange interaction between the spins is completely switched off, we are left with a quantum mechanical single particle problem with the Zeeman Hamiltonian

$$\mathcal{H}_0 = -HS^z. \tag{B.15}$$

The corresponding single-site connected correlation functions in imaginary time, respectively Matsubara-frequency representation,

$$G^{\alpha_1\ldots\alpha_n}_{\Lambda_0,\tau_1\ldots\tau_n} = \langle \mathcal{T}\left[S^{\alpha_1}(\tau_1)\ldots S^{\alpha_n}(\tau_n)\right]\rangle_{0,c}, \tag{B.16}$$

$$G^{\alpha_1\ldots\alpha_n}_{\Lambda_0,\omega_1\ldots\omega_n} = \int_{\tau\ldots\tau_n} G^{\alpha_1\ldots\alpha_n}_{0,\tau_1\ldots\tau_n} e^{i\sum_n \omega_n\tau_n}, \tag{B.17}$$

can be calculated in several ways. Historically, the lowest order functions were first presented by Vaks *et al.* [33], which used a spin analog of the familiar *Wick theorem* to construct the correlation functions recursively. A detailed description of this algorithm can be found in Ref. [35]. Another obvious possibility is to directly calculate the disconnected counter parts,

$$\langle \mathcal{T}\left[S^{\alpha_1}(\tau_1)\ldots S^{\alpha_n}(\tau_n)\right]\rangle_0 = \frac{\sum_n \langle n|e^{\beta HS^z}\mathcal{T}S^{\alpha_1}(\tau_1)\ldots S^{\alpha_n}(\tau_n)|n\rangle}{\sum_n \langle n|e^{\beta HS^z}|n\rangle}, \tag{B.18}$$

for a given spin $S$-representation, from which the connected correlation functions can be constructed. Both procedures straightforwardly yield the imaginary time representation, but the Fourier transformation of the eventual results to the frequency domain is rather tedious. Since we are mainly interested in the frequency representation of the correlation functions, it is thus more convenient to use a recursion relation which was derived by Dmytro Tarasevych and outlined in appendix B and C of our publication Ref. [3]. Introducing the notation

$$G^{\overbrace{+\ldots+}^{n}\overbrace{-\ldots-}^{n}\overbrace{z\ldots z}^{m}}_{\Lambda_0,\omega_1\ldots\omega_n;\omega'_1\ldots\omega'_n;\omega''_1\ldots\omega''_m} = \delta\left(\omega_1+\ldots+\omega''_m\right) G^{(n,n,m)}_{\Lambda_0}(\omega_1\ldots\omega_n;\omega'_1\ldots\omega'_n;\omega''_1\ldots\omega''_m), \tag{B.19}$$

where the frequency conserving delta function can be factored out due to imaginary-time translational invariance, this recursion scheme reads

$$\begin{aligned}(H - i\omega_1)\, G^{(n,n,m)}_{\Lambda_0}(\omega_1\ldots\omega_n;\omega'_1\ldots\omega'_n;\omega''_1\ldots\omega''_m) = \\ -\sum_{\nu=1}^{m} G^{(n,n,m-1)}_{\Lambda_0}(\omega_1+\omega''_\nu,\omega_2\ldots\omega_n;\omega'_1\ldots\omega'_n;\omega''_1\ldots\not{\omega}''_\nu\ldots\omega''_m) \\ +\sum_{\nu=1}^{n} G^{(n-1,n-1,m+1)}_{\Lambda_0}(\omega_2\ldots\omega_n;\omega'_1\ldots\not{\omega}'_\nu\ldots\omega'_n;\omega''_1\ldots\omega''_m,\omega_1+\omega'_\nu).\end{aligned} \tag{B.20}$$

Here, the slashed symbol $\not{\omega}''_\nu$ indicates that the argument $\omega''_\nu$ should be omitted. Eq. (B.20) follows from solving the hierarchy of motions of the connected correlation functions in the

limit of vanishing exchange interaction. The detailed derivation can be found in appendix C of Ref. [3]. Having calculated the purely longitudinal functions [using e.g. Eq. (B.18)]

$$G^{z}_{\Lambda_0}(i\omega) = \delta(\omega) b, \tag{B.21a}$$

$$G^{zz}_{\Lambda_0}(i\omega_1, i\omega_2) = \delta(\omega_1)\delta(\omega_2) b', \tag{B.21b}$$

$$\vdots$$

$$G^{\overbrace{z\dots z}^{n}}_{\Lambda_0}(i\omega_1, \dots, i\omega_n) = \delta(\omega_1)\dots\delta(\omega_n) b^{(n)}, \tag{B.21c}$$

where $\delta(\omega) = \beta\delta_{\omega,0}$, $b_{\Lambda_0} = b(\beta H)$, and $b^{(n)}_{\Lambda_0} = b^{(n)}(\beta H)$ are determined by the spin-$S$ Brillouin function

$$b(y) = \left(S + \frac{1}{2}\right) \coth\left[\left(S + \frac{1}{2}\right) y\right] - \frac{1}{2}\coth\left[\frac{y}{2}\right], \tag{B.22}$$

respectively its nth-derivative, Eq. (B.20) allows to successively construct all transverse and mixed transverse-longitudinal correlation functions. Up to fourth order we find

$$G^{+-}_{\Lambda_0}(i\omega, -i\omega) = G_{\Lambda_0}(i\omega), \tag{B.23a}$$

$$G^{+-z}_{\Lambda_0}(i\omega_1, i\omega_2, i\omega_3) = \frac{1}{b_{\Lambda_0}}\left[-G_{\Lambda_0}(i\omega_1)G_{\Lambda_0}(-i\omega_2) + G_{\Lambda_0}(i\omega_1)\delta(\omega_3) b'_{\Lambda_0}\right], \tag{B.23b}$$

$$\begin{aligned} G^{++--}_{\Lambda_0}(i\omega_1, i\omega_2, i\omega_3, i\omega_4) = \frac{1}{b^2_{\Lambda_0}}\Big[ &- G_{\Lambda_0}(i\omega_1)G_{\Lambda_0}(i\omega_2)[G_{\Lambda_0}(-i\omega_3) + G_{\Lambda_0}(-i\omega_4)] \\ &+ G_{\Lambda_0}(i\omega_1)G_{\Lambda_0}(i\omega_2)[\delta(\omega_1+\omega_3) + \delta(\omega_1+\omega_4)] b'_{\Lambda_0}\Big], \end{aligned} \tag{B.23c}$$

$$\begin{aligned} G^{+-zz}_{\Lambda_0}(i\omega_1, i\omega_2, i\omega_3, i\omega_4) = \frac{1}{b^2_{\Lambda_0}}\Big[ &\; G_{\Lambda_0}(i\omega_1)G_{\Lambda_0}(-i\omega_2)[G_{\Lambda_0}(i\omega_1+i\omega_3) + G_{\Lambda_0}(i\omega_1+i\omega_4)] \\ &- G_{\Lambda_0}(i\omega_1)G_{\Lambda_0}(-i\omega_2)[\delta(\omega_3) + \delta(\omega_4)] b'_{\Lambda_0} + G_{\Lambda_0}(i\omega_1)\delta(\omega_3)\delta(\omega_4) b_{\Lambda_0} b''_{\Lambda_0}\Big], \end{aligned} \tag{B.23d}$$

where

$$G_{\Lambda_0}(i\omega) = \frac{b_{\Lambda_0}}{H - i\omega}. \tag{B.24}$$

# Additions to chapters 3 and 4

## C.1 Technical details

### C.1.1 Low temperature approximation of the momentum sums

Hereafter, we summarize the details of the low temperature evaluation of the momentum sums as frequently carried out in chapter 3 and 4. As a representative example, let us consider the magnon correction to magnetization flow

$$I_{1,\Lambda} = \frac{1}{N} \sum_{\boldsymbol{k}} n\left(\beta E_\Lambda(\boldsymbol{k})\right), \tag{C.1}$$

as derived in Eq. (3.26) on page 53. In the thermodynamic limit $N \to \infty$, the momentum sum can be replaced by an integration such that we obtain

$$I_{1,\Lambda} = \frac{a^D}{(2\pi)^D} \int_{\mathrm{BZ}} d^D k \, n\left(\beta E_\Lambda(\boldsymbol{k})\right), \tag{C.2}$$

where the integration is restricted to momenta inside the first Brillouin zone of the underlying lattice.

#### The case $\Lambda = 1$

We begin with a discussion of the magnon correction at the end of the flow. In particular, recall that the Bose distribution function $n(x) = (e^x - 1)^{-1}$ is exponentially small at arguments $x \gg 1$. In the temperature range $T < SJ_0$ considered throughout this thesis, this implies that the thermal momentum $k \leq k_{\mathrm{th}}$, determined by the low momentum expansion of the magnon dispersion

$$E_{\Lambda=1}(\boldsymbol{k}) \approx H + k^2/(2m), \tag{C.3}$$

effectively acts as an ultraviolet cutoff in the momentum integration of Eq. (C.6). The precise form of the magnon mass $m$ follows from the underlying exchange interaction. E.g. for a nearest neighbor interaction of strength $J$, where $J_{\boldsymbol{k}}$ is given by

$$J_{\boldsymbol{k}} = 2J \sum_{i=1}^{D} \cos(k_i a), \tag{C.4}$$

one finds $m = 1/(2JM_0a^2) \approx 1/(2JSa^2)$ and correspondingly

$$k_{\mathrm{th}} a = \sqrt{2mT} \approx \sqrt{T/(JS)}. \tag{C.5}$$

Within this low momentum expansion, the integral in Eq. (C.2) can therefore be approximated as

$$I_{1,\Lambda=1} \approx \frac{\Omega_D a^D}{(2\pi)^D} \int_0^{k_{\text{th}}} dk \, \frac{k^{D-1}}{e^{\beta H + k^2/k_{\text{th}}^2} - 1} = \frac{\Omega_D \, (k_{\text{th}} a)^D}{2(2\pi)^D} \int_0^1 d\epsilon \, \frac{\epsilon^{\frac{D-2}{2}}}{e^{\beta H + \epsilon} - 1}, \tag{C.6}$$

where we substituted $\epsilon = \sqrt{k/k_{\text{th}}}$ in the second identity. Furthermore, given that the integrand in Eq. (C.6) is exponentially small for $\epsilon \gg 1$, the upper integration boundary may be shifted to infinity such that we finally recover

$$I_{1,\Lambda=1} = \frac{(k_{\text{th}} a)^D}{c_D} \text{Li}_{D/2}\left(e^{-\beta H}\right), \quad c_D = 2^D \pi^{D/2}, \tag{C.7}$$

where the Polylogarithm function $\text{Li}_s(z)$ was introduced in Eq. (3.30) on page 54.

**The case $0 < \Lambda < 1$**

The evaluation of the momentum sums along the flow is a little more subtle. In particular recall, that the $\Lambda$-dependent dispersion is given by

$$E_\Lambda(\boldsymbol{k}) = \Delta_\Lambda + \Lambda \varepsilon_{\boldsymbol{k}}. \tag{C.8}$$

Due to the additional $\Lambda$-factor in front of the momentum dependent part of the magnon dispersion, a restriction of the momentum integration to small momenta $k \leq k_{\text{th}}$ is thus not justified for $\Lambda < \Lambda_c$, where $\Lambda_c$ is of the order of $T/(SJ_0)$. In principle, the momentum integrals should hence be carried out with the full dispersion relation. This is the procedure followed in section 3.4 where we quantitatively compare our spin FRG results to the literature. However, for a qualitative discussion, an approximation of the magnon dispersion in the form $\varepsilon_{\boldsymbol{k}} = k^2/(2m)$ is still sufficient. This is because the Bose distribution function in the flow region $\Lambda < \Lambda_c$ is exponentially suppressed by the corresponding gap term $\beta\Delta_\Lambda \approx \beta S J_0 \gg 1$. Upon integrating over $\Lambda$, the region $\Lambda < \Lambda_c$ thus does not significantly contribute to the final result, irrespective of the precise form of $\varepsilon_{\boldsymbol{k}}$. In the present work these considerations are only relevant in section 3.3.3, where the flow of the magnetization within the Ward identity truncation is qualitatively discussed. In particular, the momentum sum in Eq. (3.39)

$$I_{2,\Lambda} = \frac{1}{N} \sum_{\boldsymbol{k}} J_{\boldsymbol{k}} n\big(\beta \tilde{E}_{\Lambda,\boldsymbol{k}}\big) \Big[ n\big(\beta \tilde{E}_{\Lambda,\boldsymbol{k}}\big) + 1 \Big], \tag{C.9}$$

is approximated by

$$I_{2,\Lambda} \approx J_0 \frac{\Omega_D a^D}{(2\pi)^D} \int_0^{k_{\text{th}}} dk \, \frac{k^{D-1} e^{\beta\tilde{\Delta}_\Lambda + \Lambda k^2/k_{\text{th}}^2}}{\left(e^{\beta\tilde{\Delta}_\Lambda + \Lambda k^2/k_{\text{th}}^2} - 1\right)^2} = J_0 \frac{\Omega_D (k_{\text{th}} a)^D}{(2\pi)^D \Lambda^{D/2}} \int_0^\Lambda d\epsilon \, \frac{\epsilon^{\frac{D-2}{2}} e^{\beta\tilde{\Delta}_\Lambda + \epsilon}}{\left(e^{\beta\tilde{\Delta}_\Lambda + \epsilon} - 1\right)^2}. \tag{C.10}$$

Noteworthy, shifting the integration boundary from $\Lambda$ to infinity is not allowed in this case, given that the integral would otherwise diverge in the region $\Lambda < \Lambda_c$. Note, that in generating Fig. 3.3 we hence evaluated the magnon correction $I_{1,\Lambda}$ in Eq. (3.26) in the form of Eq. (C.6) [and not in the form of (C.7)] for reason of consistency. The resulting qualitative picture is of course independent of this choice.

### C.1.2 The polylogarithm function

We shortly summarize the essential convergence properties of the polylogarithm function, introduced in the previous section (respectively in chapter 3) to facilitate the calculation of momentum sums over the Bose-distribution function. In this work we encounter the integral representation of the polylogartihm function

$$\mathrm{Li}_s(z) = \frac{1}{\Gamma(s)} \int_0^\infty d\epsilon \, \frac{\epsilon^{s-1}}{e^\epsilon/z - 1}, \tag{C.11}$$

at arguments $z \in \mathbb{R}$, with $|z| < 1$, and integer and half integer values of $s$, i.e. $s = \{\ldots, -3/2, -1/2, 1/2, 1, 3/2, 2, \ldots\}$. Here, $\Gamma(s)$ is the Gamma-function, which can be defined in terms of the integral representation

$$\Gamma(s) = \int_0^\infty d\epsilon \, \epsilon^{s-1} e^{-\epsilon}. \tag{C.12}$$

The asymptotic behavior in the limit $|z| \to 1$ is of essential interest, satisfying

$$\lim_{|z|\to 1} \mathrm{Li}_s(z) = \begin{cases} \zeta(s) & s > 1, \\ \infty & s \leq 1, \end{cases} \tag{C.13}$$

where $\zeta(s)$ is the Riemann-zeta function. In the divergent case $s \leq 1$, the asymptotic behavior is conveniently expressed in terms of a chemical potential variable $\mu = -\ln(z)$. At $s = 1$, the polylogarithm reduces to $\mathrm{Li}_1(z) = -\ln(1-z)$ and one hence finds

$$\mathrm{Li}_1(e^{-\mu}) \overset{\mu\to 0^+}{\sim} -\ln(\mu), \tag{C.14}$$

while for $s < 1$ the asymptotics are given by [154]

$$\mathrm{Li}_s(e^{-\mu}) \overset{\mu\to 0^+}{\sim} \Gamma(1-s)\mu^{s-1}. \tag{C.15}$$

Finally let us collect the relevant values of $\zeta(s)$ and $\Gamma(s)$ encountered throughout this work:

$$\begin{aligned} &\zeta(3/2) \approx 2.612, \quad \zeta(2) = \pi^2/6, \quad \zeta(5/2) \approx 1.341, \\ &\Gamma(1/2) = \sqrt{\pi}, \quad \Gamma(1) = 1, \quad \Gamma(3/2) = \sqrt{\pi}/2, \quad \Gamma(2) = 1. \end{aligned} \tag{C.16}$$

### C.1.3 Numerical evaluation of the longitudinal structure factor

This section is a reformulation of appendix C of Ref. [4], written by the author in 2020. Hereafter, the numerical evaluation of the longitudinal structure factor

$$S^{zz}(\boldsymbol{q}, \omega) = \frac{1}{\pi} \frac{e^{\beta\omega}}{e^{\beta\omega} - 1} \mathrm{Im} \left[ \frac{P\left(\frac{\omega + i\delta}{v_{\mathrm{th}} q}\right)}{(1+\rho)^2 + J_0 P\left(\frac{\omega + i\delta}{v_{\mathrm{th}} q}\right)} \right], \tag{C.17}$$

shown graphically in Fig. 4.2 on page 76 is briefly explained. Likewise, the dimensionless zero-magnon velocity $x_0 = \omega_{\boldsymbol{q}}/(v_{\mathrm{th}} q)$ and the damping $\gamma_{\boldsymbol{q}} = y_0 v_{\mathrm{th}} q$ shown graphically in Fig. 4.3 are obtained from the solution of

$$0 = (1+\rho)^2 + J_0 \mathrm{Re}\, P(x_0 + i0^+), \tag{C.18}$$

respectively

$$y_0 = \frac{\operatorname{Im} P(x_0 + i0^+)}{\operatorname{Re} P'(x_0 + i0^+)}. \tag{C.19}$$

To evaluate the function $P(z)$ defined in Eq. (4.35) on page 74, the explicit expressions of the angular average $g_D(z)$ in dimensions $D = 1, 2, 3$ are required; in particular the corresponding imaginary and real parts of the analytical continuation $g_D(x + i0^+)$ with $x \in \mathbb{R}$. The analytic properties of $g_D(x + i0^+)$ are summarized in [155]. For the real part, we obtain

$$\operatorname{Re} g_1\left(x + i0^+\right) = \begin{cases} 0, & |x| = 1 \\ \frac{1}{1-x^2}, & |x| \neq 1 \end{cases}, \tag{C.20a}$$

$$\operatorname{Re} g_2\left(x + i0^+\right) = \begin{cases} 1, & |x| \leq 1 \\ 1 - \frac{|x|}{\sqrt{x^2-1}}, & |x| > 1 \end{cases}, \tag{C.20b}$$

$$\operatorname{Re} g_3\left(x + i0^+\right) = 1 - \frac{x}{2} \ln\left|\frac{1+x}{1-x}\right|. \tag{C.20c}$$

Please note, that for $x \gg 1$ we can approximate

$$\operatorname{Re}\, g_D\left(x + i0^+\right) \approx -\frac{1}{Dx^2}, \tag{C.21}$$

as used in the main text. Likewise, the imaginary part is given as

$$\operatorname{Im} g_1\left(x + i0^+\right) = \frac{\pi}{2}|x|\left[\delta(1-x) + \delta(1+x)\right], \tag{C.22a}$$

$$\operatorname{Im} g_2\left(x + i0^+\right) = \frac{x}{\sqrt{1-x^2}}\Theta(1-|x|), \tag{C.22b}$$

$$\operatorname{Im} g_3\left(x + i0^+\right) = \frac{\pi}{2}x\Theta(1-|x|). \tag{C.22c}$$

Substituting these expressions into the definition (4.35) of $P(z)$ yields for the real part

$$\operatorname{Re} P_{D=1}(x + i0^+) = -\frac{k_{\text{th}}a}{2\pi T}\mathcal{P}\int_0^\infty d\epsilon\, \frac{\sqrt{\epsilon}}{(x^2-\epsilon)}\frac{e^{\beta H+\epsilon}}{(e^{\beta H+\epsilon}-1)^2}, \tag{C.23a}$$

$$\operatorname{Re} P_{D=2}(x + i0^+) = \frac{(k_{\text{th}}a)^2}{4\pi T}\left[\frac{1}{e^h - 1} - \int_0^{x^2} d\epsilon\, \frac{x}{\sqrt{x^2-\epsilon}}\frac{e^{\beta H+\epsilon}}{(e^{\beta H+\epsilon}-1)^2}\right], \tag{C.23b}$$

$$\operatorname{Re} P_{D=3}(x + i0^+) = \frac{(k_{\text{th}}a)^3}{4\pi^2 T}\left[\frac{\sqrt{\pi}}{2}\operatorname{Li}_{\frac{1}{2}}\left(e^{-\beta H}\right) - \frac{x}{2}\int_0^\infty d\epsilon \ln\left|\frac{\sqrt{\epsilon}+x}{\sqrt{\epsilon}-x}\right|\frac{e^{\beta H+\epsilon}}{(e^{\beta H+\epsilon}-1)^2}\right], \tag{C.23c}$$

where $\mathcal{P}$ denotes the Cauchy principal value. The imaginary part is given by

$$\operatorname{Im} P_{D=1}(x + i0^+) = \frac{k_{\text{th}}a}{2T}\frac{xe^{\beta H+x^2}}{\left[e^{\beta H+x^2}-1\right]^2}, \tag{C.24a}$$

$$\operatorname{Im} P_{D=2}(x + i0^+) = \frac{(k_{\text{th}}a)^2}{4\sqrt{\pi}T}x\operatorname{Li}_{-\frac{1}{2}}\left(e^{-\beta H-x^2}\right), \tag{C.24b}$$

$$\operatorname{Im} P_{D=3}(x + i0^+) = \frac{(k_{\text{th}}a)^3}{8\pi T}\frac{x}{e^{\beta H+x^2}-1}. \tag{C.24c}$$

The longitudinal structure factor (C.17), the zero-magnon velocities (C.18), and the damping rates (C.19) can now be displayed by calculating the expressions (C.23) for $\mathrm{Re}\, P_D(x+i\delta)$ and (C.24) for $\mathrm{Im}\, P_D(x+i\delta)$ numerically.

## C.2 Transverse spin dynamics

For completeness, we briefly discuss the characteristics of the transverse spin dynamics as obtained within the deformation/truncation scheme presented in chapter 3. Thereto, let us consider the transverse part of the dynamical structure factor

$$\mathcal{S}^{\perp}_{\Lambda}(\boldsymbol{q},\omega) = \frac{1}{\pi}\frac{e^{\beta\omega}}{e^{\beta\omega}-1}\mathrm{Im}\, G_{\Lambda}(\boldsymbol{q},\omega+i\delta), \tag{C.25}$$

which is determined by analytically continuing the magnon propagator $G_\Lambda(Q)$ to real frequencies. Following the deformation process outlined in chapter 3, the $\Lambda$-dependence of the transverse propagator can hereby be summarized as

$$G_{\Lambda}(Q) = \begin{cases} \frac{b(\beta H)}{H-i\omega}, & \Lambda=-1, \\ \frac{M_0}{H+M_0J_0-i\omega}, & \Lambda=0, \\ \frac{M_0}{E_{\boldsymbol{q}}-i\omega+M_0\Sigma(Q)}, & \Lambda=1, \end{cases} \tag{C.26}$$

where - as a reminder - $b(x)$ is the Brillouin function, $M_0$ the mean-field magnetization, and $\Sigma(Q)$ the self energy which accounts for the higher order vertex corrections [cf. Eqs. (3.4), (3.7), and (3.23)].

### C.2.1 Mean-field and one-loop solutions

At $\Lambda=-1$, where the sites are completely decoupled, the transverse structure factor is simply given by a momentum independent delta contribution at $\omega=H$ which is shifted to $\omega=H+M_0J_0$ at mean-field level ($\Lambda=0$). Upon taking into account the transverse interaction from $\Lambda=0$ to $\Lambda=1$, the infinite hierarchy of flow equations then introduces a particular momentum and frequency dependence in the transverse propagator. E.g., to one-loop order, the structure factor is given by

$$S^{\perp}_{\text{one-loop}}(\boldsymbol{q},\omega) \sim \delta(E_{\boldsymbol{q}}-\omega), \tag{C.27}$$

where $E_{\boldsymbol{q}} = H + M_0(J_0 - J_{\boldsymbol{q}})$ is the magnon dispersion introduced in Eq. (3.22).

### C.2.2 Self-energy corrections

The self energy contributions in the transverse propagator renormalize the magnon dispersion, lifetime, and spectral weight.

### Parameterization

To discuss these effects, let us follow section 3.3.4 and parameterize the self energy in the form

$$\Sigma_\Lambda(Q) = \Sigma_\Lambda(0) + M_0^{-1}\left[\left(1 - Z_\Lambda^{-1}\right) i\omega + \sigma_\Lambda(Q)\right] \tag{C.28}$$

where $Z_\Lambda$ is the wave function renormalization, while $\sigma_\Lambda(K)$ accounts for the momentum and frequency dependent contribution to the magnon dispersion and damping. To separate the latter two, the corresponding analytically continued version of $\sigma_\Lambda(K)$ is hereby parameterized as

$$\sigma_\Lambda(\boldsymbol{q}, i\omega \to \omega + i\delta) = \sigma^r_\Lambda(\boldsymbol{q},\omega) - i\gamma_\Lambda(\boldsymbol{q},\omega), \tag{C.29}$$

where $\sigma^r_\Lambda(\boldsymbol{k},\omega)$ accounts for the renormalization of the magnon energy and $\gamma_\Lambda(\boldsymbol{k},\omega)$ for damping processes. Upon substituting this self energy parameterization in the transverse propagator, the transverse structure factor at $\Lambda = 1$ can thus be expressed in the Lorentzian form

$$\mathcal{S}^\perp_{\Lambda=1}(\boldsymbol{q},\omega) = \frac{1}{\pi}\frac{e^{\beta\omega}}{e^{\beta\omega}-1}\frac{Z^2\gamma(\boldsymbol{q},\omega)M_0}{\left[Z\mathcal{E}(\boldsymbol{q},\omega)-\omega\right]^2 + \left[Z\gamma(\boldsymbol{q},\omega)\right]^2}, \tag{C.30}$$

with $Z = Z_{\Lambda=1}$, $\gamma(\boldsymbol{q},\omega) = \gamma_{\Lambda=1}(\boldsymbol{q},\omega)$, and the renormalized magnon dispersion

$$\mathcal{E}(\boldsymbol{q},\omega) = E_{\Lambda=1,\boldsymbol{q}} + M_0\Sigma_{\Lambda=1}(0) + \sigma^r_{\Lambda=1}(\boldsymbol{q},\omega). \tag{C.31}$$

### Self energy flow in one-loop approximation

Let us now consider the flow of three coefficients, $Z_\Lambda$, $\sigma^r_\Lambda(\boldsymbol{k},\omega)$, and $\gamma_\Lambda(\boldsymbol{k},\omega)$, which follow from an appropriate analysis of the flow of the self energy. The latter was already derived on page 59 as[2]

$$\begin{aligned}\partial_\Lambda\Sigma_\Lambda(Q) = \int_K \dot{G}_\Lambda(K)\Big[&\Gamma^{++--}_\Lambda(Q,K,-K,-Q) - F_\Lambda(0)\Gamma^{+-z}_\Lambda(Q,-Q,0)\Gamma^{+-z}_\Lambda(K,-K,0)\\ &- F_\Lambda(Q-K)\Gamma^{+-z}_\Lambda(Q,-K,K-Q)\Gamma^{+-z}_\Lambda(K,-Q,Q-K)\Big].\end{aligned} \tag{C.32}$$

In principle, a solution of Eq. (C.32) thus requires the consistent calculation of the various higher order vertices on the right side of the upper flow equation. Such a procedure is beyond the scope of this appendix, and at this point we restrict the discussion to the approximations introduced in chapter 3. In particular, we demand that the momentum and frequency independent part of the selfenergy $\Sigma_\Lambda(0)$ is given by the expression (3.36) which ensures that the Ward identity in Eq. (3.35) is fulfilled. For simplicity, we furthermore neglect the self energy correction $\sigma^r_\Lambda(\boldsymbol{q},\omega)$ to the magnon energy, whose inclusion should primarily correspond to a rescaling of the frequency scale. Within these approximations, the renormalized magnon dispersion assumes the familiar form

$$\mathcal{E}_\Lambda(\boldsymbol{q},\omega) = \tilde{E}_{\Lambda,\boldsymbol{q}} = \tilde{\Delta}_\Lambda + \Lambda\varepsilon_{\boldsymbol{k}}, \quad \tilde{\Delta}_\Lambda = H\frac{M_0}{M_\Lambda} + M_0J_0(1-\Lambda), \quad \varepsilon_{\boldsymbol{k}} = M_0(J_0 - J_{\boldsymbol{k}}), \tag{C.33}$$

encountered in section 3.3.3 and we are left with an analysis of the flow of the wave function renormalization and the damping coefficient. To one-loop order, the flow of $\gamma_\Lambda(\boldsymbol{k},\omega)$ and $Z_\Lambda$

[2]Note, that the momentum-frequency labels $K$ and $Q$ are interchanged compared to Eq. (3.51).

is obtained by replacing the higher order vertices on the right of the flow equation (C.32) by their mean field expression derived in section 3.3.1. This yields

$$\partial_\Lambda \Sigma_\Lambda(Q) = \int_K \dot{G}_\Lambda(K) \left[ I_a(K,Q) + I_b(K,Q) \right], \tag{C.34}$$

where the abbreviations $I_{a,b}(K,Q)$ are given by

$$\begin{aligned} M_0^2 I_a(K,Q) = {} & G_0^{-1}(i\omega_k) + G_0^{-1}(i\omega_q) - J_{\boldsymbol{k}-\boldsymbol{q}} - J_0 \\ & + \beta b_0' \Big[ - G_0^{-1}(i\omega_q) G_0^{-1}(i\omega_k) - \frac{J_0^2}{1-\beta b_0' J_0} \left[1 - \beta b_0' G_0^{-1}(i\omega_q)\right] \left[1 - \beta b_0' G_0^{-1}(i\omega_k)\right] \\ & + J_0 \left[ G_0^{-1}(i\omega_q) + G_0^{-1}(i\omega_k) - \beta b_0' G_0^{-1}(i\omega_q) G_0^{-1}(i\omega_k) \right] \Big], \end{aligned} \tag{C.35}$$

respectively

$$M_0^2 I_b(K,Q) = -\beta b_0' \delta_{\omega_k,\omega_q} \frac{\left[G_0^{-1}(i\omega_q) - J_{\boldsymbol{k}-\boldsymbol{q}}\right]^2}{1-\beta b_0' J_{\boldsymbol{k}-\boldsymbol{q}}}. \tag{C.36}$$

At low temperatures, all terms $\propto b_0'$ can be neglected and the flow of $\Sigma_\Lambda(K)$ is solely determined by the first line in Eq. (C.35). By comparing the terms in the flow Eq. (C.34) with the parameterization introduced in Eq. (C.28), we obtain for the flow of the wave function renormalization

$$\partial_\Lambda Z_\Lambda = -Z_\Lambda^2 / M_0^2 \int_K \dot{G}_\Lambda(K). \tag{C.37}$$

Likewise, there is no contribution to the flow of the damping coefficient, which can thus be neglected at low temperatures. Within the present truncation-scheme, the transverse structure factor at low temperatures is thus simply given by a delta contribution at magnon energy $\tilde{E}_{\boldsymbol{k}}$.

### C.2.3 Magnon damping due to classical longitudinal fluctuations

The previous considerations allow us - once more - to make contact with the perturbative calculations of Vaks *et al.* [33,34]. In particular, let us analyze the damping processes encoded in the one-loop expression of the self energy flow in the intermediate temperature regime $T \sim S J_0$. In this case, the terms $\propto b_0'$ in Eq. (C.34) can no longer be neglected and the flow of the damping coefficient is determined by the $I_b(K,Q)$-contribution as

$$\begin{aligned} \partial_\Lambda \gamma_\Lambda(\boldsymbol{q},\omega) &= -M_0 \partial_\Lambda \mathrm{Im}\, \Sigma_\Lambda(\boldsymbol{q}, \omega + i\delta) \\ &= \frac{b_0'}{M_0} \mathrm{Im} \left[ \frac{1}{N} \sum_{\boldsymbol{k}} \dot{G}_\Lambda(\boldsymbol{k}, \omega + i\delta) \frac{\left[G_0^{-1}(\omega + i\delta) - J_{\boldsymbol{k}-\boldsymbol{q}}\right]^2}{1-\beta b_0' J_{\boldsymbol{k}-\boldsymbol{q}}} \right]. \end{aligned} \tag{C.38}$$

If we neglect the self energy contributions to the single-scale propagator in the above flow equation, this can be straightforwardly integrated and we obtain

$$\begin{aligned} \gamma_{\Lambda=1}(\boldsymbol{q},\omega) &= \frac{b_0'}{M_0} \mathrm{Im} \left( \frac{1}{N} \sum_{\boldsymbol{k}} G_\Lambda(\boldsymbol{k}, \omega + i\delta) \frac{\left[G_0^{-1}(\omega + i\delta) - J_{\boldsymbol{k}-\boldsymbol{q}}\right]^2}{1-\beta b_0' J_{\boldsymbol{k}-\boldsymbol{q}}} \right) \Bigg|_{\Lambda=0}^{\Lambda=1} \\ &= \frac{\pi b_0'}{N} \sum_{\boldsymbol{k}} \delta\left(E_{\boldsymbol{k}} - \omega\right) \frac{\left[J_{\boldsymbol{k}} - J_{\boldsymbol{k}-\boldsymbol{q}}\right]^2}{1-\beta b_0' J_{\boldsymbol{k}-\boldsymbol{q}}} - \gamma_0(\omega), \end{aligned} \tag{C.39}$$

where the initial contribution

$$\gamma_0(\omega) = \frac{\pi b_0'}{N} \sum_{\boldsymbol{k}} \frac{J_{\boldsymbol{k}}^2}{1 - \beta b_0' J_{\boldsymbol{k}}} \delta\left(H + M_0 J_0 - \omega\right), \tag{C.40}$$

does not contribute to structure factor at finite momenta and will hence be neglected in the following. This result for the magnon damping recovers the leading perturbative contribution obtained in Ref. [34], which is connected with the coupling of magnons to classical longitudinal fluctuations.

In one and two dimensions, the above expression is not valid for small magnetic field, since we know that the Ward-identity Eq. (3.35) is not fulfilled if the self-energy corrections are neglected. A consistent inclusion of these self-energy corrections requires the consideration of the flow of the higher order vertices, which is beyond the scope of this work. Phenomenologically, these corrections can be taken into account by a replacement of the magnetic field $H$ by the gap $\tilde{\Delta} = HM_0/M(H,T)$, and a rescaling of the external frequency by the wave-function renormalization factor $Z$ in the damping. These modifications yield the semi-phenomenological damping coefficient

$$\tilde{\gamma}(\boldsymbol{q},\omega) = \frac{\pi b_0' Z}{N} \sum_{\boldsymbol{k}} \delta\left(Z\tilde{E}_{\boldsymbol{k}} - \omega\right) \frac{\left[J_{\boldsymbol{k}} - J_{\boldsymbol{k}-\boldsymbol{q}}\right]^2}{1 - \beta b_0' J_{\boldsymbol{k}-\boldsymbol{q}}}. \tag{C.41}$$

The corresponding transverse structure factor

$$\mathcal{S}^{\perp}(\boldsymbol{q},\omega) = \frac{1}{\pi} \frac{e^{\beta\omega}}{e^{\beta\omega}-1} \frac{Z^2 \tilde{\gamma}(\boldsymbol{q},\omega) M_0}{\left[Z\tilde{E}(\boldsymbol{q},\omega) - \omega\right]^2 + \left[Z\tilde{\gamma}(\boldsymbol{q},\omega)\right]^2}, \tag{C.42}$$

is depicted graphically in Fig. C.1 as a function of temperature and magnetic field for a generic momentum $\boldsymbol{k}_0$. In order to generate the plot of $\mathcal{S}^{\perp}(\boldsymbol{q},\omega)$, the magnetization and wave function renormalization were calculated solving the set of flow equations (3.61), derived in chapter 3 (cf. page 61). Since we are only interested in the qualitative behavior, the renormalization of the longitudinal two-point vertex $\Gamma_{\Lambda}^{zz}$ and the mixed three-point vertex $\Gamma_{\Lambda}^{+-z}$ were hereby neglected. Furthermore, all momentum sums - including the sum in the definition of $\tilde{\gamma}(\boldsymbol{k},\omega)$ - were evaluated within a low momentum expansion. Note, that the $\delta$-function in Eq. (C.39) introduces a threshold, which sets $S(\boldsymbol{k},\omega) = 0$ for $\omega < Z\tilde{\Delta}$. In the limit of vanishing magnetic field this implies that the spectral weight of the magnons in $S(\boldsymbol{k},\omega)$ vanishes for $\omega < ZM_0/\chi(0,T)$, where $\chi(0,T)$ is the zero-field susceptibility whose behavior was discussed in chapter 3. Increasing the magnetic field and decreasing the temperature the resulting quasiparticle-peaks sharpen and grow. In this regime the magnons are stabilized. The same behavior is observed if the magnitude of the momentum $k_0$ is lowered. Furthermore, please note that the momentum and frequency dependence of $\tilde{\gamma}(\boldsymbol{k},\omega)$ leads to an asymmetry of the spectral lineshape. This asymmetry increases when the quasiparticle-peaks broaden. Finally, let us emphasize once more that the damping term $\tilde{\gamma}(\boldsymbol{k},\omega)$ is proportional to $b_0'$ and hence exponentially small at low temperatures. In this regime the damping is dominated by processes such as two-magnon scattering, which are not accounted for in the present truncation/deformation scheme.

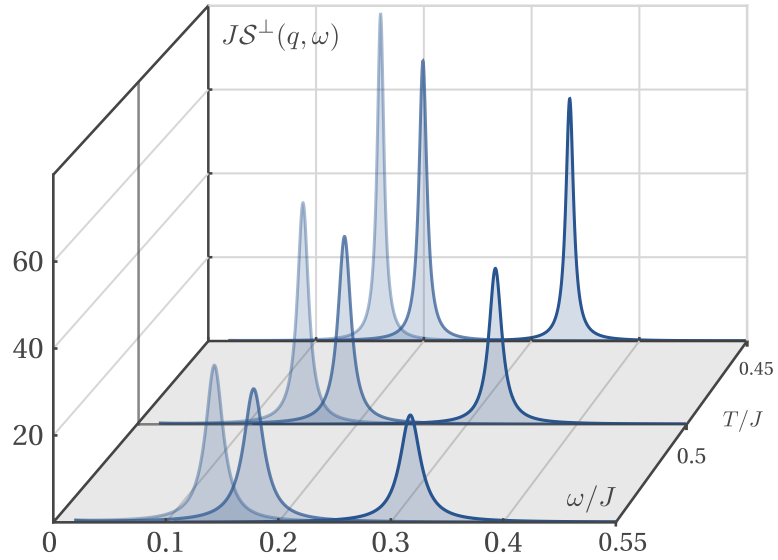


Figure C.1: Transverse structure factor $\mathcal{S}^{\perp}(\boldsymbol{q},\omega)$ (Eq. C.42) of the two-dimensional $S = 1/2$ Heisenberg ferromagnet as a function of frequency and temperature for momentum $k_0 a = 0.75$ and magnetic fields $H/J = 0.001, 0.01, 0.1$ (left to right). Note, that the quasi-particle peaks sharpen with increasing magnetic field strength and decreasing temperature. Furthermore, the lineshapes of the peaks are not symmetrical around the pole $\omega = Z\tilde{E}_{\boldsymbol{k}_0}$ but show a slight asymmetry due to the frequency dependence of the damping $\tilde{\gamma}(k_0,\omega)$. (To be consistent with chapter 3, the energy scale is fixed assuming a nearest neighbor exchange interaction of strength $J$).

# III

# Formalia

# Deutsche Zusammenfassung

## D.1 Überblick

In dieser Arbeit untersuchen wir die thermodynamischen und dynamischen Eigenschaften des $D$-dimensionalen ferromagnetischen Heisenberg Modells im Rahmen der sogenannten *funktionalen Spin Renormierungsgruppe* (spin FRG); ein Formalismus, der die Evolution der Observablen des Systems hinsichtlich einer artifiziellen Modifikation der magnetische Austauschwechselwirkung beschreibt. Wie zu Beginn erwähnt basieren die im Folgenden zusammengefassten Inhalte dabei partiell auf den Publikationen [3] und [4].

## D.2 Das ferromagnetische Heisenberg Modell

Wir beginnen mit der Definition des Modells: Der Hamiltonoperator des Heisenberg Modells ist gegeben als

$$\mathcal{H} = -H \sum_{i=1}^{N} S_i^z - \frac{1}{2} \sum_{ij}^{N} J_{ij} \boldsymbol{S}_i \cdot \boldsymbol{S}_j, \tag{D.1}$$

wobei die Indices $i$ und $j$ die $N$ Gitterpunkte eines $D$-dimensionalen kubischen Gitters durchnummerieren, und $J_{ij} = J(r_{ij}) > 0$, mit $r_{ij} = |\boldsymbol{r}_i - \boldsymbol{r}_j|$ die räumlich isotrope Austauschwechselwirkung bezeichnet. Die Spinoperatoren $S_i^\alpha$ mit $\alpha \in \{x, y, z\}$ erfüllen hierbei die SU(2) Kommutatorrelationen $[S_i^\alpha, S_j^\beta] = i\delta_{ij}\varepsilon^{\alpha\beta\gamma} S_i^\gamma$ und die Normierungsbedingung $\boldsymbol{S}_i^2 = S(S+1)$ wobei $\varepsilon^{\alpha\beta\gamma}$ den vollständig antisymmetrischen Levi-Civita Tensor und $S$ die Spinquantenzahl darstellt. Des Weiteren wurde der Hamiltonoperator um eine Zeemankopplung erweitert. $H$ ist dabei das magnetische Feld in Einheiten der Energie.

## D.3 Die funktionale Spin Renormierungsgruppe

In Kapitel 2 geben wir eine kurze Einführung in das methodische Fundament dieser Arbeit; die funktionale Spin Renormierungsgruppe, die in den Arbeiten von Krieg und Kopietz [1] und Krieg [2] eingeführt wurde. Die grundlegende Idee dieses Formalismus ist es, den Hamiltonoperator artifiziell so zu modifizieren, dass eine kontrollierte Berechnung der dazugehörigen Observablen möglich wird. Dazu wird der wechselwirkenden Teil des Hamiltonoperators durch den Ausdruck

$$\mathcal{V}_\Lambda = -\frac{1}{2} \sum_{ij} \left[ J_{\Lambda,ij}^\perp \left( S_i^+ S_j^- + S_i^- S_j^+ \right) + J_{\Lambda,ij}^z S_i^z S_j^z \right], \tag{D.2}$$

ersetzt. Hierbei sind $S_i^{\pm} = 1/\sqrt{2}\,(S_i^x \pm iS_i^y)$ die Spinleiteroperatoren und

$$J^{\perp}_{\Lambda,ij} = J^{\perp}_{ij} - R^{\perp}_{\Lambda,ij}, \quad J^{z}_{\Lambda,ij} = J^{z}_{ij} - R^{z}_{\Lambda,ij}, \tag{D.3}$$

der transversale und longitudinale Anteil der modifizierten Austauschwechselwirkung. Die Regulatoren $R^{\perp}_{\Lambda,ij}$ und $R^{z}_{\Lambda,ij}$ bestimmen hierbei den genauen Modifikationsprozess der durch die Variable $\Lambda$ parametrisiert wird. Der Evolution der Observablen des Systems hinsichtlich dieses Modifikationsprozesses kann nun im Rahmen eines allgemeinen Renormierungsgruppenformalismus Rechnung getragen werden. Dazu führen Krieg und Kopietz das generierende Funktional $\mathcal{G}_\Lambda[\boldsymbol{h}]$ der imaginärzeitlich geordneten Spinkorrelationfunktionen ein, dessen entsprechende Evolution durch eine allgemeine Flussgleichung $\partial_\Lambda \mathcal{G}_\Lambda[\boldsymbol{h}]$ beschrieben wird. Die Spinkorrelationfunktionen können dabei die funktionales Ableiten hinsichtlich der Quellenfelder erzeugt werden. Analog zu fermionischen oder bosonischen Systemen ist es allerdings signifikant effizienter die relevanten Observablen mithilfe diagramatisch irreduzibler Größen zu berechnen. Im Rahmen konventioneller FRG Formalismen, wird dazu die entsprechende funktionale Legendretransformierte des Funktionals $\mathcal{G}_\Lambda[\boldsymbol{h}]$ eingeführt. Unglücklicherweise ist das in diesem Fall nicht im Allgemeinen möglich; insbesondere nicht für einen initialen Zustand für den die Austauschwechselwirkung komplett verschwindet.

Um dieser technischen Komplikation gerecht zu werden, haben wir in Ref. [3] einen Hybridformalismus entwickelt, der diese Einschränkung geschickt umschifft und dabei gleichzeitig eine irreduzible Struktur gewährleistet. Dieser Formalismus basiert auf einer asymmetrischen Behandlungen transversaler und longitudinal Fluktuationen und erlaubt daher insbesondere eine elegante Untersuchung der symmetriegebrochenen Phase. Konkret wird dazu das generierede Funktional der sogenannte *partiell amputierten Spinkorrelationfunktionen* $\mathcal{F}_\Lambda[\boldsymbol{j}]$ eingeführt, deren Relation zu den physikalisch relevanten Spinkorrelationfunktionen explizit konstruiert werden kann. Gleichzeitig ist nun auch eine Definition der entsprechenden Legendretransformierten $\Gamma_\Lambda\,[\boldsymbol{\varphi}]$ möglich. Eine Taylorentwicklung der dazugehörigen Flussgleichung $\partial_\Lambda \Gamma_\Lambda[\boldsymbol{\varphi}]$ führt schlussendlich zu einer unendlichen Hierarchie gekoppelter Integrodifferentialgleichungen, welche die Basis der im Folgenden zusammengefassten Rechnungen darstellt.

## D.5 Thermodynamik in Dimensionen $D \leq 2$

In Kapitel 3 wird der Hybridformalismus im Rahmen einer Berechnung der thermodynamischen Eigenschaften des ein- und zweidimensionalen Heisenberg Modells bei niedrigen Temperaturen und endlichen Magnetfeldern konzeptionell etabliert. Der grundsätzlichen Idee der Spin FRG folgend gehen wir dabei von einem System vollständig entkoppelter Gitterplätze aus und integrieren die Wechselwirkungseffekte durch (näherungsweises) Lösen der Hierarchie von Integrodifferentialgleichungen.

### Modifikationschema & Anfangsbedingungen

Um unseren Formalismus in Beziehung zur konventionellen Formulierung der Mean-Field- und Spinwellen Theorie zu setzen, wählen wir in dieser Arbeit ein Modifikationschema welches longitudinale und transversale Wechselwirkung nacheinander einschaltet. Im ersten Teil des Flusses betrachten wir den longitudinalen Anteil und lösen die Flussgleichungen in einer sogenannten *Tadpoleapproximation*, welche die Mean-Field Lösungen reproduziert. Im zweiten

Teil wird anschließend der transversale Anteil hochgefahren; implizit wird dabei der Effekt der Spinwellenanregungen auf die thermodynamischen Eigenschaften des System betrachtet.

Für die explizite Lösung der Tadpoleapproximation während des ersten Teil des Flusses verweisen wir an dieser Stellen auf Kapitel 3. Die resultierenden Anfangsbedingungen für den zweiten Teil des Flusses sind sogenannte Mean-Field Vertexfunktionen, die aus Summen von Termen proportional zur Brillouinfunktion $b_0 = b(H + J_0 M_0)$ und deren Ableitungen $b_0^{(n)} = b^{(n)}(H + J_0 M_0)$ bestehen. Hierbei ist $J_0$ die $\boldsymbol{k} = 0$ Komponente der Fouriertransformation der Austauschwechselwirkung und $M_0$ der Mean-Field Ausdruck für die Magnetisierung. Bei niedrigen Temperaturen $T \ll SJ_0$ erfüllt die Brillouinfunktion die Hierarchie

$$b_0 \ll b_0' \ll b_0'' \ll \dots \,. \tag{D.4}$$

Dies erlaubt es die unendliche Anzahl an Vertexfunktionen hinsichtlich ihrer Anfangsbedingung zu klassifizieren. Insbesondere betrachten wir während des zweiten Teil des Flusses nur die Beiträge, deren Mean-field Ausdrücke $\propto b_0$ sind.

### Infrarotkatastrophe & Ward-Identitätkorrektur

Die Ergebnisse konventioneller Spinwellentheorie werden in unserem Formalismus durch eine einfache One-loop Approximation der Flussgleichungen reproduziert. Dazu vernachlässigen wir die Renormierung aller Vertexfunktionen der Ordnung $\geq 2$. In dieser Näherung finden wir für die fließende Magnetisierung

$$M_\Lambda \approx M_0 - \frac{1}{N} \sum_{\boldsymbol{k}} n\left(\beta E_{\Lambda,\boldsymbol{k}}\right), \quad \Lambda \in (0,1), \tag{D.5}$$

wobei

$$E_{\Lambda,\boldsymbol{k}} = \Delta_\Lambda + \Lambda \varepsilon_{\boldsymbol{k}}, \tag{D.6}$$

mit $\Delta_\Lambda = H + M_0 J_0 (1 - \Lambda)$ und $\varepsilon_{\boldsymbol{k}} = M_0(J_0 - J_{\boldsymbol{k}})$ die Spinwellendispersion darstellt, und $n(x) = [\exp(x) - 1]^{-1}$ die Bosedistributionsfunktion. Diese Lösung beschreibt das qualitative Verhalten des dreidimensionale Modells. Allerdings divergiert der Spinwellenkorrekturterm in Gl. (D.5) für hinreichend kleine Magnetfelder in niedrigen Dimensionen. Dies hat seinen Ursprung in der Vernachlässigung der transversalen Selbstenergie. Um diesem Rechnung zu tragen komplementieren wir unser Approximationsssschema um eine Ward-Identität , welche die Magnetisierung in Bezug zum transversalen Propagator setzt. In unserem Schema gewährleisten wir diese Identität indem wir die transversale Selbstenergie bei verschwindendem Impuls und Frequenz entsprechend festsetzen. Effektiv führt das zu der modifizierten Spinwellendispersion

$$\tilde{E}_{\Lambda,\boldsymbol{k}} = \tilde{\Delta}_\Lambda + \Lambda \varepsilon_{\boldsymbol{k}}, \tag{D.7}$$

mit $\tilde{\Delta}_\Lambda = H M_0 / M_\Lambda + M_0 J_0 (1 - \Lambda)$. Diese Korrektur hebt die Divergenz auf und führt zu Magnetisierungskurven die qualitativ mit dem Mermin-Wagner-Theorem übereinstimmen.

### Magnetisierungs- & Suszptibilitätskurven

Schlussendlich erlaubt uns die Ward-Identität auch näherungsweise den Einfluss der höheren Vertexkorrekturen abzuschätzen. Effektiv ergibt sich dann aus der Kombination unseres Approximationsschemas und der Ward-Identität ein gekoppeltes System an Integrodifferentialgleichungen für die Magnetisierung $M_\Lambda$, die Wellenfunktionsrenormierungskonstante $Z_\Lambda$,

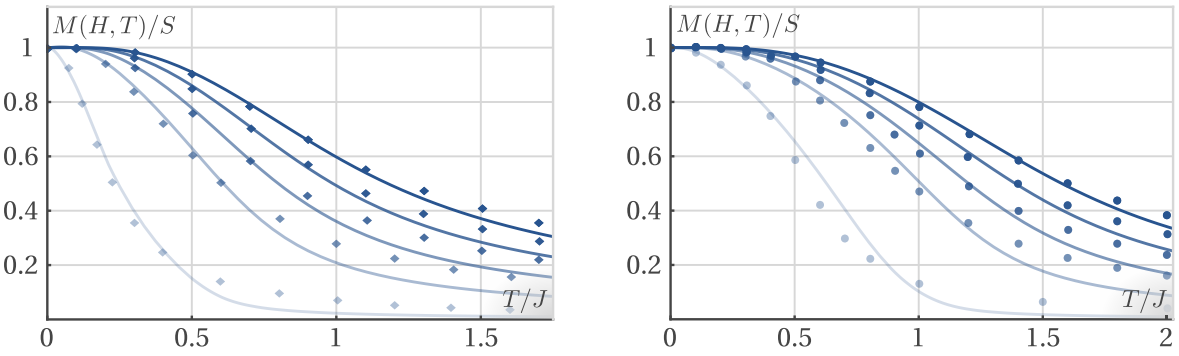


(a) $D = 1$ (b) $D = 2$

Abb. D.1: Magnetisierungskurven $M(H,T)$ des ein- und zweidimensionalen $S = 1/2$ ferromagnetischen Heisenberg Modells als Funktion der Temperatur für Magnetfelder $H/J = 1.0, 0.8, 0.6, 0.4, 0.1$ (von oben nach unten). Die Referenzpunkte beziehen sich auf die Bethe-Ansatz Ergebnisse aus Ref. [123] (◆), respektive auf die Monte Carlo Simulationen aus Ref. [125] (●). Die Energieskala $J$ gibt die Stärke der zugrundeliegenden Austauschwechselwirkung an.[3]

und den longitudinalen Zweipunktvertex bei verschwindendem Impuls und Frequenz $\Gamma^{zz}_{\Lambda}(0)$. Die entsprechende numerische Lösung dieses Gleichungssystems führt zu Magnetisierungs- und Suzeptibilitätskurven die für niedrige Temperaturen und endliche Magnetfelder in guter Übereinstimmung mit der Literatur sind, siehe Abb. D.1.

## D.6 Longitudinale Dynamik

In Kapitel 4 dieser Arbeit untersuchen wir die longitudinale Spindynamik bei tiefen Temperaturen. Insbesondere gehen wir der Existenz einer möglichen kollektiven Schallmode (Zero-sound), d.h. einer wellenförmigen Ausbreitung der Magnetisierungsfluktuationen, nach.

### Zero-sound Approximation & Generalized Random Phase Lösung

Um die wesentliche Struktur der longitudinalen Fluktuationen bei niedrigen Temperaturen aus der unendlichen Hierarchie an Flussgleichungen zu extrahieren, vereinfachen wir diese in zwei Schritten. Erstens orientieren wir uns an Kapitel 3 und klassifizieren die Vertexfunktionen anhand ihrer Mean-Field Beiträge, d.h. alle Terme $\sim b_0'$ und höher werden vernachlässigt. Zweitens ordnen wir die übriggebliebenden Terme anhand der Anzahl an longitudinalen Propagatoren $F_\Lambda(K)$, was effektive einer Entwicklung der Flussgleichungen in der inversen Austauschreichweite entspricht. In dieser Arbeit behalten wir nur die Beiträge $\mathcal{O}(F_\Lambda(K))$ und vernachlässigen des Weiteren die sogenannten *Exchange* und *Particle-particle* Beiträge zur Renormierung des Vierpunktvertex. Das resultierende System an Integrodifferentialgleichungen kann für Magnetfelder $H > H_l(T)$ anhand eines Ansatzes, der sich an den Anfangsbedingungen orientiert, gelöst werden. Hierbei bezeichnet $H_l(T)$ das kritische Magnetfeld für das die One-loop Magnetisierung verschwindet. Dies ergibt die sogenannte *Generalized Random Phase Lösung* für die longitudinale Korrelationsfunktion, deren algebraische Struktur mit der

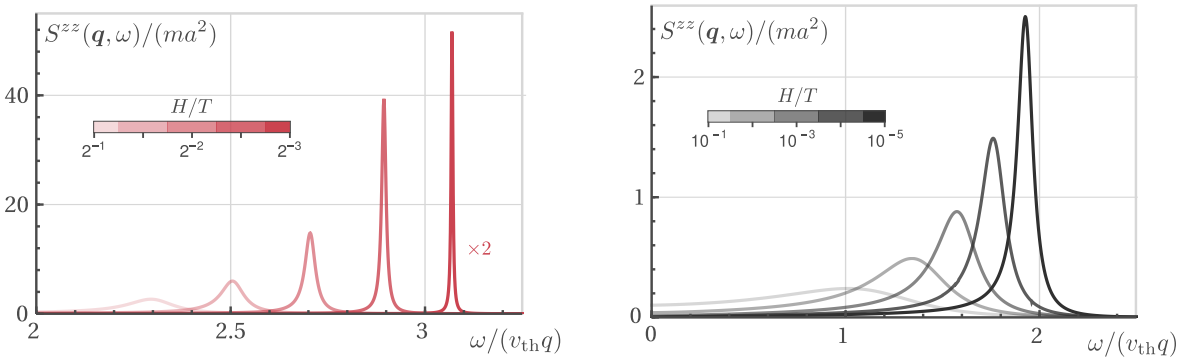


(a) $D = 1$ (b) $D = 2$

Abb. D.2: Longitudinaler dynamischer Strukturfaktor $S^{zz}(\boldsymbol{q},\omega)$ des ein- und zwei-dimensionalen Heisenberg Ferromagnet für $q = k_{\mathrm{th}}/4$, Temperatur $Tma^2 = 10^{-2}$ und Magnetfeld im Bereich $H < T \ll 1/(ma^2)$.[3] Mit Genehmigung aus Ref. [4] übernommen © [2020] American Physical Society.

komplizierten nichtperturbativen Lösung von Izyumov *et al.* aus Ref [36] übereinstimmt. Für die genaue Form dieser Lösung verweisen wir auf Kapitel 4.

### Zero-magnon Schall

Der resultierende longitudinale Strukturfaktor zeigt abhängig von der Dimension ein qualitativ unterschiedliches Verhalten: In $D = 3$ führt der große Phasenraum, der für den Zerfall in transversale Magnonen zur Verfügung steht, lediglich zu einem um die Nullfrequenz zentrierten Peak dessen Breite linear mit dem Impuls skaliert. Im Gegensatz dazu tritt in $D \leq 2$ bei niedrigen Temperaturen $T \ll SJ_0$ und im Magnetfeldbereich $H_l(T) < H < T$ [3], d.h. in der Umgebung des kritischen Punktes $(T_c, H_c) = (0, 0)$, ein wohldefinierter Quasiteilchenpeak mit linearer Dispersion in Erscheinung, den wir als eine Signatur des zero-magnon Schalls interpretieren, siehe Abb. D.2. Dies ist unseres Wissens nach die erste Beschreibung eines solchen Phänomens. Für eine Analyse der entsprechenden Schallgeschwindigkeit und Dämpfung sowie eine Abschätzung des relevante Frequenz- und Impulsbereich verweisen wir wiederum auf Kapitel 4.

---

Insgesamt stellen die hier zusammengefassten Berechnungen eine der ersten erfolgreichen Anwendungen des neuen nichtperturbativen Spin FRG Formalismusses dar. Entsprechend sollten zukünftig auch kompliziertere Quantenspinsysteme mithilfe der spin FRG Methode analysiert werden können, vorausgesetzt, es kann ein physikalisch sinnvolles Modifikations- und Approximationsschema für die entsprechende Hierarchie gekoppelter Flussgleichungen gefunden werden.

[3] Alle Größen in Einheiten der Energie. Die Energieskala $1/(ma^2)$ ist hierbei durch die Gitterkonstante $a$ und durch die Spinwellendispersion bei kleinen Impulsen $\varepsilon_{\boldsymbol{k}} \approx k^2/(2m)$ gegeben. Letztere ist durch die zugrundeliegende Wechselwirkung bestimmt. Für eine Wechselwirkung zwischen nächsten Nachbarn der Stärke $J$ ergibt sich für $S = 1/2$ bei tiefen Temperaturen $ma^2 \approx 1/J$. Thermische Geschwindigkeit und Wellenvektor sind außerdem gegeben als $k_{\mathrm{th}} = mv_{\mathrm{th}} = \sqrt{2mT}/a$.

# Bibliography


[1] J. Krieg and P. Kopietz, Exact renormalization group for quantum spin systems, Phys. Rev. B **99**, 060403(R) (2019).

[2] J. Krieg, *Functional renormalization group approach to classical and quantum spin systems*, (PhD thesis, Johann Wolfgang Goethe-Universität, Frankfurt am Main, 2019).

[3] R. Goll, D. Tarasevych, J. Krieg, and P. Kopietz, Spin functional renormalization group for quantum Heisenberg ferromagnets: Magnetization and magnon damping in two dimensions, Phys. Rev. B **100**, 174424 (2019).

[4] R. Goll, A. Rückriegel, and P. Kopietz, Zero-magnon sound in quantum Heisenberg ferromagnets, Phys. Rev. B **102**, 224437 (2020).

[5] R. Goll and P. Kopietz, Renormalization group for the $\varphi^4$ theory with long-range interaction and the critical exponent $\eta$ of the Ising model, Phys. Rev. E **98**, 022135 (2018).

[6] D. C. Mattis, *The Theory of Magnetism Made Simple*, (World Scientific, Singapore, 2006).

[7] H-J. Van Leeuwen, Problèmes de la théorie électronique du magnétisme, J. Phys. Radium **2**, 361 (1921).

[8] W. Pauli, Exclusion Principle and Quantum Mechanics, Nobel Lecture, (1946).

[9] G. E. Uhlenbeck and S. Goudsmit, Ersetzung der Hypothese vom unmechanischen Zwang durch eine Forderung bezüglich des inneren Verhaltens jedes einzelnen Elektrons, Die Naturwissenschaften **13**, 953 (1925).

[10] W. Pauli, Zur Quantenmechanik des magnetischen Elektrons, Z. Phys. **43**, 601 (1927).

[11] W. Heisenberg, Zur Theorie des Ferromagnetismus, Z. Phys., **49**, 619 (1928).

[12] P. Dirac, On the theory of quantum mechanics, Proc. R. Soc. London, Ser. A **112**, 661 (1926).

[13] P. Dirac, Quantum mechanics of many-electron systems, Proc. R. Soc. London, Ser. A **123**, 714 (1929).

[14] P. Coleman, *Introduction to Many-Body Physics*, (Cambridge University Press, Cambridge, 2015).

[15] P. Fazekas, *Lecture notes on Electron Correlation and Magnetism*, (World Scientific, Singapore, 1999).

[16] M. L. Néel, Propriétés magnétiques des ferrites ; ferrimagnétisme et antiferromagnétisme, Ann. Phys. (Paris) **3**, 137 (1948).

[17] P. W. Anderson, Localized Magnetic States in Metals, Phys. Rev. **124**, 41 (1961).

[18] J. Kondo, Resistance Minimum in Dilute Magnetic Alloys, Prog. Theor. Phys. **32**, 37 (1964).

[19] L. Savary and L. Balents, Quantum spin liquids: a review, Rep. Prog. Phys. **80**, 016502 (2017).

[20] J. Zinn-Justin, *Quantum field theory and critical phenomena*, (Clarendon Press, Oxford, 2010).

[21] F. Keffer, in *Handbuch der Physik*, edited by F. Flügge, (Springer, Berlin, 1966).

[22] V. N. Krivoruchko, Longitudinal magnetization dynamics in Heisenberg magnets: Spin Green functions approach, Fiz. Nizk. Temp. **43**, 1245 (2017).

[23] O. O. Boliasova and V. N. Krivoruchko, Longitudinal Spin Dynamics in the Heisenberg Antiferromagnet: Two-Magnon Excitations, Ukr. J. Phys. **65**, 865 (2020).

[24] J. F. Rodriguez-Nieva, D. Podolsky, and E. Demler, Hydrodynamic sound modes and Galilean symmetry breaking in a magnon fluid, arXiv:1810.12333v2.

[25] D. Pines and P. Nozieres, *The Theory of Quantum Liquids: Normal Fermi Liquids*, (W. A. Benjamin, New York, 1966). *The Theory of Quantum Liquids: Superfluid Bose Liquids*, (Addison-Wesley, Redwood City, 1990).

[26] T. Izuyama and M. Saitoh, Zero sound oscillation in the magnon assembly, Phys. Lett. A **29**, 581 (1969).

[27] C. R. Natoli and J. Ranninger, High frequency collective mode in a Heisenberg ferromagnet, Phys. Lett. A **32**, 11 (1970).

[28] D. L. Huber, Longitudinal Susceptibility of a Planar Ferromagnet, Phys. Rev. B **3**, 805 (1971).

[29] A. B. Harris, Longitudinal Dynamical Susceptibility of the Heisenberg Ferromagnet at Short Wavelengths and Low Temperatures, Phys. Rev. B **3**, 3065 (1971).

[30] T. L. Reinecke, Longitudinal susceptibility and the question of zero magnons in low-temperature magnetic insulators, Phys. Rev. B **10**, 200 (1974).

[31] C. R. Natoli and J. Ranninger, Spin-wave interaction effects on the longitudinal dynamical susceptibility in Heisenberg ferromagnets, J. Phys. C **7**, 3603 (1974).

[32] G. Dewel, The dynamical longitudinal correlation function of the Heisenberg model at low temperatures, Physica A **82**, 365 (1976). The dynamical longitudinal correlation function of the Heisenberg model at low temperatures II, Physica A **89**, 245 (1977).

[33] V. G. Vaks, A. I. Larkin, and S. A. Pikin, Thermodynamics of an ideal ferromagnetic substance, Zh. Eksp. Teor. Fiz. **53**, 281 (1967) [Sov. Phys. JETP **26**, 188 (1968)].

[34] V. G. Vaks, A. I. Larkin, and S. A. Pikin, Spin waves and correlation functions in a ferromagnetic, Zh. Eksp. Teor. Fiz. **53**, 1089 (1967) [Sov. Phys. JETP **26**, 647 (1968)].

[35] Y. A. Izyumov and Y. N. Skryabin, *Statistical Mechanics of Magnetically Ordered Systems*, (Springer, Berlin, 1988).

[36] Y. A. Izyumov, N. I. Chaschin, and V. Y. Yushankai, Longitudinal spin dynamics in the Heisenberg ferromagnet: Diagrammatic approach, Phys. Rev. B **65**, 214425 (2002).

[37] A. Auerbach, *Interacting Electrons and Quantum Magnetism*, (Springer, New York, 1998).

[38] E. Koch, *Exchange Mechanisms*, (Lecture notes, Autumn School on Correlated Electrons, Juelich, 2012).

[39] C. Timm. *Theory of Magnetism*, (Lecture notes, International Max Planck Research School for Dynamical Processes in Atoms, Molecules and Solids, Dresden, 2009).

[40] W. Nolting, *Quantentheorie des Magnetismus - Teil 2*, (Teubner, Stuttgart, 1986).

[41] H. A. Kramers, L'interaction Entre les Atomes Magnétogènes dans un Cristal Paramagnétique, Physica, **1**, 182 (1934).

[42] P. W. Anderson, Antiferromagnetism. Theory of Superexchange Interaction, Phys. Rev. **79**, 350 (1950).

[43] B. T. Matthias, R. M. Bozorth, and J. H. Van Vleck, Ferromagnetic Interaction in EuO, Phys. Rev. Lett. **7**, 160 (1961).

[44] J. B. Goodenough, Theory of the Role of Covalence in the Perovskite-Type Manganites [La, $M$(II)]$MnO_3$, Phys. Rev. **100**, 564 (1955).

[45] J. Kanamori, Superexchange interaction and symmetry properties of electron orbitals, J. Phys. Chem. Solids,**10**, 87 (1959).

[46] I. Dzyaloshinsky A thermodynamic theory of "weak" ferromagnetism of antiferromagnetics, J. Phys. Chem. Solids **4**, 241 (1958).

[47] T. Moriya, Anisotropic Superexchange Interaction and Weak Ferromagnetism, Phys. Rev. **120**, 91 (1960).

[48] R. J. Birgeneau and G. Shirane, Magnetism in one dimension, Physics Today **31**, 32 (1978).

[49] B. Pan, J. Qiu, B. Pan, X. Gong, S. Li, Y. Xu, X. Kong, M. Ding, L. Zhanga, and H. Feng, Realization of an excellent two-dimensional Heisenberg ferromagnetic system: the synthesis, structure, and thermodynamic properties of piperazinediium tetrabromocuprate, J. Mater. Chem. C **7**, 8813 (2019).

[50] H. Mikeska, A. K. Kolezhuk, in *Quantum Magnetism*, edited by U. Schollwöck *et al.*, (Springer, Berlin, 2004).

[51] Y. Nambu, Quasi-Particles and Gauge Invariance in the Theory of Superconductivity, Phys. Rev. **117**, 648 (1960).

[52] J. Goldstone, Field theories with "Superconductor" solutions, Nuovo Cim **19**, 154 (1961).

[53] H. Watanabe and and H. Murayama, Unified Description of Nambu-Goldstone Bosons without Lorentz Invariance, Phys. Rev. Lett. **108**, 251602 (2012).

[54] H. Watanabe, Counting Rules of Nambu–Goldstone Modes, Annual Review of Condensed Matter Physics, Vol. **11**, 169 (2020).

[55] A. J. Beekman, L. Rademaker, J. v. Wezel, An introduction to spontaneous symmetry breaking, SciPost Physics Lecture Notes **11**, (2019).

[56] P. W. Anderson, *Basic Notions Of Condensed Matter Physics*, (Westview Press, Boulder, 1997.)

[57] F. Bloch, Zur Theorie des Ferromagnetismus, Z. Phys. **61**, 206 (1930).

[58] P. Kopietz, *Theorie zur Supraleitung, Magnetismus und elektronische Korrelation* (Lecture Notes, Johann Wolfgang Goethe-Universität, Frankfurt am Main, 2021).

[59] N. D. Mermin and H. Wagner, Absence of Ferromagnetism or Antiferromagnetism in One- or Two-Dimensional Isotropic Heisenberg Models, Phys. Rev. Lett. **17**, 1307 (1966).

[60] P. C. Hohenberg, Existence of Long-Range Order in One and Two Dimensions, Phys. Rev. **158**, 383 (1967).

[61] V. L. Berezinskii, Destruction of long-range order in one-dimensional and two-dimensional systemspossessing a continuous symmetry group. II: Quantum systems, Zh. Eksp. Teor. Fiz. 61, 1144 (1971)[Sov. Phys. JETP34, 610 (1972)].

[62] J. M. Kosterlitz and D. J. Thouless, Ordering, metastability and phase transitions in two-dimensional systems, J. Phys. C **6**, 1181 (1973).

[63] J. M. Kosterlitz, The critical properties of the two-dimensional xy model, J. Phys. C **7**, 1046 (1974).

[64] D. R. Nelson and J. M. Kosterlitz, Universal Jump in the Superfluid Density of Two-dimensional Superfluids, Phys. Rev. Lett. **39**, 1201 (1977).

[65] B. Nachtergaele, Quantum spin systems after DLS 1978, in *Spectral Theory and Mathematical Physics: A Festschrift in Honor of Barry Simon's 60th Birthday*, edited by F. Gesztesy *et al.*, Proceedings of Symposia in Pure Mathematics **76**, 47 (2007).

[66] M. Kollar, I. Spremo, and P. Kopietz, Spin-wave theory at constant order parameter, Phys. Rev. B **67**, 104427 (2003).

[67] R. Kubo, Statistical-Mechanical Theory of Irreversible Processes. I. General Theory and Simple Applications to Magnetic and Conduction Problems, J. Phys. Soc. Jpn. **12**, 570 (1957).

[68] R. Kubo, The fluctuation-dissipation theorem, Rep. Prog. Phys. **29, 255 (1966)**.

[69] J. Schmalian, *Theory of Condensed Matter II*, (Lecture Notes, Karlsruhe Institute of Technology, Karlsruhe, 2018).

[70] A. Furrer, J. F. Mesot, and T. Stässle. *Neutron scattering in condensed matter physics*, (World Scientific, Hackensack, 2009).

[71] S. W. Lovesey, *Theory of neutron scattering from condensed matter*, (Oxford, Clarendon, 1984).

[72] G. L. Squires, *Introduction to the theory of thermal neutron scattering*, (Cambridge University Press, Cambridge, 2012).

[73] S. V. Maleev, Polarized neutron scattering in magnets, Phys.-Usp. **45**, 569 (2002).

[74] A. Kamenev, *Field theory of non-equilibrium systems*, (Cambridge Univ. Press, Cambridge, 2011).

[75] T. Matsubara, A New Approach to Quantum-Statistical Mechanics, Prog. Theor. Phys. **14**, 351 (1955).

[76] P. C. Martin and J. Schwinger, Theory of Many-Particle Systems. I, Phys. Rev. **115**, 1342 (1959).

[77] D. Bohm and D. Pines, A Collective Description of Electron Interactions: III. Coulomb Interactions in a Degenerate Electron Gas, Phys. Rev. **92**, 609 (1963).

[78] J. Hubbard, The description of collective motions in terms of many-body perturbation theory, Proc. R. Soc. London, Ser. A **240**, 539 (1957).

[79] H. Ehrenreich and M. H. Cohen, Self-Consistent Field Approach to the Many-Electron Problem, Phys. Rev. **115**, 786 (1959).

[80] A. L. Fetter and J. D. Walecka, *Quantum theory of many-particle systems*, (Dover, Mineola, 2003).

[81] G. D. Mahan, *Many-particle Phyics*, (Kluwer Academic, New York, 2000).

[82] A. A. Abrikosov and I. M. Khalatnikov, The theory of a fermi liquid (the properties of liquid $^3$He at low temperatures), Rep. Prog. Phys., **22**, 329 (1959).

[83] D. Vollhardt and P. Wölfle, *The Superfluid Phases of Helium 3*, (Taylor & Francis, London, 1990).

[84] L. P. Kadanoff and P. C. Martin, Hydrodynamic equations and correlation functions, Ann. Phys. (N.Y.), **24**, 419 (1963).

[85] D. Forster, *Hydrodynamic fluctuations, broken symmetry, and correlation functions*, (W. A. Benjamin, Reading, 1975).

[86] B. Spivak, S. V. Kravchenko, S. A. Kivelson, and X. P. A. Gao, Colloquium: Transport in strongly correlated two dimensional electron fluids, Rev. Mod. Phys. **82**, 1743 (2010).

[87] A. V. Andreev, Steven A. Kivelson, and B. Spivak, Hydrodynamic Description of Transport in Strongly Correlated Electron Systems, Phys. Rev. Lett. **106**, 256804 (2011).

[88] M. Polini, and A. Geim, Viscous electron fluids, Physics Today **73**, 6 (2020).

[89] D. A. Bandurin, I. Torre, R. Krishna Kumar, M. Ben Shalom, *et al.*, Negative local resistance caused by viscous electron backflow in graphene Science **351**, 1055 (2016).

[90] R. Krishna Kumar, D. Bandurin, F. Pellegrino, *et al.*, Superballistic flow of viscous electron fluid through graphene constrictions, Nature Phys **13**, 1182 (2017).

[91] B. E. Keen, P. W. Matthews and J. Wilks, The acoustic impedance of liquid helium-3, Proc. R. Soc. London, Ser. A. **284**, 1396 (1965).

[92] W. R. Abel, A. C. Anderson, and J. C. Wheatley, Propagation of Zero Sound in Liquid $He^3$ at Low Temperatures, Phys. Rev. Lett. **17**, 74 (1966).

[93] C. C. Ackerman and W. C. Overton, Jr., Second Sound in Solid Helium-3, Phys. Rev. Lett. **22**, 764 (1969).

[94] W. Kaminski, Hyperbolic Heat Conduction Equation for Materials With a Nonhomogeneous Inner Structure, J. Heat Transfer **112**, 555 (1990).

[95] L. Tisza, Sur la théorie des liquides quantiques. Application à l'hélium liquide. II, J. Phys. Radium **1**, 350 (1940).

[96] L. D. Landau, Two-fluid model of liquid helium II, J. Phys. U.S.S.R **5**, 71 (1941).

[97] I. M. Khalatnikov, *An introduction to the theory of superfluidity*, (W. A. Benjamin, New York, 1965).

[98] F. J. Dyson, General theory of spin-wave interactions, Phys. Rev. **102**, 1217 (1956).

[99] F. J. Dyson, Thermodynamic behavior of an ideal ferromagnet, Phys. Rev. **102**, 1230 (1956).

[100] T. Holstein and H. Primakoff, Field dependence of the intrinsic domain magnetization of a ferromagnet, Phys. Rev. **58**, 1098 (1940).

[101] S. V. Maleev, Scattering of slow neutrons in ferromagnets, Sov. Phys. JETP **6.4**, 776 (1958).

[102] J. Schwinger, *Quantum theory of angular momentum*, edited by J. L. Biedenharn and H. Van Dam, (Academic Press, New York, 1965).

[103] D. P. Arovas and A. Auerbach, Functional integral theories of low-dimensional quantum Heisenberg models, Phys. Rev. B **38**, 316 (1988).

[104] A. A. Abrikosov, Electron scattering on magnetic impurities in metals and anomalous resistivity effects, Physics Physique Fizika **2**, 5 (1965).

[105] H. Bethe, Zur Theorie der Metalle, Z. Phys. **71, 205 (1931)**.

[106] S. V. Tyablikov, *Methods in the Quantum Theory of Magnetism*, (Springer, New York, 1967).

[107] F. D. M. Haldane, Continuum dynamics of the 1-D Heisenberg antiferromagnet: Identification with the $O(3)$ nonlinear sigma model, Phys. Lett. A **93**, 464 (1983).

[108] F. D. M. Haldane, Nonlinear Field Theory of Large-Spin Heisenberg Antiferromagnets: Semiclassically Quantized Solitons of the One-Dimensional Easy-Axis Néel State, Phys. Rev. Lett. **50**, 1153 (1983).

[109] A. W. Sandvik, Computational Studies of Quantum Spin Systems, AIP Conference Proceedings **1297**, 135 (2010).

[110] S. R. White, Density-matrix algorithms for quantum renormalization groups, Phys. Rev. B **48**, 10345 (1993).

[111] N. V. Prokof'Ev, B. V. Svistunov, and I. S. Tupitsyn, Exact, complete, and universal continuous-time worldline Monte Carlo approach to the statistics of discrete quantum systems, J. Exp. Theor. Phys. **87**, 310 (1998).

[112] H. G. Evertz, The loop algorithm, Adv. Phys. **52**, 1 (2003).

[113] P. Kopietz, L. Bartosch, and F. Schütz, *Introduction to the Functional Renormalization Group*, (Springer, Berlin, 2010).

[114] J. Berges, N. Tetradis, and C. Wetterich, Non-perturbative renormalization flow in quantum field theory and statistical physics, Phys. Rep. **363**, 223 (2002).

[115] D. Tarasevych, J. Krieg, and P. Kopietz, A rich man's derivation of scaling laws for the Kondo model, Phys. Rev. B **98**, 235133 (2018).

[116] M. Salmhofer, *Renormalization: an introduction*, (Springer, Berlin, 1999).

[117] F. SchÜtz and P. Kopietz, Functional renormalization group with vacuum expectation values and spontaneous symmetry breaking, J. Phys. A: Math. Gen. **39**, 8205 (2006).

[118] M. Takahashi, One-Dimensional Heisenberg Model at Finite Temperature, Prog. Theor. Phys. **46**, 401 (1971).

[119] M. Yamada and M. Takahashi, Critical Behavior of Spin-1/2 One-Dimensional Heisenberg Ferromagnet at Low Temperatures, J. Phys. Soc. Jpn. **55**, 2024 (1986).

[120] M. Takahashi, Correlation length and free energy of the $S = 1/2$ $XYZ$ chain, Phys. Rev. B **43**, 5788 (1991).

[121] P. Kopietz and S. Chakravarty, Low-temperature behavior of the correlation length and the susceptibility of a quantum Heisenberg ferromagnet in two dimensions, Phys. Rev. B **40**, 4858 (1989); P. Kopietz, Low-temperature behavior of the correlation length and the susceptibilty of the ferromagnetic quantum Heisenberg chain, *ibid.* **40**, 5194 (1989).

[122] M. Takahashi, Few-dimensional Heisenberg ferromagnets at low temperature, Phys. Rev. Lett. **58**, 168 (1987).

[123] I. Junger, D. Ihle, J. Richter, and A. Klümper, Green-function theory of the Heisenberg ferromagnet in a magnetic field, Phys. Rev. B **70**, 104419 (2004).

[124] I. Juhász Junger, D. Ihle, L. Bogacz, and W. Janke, Thermodynamics of Heisenberg ferromagnets with arbitrary spin in a magnetic field, Phys. Rev. B **77**, 174411 (2008).

[125] P. Henelius, A. W. Sandvik, C. Timm, and S. M. Girvin, Monte Carlo study of a two-dimensional quantum ferromagnet, Phys. Rev. B **61**, 364 (2000).

[126] C. Timm, S. M. Girvin, P. Henelius, and A. W. Sandvik, $1/N$ expansion for two-dimensional quantum ferromagnets, Phys. Rev. B **58**, 1464 (1998).

[127] P. M. Chaikin and T. C. Lubensky, *Principles of Condensed Matter Physics*, (Cambridge University Press, Cambridge, 1995).

[128] A. Z. Patashinskii and V. L. Prokrovskii, Longitudinal susceptibility and correlations in degenerate systems, Zh. Eksp. Teor. Fiz. **64**, 1445 (1973) [Sov. Phys. JETP **37**, 733 (1973)].

[129] A. A. Katanin, Fulfillment of Ward identities in the functional renormalization group approach, Phys. Rev. B **70**, 115109 (2004).

[130] J. Reuther and P. Wölfle, $J_1$-$J_2$ frustrated two-dimensional Heisenberg model: Random phase approximation and functional renormalization group, Phys. Rev. B **81**, 144410 (2010).

[131] J. Kondo and K. Yamaji, Green's-function formalism of the one-dimensional Heisenberg spin system, Prog. Theor. Phys. **47**, 807 (1972).

[132] Wolfram Research, Inc., MATHEMATICA (VERSION 12.0), (Champaign, 2021).

[133] D. Tarasevych and P. Kopietz, Dissipative spin dynamics in hot quantum paramagnets, Phys. Rev. B **104**, 024423 (2021).

[134] B. I. Halperin and P. C. Hohenberg, Hydrodynamic Theory of Spin Waves, Phys. Rev. **188**, 898 (1969).

[135] G. Reiter, Magnon Density Fluctuations in the Heisenberg Ferromagnet, Phys. Rev. **175**, 631 (1968).

[136] F. Schwabl and K. H. Michel, Hydrodynamics of Heisenberg Ferromagnets, Phys. Rev. B **2**, 189 (1970).

[137] K. H. Michel and F. Schwabl, Hydrodynamic Modes in a Gas of Magnons, Phys. Kondens. Mater. **11**, 144 (1970).

[138] Y. G. Rudoy, Collective Green Function and Longitudinal susceptibility of anisotropic Heisenberg Ferromagnets at low temperatures, Ukr. J. Phys. **50**, 770 (2005).

[139] V. Tiberkevich, I. V. Borisenko, P. Nowik-Boltyk, V. E. Demidov, A. B. Rinkevich, S. O. Demokritov, and A. N. Slavin, Excitation of coherent second sound waves in a dense magnon gas, Sci Rep **9**,9063 (2019).

[140] S. Streib, N. Vidal-Silva, K. Shen, and G. E. W. Bauer, Magnon-phonon interactions in magnetic insulators , Phys. Rev. B **99**, 184442 (2019).

[141] S. M. Winter, K. Riedl, P. A. Maksimov, A. L. Chernyshev, A. Honecker, and R. Valentí, Breakdown of magnons in a strongly spin-orbital coupled magnet, Nat. Commun. **8**, 1152 (2017).

[142] L. J. De Jongh, W. D. Van Amstel, and A. R. Miedema Magnetic measurements on $(C_2H_5NH_3)_2$ $CuCl_4$: Ferromagnetic layers coupled by a very weak antiferromagnetic interaction, Physica **58**, 277 (1972).

[143] L. J. De Jongh, Observation of lattice- and spin-dimensionality crossovers in the susceptibility of quasi 2-dimensional Heisenberg ferromagnets, Physica B+C **82**, 247 (1976).

[144] P. Zhou and J. E. Drumheller, Magnetic critical behavior and exponents of the quasi-two-dimensional ferromagnet $[NH_3(CH_2)_9NH_3]CuBr_4$, Jour. Appl. Phys. **67**, 5755 (1990).

[145] A. Vasiliev, O. Volkova, E. Zvereva, and M. Markina, Milestones of low-D quantum magnetism, NPJ Quant. Mater. **3**, 18 (2018).

[146] I. Affleck, Model for Quasi-One-Dimensional Antiferromagnets: Application to $CsNiCl_3$, Phys. Rev. Lett. **62**, 474 (1988).

[147] C. Gros, P. Lemmens, M. Vojta, R. Valentí, K.-Y. Choi, H. Kageyama, Z. Hiroi, N. V. Mushnikov, T. Goto, M. Johnsson, and P. Millet, Longitudinal magnon in the tetrahedral spin system $Cu_2Te_2O_5Br_2$ near quantum criticality, Phys. Rev. B **67**, 174405 (2003).

[148] H. J. Schulz, Dynamics of Coupled Quantum Spin Chains, Phys. Rev. Lett. **77**, 2790 (1996).

[149] I. Affleck, G. F. Wellmann, Longitudinal modes in quasi-one-dimensional antiferromagnets, Phys. Rev. B **46**, 8934 (1992).

[150] Y. Kulik and O. P. Sushkov, Width of the longitudinal magnon in the vicinity of the $O(3)$ quantum critical point Phys. Rev. B **84**, 134418 (2011).

[151] S. G. Ovchinnikov, *Hubbard operators in the theory of strongly correlated electrons* (Imperial College Press, London, 2004).

[152] Y. A. Izyumov and B. M. Letfulov, A diagram technique for Hubbard operators: the magnetic phase diagram in the (t-J) model, J. Phys.: Condens. Matter **2**, 8905 1990.

[153] K. Yosida, *Theory of Magnetism*, (Springer, Berlin, 1998).

[154] D. C. Wood, *The computation of polylogarithms*, (Technical report. UKC, University of Kent, Canterbury, 1992).

[155] P. Kopietz, *Bosonization of Interacting Fermions in Arbitrary Dimensions*, (Springer, Berlin, 1997).